5-2016

EVALUATING DIFFERENTIAL NUCLEAR DNA YIELD RATES AMONG HUMAN BONE TISSUE TYPES: A SYNCHROTRON MICRO-CT APPROACH

Janna Michelle Andronowski
University of Tennessee - Knoxville, jandrono@vols.utk.edu

To the Graduate Council:

I am submitting herewith a dissertation written by Janna Michelle Andronowski entitled "EVALUATING DIFFERENTIAL NUCLEAR DNA YIELD RATES AMONG HUMAN BONE TISSUE TYPES: A SYNCHROTRON MICRO-CT APPROACH." I have examined the final electronic copy of this dissertation for form and content and recommend that it be accepted in partial fulfillment of the requirements for the degree of Doctor of Philosophy, with a major in Anthropology.

Amy Z. Mundorff, Major Professor

We have read this dissertation and recommend its acceptance:

Dawnie W. Steadman, Benjamin M. Auerbach, Yong C. Bradley, Christian M. Crowder, David M. L. Cooper

Accepted for the Council:

Carolyn R. Hodges

Vice Provost and Dean of the Graduate School

(Original signatures are on file with official student records.)

EVALUATING DIFFERENTIAL NUCLEAR DNA YIELD RATES AMONG HUMAN BONE TISSUE TYPES: A SYNCHROTRON MICRO-CT APPROACH

A Dissertation Presented for the
Doctor of Philosophy
Degree
The University of Tennessee, Knoxville

Janna Michelle Andronowski
May 2016

DEDICATION

For Daniel C. Harvey (Harvey M. Harvey), my longest and truest friend. I could not have successfully completed this endeavor (or learned to play the tuba) without your love and support.

ACKNOWLEDGEMENTS

I could not have accomplished this goal without the contributions and support of many colleagues and friends. First and foremost, I would like to express my deepest thanks to my advisor Dr. Amy Z. Mundorff for her role in shaping this work. Her support and direction over the past (almost) four years has allowed me to excel in my studies.

I am indebted to my longtime mentor, committee member, and friend, Dr. Christian Crowder. I greatly appreciate all of the time he spent teaching me how to prepare bone thin-sections, and proficiency in histological analysis. Without his mentorship and friendship, I certainly would not be where I am today. I am grateful to have had the privilege of working with Dr. David Cooper on this project. His knowledge and expertise in synchrotron science and 3D bone imaging have been invaluable, and without his support and encouragement this work certainly would not have been possible. I also wish to thank Dr. Cooper for the remote use of his laboratory computing facilities for data processing. I would like to thank the remaining members of my committee: Drs. Dawnie Steadman, Benjamin Auerbach, and Yong Bradley for providing direction, insightful comments, and advice regarding this research. I especially want to offer my gratitude to Dr. Dawnie Steadman who granted me permission for the use of skeletal material from the William M. Bass Donated Skeletal Collection. I feel privileged to have worked with this valuable collection. Thanks to Dr. Bradley for providing access to the clinical CT scanner at the University of Tennessee Medical Center, and to Shelley Acuff for operating the CT system and assisting with bone set-up prior to scanning. I am also very grateful to Josh Price who provided helpful statistical advice regarding data analysis and interpretation.

I wish to thank Dr. Graciela Cabana for providing space in the Molecular Anthropology Laboratory for me to prepare my skeletal samples. Thank you also to Drs. Yasmin Carter, Alix Black, and Steve Thomopouloss who offered helpful advice regarding bone sectioning for SR micro-CT. And many thanks to Hannah Johnson who helped to prepare bone specimens for 3D imaging over her summer break.

Financial resources for this research have come from a number of sources. I would like to acknowledge the Canadian Light Source (CLS) in Saskatoon, Saskatchewan, Canada, and the Forensic Anthropology Center and Department of Anthropology at the University of Tennessee, Knoxville for funding a portion of this project through the Walter Leitner and Kneberg-Lewis Doctoral Completion Awards.

I extend my deepest appreciation to the Biomedical Imaging and Therapy beamline (BMIT) staff at the CLS. To Dr. George Belev, thank you for providing endless user support and beam line troubleshooting during my many experimental shifts. My experiments would not have been possible without your extensive knowledge and dedication to their success at the beam line. I also want to sincerely thank Drs. Tomasz Wysokinski, Adam Webb, and Ning Zhu for providing additional user support and advice regarding my experimental set-up. I am forever indebted to my fantastic beam team, Isaac Pratt, Danielle Kabatoff, Kim Harrison, and Dr. David Cooper. Without your assistance, companionship, and camaraderie during many long continuous days of beam time I would have surely gone mad. I am especially indebted to Isaac Pratt for teaching me the ropes at the CLS, running paperwork around for me, providing late-night software teaching sessions, and both intellectual and emotional support at the beam line during data collection. This research would not have been possible without your help and

dedication. Thank you to Tracey MacDonald, Mylene Tham, and Kelly Summers for the ice cream trips, board game playing, and overall friendship and company during long stints of beam time. I cannot wait to work and spend time with you all in the upcoming years in Saskatoon.

I wish to sincerely thank two other scholars, colleagues, and mentors who helped shape my interest in bone histology. To Dr. Lynne Bell, who first sparked my interest in bone histology and provided me with many invaluable learning opportunities during my undergraduate career. Thank you for starting it all. Your fire in the belly was contagious! And to my Master's advisor, Dr. Susan Pfeiffer, you have perfected the art of mentorship and your enthusiasm for research continues to be an inspiration to me.

I am immensely indebted to my family and friends who have supported me through my entire tenure in graduate school. I extend a special thank you to my beautiful Mom, Karen Andronowski, and Dad, Max Andronowski, for their unconditional love, support, and encouragement during my graduate career. There are no words to express how appreciative I am of their undying love and support. They have championed my academic career goals from the very beginning and have always supported me in my endeavors, no matter how far away from home they took me. They have made it a top priority to help me achieve my goals and I truly strive to make them proud. To my brother, John, thank you for not allowing me to take myself too seriously. I always greatly enjoy our visits in the Motherland and have fond (yet painful) memories from when you ventured to the Knoxville area. Thank you for always being there for me.

To my best friends in Western Canada who have been by my side throughout my undergraduate and graduate school years, Heather Broski, Ashley Turrie, and Nicole

Scott. Thank you for being so understanding and supportive of my career goals (and for the endless fun times, of course!). I know that no matter how far apart we are, we will always stay in touch and remain the best of friends. To Alexs Hermans, thank you for being my rock and platonic Knoxville life partner. Your home cooked meals allowed me to finish my dissertation without going hungry. You have truly made my life a little sweeter over this past year and I am greatly appreciative for that. I also want to thank Chris Agee for standing by me throughout the writing process. Thank you for listening to my endless ramblings about bone biology and forensic anthropology.

To my anthropology peers and friends who have commiserated with me both near and far, especially Ashley Kendall, Michelle Cameron, Dr. Catherine Merritt, Hilary Duke, Guy Duke, Dr. Sarah M. Rowe, Jonathon Eaton, Sean Tallman, Dr. Audrey Scott, Dr. Giovanna Vidoli, Dr. Cate Bird, Christina Fojas, and Katie Corcoran. You have all given me a wealth of personal and academic advice and enriched my life.

ABSTRACT

Molecular human identification has conventionally focused on DNA sampling from dense, weight-bearing cortical bone tissue from femora or tibiae. A comparison of skeletal elements from three contemporary individuals demonstrated that elements with high quantities of cancellous bone yielded nuclear DNA at the highest rates, suggesting that preferentially sampling cortical bone is suboptimal (Mundorff & Davoren, 2014). Despite these findings, the reason for the differential DNA yields between cortical and cancellous bone tissues remains unknown.

The primary goal of this research is to ascertain whether differences in bone microstructure can be used to explain differential nuclear DNA yield among bone tissue types, with a focus on osteocytes and the 3D quantification of their associated lacunae. Osteocytes and other bone cells are recognized to house DNA in bone tissue, thus examining the density of their lacunae may explain why nuclear DNA yield rates differ among bone tissue types. Methods included: (1) quantifying cortical and cancellous bone volume from each bone-sampling site using Computed Tomography (CT), and (2) visualizing and quantifying osteocyte lacunae using synchrotron radiation micro-Computed Tomographic imaging (SR micro-CT). Regions of interest (ROIs) from cortical and cancellous bone tissues (n=129) were comparatively analyzed from the three skeletons sampled for Mundorff and Davoren's (2014) study. Analyses tested the primary hypothesis that the abundance and density of bone's cellular spaces vary between cortical and cancellous bone tissue types.

Results demonstrated that osteocyte lacunar abundance and density vary between cortical and cancellous bone tissue types, with cortical bone ROIs containing a higher lacunar abundance

and density. The osteocyte lacunar density values are independent of nuclear DNA yield, suggesting an alternative explanation for the higher nuclear DNA yields from predominantly cancellous bones. It is hypothesized that soft tissue remnants within the medullary cavities of primarily cancellous skeletal elements are driving the high nuclear DNA yields.

These findings have significant implications for bone-sample selection for nuclear DNA analysis in a forensic context. The procurement of small, primarily cancellous bones with associated soft tissues should be preferentially sampled, and no longer dismissed as potential DNA sources in favor of cortical bone tissue.

TABLE OF CONTENTS

LIST OF TABLES

LIST OF FIGURES

LIST OF ABBREVIATIONS

° = degrees
2D = two-dimensional
3D = three-dimensional
ANOVA = Analysis of Variance
APS = Advanced Photon Source
ASBMR = American Society of Bone and Mineral Research
ARF= Anthropology Research Facility
BPs = bisphosphonates
BMU = Basic Multicellular Unit
BMIT = BioMedical Imaging and Therapy
BM = bending magnet
CLS = Canadian Light Source
CT = Computed Tomography
DEI = Diffraction Enhanced Imaging
DNA = Deoxyribonucleic Acid
DVI = Disaster Victim Identification
EV = eigenvalue
FAC = Forensic Anthropology Center
FEM = Finite Element Analysis
HR-pQCT = High Resolution Peripheral Quantitative Computed Tomography
GPU = Graphics Processing Unit
Gy - Grays
ICMP = International Commission on Missing Persons
ID = Insertion Device
ISFG = International Society for Forensic Genetics
KES= K-edge Subtraction Computed Tomography
keV = kiloelectronvolt
MESm = minimum effective strain set-points
MESr = minimum effective strain for remodeling
MFIs = Mass Fatality Incidents
MMA= Methylmethacrylate
mm = millimeter
mtDNA = mitochondrial DNA
NAME = National Association of Medical Examiners
NIJ = National Institute of Justice
OPD = osteon population density
PCI = Phase Contrast Imaging
PCR = Polymerase Chain Reaction
PMI= Post Mortem Interval
pQCT = Peripheral Quantitative Computed Tomography
RFLP = Restricted Fragment Length Polymorphisms
ROI = Region Of Interest

SEM = standard error
SK = Saskatchewan
SMI= Structural Model Index
SR = synchrotron radiation
STR = Short Tandem Repeat
UV = ultraviolet
vs = versus
μCT = micro-computed tomography
μm = micrometer

CHAPTER ONE: INTRODUCTION

Molecular human identification has long focused on extracting nuclear DNA from sampling sites containing dense cortical bone, such as areas in the femur or tibia. A recent comparison of modern skeletal elements from three individuals demonstrated that elements with high quantities of cancellous bone yield nuclear DNA at the highest rates, suggesting that preferentially sampling cortical bone is suboptimal (Mundorff & Davoren, 2014). This finding has significant implications in the context of human identification since cancellous bone is typically dismissed as a potential DNA source in favor of cortical bone. As DNA is increasingly relied upon for human identification, the development of- and an understanding behind-improved sample-selection are paramount. Following a mass disaster or grave excavation, human remains may be fragmentary, commingled, degraded, or otherwise compromised, limiting the choice of elements that can be DNA sampled. If small elements such as phalanges, tarsals, and patellae are recoverable, their intact removal has the potential to simplify collection and processing as higher levels of DNA often allow for successful extraction. While recent research by Mundorff and Davoren (2014) indicated that bones with high cancellous quantity yield DNA at higher rates, the reason remains unknown. Evidence from bone microarchitecture may help explain this variation and enrich our understanding of the density and morphology of bone microstructural features.

Biological anthropologists have evaluated human cortical bone tissue to gain insight into the lives of past and current populations. Bone's unique properties make it an ideal tissue for histological investigations since it maintains a dynamic structure throughout an individual's lifespan, providing a temporal record of remodeling events. This continuous response allows for

the maintenance of bone's microstructural organization when exposed to various physiological, mechanical, and metabolic demands. Because of this remodeling process, microscopic features accumulate in bone tissue that are believed to aid in understanding circumstances encountered during life. Histological studies have focused on the influences of physical activity, metabolism, nutrition, and age-related change (Agarwal, 2008; Ruff, 2008; Kerley, 1965). Such analyses have been applied in forensic, archaeological, and ancient contexts and thus have great potential for new research endeavors in anthropology and forensic identification. Despite the various applications of bone histological methods in anthropology, they are infrequently employed. The lack of applied histology in anthropology has been attributed to recognized methodological and theoretical issues, and a lack of instructional texts, both of which have hindered its advancement (Crowder et al., 2012). As such, improvements to bone histological methods are necessary in order to increase its utility in anthropological investigations.

Applications of three-dimensional (3D) imaging modalities to cortical bone microstructure have provided researchers with a more comprehensive understanding of bone histology than was possible using two-dimensional (2D) techniques (Cooper et al., 2003; 2006). Micro-Computed Tomography (micro-CT) technology has allowed for the quantitative analysis of minute microscopic features, including osteocyte lacunae, in 3D. As soft tissue structures, osteocytes cannot be visualized using currently available x-ray imaging techniques (Carter et al., 2013a). As such, their associated cellular spaces (lacunae) are used as substitutes. Osteocytes and their lacunae have been studied in both human and non-human animals. However, quantifying osteocyte population density has been problematic due to limitations of traditional lower-resolution imaging techniques (Qiu et al., 2003b; Carter et al., 2013a).

Recent approaches for visualizing cortical and cancellous bone tissue including synchrotron radiation micro-Computed Tomographic imaging (SR micro-CT) offer an avenue for studying bone microarchitecture, bone quality, and microstructural features. SR micro-CT is a proven method for visualizing osteocyte lacunar density, morphology and orientation in cortical bone from human femora (Carter et al., 2013a; 2013b; 2014a). Carter and colleagues (2013a) revealed a higher number of osteocyte lacunae present in human femoral bone than had been recorded previously using 2D methods. Osteocyte lacunar densities in many other skeletal elements, and bones with high cancellous content, have yet to be examined using high-resolution 3D imaging.

The preservation and quantification of osteocytes have been further examined in a forensic identification context. For example, Soler and colleagues (2011) compared the number of osteocytes present in compact femoral bone to nuclear DNA yield. Osteocytes and other bone cells are recognized to house DNA in bone tissue (Campos et al., 2012), thus, examining the density of their lacunae may explain why DNA yield rates differ among bone tissue types. The current study will further investigate the potential correlation of osteocyte density and recoverable nuclear DNA using SR micro-CT. It will be the first study to focus extensively on inter-element variation in osteocyte lacunar parameters using SR micro-CT in human bone tissue.

Research Purpose and Questions

The purpose of this study is to ascertain whether differences in bone microstructure can be used to explain differential nuclear DNA yield among bone tissue types, with a focus on osteocytes and the 3D quantification of their associated lacunae.

Three central research questions are posed in this dissertation: 1) How does osteocyte lacunar density and the amount of bone matrix surrounding osteocytes compare between cortical and cancellous bone tissue types? 2) Can osteocyte lacunar density in cortical and cancellous bone be used to explain differential nuclear DNA yield? 3) Do the relative volumes of cortical and cancellous bone procured by Mundorff and Davoren (2014) vary between each sampling sites to achieve the desired testing weight for nuclear DNA analysis?

The following hypotheses and background chapters will focus on the proposed research questions, with the background sections providing justification for the hypotheses.

Hypotheses

The following section introduces four hypotheses that were tested to determine whether the 3D histomorphometric examination of modern human bone microstructure can be used to explain differential nuclear DNA yield among bone tissue types previously tested for DNA. The first set of hypotheses were concerned with differences in osteocyte lacunar abundance and density in cortical and cancellous bone tissues. Hypotheses three and four pertained to the relationship between the clinical CT and SR micro-CT histomorphometric variables and nuclear DNA yield.

1. There will be differences in osteocyte lacunar density between cortical and cancellous bone.
2. Cancellous bone will have greater osteocyte lacunar densities.
3. The osteocyte lacunar density in cortical and cancellous bone is correlated with differential DNA yield.
4. The relative volumes of cortical and cancellous bone procured by Mundorff and Davoren (2014) will vary between sampling sites to achieve the desired testing weight for nuclear DNA analysis.

Organization of the Dissertation

The current research details a study conducted over the past three years (2012-2015) at The Canadian Light Source, Saskatchewan (SK), Canada, and University of Tennessee, Knoxville. Chapter two documents broad issues associated with DNA bone sampling protocols in the forensic identification literature, and reviews previous studies examining DNA yield rate by skeletal element. Chapter three provides a comprehensive overview of basic bone biological principles including normal human bone gross composition, histomorphology and basic mechanisms of bone turnover. Chapter four introduces 3D imaging modalities as alternatives to traditional 2D methods, provides a brief history of 3D imaging techniques, and describes various imaging modalities used in both clinical and anthropological research. Chapter five details the study's skeletal sample and the unique bone preparation methodology necessary for this type of analysis. This chapter also presents an overview of data collection using 3D imaging modalities and the process for their subsequent analyses. Chapter six presents the results. Chapter seven is a discussion of the results and how they apply to human DNA identification, including the perspectives gained from the study and the potential for future research as they relate to anthropology and bone biology. Chapter eight is a brief conclusion, which summarizes the conclusions drawn from the current work in response to the three research questions posed in Chapter 1.

CHAPTER TWO: DNA ANALYSIS AND HUMAN IDENTIFICATION

Despite growing reliance on nuclear DNA extraction as a preferred method for human identification of skeletonized remains, few studies exist that examine differential DNA yield by bone tissue or skeletal element type to inform sampling guidelines. This chapter discusses broad issues associated with current DNA bone sampling protocols in the forensic identification literature, and reviews previous studies examining DNA yield rate by bone tissue type or skeletal element. To contextualize the proposed problem of extracting usable DNA from skeletal remains, the following topics will be discussed: (1) general difficulties associated with obtaining DNA profiles from degraded skeletal remains, (2) the influence of the postmortem environment on bone preservation, and (3) the ability to extract usable DNA for human identification.

Obtaining Genetic Profiles from DNA for Human Identification

DNA extraction from human tissues has been extensively relied upon to identify deceased individuals, mass fatality victims, and victims of mass atrocity often characterized by skeletonized or otherwise compromised remains. As such, its utility is invaluable to the medicolegal community.

DNA profiling is the dominant forensic identification modality used to positively identify fragmentary, damaged, or commingled human remains (Mundorff et al., 2009). Nuclear DNA is the preferred type for forensic identification because the genetic information is derived from both parents. It is individually specific and powerfully discriminating (Marjanovic et al., 2007), Many biological tissues have been used for testing, often successfully, despite decomposition and other environmental conditions. Moreover, antemortem reference samples are often available for comparative purposes (Weedn & Baum, 2011).

Mitochondrial DNA (mtDNA) is not as discriminatory as nuclear DNA and therefore is rarely employed in forensic identification efforts (Misner et al., 2009), though it may be used for exclusionary purposes if a matrilineal reference sample is available. mtDNA has different properties than nuclear DNA. It resides in the mitochondria of cells instead of the nucleus, and is only maternally inherited. mtDNA has a 'high copy number', which refers to the presence of thousands of copies of mtDNA for every copy of nuclear DNA, thus increasing the likelihood of retrieving sufficient amounts from compromised samples (Weedn & Baum, 2011). mtDNA remains viable in cells for longer time periods than nuclear DNA, and has proven valuable for typing ancient or degraded samples (Shook & Smith, 2008). As this study focuses on the quantity of nuclear DNA as it relates to bone microarchitecture, mtDNA will not be further considered here.

Overall, obtaining genetic profiles from forensic samples can prove difficult if the sample is highly degraded. Degradation diminishes the amount of viable nuclear DNA available for extraction, resulting in amounts that fall below the amplification kit's specified concentrations (Marjanovic et al., 2007; Just et al., 2009). Thus, a number of techniques have been devised to improve profiling success from extracted DNA, and a general overview is presented below.

Methods Employed in DNA Analysis

Though many methods for DNA sequencing exist, not all are acceptable or possible if DNA is degraded. A traditional DNA sequencing method, Restricted Fragment Length Polymorphisms (RFLPs), requires high DNA quantities (Parsons & Weedn, 1997). RFLPs involve using restriction enzymes to segment portions of DNA, which are then sized using gels. If DNA is degraded, the enzymes will fail at determining where to make cuts and the fragment lengths will be inaccurate and thus inappropriate for use with fragmented DNA.

Short Tandem Repeat (STR) analysis has the advantage of requiring less DNA overall, and is one of many methods that make use of Polymerase Chain Reaction (PCR) to amplify the sample for sequencing. PCR is a sensitive, repetitive, cyclical process that allows for DNA amplification. This form of analysis involves commercial test kits for specific STR genetic loci. STR typically performs well despite suspected DNA degradation.

If STR is unsuccessful, Mini-STRs can be applied to amplify smaller DNA fragments. Single Nucleotide Polymorphisms (SNPs) can be utilized for very degraded samples since it can identify small changes, such as a single base pair alteration, but it is not robust enough to establish a forensic identification. Overall, STR is the preferred testing method, followed by Mini-STRs, mtDNA, and SNPs (Weedn & Baum, 2011). However, success of postmortem DNA extraction largely depends on the specific remains recovered and their condition.

DNA Degradation

DNA begins to degrade directly following an organism's death. Cellular autolysis and bacterial digestion are the primary agents in DNA degradation, and with progressive putrefaction, DNA integrity rapidly breaks down (Schwark et al., 2011; Weedn & Baum, 2011). Though the relationship between DNA degradation and environmental exposure is not fully understood, taphonomic factors that promote human decomposition are recognized as influencing bone preservation and DNA degradation. Numerous studies implicate common environmental agents including ground water, fungi, pH balance, exposure to ultraviolet (UV) light exposure, temperature, humidity, bacteria, and cyanobacteria (Jans et al., 2004; Turner-Walker & Jans, 2008; Turner-Walker, 2008; Golubic et al., 2005; Bell, 1990; Graw et al., 2000; Jackes et al., 2001; Bell & Elkerton, 2008).

The ability to extract usable DNA from human tissues is generally presented in terms of

success or failure. Failure is often attributed to degraded samples. Genetic material may deteriorate more slowly in hard tissue, such as bones and teeth, than in soft tissues, such as skin and organs, because the composition of hard tissue structures can act as a physical barrier to external influences (Campos et al., 2012; Graw et al., 2000; Ye et al., 2004). The resilient structure of skeletal tissue can be attributed in part to bone density and microarchitectural composition. In cortical bone, osteocytes embedded between concentric layers of lamellae within the periphery of osteons (~250 μm in diameter), and in interstitial bone, are further away from the larger surface area of the trabecular network and thus may be isolated and/or protected from environmental insults (Qiu et al., 2002; D.M.L. Cooper, personal communication). In cancellous bone, however, osteocytes are likely closer to the larger surface area of the trabecular network (i.e. trabecular thickness of 100-150 μm). As such, the open-nature of cancellous bone may result in an easier introduction of microorganisms, and other chemical destructive entities of DNA.

DNA degradation in hard tissue has been linked to collagen and crystallinity loss of the hydroxyapatite, which both play a crucial role in DNA preservation (Gotherstrom et al., 2002). Taphonomic factors, specifically diagenesis, can affect the integrity and appearance of bone microstructure and affect the reliability of DNA extraction, histological age estimation methods, and biomechanical analyses. Understanding DNA preservation and degradation in hard tissue necessitates understanding diagenetic alterations to bone microstructural integrity.

The Influence of the Postmortem Environment on Bone Preservation

Following decomposition, bone and teeth are often the only remaining tissues of an organism. These hard tissues can provide excellent sources of DNA for human identification. A phenomenon called diagenesis, however, can alter the chemical and physical environment within

bone that surrounds DNA. The following section will define diagenesis as it applies to bone, and consider various diagenetic agents that may hinder successful DNA extraction.

Defining Diagenesis

Diagenesis is a term borrowed from geology referring to physical, biochemical and physico-chemical processes that occur during the formation of a sedimentary deposit (Bell, 1990; 1995; Turner-Walker & Jans, 2008; Hedges, 2002; Hedges & Millard, 1995). Diagenesis adapted to skeletal material describes a complex of alterations to bone tissue in the burial environment (Hedges & Millard, 1995; Hedges, 2002). These processes include, but are not limited to, desiccation, bleaching, mineral replacement, compaction, and decomposition of organic compounds (Bell, 1995).

Autolysis and hydrolysis are chemical processes associated with soft tissue decomposition and also includes degrading bone collagen (Jans, 2008). These reactions, or diagenetic alterations, are extremely variable from one environment to another. Diagenetic agents such as ground water, fungi, pH balance, bacteria, and cyanobacteria that can potentially alter bone microstructure will be reviewed below (Jans et al., 2004; Turner-Walker & Jans, 2008; Turner-Walker, 2008; Bell, 1990; Jackes et al., 2001; Bell & Elkerton, 2008).

The Presence of Water

Water's presence and movement within a burial may influence the microstructural preservation of bone (Turner-Walker, 2008; Bell & Elkerton, 2008). Water flow can penetrate submerged bone through the network of vascular canals. Repeating cycles of wetting and drying leach calcium and phosphate from bones and they become porous and weak. Water is also the medium for almost all chemical reactions that occur within the soil (Turner-Walker, 2008). In the

body, bone is in a relatively closed system surrounded by fluid with a strictly controlled pH (Ortner & Turner-Walker, 2003; Turner-Walker, 2008). In contrast, the soil is an open, unregulated system and bone is vulnerable to its degradative influences. The presence of water also supports microbial activity and metabolism.

Damp or wet conditions can be detrimental to DNA survivability in skeletal remains (Graw et al., 2000; Iwamura et al., 2005; Schwark et al., 2011; Ye et al., 2004). For example, Graw and colleagues (2000) found that bones and teeth exposed to damp conditions are subject to rapid DNA degradation. Iwamura and colleagues (2005) reported on DNA degradation of skeletal material after submersion in fresh water. Schwark and colleagues (2011) evaluated DNA extracted from soft tissues such as the aorta, kidney, muscle, and liver from individuals of various decompositional stages. The authors found that DNA yield was poor from individuals in advanced stages of decomposition that were wet and/or damp from decompositional fluids.

Bone Degradation in Soil

Two mechanisms of degradation affect skeletal material recovered from within a soil context: (1) chemical hydrolysis, and (2) microbial degradation (Turner-Walker, 2008; Turner-Walker & Jans, 2008). These processes can occur concurrently. Various agents of decay work in concert with these diagenetic trajectories within a soil burial environment. Decomposition is generally governed by external microflora commonly present in ground soil (Bell et al., 1996). During decomposition, microbes found within a cadaver and the surrounding soils invade bone and degrade organic molecules, and presumably DNA (Mundorff & DeBruyn, 2015). For example, a recent study by Lauber and colleagues (2014) described the effects of various soil microbial communities on vertebrate decomposition using a mouse model. The authors noted a

much quicker rate of decomposition for subjects placed on soil with intact microbial communities compared to those placed on sterile soil.

Taphonomic factors such as temperature, pH balance and the availability of groundwater, influences the types of soil microorganisms present, which then affects the amount of tissue decay that occurs (Turner-Walker, 2008; Henderson, 1987). Higgins and colleagues (2015) found that soil temperatures within burials had a substantial impact on DNA preservation in different tissues of the tooth (Higgins et al., 2015). Their results further demonstrated variable postmortem preservation of both nuclear and mtDNA in single teeth, with varying degradation rates for each tissue type. Pulp tissue was found to decay quickly, while cementum maintained its structural integrity over an extended period of time (Higgins et al., 2015).

Further, the pH of groundwater has been shown to affect the degree of microstructural degradation of bone (Tibbet & Carter, 2008; Jans et al., 2004). If grave soil has a neutral alkaline pH balance, the destruction of bone microstructure is not as severe. Bones recovered from alkaline soils tend to be white, or cream in color since metal ions present in the groundwater are insoluble at a neutral pH (Turner-Walker, 2008). If the soil condition is acidic, the inorganic components of bone tissue will deteriorate. Bones recovered from these environments tend to be brown in color due to the presence of soluble transition-metal ions (Turner-Walker, 2008), and microstructural features such as osteons are often soil stained.

Microbial Diagenesis of Bone

Microbes can speed the rate of decomposition and alter both the surface and interior structures of bone. Bacteria infiltrate the vascular networks, and seem to follow the course of collagen fibers, creating tunnel structures (Bell et al., 1996; Jans, 2008; Turner-Walker, 2008).

Two broad classes of bacteria have been identified: (1) aerobic, and (2) cyanobacteria (Bell, 1990).

Fungi have also been implicated in the postmortem alteration of bone tissues (Piepenbrink, 1986; Turner-Walker, 2008; Jans, 2008). Piepenbrink (1986) successfully isolated and identified various species of fungi from samples of excavated archeological human material. Fungi penetrate the cortex of bone and infiltrate the bone matrix with branching tunnel structures (Jans, 2008). These are referred to as Wedl's tunnels.

A distinct form of micro-boring has been identified by Bell and Elkerton (2008). Boring microbes are associated with microstructural degradation of bone recovered from aquatic environments and include: fungi, bacteria and cyanobacteria (Raghukumar et al., 2001). Aquatic microbes are known degraders of various calcareous marine substrates (Raghukumar et al., 2001), and tunnel inside skeletal remains for use as dwellings (Turner-Walker, 2008; Bell et al., 1996).

Networks of microscopic tunnels have been observed that occur peripherally in distribution on prepared thin sections, referred to as endolithic tunnels (Bell & Elkerton, 2008). No boundary of remineralization is evident in this type of structural modification. The microorganism's activities vary depending on temperature, depth, and light exposure (Bell & Elkerton, 2008). Microbial endoliths can occupy a variety of niches, including human bone, and the tunnels created vary depending on whether the organisms are phototrophic or heterotrophic (Golubic et al., 2005). Heterotrophic organisms, such as species of fungi, tend to invade bone in the marine environment. The organic components of bone provide a nutrient rich food source for these fungi. Heterotrophic organisms show variable boring patterns, but the tunnels created are fairly consistent in diameter (Golubic et al., 2005).

Particular extrinsic factors including temperature affect microbial activity, and in turn, DNA and bone microstructural and DNA preservation (Burger et al., 1999; Lee et al., 2010; Iwamura et al., 2005). Burger and colleagues (1999) investigated the effect of various environmental factors on the preservation of nuclear DNA. Through simulation of various environmental conditions, the authors documented that high humidity and heat resulted in the most severe decreases in DNA quantity and quality. Further, Lee and colleagues (2010) analyzed human skeletal remains for nuclear DNA following exposure to various maceration techniques. Overall, the authors found that maceration for longer periods of time in hot water resulted in the poorest DNA amplification rates. A study conducted by Iwamura and colleagues (2005) investigated the presence of osteocytes using two-dimensional (2D) histologic sections following bone maceration. They reported that DNA extracted from previously boiled femoral bone samples was either unattainable or severely degraded. The authors further discovered that boiling bones appeared to remove and/or destroy osteocytes, which are recognized to contain DNA (Hedges, 2002; Soler et al., 2011).

Conversely, a recent study by Frank and colleagues (2015) investigated the effects of three common processing techniques commonly employed prior to skeletal analyses: (1) maceration in hot water, (2) Computed Tomography (CT) scanning, and (3) X-ray imaging. The authors aimed to determine if these commonly used practices impacted nuclear DNA yield success rates. Data revealed that DNA yields from bone were highly variable following hot water maceration, but that none of the three processes in isolation caused a statistically significant reduction in profile completeness. However, the combined effects of hot water maceration, CT scanning, and X-ray imaging revealed statistically significant decreases in DNA success rates (Frank et al., 2015), suggesting an additive effect from these processing techniques.

In sum, the above works demonstrate the influence of microbial activity on hard tissues and the potential effects high-heat and humidity have on microbes. In general, these variables are shown to assault DNA by increasing microbial activity, which may influence the destruction of bone microstructure including DNA-housing bone cells (Hedges, 2002).

Modeling Bone Diagenesis

The diagenesis literature typically documents qualitative features in which degenerative change has been identified (Bell, 1990; Hackett, 1981; Jans, 2008). Hedges and colleagues have accomplished a considerable amount of qualitative work in the realm of bone diagenesis (Hedges, 2002; Hedges & Millard, 1995a; 1995b). The authors have enhanced our understanding of diagenetic processes and provide a histological index for the possible quantification of diagenetic features. Hedges and Millard (1995) also discuss how concepts developed from soil studies can be applied to the examination of buried bone and our understanding of diagenesis. They identified modes of interaction between soil and bone based on local hydrology. Considering certain variables such as increased crystallinity in bone, porosity, and uptake of uranium, the authors model bone diagenesis. The authors further demonstrated that soil structure and moisture, the resulting physical state of bone, and bone chemistry can provide evidence for the manner of the diagenetic process experienced.

Due to the wide range of factors influencing the chemical and physical changes to bone, however, a valid mathematical method does not exist for quantifying bone diagenesis. As these alterations ultimately affect skeletal preservation, the integrity of bone microstructure must be considered prior to histological analyses. All areas of bone cortex are not always affected by diagenesis, and so areas displaying less microscopic damage may still be suitable for histological assessment.

DNA Survivability

Significant technological advances in molecular analyses of skeletal remains have emerged in recent years. Nevertheless, DNA survivability remains affected by taphonomic factors that encourage bone and DNA degradation, creating challenges for DNA analysis. Early studies have ranked these factors according to their adverse effects on DNA preservation (Hochmeister et al., 1991; Parsons & Weedn, 1997; Burger et al., 1999; Graw et al., 2000; Crainic et al., 2002; Imaizumi et al., 2004; Ye et al., 2004; Cockle et al., 2005; Iwamura et al., 2005), providing a foundation for more recent works (Putkonen et al., 2010; Schwark et al., 2011; Mameli et al., 2014).

Environmental Effects on DNA Yield

Case studies and actualistic research have been used to demonstrate that high heat and humidity, damp and wet conditions, or submersion in water, are detrimental to DNA survivability in bone. For example, Hochmeister and colleagues (1991) documented the difficulties associated with DNA extraction and amplification from human remains submerged in a river. The researchers could not recover amplifiable DNA from decedents immersed in water for multiple months prior to recovery. Graw and colleagues (2000) also found that human remains exposed to damp conditions were subject to rapid DNA degradation. In each skeletal case recovered from a damp environment, DNA typing from hard tissues was impossible. Burger and colleagues (1999) further investigated the effect of various environmental factors on the preservation of nuclear DNA extracted from archaeological tooth samples. Various environmental conditions were simulated experimentally, and included temperature, humidity, pH value, and presence of bacteria. Overall, the authors documented that high humidity and heat resulted in decreased DNA quantity and greatly reduced DNA quality.

A case study by Crainic and colleagues (2002) addressed the challenges of extracting and amplifying DNA from human tissue retrieved from a dam. The authors sampled decomposing muscle tissue and a clavicular fragment for nuclear and mtDNA analyses. The clavicle was chosen since significant portions of the recovered remains were missing (Crainic et al., 2002). The degraded soft tissues failed to produce a successful DNA profile, though the bone sample proved to be suitable following positive PCR amplifications. Further, Imaizumi and colleagues (2004) examined PCR assays that were applied to different human tissues (i.e. bone, nails, hair) exposed to various environmental contexts. Results indicated that strong PCR inhibition was observed in the DNA extracted from bones buried in soil, with the most rapid decrease in DNA yield seen in tissues immersed in water. The authors found that exposure to various environmental stimuli greatly affect the quantity and quality of recoverable DNA.

More recent studies further indicate that varying taphonomic factors result in differing levels of DNA degradation. Schwark and colleagues (2011) evaluated procedures for the extraction and amplification of DNA from soft tissues such as the aorta, kidney, skeletal muscle, and liver from individuals of various decompositional stages. DNA quality and quantity results indicated high variability in DNA preservation from individual to individual. DNA yield was poorer from individuals in advanced stages of decomposition. Mummified individuals, or those who displayed adipocere formation, yielded better DNA results than those who were wet and/or damp from decompositional fluids or processes.

To improve DNA extraction modalities from skeletal remains recovered from aquatic environments, Mameli and colleagues (2014) developed a method specifically for DNA profiling human remains submerged in seawater. The study was inspired by a case in which a decedent was retrieved from seawater after approximately eight months. The authors retrieved sections of

a well-preserved mandibular body, and employed three DNA extraction protocols. Two techniques were created specifically for bones retrieved from freshwater environments (Mameli et al., 2014). Extracted DNA was quantified using PCR and STR profiles generated. No measurable amounts of DNA were usable from the first and second freshwater protocols. The third method was successful in recovering low copy number DNA from the mandible, although it was highly degraded. This technique used additional bone powder and included an additional concentration step (Mameli et al., 2014). This case highlights advancements in DNA profiling techniques that have increased the likelihood of extracting adequate DNA from poorly preserved samples.

Overall, the quantity and quality of nuclear DNA that can be extracted and amplified highly depends on the deposition environment. The above review demonstrated that bones exposed to high-heat and wet environments show a reduction in the quantity and quality of extractable DNA. Conversely, certain conditions demonstrate the ability to limit or slow bacterial growth and thus inhibit the degradation of DNA. As such, bones recovered from temperate, relatively cold, or dry environments exhibit better preserved collagen and nuclear DNA for extraction (Sosa et al., 2013; Iwamura et al., 2005; Leney, 2006). For example, Leney (2006) documented that skeletal elements recovered from temperate environments promoted DNA preservation. He further demonstrates that remains recovered from a temperate environment, even from a prolonged postmortem interval, yielded better results than those recovered from a wet environment with a short postmortem interval.

Storage and Preservation Following Mass Disasters

Few mass fatality incidents (MFIs) occur in environments that encourage DNA preservation, and scene processing is often impossible before the onset of decomposition.

Therefore, the storage and preservation of human biological material can further challenge the identification process. As such, various researchers have developed procedures for short- and long-term human tissue storage to preserve the quality of DNA and delay the effects of degradation (Caputo et al., 2011; Michaud & Foran, 2011; Graham et al., 2008; Holland et al., 2003; Li, 2006). These efforts are essential, especially in disaster situations where subsequent DNA analysis for victim identification is critical.

Typically, DNA samples for human identification are often stored at -20 C to halt the DNA degradation process. However, when the tissue thaws, endogenous enzymes are released that may threaten to degrade DNA (Caputo et al., 2011). In temporary mortuary sites following a mass disaster, even immediate sample refrigeration is often not possible.

Caputo and colleagues (2011) proposed the use of table salt (NaCl) for rapid dehydration of tissue samples to allow for reliable DNA extraction. Graham and colleagues (2008) investigated the use of various buffer solutions for the preservation of soft tissue samples to aid in conservation of nuclear DNA in the context of disaster victim identification. Using this method, samples can be stored at room temperature for up to six months. Based on their work on the World Trade Center remains, Holland and colleagues (2003) developed a high quality DNA extraction procedure for bone and two new STR multiplexes, thus enhancing the ability to obtain DNA results from very challenging samples.

Michaud and Foran (2011) compared different techniques for field-preservation of tissues for later DNA analysis. Swine skin and muscle tissues were preserved using cold storage, desiccation, or room temperature storage in preservation fluid for a maximum of six months. DNA was extracted shortly after and amplified via PCR. Results indicated that simple

preservation in solutions such as rubbing alcohol and ethanol result in substantially better DNA quality than delaying preservation.

Allouche and colleagues (2008) investigated nail clippings as an alternative nuclear DNA source from decomposed cadavers. Though nails are not often used as a DNA source, the authors determined the amount of nail clippings required to establish nuclear DNA profiles (5-50 milligrams), and evaluated the quality of nail-derived DNA. Overall, they found that nails demonstrate a satisfactory resistance to decay and are straightforward to sample.

Li (2006) developed a straightforward sample processing method for nuclear DNA isolation to address difficulties in cleaning and extracting DNA from bone, especially in cases where only small amounts of DNA are present. This method involved the use of trypsin, a digestive enzyme, to degrade various types of proteins found on the bone's surface. Li (2006) further examined the effects trypsin had on subsequent DNA yields and on the quality of the DNA obtained. Light microscopy and SEM revealed that trypsin did not have any adverse effects on the bone, and the DNA extracted following treatment was sufficient for amplification and analysis.

Conclusions

Overall, there appears to be consensus in the literature regarding the application of inexpensive and easily employable preservation methods for delaying decomposition and subsequent DNA degradation in human tissues recovered in MFIs. It should be noted, however, that there are no consistent rules indicating whether a particular approach will be successful since every case or context is unique.

Current DNA Sampling Protocols for Human Identification

Hard tissues, such as bones and teeth, are often the only remaining suitable material available for DNA extraction. Sampling and cleaning strategies for bone and teeth are typically specialized and time consuming particularly when the material has been exposed to harsh environmental conditions (Li, 2006; Davoren et al., 2007; Milos et al., 2007). Contamination issues must be considered as it interferes with DNA analysis. Generally speaking, contamination can result from the introduction of extraneous DNA from physical contact, or occur via cross-contamination between samples.

The improvement of DNA extraction and amplification techniques has altered the human identification standards and protocols, particularly following MFIs characterized by small and degraded samples. DNA sampling techniques used in recent MFIs are highly variable, however, and are often tailored to each unique circumstance (Mundorff et al., 2009). Until recently, there were few detailed guidelines outlining bone-sampling protocols for DNA analysis following MFIs. For example, in the 2004 Thailand tsunami disaster, ribs and teeth were initially sampled for DNA (Cockle et al., 2005), and for victims of the 2005 Hurricane Katrina, anterior mid-shaft portions of tibiae were procured. To speak to these disparities in DNA sampling strategies, specialists in mass fatality management have begun collaborating to produce manuals containing general human identification guidelines. Agencies such as the International Commission on Missing Persons, the National Institute of Justice, the National Association of Medical Examiners, Interpol, and the International Society for Forensic Genetics have devised sampling recommendations for DNA specimen collection.

International Commission on Missing Persons (ICMP)

The International Commission on Missing Persons (ICMP) uses an effective DNA extraction protocol developed by Amory and colleagues (2012). This method involves demineralization and purification of bone samples and appears to limit environmental impacts (Hines et al., 2014). Based on results of an extensive analysis of DNA extractions from numerous skeletal elements (n=11,650) by Hines and colleagues (2014), the ICMP outline suggestions for effective sampling strategies for incomplete human remains.

The ICMP prioritizes sampling teeth for DNA analysis, followed by femora, tibiae, and os coxae (ICMP, 2015). Tarsals were found to yield consistently high DNA STR profiles in the study by Hines and colleagues (2014), however, it was determined that these elements are not ideal to sample from a commingled mass grave as they may be difficult to reassociate with other skeletal remains.

In addition to prioritizing elements for sampling based on DNA success rates, ICMP advises practitioners to consider the circumstances surrounding the skeletal recovery, and the durability and simplicity involved in removing the sample (Hines et al., 2014). Completeness and preservation of the specimen should also be considered. More detailed guidelines can be found in the publication (Hines et al., 2014).

National Institute of Justice (NIJ)

The *Mass Fatality Incidents: A Guide for Forensic Human Identification* (2005) was designed for medical examiners and coroners to aid in the creation of mass disaster plans. Overall, this guide provides a comprehensive section on DNA sampling. NIJ provides twelve general tissue extraction guidelines. The preferred samples from human remains listed in order of preference include: (1) blood, (2) soft tissues such as skeletal muscle, organ tissue, and skin, and

(3) hard tissues such as cortical bone tissue and teeth. In terms of sampling bone for DNA, NIJ encourages a preference for sampling dense cortical bone from weight-bearing lower limb bones yet neglect to include citations that lead to this determination.

The National Association of Medical Examiners (NAME)

The National Association of Medical Examiners (NAME) mass fatality plan is generally directed towards coroner and medical examiner offices to aid in developing disaster response plans. It is comprehensive and contains additional pages of forms for the recording of postmortem data. The NAME mass fatality plan addresses DNA sampling procedures in the section titled *DNA Specimen Collection Guidelines.* These recommendations specify that hard tissues such as long bones (either intact or 6 inches of the diaphysis), rib cuttings, or teeth with intact roots be retrieved when sampling decomposed human remains (National Association of Medical Examiners, 2010).

Interpol

The Interpol Disaster Victim Identification (DVI) manual is arguably the most comprehensive guide available for professionals involved in mass fatality management. It is updated regularly in response to the experiences of Interpol DVI personnel during disaster situations. Additionally, the information provided is compatible with international DVI procedures, and as such is available in over one hundred countries and in multiple languages (Interpol, 2014). In terms of DNA sampling, the report suggests preferentially sampling 4-6 cm from long bones with dense cortical bone tissue, healthy teeth, or other available cortical bone. It further indicates that samples retrieved from cancellous bone may be difficult to preserve (Interpol, 2014).

International Society for Forensic Genetics (ISFG)

Prinz and colleagues (2007) reported guidelines for forensic geneticists involved in mass disasters set forth by the International Society for Forensic Genetics (ISFG). This group includes international members who are leaders in the field of human identification. The authors recommend an interdisciplinary approach to human identification that involves DNA identification and additional methods such as fingerprint and dental record analysis. Regarding DNA sampling, Prinz and colleagues (2007) recommend that numerous sample types should be collected for DNA testing (i.e. blood and buccal swab if not decomposed, muscle tissue, long primarily cortical bones, healthy teeth). All specimens should be retrieved at the earliest possible stage following recovery, and from each recognizable body part. These general guidelines are quite broad, however, and do not specify which particular skeletal elements are most likely to produce sufficient DNA profiles if skeletal remains are fragmentary or if limb bones are unavailable (Mundorff et al., 2012). Additionally, there is no mention of which bones might consistently produce full DNA profiles, especially following exposure to harsh environmental conditions.

Guidelines for Mass Fatality DNA Identification Operations

Sozer and colleagues (2010) prepared the Guidelines for Mass Fatality DNA Identification Operations to provide a review of the factors and protocols involved in DNA identification procedures in response to MFIs. The authors emphasize that their manual is based on experiences from previous disasters, and does not aim to set standards. The document is thorough and well organized. There are coherent sections that describe overall mass disaster program management, and technical considerations for DNA sample collection and testing. The authors also include appendices with references for suggested reading, and resources for using

Bayesian statistics in paternity testing. In their review of sample collection for DNA, Sozer and colleagues (2010) recommend sampling biological tissues with the best potential for DNA survival as well as the contracting laboratory's ability and expertise to work with certain sample types. Although various laboratories retrieve different minimum sample requirements, the authors recommend that skeletal muscle, nails, long bones, and healthy teeth be recovered if possible.

The following section will examine the existing state of knowledge regarding DNA sampling techniques by skeletal element. This review emphasizes the need for additional studies evaluating differential preservation of DNA by skeletal element under controlled conditions.

Studies Examining DNA Yield by Skeletal Element

Until recently (Hines et al., 2014; Mundorff & Davoren, 2014), DNA sampling protocols for human identification have been largely based on the collective wisdom of practitioners. Pooled experience suggested that weight-bearing lower limb bones, specifically femora and tibiae, yielded higher quantities of DNA than other skeletal elements and were therefore favored for sampling. In fact, the aforementioned government agencies including the International Commission on Missing Persons, National Institute of Justice, The National Association of Medical Examiners, and Interpol have proposed DNA sampling strategies encouraging the preferred extraction of dense cortical bone from the lower limb. As such, DNA testing using non-weight-bearing bones, or small bones with high cancellous content have been marginalized, resulting in a dearth of information on their actual potential. As DNA technology has become more refined, various researchers have aimed to demonstrate which skeletal elements and bone tissue types (cancellous and cortical bone) best preserve DNA. The following chronological review presents current evidence from the forensic identification literature.

Alonso and colleagues (2001) examined the influence of bacterial contaminants on nuclear DNA extracted from hard-tissue samples. The authors analyzed eight-to-fifty year-old skeletal material from the skull, ribs, and teeth. Results indicated that the quality and quantity of DNA obtained from long bones is higher than that from the ribs or skull. Edson and colleagues (2004) also agree that bones from the lower limb, such as femora and tibiae, should be preferentially sampled for DNA. The authors evaluated the rate of successful mtDNA extraction from an array of degraded human skeletal elements such as long bones, metatarsals, os coxae, and ribs.

Anđelinović and colleagues (2005) analyzed DNA from bone and teeth samples from victims of past conflicts in Croatia, Bosnia and Herzegovina (BH) between 1993 and 2005. Their sample consisted of hard tissues, primarily long bones and teeth, from 674 individuals recovered from various mass graves sites in Croatia and BH. Anđelinović and colleagues (2005) found that successful DNA typing from skeletal material depended on employing an appropriate DNA isolation procedure. The authors saw a drastic increase in success from 1993-2004 due to vast increases in DNA technology. They reported that the DNA quality from teeth was generally higher than that retrieved from bone. It was also noted that femoral samples with dense cortical bone better preserved DNA, although the environmental context in which the bones were recovered influenced the state of DNA quality (Anđelinović et al., 2005).

Although focused on mtDNA instead of nuclear DNA, Leney (2006) sampled archaeological skeletal remains to identify which skeletal element, by sample weight, performed best. He found that the larger the bone sample taken for DNA analysis, the greater the likelihood it would yield an acceptable DNA profile. Results further indicated that dense cortical bone from femora, followed by humerii were the most successful for mtDNA extraction.

In 2007, work by Milos and colleagues utilized data from human skeletal remains recovered from mass graves in the former Yugoslavia. They aimed to examine nuclear DNA yield from various skeletal elements from different postmortem intervals. The authors tested a large sample of bones including upper and lower limb bones, teeth, and small elements such as vertebrae and metatarsals. DNA success rates were found to be highly variable. Their results further suggested that dense cortical bone (i.e. from long bones) yielded the best DNA profiles, and should thus be preferentially sampled. The authors state that bones with a greater proportion of cancellous bone performed poorly in comparison (Milos et al., 2007).

An important study by Misner and colleagues (2009) investigated whether there was a correlation between skeletal weathering, or bone's overall macroscopic preservation, and mtDNA quality and quantity. Archaeological bones were tested for DNA quality and quantity and included ribs, femora, and os coxae. Results suggested that there is in fact no correlation between skeletal weathering and the quantity and quality of mtDNA. This finding contradicts previous literature that suggests bone's gross appearance is often an indicator of DNA preservation. As such, factors that degrade bone do not necessarily have the same effect on DNA. Moreover, the authors state that the greatest differences in DNA quantity and quality existed between femora and os coxae, regardless of the level of weathering. Misner and colleagues (2009) assert that cortical bone (i.e. femora) performed better overall than ribs and os coxae, with the pelvic material producing the poorest results.

Mundorff and colleagues (2009) evaluated a subset of remains from the World Trade Center Human Identification Project to measure differential nuclear DNA preservation by skeletal element. The authors found that variables such as the recovery location of the remains (Ground Zero versus the Staten Island Landfill), sex of the decedent, and decedent type did not

appear to influence DNA preservation. Contradictory to previous studies, the higher-yield producing bones included several smaller elements including patellae, metatarsals, and foot phalanges, which are generally overlooked in DNA sampling. These smaller bones can be removed easily using a disposable scalpel while sectioning mid-shaft femora is more time consuming, increases the risk of DNA contamination, and requires a bone saw. As such, the authors argue that their results should be considered when DVI managers are developing DNA sampling protocols.

Ferreira and colleagues (2011) discussed two mass disasters in Rio de Janeiro, Brazil: a mudslide event and an aircraft crash. The authors presented results from nuclear DNA sampling, fingerprinting, and dental analyses for victim identification. In relatively intact decedents, the authors preferentially sampled hard tissues such as lower limb bones, particularly metatarsals and foot phalanges, and teeth for DNA analyses. Long bones and teeth were also collected from fragmented or burned remains. In accordance with Mundorff and Davoren's (2014) results, the authors found that metatarsals and foot phalanges had high DNA success rates. Comparable to Mundorff and colleagues (2009), the authors noted that these small bones were easy to collect using disposable equipment that prevented DNA contamination (Ferreira et al., 2011). In a second study, the authors analyzed twenty foot-phalanges and knee cartilage samples from intact victims from the Brazil forest floor and mudslide incidents of 2011 (Ferreira et al., 2013). They compared the DNA profiles and yields from the cartilage samples to the bone specimens. While all of the samples yielded full DNA profiles regardless of tissue type, the yield rates were variable. Based on these findings, the authors recommended preferentially sampling phalanges instead of conventional bones, such as femora.

Notable work by Hines and colleagues (2014) provides a comprehensive analysis of DNA extractions from numerous skeletal elements (*n*=11,650) retrieved from varying environmental contexts. The skeletal sample was recovered throughout the Western Balkans by the ICMP (Hines et al., 2014). The authors presented their nuclear DNA extraction results for all skeletal elements in four tiers, with the first tier providing the best data. Results indicated that teeth, tarsals (particularly the talus), the petrous portion of temporal bones, vertebrae, metatarsals, and the femora and tibiae offered the highest success rates (Hines et al., 2014). Patellae also exhibited promising results but the sample size was too small (n=<10) to be included. Alternatively, skeletal elements exhibiting a DNA success rate of 50% or less included the ribs, cranial bones, humerii, ulnae, radii, and clavicles. In accordance with the findings of Mundorff and colleagues (2009), small bones composed predominantly of cancellous bone yielded more full DNA STR profiles than dense cortical bone retrieved from long bones.

Most recently, Kaneko and colleagues (2015) analyzed forty-two hard tissue samples at varying states of degradation including teeth, nails, second ribs, and cranial bones. Their results demonstrated that teeth provided the highest nuclear DNA concentrations and most complete profiles. DNA concentration retrieved from ribs was low compared to the other hard tissues. Three of the hard tissue types (rib, skull, and nails) exhibited a high loci number up to one month following death. After three months, approximately half of the loci from nail samples were non-demonstrable, and after five months, the number of loci from the three hard tissue types also dropped.

The majority of the above studies were retrospective analyses in which the researchers did not evaluate all element types within a single skeleton. Notably, while smaller bones with a higher quantity of cancellous bone tissue were often excluded from these studies, when they

were included they often out-performed other bones. Until recently, the majority of studies ignored small bones with high cancellous content. Consequently, the conclusions were based on testing limited samples and then misapplied to represent results from the entire skeleton.

Only one empirical study currently exists that has evaluated the differential preservation of nuclear DNA by all skeletal element types within the same skeleton and between multiple individuals recovered from one environment and point in time.

Mundorff and Davoren (2014)

Mundorff and Davoren (2014) presented a recent comparison of nuclear DNA quantity and quality from modern skeletal elements from three individuals with similar demographics (i.e. year of death, sex, age). A unique feature of their work is that they tested representatives of all element types within each skeleton. While it was not necessary or feasible to test all 206 bones in each skeleton, their sampling strategy captured at least one of each specific bone (i.e. one femur, one cervical vertebrae, all cranial elements). This was the first empirical study to evaluate the differential preservation of DNA by skeletal element under controlled conditions. The researchers compared 55 skeletal elements from three recently deceased individuals (n=165). Results revealed that bones such as phalanges, tarsals, and patellae yielded both higher quantity and better quality DNA for human identification. Results further demonstrated that elements with high quantities of cancellous bone yield and may preserve DNA at the highest rates, suggesting that preferentially sampling cortical bone may be suboptimal. As such, their findings have significant implications for the extraction of DNA, since cancellous bone is typically dismissed as a potential DNA source in favor of cortical bone. While the results presented by Mundorff and Davoren (2014) clearly indicated that bones with high cancellous quantity better preserve DNA, the reason is unknown. As DNA is becoming the preferred human identification

method, understanding why these results diverge from expectations requires further scientific investigation.

Summary

Nuclear DNA extraction from bone for forensic identification has long relied on preferentially sampling dense lower limb bones, specifically femora and tibiae. Certain studies further argue that primarily cancellous elements with little weight-bearing capability perform less well and should be avoided when selecting a bone to sample. However, a similarity among many of the aforementioned studies is their retrospective approach. As such, the authors did not evaluate all skeletal element types within a single individual. Further research quantifying DNA yield rates from all skeletal elements and cortical and cancellous bone tissue types within the same skeleton are warranted.

The current research methodology offers promise to refine our understanding of DNA sample-selection protocols for human identification. It will identify potential reasons for variation in DNA preservation among bone tissue types, and aid in understanding why particular bones may better preserve DNA. As a result, the findings have wide ranging implications in bone biology and will likely impact various fields within anthropology including biological anthropology, molecular anthropology, and forensic anthropology.

CHAPTER THREE: BASIC BONE BIOLOGY

''…between muscle and bone there can be no change in the one but it is correlated with changes in the other;…they are parts of a whole…''
- D'Arcy Wentworth Thompson (1917)

The current study aims to identify potential reasons why nuclear DNA yield varies among skeletal elements with differing proportions of cortical and cancellous bone tissues. To address the proposed question, an extensive knowledge of bone biology is essential to understanding histomorphological variation in human bone tissue. The following review of normal bone gross morphology and histomorphology provides an overview of bone microstructure pertaining to differential DNA yield among human bone tissue types.

Composition and Structure of Bone

The skeletal system performs a variety of metabolic and structural functions in the human body. Bone functions metabolically as a reservoir for minerals such as phosphorus and calcium, and is involved in maintaining their homeostasis (Martin et al., 2015). It also serves structurally as a lever system in which muscles attach allowing for movement. The framework it provides supports and anchors the soft tissues of the body while offering protection to internal organs. As such, the composition and structure of bone at the molecular, microscopic, and gross levels allows the skeleton to perform these functions.

Molecular Structure of Bone

Human bone is a connective tissue that is composed of 67% inorganic material and 33% organic material (Nanci, 2008). Twenty-eight percent of the organic matrix is composed of Type I collagen, organized into long fiber bundles (Nanci, 2008). This structural organization provides bone with strength and slight flexibility. Inorganic bone material is composed of hydroxyapatite,

a poorly crystallized mineral that infuses the organic bone matrix (Nanci, 2008). It is this mineral that constitutes the remaining 67% of bone material, and provides bone with its dense and rigid structure (Nanci, 2008; Martin et al., 2015). Integration of protein and minerals give bone tissue combined mechanical properties that differ from the sum of the individual components. The presence of organic and inorganic components allows bone to function in the support and protection for the many intricate body systems. This composition also permits locomotion, resistance to compressive forces, and as a storage reservoir for minerals (Robling, 1998; Goldman, 2001; Nanci, 2008). Human bones greatly differ in size and shape, but this structurally sound composition is consistent despite the gross appearance.

Composition of Bone

Bone is a mechanically active and dynamic tissue that changes in structure over the human lifespan. It can be differentiated into two main structural types: cortical and cancellous. Generally speaking, long bones possess a diaphysis and two or more epiphyses, composed of an outer cortex of cortical bone and cancellous bone within the medullary cavity (Carter & Beaupré, 2001). The outer surface of the cortex is covered by periosteum, a soft-tissue layer composed of a highly vascularized fibrous membrane, and an inner layer containing osteogenic cells (Martin et al., 2015). The inner surface of the bone's cortex is the endosteum, which forms the boundary of the medullary canal.

Cortical, or compact bone is dense and comprises the external surface of bones (**Figure 3.1**). It protects the medullary cavities, covers the diploe of cranial bones, and is recognized to exhibit three envelopes: periosteal, intracortical and endosteal (Frost, 2003; Robling et al., 2006). Cortical bone accounts for the majority of bone mass (~80%) and is composed of highly organized primary lamellar and secondary osteonal bone tissues (Carter & Beaupré, 2001).

Primary lamellar bone tissue is formed during appositional growth or endochondral ossification (Scheur & Black, 2000), and is vascularized by primary vascular canals. Secondary osteonal bone tissue, or Haversian bone, refers to lamellar bone tissue that has replaced older bone tissue through bone remodeling (discussed later in this chapter). Concentric lamellar rings bordered by a cement, or a reversal line, characterize secondary osteonal bone tissue. Reversal lines are composed of highly mineralized collagen matrix, and separate secondary lamellar tissue from previously existing bone tissue (Crowder & Stout, 2012). Each osteonal system contains several specialized bone cells.

Cancellous bone is composed of thin plate-like structures called trabeculae (**Figure 3.1**) and has a spongy appearance (Nanci, 2008; Carter & Beaupré, 2001). It is typically found at the metaphyseal ends of bones and within the medullary cavities that house red and yellow bone marrow during life. For the most part, lamellae are arranged parallel to the trabecular surface forming half osteons called hemiosteons. One surface of the hemiosteon borders the bone marrow cavity, rather than a Haversian canal as seen in cortical bone (Burr & Allen, 2013). As such, cancellous bone's microstructure is comparable to that of cortical bone, with the exception that the latter includes Haversian systems.

Bone Cells

Three primary cell types are responsible for the resorption, formation and maintenance of skeletal tissue: osteoclasts, osteoblasts, and osteocytes. These cells are histologically distinct and are differentiated by their origins, form, function, and locations within the bone matrix.

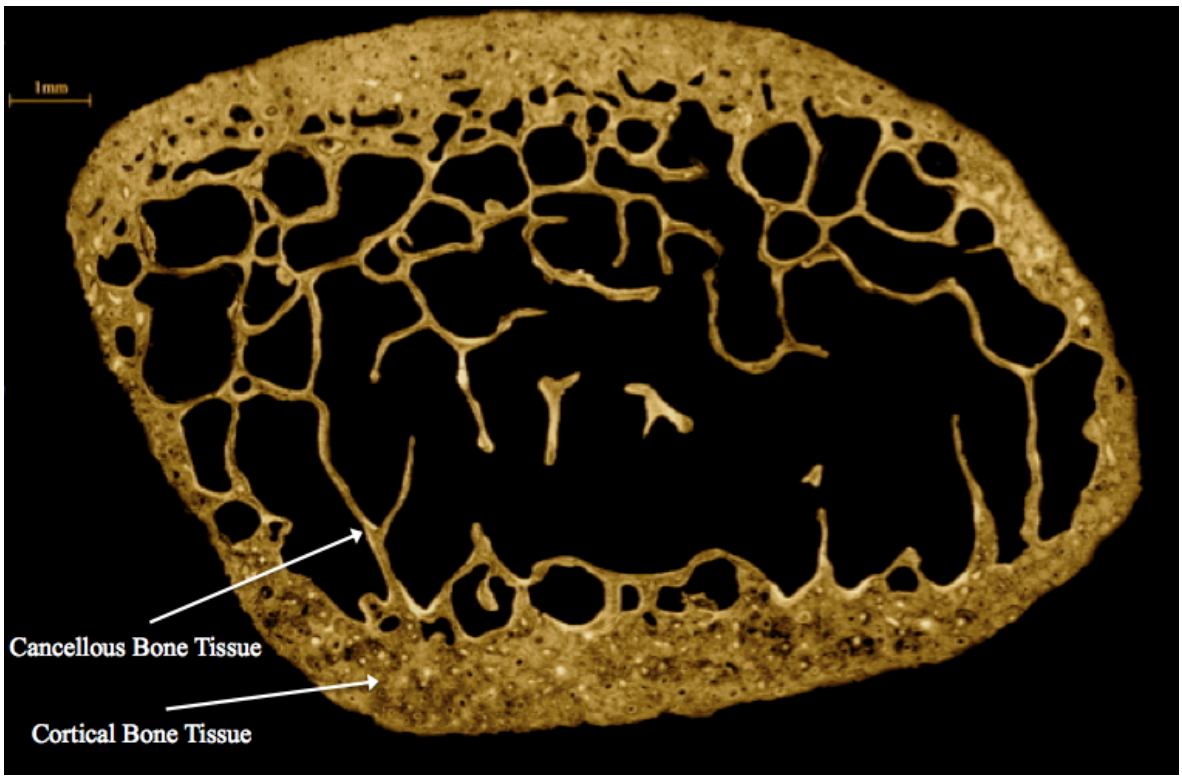

Figure 3.1: Bone cross-section of an adult human rib exhibiting cortical and cancellous bone tissue. This image was captured under transmitted light with 10x objective magnification (Credit: JM. Andronowski).

Osteoclasts

Osteoclasts are bone cells of hematopoietic origin that are responsible for the resorption of both inorganic and organic bone material. These are the largest of the three bone cells and are multinucleated. Osteoclasts remove excess bone tissues and microfractures, and release minerals stored in mature bone tissue to assist with maintenance of mineral homeostasis (Robling et al., 2006). The activity and control of these cells play a large role in maintaining the balance between bone resorption and deposition that is required for healthy bone tissue. Osteoclasts and their precursors undergo a series of transformations during bone modeling and remodeling that include identified stages of activation, mobilization, resorption, and cessation. Numerous genes

are essential for osteoclast differentiation that include: transcription factors PU.1, c-Fos, NFKB1and 2, growth factors M-CSF and RANKL, and the receptor RANK (Robling et al., 2006; Allen & Burr, 2013).

Bone resorption begins with immature osteoclasts differentiating into mature osteoclasts regulated by RANKL and M-CSF (Allen & Burr, 2013). Mature osteoclasts then migrate to the resorption site, where they are activated, and attach themselves to the internal cellular structures by means of a plasma membrane. A tight seal (actin ring) forms between the plasma membrane and the adjacent bone forming an area referred to as the sealing zone (Allen & Burr, 2013). Once the cells are mobilized, a space is created between the two surfaces where protons and other proteolytic enzymes are secreted (Robling et al., 2006; Teitelbaum, 2000). A highly convoluted membrane forms the characteristic ruffled appearance of osteoclast borders (Allen & Burr, 2013). These membranes contain large quantities of targeted transport vesicles, lysosomes, and proton pumps (Teitelbaum, 2000). Bone removal across the inorganic matrix proceeds by acidification of the extracellular spaces through proton secretion across the ruffled border (Allen & Burr, 2013). The structure of osteoclasts allows for the dissolved bone matrix to be continually removed without compromising the tight bond of the actin ring. The dissolution of the bone matrix results in a depression termed a Howship's lacuna. Once the Howship's lacuna has been eroded, the osteoclast detaches and relocates (Teitelbaum, 2000). The disintegrated matrix will then be either internalized by the cells, or released into the surrounding microenvironment once the osteoclast retracts from the Howship's lacuna (Allen & Burr, 2013). Following osteoclastic bone removal, bone formation by bone forming cells (osteoblasts) occurs.

Osteoblasts

The osteoblast is a uninucleated, mesenchymal-derived cell involved in the synthesis of bone proteins and the deposition of new bone material (Parfitt, 1983a). Osteoblasts form cell layers over existing bony material and collectively act as a barrier to control the passage of ions in and out of bone. These cells are involved in the secretion of cytokines that regulate the formation of bone (Ortner & Turner-Walker, 2003). Osteoblasts are considerably smaller than osteoclasts, thus requiring 100-150 cells to form the amount of bone that can be broken down by the activity of a single osteoclast (Crowder, 2005). As such, maintaining the balance between resorbed and new bone tissue is an ongoing process in which disruption of the normal activity of either osteoclastic or osteoblastic activity could be detrimental to bone health.

Similar to osteoclastic bone resorption, the transcription factors responsible for osteoblast proliferation and differentiation are regulated by various hormones and growth factors. These include: PTH, estrogens, insulin like growth factor (IGF), fibroblast growth factor 23 (FGF23), bone morphogenetic protein, glucocorticoids and vitamin D (Allen & Burr, 2013; Zaidi, 2007). Following differentiation and proliferation of osteoblasts, the cells migrate to bone remodeling or modeling sites to secrete osteoid, composed of proteins, type I collagen, osteocalcin, and alkaline phosphatase, on the resorbed bone's surface (Robling et al., 2006). A border of unmineralized matrix, referred to as an osteoid seam, is then formed. The boundary between the osteoid seam and the unremodeled bone surface is called the mineralization front. As the process of bone formation progresses, a small number of osteoblasts become entombed in pits called lacunae within the surrounding mineralized matrix and undergo osteocytogenesis (Allen & Burr, 2013). Radiating appendages stem from the lacunae, termed canaliculi, which allow osteocytes to communicate with neighboring osteocytes and osteoblasts, and respond to the surrounding

environment (Currey, 2002).

Since researchers have made significant progress in understanding the complex roles that osteocytes play in bone homeostasis, a further discussion of osteocytes and their proposed characteristics is presented below.

Osteocytes

Osteocytes are often cited as the most ubiquitous bone cells in mature bone, amounting to approximately 90% of all cells in cortical bone tissue (Martin et al., 2015). As they are well distributed throughout the bone matrix, communication is efficient with other osteocytes and with osteoblasts via canaliculi, as well as aid in exchanging substances via an interconnected system. Due to their small size, they only compose about 1% of total bone volume (Martin et al., 2015). Despite this fact, they have vast surface area. Though the complete nature of osteocytes remains elusive, they are considered essential to maintaining normal bone homeostasis and in the initiation of bone repair (Turner & Forwood, 1995; Martin et al., 2015). As such, osteocytes play an important role as sensors and represent a key element in the mechanosensory system. Some remain in direct contact with osteoblasts and with the internal surface of bone. As such, this forms a network of mechanosensing. A complete understanding of the lacuno-canalicular system, however, remains elusive.

Overall, the mechanotransduction process can be divided into the following phases: (1) the pairing of biomechanical and biochemical processes in response to mechanical loads, (2) the transmission of signals by osteocytes, and (3) bone remodeling (Robling & Turner, 2009).

Osteocytes as Mechanosensors

Mechanical strain is a documented key regulator of osteoclastic and osteoblastic activity in bone tissue. Various works have investigated load-related reactions of osteocytes, which support their role in mechanotransduction (Robling & Turner, 2009; Burr, 2002; Martin, 2000). It is recognized that mechanotransduction begins when osteocytes perceive mechanical energy and convert it into cellular and structural signals (Robling & Turner, 2009). However, there is not currently a single known mechanoreceptor in osteocytes, and it is suggested that a combination of factors must be triggered for mechanosensation and transduction to occur. These molecular mechanisms are important to consider as a better understanding of those involved in mechanotransduction may provide new insight into bone biology and shed light on new applications for therapeutic intervention.

Mechanisms by which Osteocytes Sense Mechanical Loading

Once mechanical stimuli are recognized by osteoctyes, signaling events follow that promote bone gain and prevent loss (Robling & Turner, 2009). Osteocytes may be triggered to sense mechanical loads via exposure to stress on the cell body itself or on the canaliculi, or cell deformation in response to strain. For example, strain concentrations leading to deformation of the bone matrix can be triggered by the appearance of microcracks or initiated by common microstructural features of bone such as osteocyte lacunae (Burr, 2002; Robling & Turner, 2009). In addition, it is suggested that osteocytes can sense strain in their localized environment. As such, separation of lamellae can occur due to bands of stress that form around osteocyte lacunae (Burr, 2002).

The Fluid Flow Hypothesis

Osteocytes may also respond to increased fluid flow within the bone matrix that is initiated by loading. To address the hypothesis regarding the role of interstitial fluid driven by mechanical loads, Turner and Forwood (1995) discuss the fluid flow hypothesis and its influence on the integration of cellular responses. Fluid flow may be important for removing wastes from cells and supplying nutrients to tissues, and act as a stimulus for bone formation when mechanical loads are high. It is this extracellular fluid flow and the interaction with osteocytes that is essential to mechanotransduction. It is suggested that osteocyte lacunae may act as 'pumps' to push fluids along the canaliculi of loaded bone. This fluid flow can produce a drag-type force, and shear stress that may activate bone cells and thus the remodeling process (Robling et al., 2006). These triggers may occur together or independently to initiate mechanotransduction. Signals can be transferred to the Basic Multicellular Unit (BMU) via gap junctions and release of signaling molecules (i.e. prostaglandins, ATP, nitric oxide) into bone via interconnecting channels, or the lacuna-canalicular system (Robling et al., 2006).

Osteocyte Apoptosis

Mechanical stimuli are recognized as strong regulators of osteocyte apoptosis, which is also suggested to initiate remodeling (Robling & Turner, 2009; Burr, 2002). Since loading stimulates the proliferation of osteoblast precursors, rates of programmed osteocyte apoptosis are reduced (Robling et al., 2006). If the rate of damage formation in bone increases quickly due to an increased load frequency, microdamage may accumulate that can initiate osteocyte cell death. As osteocyte apoptosis occurs at sites of bone microdamage or in cases of disuse, the dying cells may send signals to osteoclasts for bone removal (Martin, 2007). Overall and generally speaking,

too little mechanical stimulation encourages apoptosis whereas too much generates damage to bone also triggering cell death.

Osteocytes and Microdamage

All structural materials that experience repetitive loading are susceptible to fatigue microdamage. Microcracks are recognized to cause damage in bone due to normal as well as high skeletal loading (Martin, 2007). Frost (1950) was the first to propose that remodeling may occur in response to microdamage. As such, osteocytes may sense this fatigue damage and release signals to activate bone remodeling in response. Additional evidence from the literature also supports this view. For example, Burr and Martin (1993) further investigated the non-random association between cracks and resorption spaces. Burr (2002) suggests that microcracks disrupted canalicular connections between osteocytes, which stimulates remodeling. He further indicates, however, that only thirty percent of microdamage is targeted by bone remodeling. The remaining seventy percent that is non-targeted, or stochastic, may be associated with metabolic factors, interstitial fluid flow, and/or regions of high strain (Martin 2002; Burr, 2002).

Bone Modeling and Remodeling

All components of the skeleton work in concert to perform mechanical, metabolic and homeostatic functions (Robling & Stout, 2008; Currey, 2002). Bone undergoes modeling and remodeling throughout life to allow for these functions.

Bone Development

Bone development begins in utero through intramembranous or endochondral ossification (Marks & Odgren, 2002). Intramembranous ossification involves the direct transformation of mesenchymal cells into osteoblasts, and is restricted to flat cranial bones, certain facial bones,

mandible, and clavicles (Scheur & Black, 2000). The remaining bones form via endochondral ossification. During this process, embryonic mesenchyme transforms into cartilage, forming a cartilaginous model through chondrocyte proliferation and hypotrophy, reflecting the final form of the bone (Carter & Beaupré, 2001). The hyperotrophic chondrocytes undergo apoptosis and are replaced by osteoblastic cells, which direct mineralization of the surrounding bone matrix. The persistence of mineralized cartilage acts as a scaffold for the deposition of subchondral bone and vasculature (Marks & Odgren, 2002). Primary ossification centers form through this process, and both intramembraneous and endochondral ossification form primary bone tissue (Marks & Odgren, 2002). After the formation of the primary ossification centers, bone formation continues through longitudinal and appositional growth. Secondary ossification centers form when chondrocytes undergo hypertrophy, while attracting vascularization and osteoblasts. Appositional growth allows for size and shape changes in bones, and occurs concurrently with longitudinal growth (Carter & Beaupré, 2001). Once longitudinal bone growth ceases, appositional growth can continue throughout life, allowing for alterations of bone morphology and cross-sectional geometry.

Modeling

Bone modeling occurs during growth and development, and for the most part, is restricted to the growing skeleton. Renewed modeling can occur in some disease states, during fracture healing, and in response to pressures of an altered mechanical loading environment (Robling & Stout, 2008). In healthy individuals, modeling results in a gain of bone volume and mass (Parfitt, 1983a; 2003). Modeling occurs via modeling drift (**Figure 3.2**), which moves bone through tissue space (Robling & Stout, 2008). This process involves the addition and removal of bone to existing surfaces, thus adjusting bone architecture. Bone modeling determines the

strength, size, and architecture of bones (Frost, 1969; 1997; Crowder, 2005), and allows for mechanical loads to be sustained or adjusted. Modeling differs from remodeling in various respects. For example, formation and resorption occur on different bone surfaces and there is no coupling between them (Parfitt, 1983a). Renewed modeling in the adult skeleton can occur, though bone remodeling dominates adult bone turnover.

Remodeling

Remodeling refers to a tissue turnover process that occurs in adults without changing the macroscopic bone architecture (Frost, 1983). Most of the physiology of bone remodeling has been defined using undecalcified bone biopsy specimens (Frost, 1969). The remodeling process is continuous throughout life, and involves a complex arrangement of cells called BMUs. BMUs remodel bone via the removal and replacement of 'packets' of bone called bone structural units (BSU) (Robling & Stout, 2008; Frost, 1969). Remodeling follows an activation, resorption, and formation (ARF) sequence. This series can be further expanded to six phases, however, that include activation, resorption, reversal, formation, mineralization, and quiescence (Martin et al., 2015). Briefly, *Activation* involves cell differentiation, and osteoclast formation. Bone *resorption* occurs at specified locations by osteoclasts, and bone *formation* occurs via osteoblastic activity (Crowder, 2005). This process removes and replaces older and/or damaged bone, in turn allowing bone to maintain its mechanical competence. BMUs move through tissue space by tunneling through bone material (**Figure 3.3**) with a leading region lined with osteoclasts (Robling & Stout, 2008). The diameter of the excavation tunnel is determined by osteoclast activity, and corresponds with the size of newly formed osteons. As BMUs transition between resorption and formation, a cement or reversal line is formed. The mineral composition of the reversal line differs from the surrounding bone matrix (Martin et al., 2015).

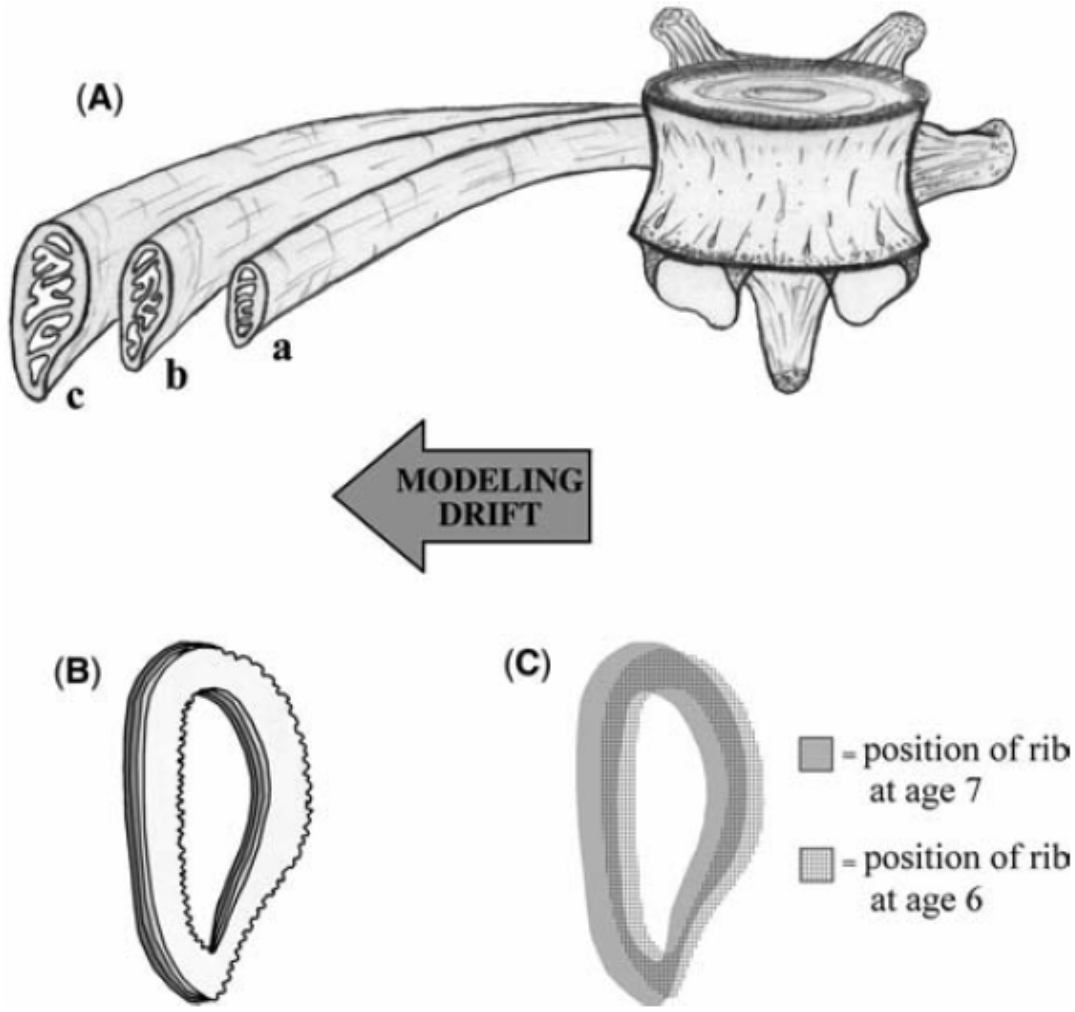

Figure 3.2: Modeling drift in human ribs. A) Changes in rib morphology due to development. None of the cortical bone tissue from the younger rib (a) remains present in the adult rib (c). B) Magnified view of the rib cortex during growth and cortical drift. The scalloped edge represents the resorptive surface and the parallel layers represent appositional growth layers. C) Changes in cortical bone tissue over one year. The majority of the cortical cross section is composed of new bone tissue. From Robling and Stout, 2008: Figure 5.1, p.150.

Osteoblasts attach to the reversal lines, and line the resorption tunnel (Goldman, 2001). Osteoid is deposited in a concentric pattern from the outer edge of the tunnel inwards. A Haversian canal is left in the center of the newly formed osteon.

Bone remodeling achieves three goals: (1) it allows the body to alter the balance of essential nutrients by increasing and/or decreasing their concentration (Burr, 2002), (2) protects bone from natural biomechanical forces that cause microscopic damage, and (3) allows microdamage to be repaired, preventing the development of macrodamage. The remodeling process continuously adjusts homeostasis within the bone matrix, and must be ideally balanced to retain bone integrity.

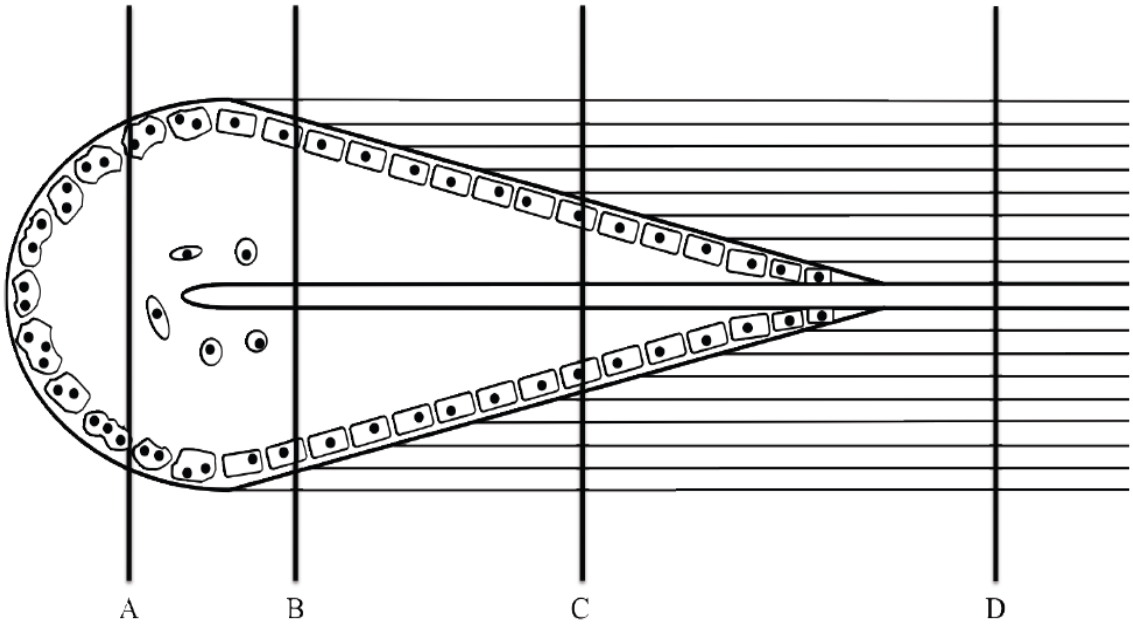

Figure 3.3: Coupled osteoclast and osteoblast activity depicted as a BMU during bone remodeling. A) osteoclastic activity near the leading edge of the cutting cone, B) initiation of osteoblastic activity, C) active osteoblast activity, D) a fully formed intact osteon depicting a Haversian Canal in the center. Used with permission from Pratt (2013), p.4.

Remodeling Theory

A diversity of viewpoints regarding bone adaptation and the impelling force behind bone remodeling exist. There remains some separation between various disciplines, as researchers from fields ranging from bioengineering and materials science to anthropology have varying viewpoints regarding the functional adaptation of bone. It is theorized, however, that remodeling may maintain the biomechanical integrity of bone (Martin, 2000; Burr, 2002). The following review will document various theoretical models pertaining to the mechanical, genetic, and chemical factors of bone remodeling.

Wolff's Law of Bone Transformation

Prior to 1892, few individuals considered the functions of bones in mechanical terms (Frost, 1998), and bone architecture was often attributed to divine design or magic (Frost, 1998). Historical researchers such as Galileo, however, considered bone structure in the context of its mechanical environment (Martin et al., 2015). These viewpoints were popularized when Julius Wolff introduced an influential theory in skeletal physiology, termed Wolff's Law. Wolff's Law generally states that the form and function of bone is followed by changes in internal architecture (Frost, 1998). Wolff's (1892) theory marked a step forward in understanding bone physiology. His theory is grounded in mathematical principles and refers to the mathematical relationship between trabecular architecture and stress trajectories (Forwood & Turner, 1995). Wolff did not formulate his proposed mathematical theory, however. As such, the basic tenets of Wolff's Law, and his misconceptions regarding skeletal biology have been met with thorough critique (Forwood & Turner, 1995; Dibbets, 1992; Pearson et al., 2004; Ruff et al., 2006). Several highly developed and biologically relevant theories have since been proposed.

Frost's Mechanostat Theory

Frost (1983) proposed a theory to explain the mechanical mechanism that controls modeling, remodeling, and bone mass during growth. Frost's mechanostat theory is based on the immensity of strain that results from mechanical loading, and is responsible for controlling bone mass (Frost, 1987). Frost (1983) maintains that bone adapts to strain via mechanical usage windows that include trivial, physiological, overload, and pathological (Forwood & Turner, 1995). Strain thresholds were introduced to explain the activation and inhibition of modeling and remodeling. Frost (1987) used a house thermometer as an analogy, stating that mechanisms controlling bone mass would turn off in the absence of strain and on in response to it. He called these strain thresholds the minimum effective strain set-points (MESm), and argued that they can be altered by intrinsic factors. Hormones, pathological agents, and other biological mechanisms may disrupt the mechanical feedback system (Frost, 1983; 1987).

During bone modeling, strains above the threshold of the minimum effective strain set-points cause modeling to turn on (Frost, 1997). This process increases the amount of bone formation. When strains are below the MESm threshold, modeling remains "turned off". Strains above the threshold of the minimum effective strain for remodeling (MESr) retains the remodeling process, and conserves bone (Frost, 1997; 2004; Crowder, 2005). If strains fall below the threshold, remodeling is inactive, and bone may be permanently removed from the endosteal envelope (Frost, 1997; 1998; 2004). This removal process can result in osteopenia, and in severe cases, osteoporosis (Carlson et al., 1976; Frost, 1997). Frost also described the effects of repeated bone strain in relation to fatigue microdramage. He proposed that strains could initiate microcracks, which in turn disrupt osteocyte canalicular networks that may stimulate remodeling (Frost, 1997).

The mechanostat is the primary hypothesis in the Utah paradigm, since it explains how load-bearing bones achieve mechanical competence (Frost, 1983; Crowder, 2005).

The Utah Paradigm

The Utah Paradigm of skeletal physiology evolved from a series of Hard Tissue Workshops sponsored by the University of Utah (Frost, 1998). The workshops were held to address the lack of multidisciplinary approaches to skeletal research (Crowder, 2005). The Utah Paradigm attempts to bridge the subfields of skeletal biology, medicine, and surgery (Frost, 1998). This theory introduced a shift from a 1960 paradigm of skeletal physiology, suggesting that effector cells (including fibroblasts, chondroblasts, osteoblasts, osteoclasts), which determine bone health, are controlled by non-mechanical agents (Stout & Crowder, 2012; Frost, 2000b).

The Utah Paradigm examines load bearing skeletal elements at the organ, tissue, and cellular level (Frost, 1998; 2004). The focus is the mechanical competence of bone (Frost, 1997; 1998). The mechanostat is the primary hypothesis in the Utah paradigm, since it explains how load-bearing bones achieve mechanical competence (Frost, 1983; Crowder, 2005). The Utah paradigm suggests that the driving force of load bearing skeletal architecture and strength are mechanical factors, and that non-mechanical factors such as hormones, minerals, sex, and age, can hinder or assist the process but do not replace it (Frost, 1998; 2004; Stout & Crowder, 2012).

The Utah Paradigm, however, does not fully explain the forces that control the cause-and-effect relationship of muscle force and bone strength. Frost (2003) introduced an updated version of the original mechanostat hypothesis indicating that genetic factors must play a role in the biological determinants of bone mass. It is not clear, however, how much genetic

predisposition accounts for the association between muscle and bone mass (Stout & Crowder, 2012).

Osteocyte Inhibitor Theory

Burr (2002) describes that bone remodeling is responsible for three important processes: (1) the repair of microdamage in bone to maintain tissue integrity, (2) adaption to the skeleton's mechanical environment, and (3) provides a mechanism for the body to maintain and balance essential minerals (Stout & Crowder, 2012; Burr, 2002). Experimental studies have revealed that new remodeling locations are frequently associated with microcracks, supporting a cause-and-effect relationship (Burr, 2002; Burr & Martin, 1993; Burr et al., 1985; Mori & Burr, 1993). Frost (1960) originally suggested that bone microdamage disrupts the canalicular connections between osteocytes, in turn stimulating remodeling.

Frost's (1983) mechanostat theory suggests that bone remodeling is activated by disuse, thus impeding modeling. Martin (2000a, 2000b), however, contends that the mechanostat does not consider the removal of microdamage resulting from high strains. It is essential to consider strain levels as they provide a mechanism to nourish osteocytes through interstitial fluid flow (Stout & Crowder, 2012; Martin 2003a). If strain levels are disturbed, a lack of nutrient supply to osteocytes may result in disrupted osteocyte networks. In turn, resorptive activity is stimulated.

Burr (2002) offers a differing view, however, suggesting that only thirty percent of microdamage is targeted by bone remodeling. The remaining seventy percent that is non-targeted, or stochastic, may be associated with metabolic factors, interstitial fluid flow, and/or regions of high strain (Martin 2002; Burr, 2002). As the relationship between targeted and stochastic bone remodeling is not fully understood, this theory has little supporting evidence and remains controversial within the scientific community.

The Principle of Cellular Accommodation Theory

Turner (1999) challenged Frost's (1983) mechanostat by introducing a mathematical theory of bone biology, the principle of cellular accommodation. Turner (1999) states that the mechanostat theory fails to explain why non-weight-bearing bones are not resorbed due to disuse (Stout & Crowder, 2012). Turner (1999) argues that Frost's (1983) mechanostat does not conform to experimental observations, and suggests his theory will address inconsistencies.

The principle of cellular accommodation theory assumes that bone cells react to their biological environment, and learn to accommodate the new environment (Turner, 1999; Stout & Crowder, 2012). Turner (1999) predicts that bone mass will stabilize once cells fully adjust to the new environment.

Altered hormone levels, or varying mechanical loads will cause a change in bone remodeling, but that reaction will change when bone cells adapt to the new environment (Turner, 1999). Turner argues that Frost's mechanostat places biomechanics at the center of bone biology, without acknowledging that bone is insensitive to mechanical loading when growth and/or parathyroid hormones are absent (Turner, 2000; Crowder, 2005). This suggests that bone mass is dependent on mechanical loading and hormonal events, and these factors play a leading role in bone formation (Turner, 1999; Stout & Crowder, 2012). Turner's approach offers a fresh perspective on bone biological principles, and represents a step towards a unified theory of bone remodeling.

Summary

Maintaining bone homeostasis involves complex interactions at the molecular, cellular and tissue level. Osteocytes play a pivotal role in mechanotransduction and transmission of information to the effector cells (osteoclasts and osteoblasts). It is essential to recognize these

interactions as a cohesive operating system that allow for the maintenance of the gross morphology, microarchitecture and mechanical properties of bone. The modeling of bone during growth and ongoing bone remodeling over the lifespan will produce indicators of skeletal health and provide information regarding skeletal age.

CHAPTER FOUR: THREE-DIMENSIONAL IMAGING OF BONE

Bone was among one of the first biological tissues to be studied microscopically. Until recently, however, the evaluation of bone microarchitecture at the micron- scale and analysis of cortical bone remodeling had been focused within the two-dimensional (2D) realm. The ideas and experimental techniques that laid the foundation for the field of bone histomorphometry, and continue to form its backbone, can be attributed to HM Frost, orthopedic surgeon, bone biologist, and self proclaimed 'Feisty, Eccentric, Old Dinosaur'. He made many breakthroughs that changed the field of bone biology, including: (1) discovering the BMU in bone remodeling, (2) introducing the mechanostat hypothesis of bone adaptation, (3) the role of osteocytes in the remodeling process, (4) devising theories of bone adaptation in response to mechanical loading, (5) introducing skeletal intermediary organization, and (6) demonstrating that non-decalcified 2D histologic bone sections can be analyzed to quantify the process of remodeling (Frost, 1969; 1983; 1987a; 1987b).

Though researchers still greatly benefit from 2D methodologies that often yield more specific or additional histological information, such as finer microstructural details or cellular/functional information from sophisticated staining techniques, 3D imaging modalities provide a much more comprehensive understanding of cortical microstructure. As such, visualizing and analyzing bone using high-resolution 3D imaging modalities will improve current understandings of bone biology and have numerous applications in both anthropology and biomedicine.

The following discussion will review topics related to 3D imaging that include: (1) a review of the history of 3D imaging and conventional histological 3D methods, (2) 3D x-ray microtomography including both desktop and synchrotron-based systems, and associated

strengths and weaknesses of these approaches, and (4) applications of 3D imaging to anthropological research.

Brief History of 3D Imaging

The following review will detail the methodological approaches used historically to evaluate cortical bone tissue in 3D. In the mid-late 1600's (1677), Anthony Van Leeuwenhoeck published what is thought to be the first description of cortical bone histology. He described the arrangement of cortical bone tissue as a series of 'pipes' and penned a 3D render of his observations (**Figure 5.1)**. In the late 1600's, Clopton Havers described types of pores that run transversely and longitudinally through cortical bone tissue to its surface. As such, he is the namesake for the longitudinal 'Haversian' canals. These early descriptions were based on observations of blocks of bone using low magnification. Todd and Bowmann (1845) first described Haversian systems, while Tomes and De Morgan later described their formation within restrictive resorption spaces (1853).

Early 3D investigations of bone microstructure were based on time consuming and tedious protocols which employed two approaches: (1) staining and/or casting of cortical canals, and (2) serial section reconstruction. Casting and/or staining bone specimens (Schnapper et al., 2002) allowed researchers to determine the positioning of vascular canals, spatial orientation of cortical bone, and osteon orientation (Hert et al., 1994; Petrtyl et al., 1996). Hert and colleagues (1994) for example, filled the vascular canals of undecalcified cortical bone with india-ink to assess the spatial microarchitecture. Other projects employing casting/staining techniques examined canal networks in various animal species, and evaluation of resorptive bay distribution (Georgia et al., 1982; Vasciaveo & Bartoli, 1961). Though allowing for visualization of canals,

these techniques historically did not provide enough quantitative data to visualize the entire 3D structure of bone samples.

As demonstrated by Cohen and Harris (1958), serial sectioning and visualization using light microscopy allowed for the examination of vascular canals in cortical bone. Sterio (1984) and Gunderson (1986) established that the number of cells per volume could be measured through serial sectioning using what is called the 'disector method'. Additionally, Tappen (1977) visualized resorptive bays evident during the remodeling process in canine bone. Reconstructed 3D sections also provided researchers with the necessary information to create 3D models out of various materials such as wire and paper (Cohen & Harris, 1958; Amprino, 1948). More recently, advancing computer technology has allowed for much more efficient 3D rendering and automation of serial sections. Stout and colleagues (1999), for example, used serial section reconstruction to analyze the 3D nature of osteons in canine bone. The authors discovered that osteons appeared to have complicated and interconnecting branching patterns, thus refuting earlier evidence suggesting that osteons display spiraling organization. A notable finding by Stout and colleagues (1999) revealed that previously described 'dumb-bell shaped' osteons are in fact bi-products of the 2D plane of sectioning. Though providing some 3D information, serial sectioning and subsequent reconstruction require destruction of study specimens, produce generally qualitative results, and are tedious in nature.

Quantitative Computed Tomography (QCT)

GN Hounsfield developed the first commercial quantitative computed tomography (QCT) system in 1973. For this innovative achievement, Hounsfield and Cormack were awarded the 1979 Nobel Prize in Physiology or Medicine. Prior to the development of QCT, a screening and diagnostic tool referred to as digital tomosynthesis allowed for the clinical identification of

pathological abnormalities in soft tissue structures (i.e. breast tumors). This early imaging modality was limited in its access to 3D information and out of plane structures were often illuminated subsequently blurring the target object.

Hounsfield's traditional CT system relied on differential x-ray absorption across materials or tissues. A series of projection x-ray images could be taken of a rotated object from 0 to 180 degrees. From these projections, the 3D structure of the object can be reconstructed. In reconstructed images, the gray levels will be inverted resulting in the denser materials being darker and areas of high absorption being brighter.

Boushey and colleagues (1983) published an early study employing QCT in a clinical context to evaluate osteoporosis. The authors employed QCT in the examination of lumbar vertebral mineral content. This technique afforded high precision compared to alternative imaging modalities available at the time of publication including radiogrammetry and photon absorptiometry.

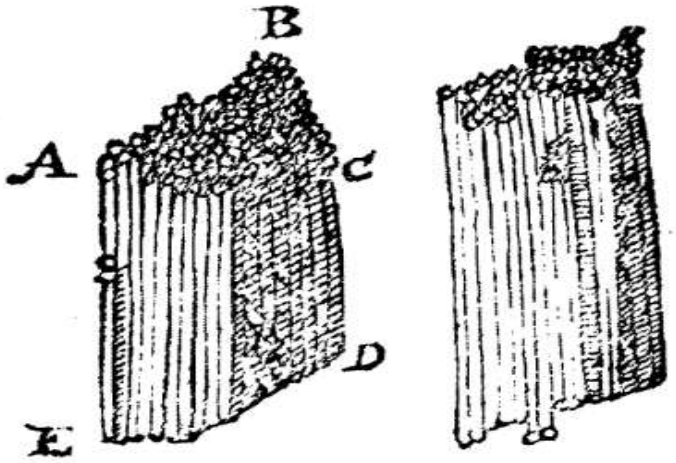

Figure 5.1: Van Leeuwenhoeck's diagrams depicting cortical bone microstructure, which he described as pipes (Leeuwenhoeck, 1677).

The aforementioned studies are few and generally yield qualitative results from small sample sizes. Findings from early conventional 3D imaging techniques demonstrate the need for further 3D analysis of cortical bone microarchitecture. The above approaches have been superseded by the use of micro-computed Tomography (micro-CT or μCT).

Micro-Computed Tomography

Micro-CT, an x-ray imaging method, has been regularly used since 1989 as an approach for analyzing 3D microstructure of cancellous bone. The original application of micro-CT to bone microstructure was to assess and quantify pathological changes and mechanical properties of bone associated with osteoporosis *in vitro (*Muller & Ruegsegger, 1995; Borah et al., 2001). The ability to quantify 3D bone architecture efficiently, and with software developed for cancellous bone analysis, is a very important advantage associated with the micro-CT approach. Micro-CT also offers the benefit of preservation of the bone specimen, as opposed to former destructive techniques such as serial sectioning. There are two primary micro-CT systems in existence that can be applied to the examination of bone tissue: (1) laboratory or desktop micro-CT systems, and (2) synchrotron radiation micro-CT (SR micro-CT).

Quantitative Assessment of Bone Microarchitecture

Traditional histomorphometric methods based on 2D histologic sections can be inadequate for defining cortical and cancellous bone microarchitecture. Employing a micro-CT approach allows for bone microarchitectural measurements to be made in 3D non-destructively. As such, there are various parameters and indices that can be applied to cortical and cancellous bone. Quantification includes measurements and statistical approaches such as counts, volumes, areas, distance measurements, distribution graphs, and porosity measurements.

Definitions

In 1987, the American Society of Bone and Mineral Research (ASBMR) histomorphometry nomenclature committee released a document designed to standardize definitions for quantitative bone histological research (Parfitt et al., 1987). This report aimed to mitigate the esoteric variety of terms in which researchers in the field of bone histomorphometry communicate with one another. What resulted was a unified system of terminology that was suitable for adoption by the Journal of Bone and Mineral Research. As general rules, the terms used to describe variables were self-explanatory and descriptive, straightforward abbreviations were employed that did not include sub-or superscripts, each symbol component used had only one meaning, and the system be flexible enough to be applied to various bone types and bone surfaces. Thus, the symbols and acronyms reported in the following review are in accordance with the nomenclature system outlined by Parfitt and colleagues (1987) in the ASBMR guidelines.

Quantitative Assessment of Cancellous bone

Bone's trabecular network has been of great clinical interest (Odgaard & Gunderson, 1993) in terms of evaluating changes in its morphology and connectivity due to disease states (i.e. osteoporosis). As such, a wealth of parameters and indices exist in order to track and measure these alterations.

Borah and colleagues (2001) described a number of parameters to quantify the various aspects of cancellous bone microarchitecture. Measurements include, but are not limited to: (1) Bone Volume/Tissue Volume (BV/TV), (2) Bone Surface/Tissue Volume (BS/TV), (3) Trabecular Thickness (TbTh), (4) Connectivity Density (Conn.D), (5) Marrow Star Volume, (6) Percent Plate, and (7) Direct Trabecular Thickness (Borah et al., 2001). Quantifying these

measures can be completed three-dimensionally by counting voxels (Müller & Rüegsegger, 1995).

Additionally, techniques exist for quantifying the orientation of trabeculae via assessing its degree of anisotropy. Anisotropy refers to a material whose properties and technical properties are different when measured in various directions. Anisotropic principles can be applied to trabeculae by evaluating their directionality. If trabeculae are biased in one preferential direction, they are thought to be anisotropic. Particular parameters have been developed to quantify the degree of anisotropy including mean intercept length, volume orientation, star volume distribution and star length distribution (Odgaard, 1997). The mean intercept length (MIL), generally involving a count of the intersections between a grid and the bone/marrow boundary, is among the most commonly applied approach. Measures of trabecular connectivity are also important parameters to consider when evaluating mechanical quality of cancellous bone (Kabel et al., 1999). Connectivity generally reflects the number of holes or gaps in the latticework-type structure (Odgaard & Gunderson, 1993). To determine an unbiased estimate of connectivity density, a topological property referred to as the Euler characteristic of 3D data, should be applied (Kabel et al., 1999; Hildebrand & Rüegsegger, 1997b).

Connectivity density is a common parameter that divides connectivity by the total volume of the region of interest (ROI). Other measures include volume fraction and surface density. Additionally, an independent morphometric parameter for assessing the Structural Model Index (SMI) of cancellous bone was developed by Hildebrand and Rüegsegger (1997b). The SMI is used to quantitatively differentiate 3D forms of trabeculae such as ‘rod-like’ and ‘plate-like’ types. As the SMI does not provide information on trabecular connectivity, it should be used in concert with the aforementioned connectivity parameters.

Parfitt and colleagues (1983b) introduced the plate model that enhanced the perception of cancellous bone structure (Odgaard & Gunderson, 1993). This model assumes that trabeculae are unbounded plates that are parallel in orientation. Assuming this particular structure, various measurements can be quantified such as trabecular plate density, and trabecular plate separation and thickness. Assumptions of this model, however, include that the architecture is indeed plate-like. Certain researchers (Kleerekoper et al., 1985) have failed to check the model assumptions, and thus results were interpreted incorrectly (Odgaard & Gunderson, 1993).

Quantitative Assessment of Cortical Bone Morphology

Cortical microarchitecture develops and remodels in three-dimensions. Thus, 3D analysis will provide a more comprehensive understanding of cortical bone dynamics. Quantification of cortical bone morphology can be accomplished on two scales: (1) gross measurements of bone morphology and bone geometry, and (2) the cortical canal network. Gross measurements for conventional 2D histomorphometric analysis include: Total Subperiosteal Area (Tt.Ar), the area under the subperiosteum including endosteal area, (2) Endosteal Area (En.Ar), the area of the marrow cavity, (3) Cortical Area (Ct.Ar), the amount of cortical bone in a rib cross-section, (4) Cortical Thickness (Ct.Th), mean thickness of the cortex (Parfitt et al., 1987).

Cortical Bone Microstructure

Since the introduction of 3D imaging of bone microstructure in 1989 (Feldkamp et al., 1989), numerous studies have employed micro-CT to image the complicated cortical canal network in human bone (Basillais et al., 2007; Borah et al., 2010; Cooper et al., 2006). Cooper and colleagues (2003), however, were the first to report on cortical bone porosity and the cortical canal network using micro-CT.

Basillais and colleagues (2007) suggested a voxel size of 10 microns or less is necessary for quantifying the 3D structure of cortical canal networks due to their complicated nature. Thus, applications of geometric assessment parameters are preferred in lieu of topological approaches (Cooper et al., 2003). Measures such as tissue volume, canal volume, and canal surface can be measured in 3D. To measure canal connectivity (Ca.ConnD) and canal length (Ca.Le), Cooper and colleagues (2003) developed imaging analysis software to analyze results of a skeletonization technique. This approach is generally accomplished by applying a 3D algorithm that strips away layers of voxels to revel a skeleton of an image. Canal connectivity and canal length can be subsequently measured by assessing the number of canal intersections and the distance between the interconnecting nodes. The SMI is also applicable to cortical canals since their cylindrical shape is in general accordance with the 'rod-like' trabecular type discussed by Hildebrand and Rüegsegger (1997b). In addition to the examination of cortical canal networks, Cooper and colleagues (2006) used micro-CT to assess age, sex, and morphological differences of BMU-related resorption spaces in human femora.

Micro-CT: Desktop

There are two primary micro-CT systems in existence that can be applied to the examination of bone tissue: (1) laboratory or desktop, and (2) SR micro-CT.

Laboratory or desktop micro-CT systems have been used as a tool to analyze bone in 3D since 1989 (Feldkamp, 1989). These self-contained commercial systems use polychromatic microfocus x-ray tubes to image specimens at high resolutions. The potential of micro-CT to fields such as bone biology and anthropology was quickly recognized. The desktop systems have been used broadly and studies span from the evaluation of cancellous bone morphology in humans and non-human primates, to the analysis of teeth and examination of fossil remains

(Cooper et al., 2012). The non-destructive nature is a crucial factor in its popular use, as well as the ability to quantitatively analyze the resulting 3D images following reconstruction. The resolution of these systems is limited by the spot size and energy of the x-ray tube, which are mutually exclusive.

Micro-CT: Synchrotron radiation micro-CT

In the 1960's, first generation SR sources were introduced which functioned by retrieving synchrotron radiation parasitically from a ring used in particle physics research. In the late 1960's-1980's, 1.5 generation sources were in existence which acquired SR from an electron storage ring. Second generation sources retrieved SR from an electron storage ring specifically built as light sources for the production of SR. The addition of wiggler insertion devices was later added to the second-generation sources. Third generation sources, including the Canadian Light Source, were introduced in the mid-1990's. These are high throughput facilities that use smaller electron beams and undulator magnets, and have dedicated electron storage beam sources designed to maximize brightness. The most recent are fourth generation SR sources (2005-present), which use high-energy linear accelerators and offer a great increase in brightness (Wurtz, 2014; CLS Summer School Lecture: Synchrotron 101).

In SR micro-CT facilities, x-rays are produced by the passage of an electron beam that travels close to the speed of light through electromagnets. The generated x-ray beam travels down a beamline where it can be optionally filtered by a monochromator. As such, radiation of a specific wavelength or energy can be selected for. The flux, or number of x-ray photons passing through an area over a given time, is much greater in magnitude than desktop micro-CT systems. As a result, high-resolution submicron level imaging can be achieved (Schneider et al., 2007). The brilliance of radiation can produce high-resolution images of spectacular quality, reduced

scan times, faster and more accurate quantitative measurements, and certain beamlines have the potential to handle much larger objects than desktop CT (Cooper et al., 2012; Carter et al., 2013b).

Synchrotron Techniques

Imaging biological tissues at synchrotron facilities also allows for the application of additional contrast mechanisms. Specialized imaging techniques that can be combined with SR micro-CT include, but are not limited to, *K*-edge Subtraction Computed Tomography (KES), Diffraction Enhanced Imaging Computed Tomography (DEI), and Phase Contrast Imaging (PCI).

To summarize the techniques generally, KES allows for the quantifiable 3D imaging of contrast materials (either natural or induced) such as iodine, barium, strontium or lead (Zhu et al., 2014). This technique has been applied to studies of human vasculature and lungs, and brain tumor imaging (Thompson et al., 1984; Kelly et al., 2007; Suhonen et al., 2008; Adam et al., 2005). KES can also be used to track the accumulation of bone turnover *in vivo* using elemental tracers such as strontium (Cooper et al., 2012b). Though KES is a powerful approach, it is limited by the need for high quality images that are perfectly matched. The subject or sample must be imaged twice at two energies at separate times, thus movement during imaging is a serious concern.

DEI relies on the use of an analyzer crystal between the object and detector. As the x-ray beam passes through an object, it refracts across tissue or materials in the sample and alters the angle of various parts of the beam. This technique allows for the extraction of absorption and refraction information, provides great tissue contrast, and produces images that are almost completely free of scatter (Chapman et al., 1997).

PCI is an intuitive and commonly employed technique at synchrotron facilities that provides excellent image quality of soft tissue structures. Conventional medical imaging systems use polychromatic beams that rely almost completely on x-ray absorption, while ignoring information produced by scattering within tissues. Phase shifts, generated as photons pass through tissues and scatter, are capable of producing greatly enhanced contrast (Zhou & Brahme, 2008). The resulting phase contrast decreases at a slower rate with increasing x-ray energy than absorption contrast, while being more tolerant to noise. There are several methodologies, including interferometry, DEI, and diffraction grating phase contrast, used for exploiting phase shift that have been incorporated into synchrotron-based techniques. The majority of these techniques use a monochromatic x-ray beam combined with further crystal optics to refine it. PCI has also been demonstrated to have potential for imaging porosity, delineating osteon boundaries in cortical bone (Cooper et al., 2011), and osteocyte lacunae (Carter et al., 2013a).

SR micro-CT and Osteocyte Imaging

SR micro-CT is revolutionizing the current understanding of bone structural biology by contributing novel 3D data. SR micro-CT has recently been extended to examining human bone at the cellular level, which will continue to contribute to the understanding of bone adaptation, disease, and aging (Schneider et al., 2007; Maggiano et al., 2016; Carter et al., 2013a; 2013b; 2014a).

Micro-CT technology has allowed researchers to quantitatively analyze osteocyte lacunae. Since osteocytes are soft tissue structures which are deeply encased within the bone matrix, they cannot be visualized using available X-ray imaging techniques. As such, their associated cellular spaces (lacunae) are used as substitutes. Though former studies have examined osteocytes and their lacunae in both human and non-human animals, quantifying

osteocyte population density has been problematic due to limitations of traditional lower-resolution imaging techniques (Qiu et al., 2003b; Carter et al., 2013a).

Prior research examining cellular spaces has been achieved using 2D histologic modalities (Parfitt, 1983b; Qie et al., 2002; Vashishth et al., 2005; Mullender et al., 1996). For example, Parfitt (1983b) described the subjectivity in determining osteocyte lacunar geometry using 2D histologic sections. He presented measurement data from three sectioning planes (major longitudinal, transverse, and minor longitudinal), combining them to form a reconstructed 3D image. The author states, however, that a single osteocyte lacuna will display a great variety of shapes and sizes depending on the sectioning plane employed. Also, Qiu and colleagues (2003) noted that penetration depth associated with traditional light microscopy could only reach a few microns below the bone specimen's surface. As such, results concerning osteocyte density were extrapolated and assumed for the entire bone section. Disadvantages of these methods include their inherent 2D nature, which leads to extrapolation of results and the possibility of introducing a large margin of error, variation in sectioning planes, limited penetration depths and regions of interest, and destruction of samples.

Confocal microscopy has been used to acquire high-resolution microscopic images while also allowing for 'optical sectioning' of cortical bone (Cooper et al., 2012). Using this technique, serial images are acquired that can be amended to 3D reconstruction and further analyses. Due to the high-resolution images acquired, minute bone features such as osteocyte lacunae, as well as very small canaliculi, can be assessed (Qiu et al., 2002). A disadvantage of this technique, however, is that the penetration depth achievable is only 1 mm. Thus, osteon morphology and canal network organization cannot be ideally assessed quantitatively.

Alternatively, employing SR micro-CT imaging has allowed for hundreds of thousands of osteocytes to be visualized and analyzed. This high-resolution imaging modality presents an opportunity to consider osteocytes individually, as well as examine them in terms of the larger population. Carter and colleagues (2013a) were the first to examine osteocyte lacunar density and morphology between cross-sectional regions in human femora.

Lacunar morphology has not been widely studied, and little is known regarding their normal variation in human skeletal elements. Carter and colleagues (2013a; 2013b; 2014a) have recently evaluated osteocyte morphology, spatial distribution, regional variation, and density in human femora. In their 2013a study, the authors examined osteocyte lacunar density and morphology between cross-sectional regions in human femora. Results indicated that extensive regional variation (~30%) in osteocyte lacunar density exists, with the medial and lateral segments having the most lacunae and the anterior and posterior displaying the least (Carter et al., 2013a). In terms of lacunar shape, the anterior and posterior regions revealed more elongated lacunae than other segments. Additionally, the authors reported a higher total number of osteocyte lacunae compared to previous studies based on 2D imaging techniques (Carter et al., 2013a). These differences may be attributed to the employment of SR micro-CT and the evaluation of a larger region of interest.

Anthropological Potential of SR micro-CT

Non-destructive 3D imaging methods offer a wealth of potential for the anthropologist. The ability to image bone in 3D provides an additional tool to investigate age-related changes associated with bone remodeling. For example, Cooper (2005) has demonstrated that examining the cortical canal network in 3D offers useful information regarding adult age at death.

The 3D examination of bone microarchitecture also holds promise for examining bone loss in past populations. Scholars have warned against the use of certain clinical technologies, particularly dual energy x-ray absorptiometry (DXA), for the examination of bone loss in archaeological remains. In comparison with many other histological techniques such as light microscopy, DXA performed poorly (Cooper et al., 2012a). As such, using 3D imaging techniques provide a more accurate and direct comparison between archaeological and modern samples.

Overall, the application of 3D imaging technologies to biomedical and bone biology research is considerable and offers tremendous future potential to the field of anthropology.

Summary

Since cortical bone develops and remodels in three-dimensions, examining bone's histomorphology in 3D provides a more comprehensive and accurate understanding of its true structure than is possible with 2D techniques. The preceding discussion provided a brief history of 3D imaging and conventional histological 3D methods, and compared and contrasted both desktop and synchrotron-based micro-CT systems. The associated strengths and weaknesses of these approaches were presented, and applications of 3D imaging to anthropological research was discussed.

For the most part, the above imaging modalities offer a tremendous improvement over traditional 2D cross-sectional methods for the visualization of cancellous and cortical bone. As such, visualizing and analyzing bone using high-resolution 3D imaging modalities will continue to improve current understandings of bone biology.

CHAPTER FIVE: METHODS

This study examines whether histological structure that distinguishes cortical and cancellous bone relate to different nuclear DNA yields among skeletal elements. To investigate this question, skeletal samples from adult human cadaveric remains were used. This chapter discusses the selection criteria of these skeletons and the methods used to image their bones in three-dimensions at high microscopic resolution. Methods for measuring and statistically analyzing these images are further discussed.

The William M. Bass Donated Skeletal Collection

Data for this dissertation were sourced from the William M. Bass Donated Skeletal Collection, housed in the Department of Anthropology at the University of Tennessee, Knoxville. The William M. Bass Donated Skeletal Collection was founded in 1981 and has since grown exponentially. As of this writing, the collection consists of human skeletal remains from approximately 1,600 modern individuals. The collection demographics include Americans of European (91%), African (7%) and Hispanic (2%) ancestry, which generally reflects the demographic composition of the East Tennessee region (Shirley et al., 2011; Vidoli, 2015). It is comprised of approximately 70% males and 30% females with ages at death ranging from fetal to 101 years.

Over 2,000 individuals currently have pre-donation paperwork on file indicating their requests for their bodies to be donated to the Forensic Anthropology Center (FAC) for research purposes. The FAC donation paperwork requires information from prospective donors including sex, weight, date and place of birth, photographs, and medical and dental history, among other attributes. Information is self-reported by donors, however family members may also provide data to the best of their knowledge. A wealth of postmortem information is also gathered at the

time of donor intake. This process involves documenting height and weight, as well as the retrieval of blood, hair, and nail samples prior to placement at the Anthropology Research Facility (ARF) for natural decomposition.

Study Sample

The study sample comprised cortical and cancellous bone tissues from the three skeletons used in the Mundorff and Davoren (2014) study. The three individuals are male donors who: (1) died in the same calendar year, (2) decomposed on a designated plot of land and in the same position (prone on the ground surface) at the ARF at the University of Tennessee, Knoxville, (3) were between the ages of 40 and 69 years at the time of death, and (4) had no known bone-affecting conditions at the time of death (Mundorff et al., 2012). Confounding taphonomic variables were limited by studying donated individuals who were exposed to the same gross environmental conditions, and decomposed in the same geographic location (Mundorff & Davoren, 2014).

The William M. Bass Donated Skeletal Collection donation numbers were assigned research numbers of: #1, #2, and #3. Individual #1 was a 50-year-old male. Duration of placement at the ARF lasted twelve months and twenty-seven days. Individual #2 was a 47-year-old male, and placement lasted fifteen months and twenty-six days. Individual #3 was a 69-year-old male. Placement lasted twenty-two months and twenty-two days.

Placement ranges varied according to the month the individual died, and the availability of FAC staff for skeletal recovery (Mundorff et al., 2012). Recovery of the remains included removing the bones from the ground surface followed by screening the dirt and debris surrounding and beneath each skeleton. All skeletal elements were transported to the former Lake Avenue processing building on the University of Tennessee, Knoxville campus. Adhering

dirt and/or tissue from the surface of the bones was removed with room-temperature water and a toothbrush. The remains of each individual were separately placed on metal trays and then transferred to a drying rack. The dry skeletal remains were then transported to Dr. Amy Mundorff's office in the Department of Anthropology to be photographed, marked for sampling, and shipped to the DNA laboratory for testing. Specific element and sample site selection criteria were established between Mundorff and FAC management.

Methods

The following section describes the methodological approaches employed to ascertain whether differences in bone microstructure can be used to explain differential nuclear DNA yield among bone tissue types. The Canadian Light Source (CLS) synchrotron facility in Saskatoon, Saskatchewan (SK), Canada, is also described here.

Bone Sampling Methodology for 3D Imaging

Prior to bone sampling, ethical approval was obtained from the University of Tennessee (UTK IRB-15-02071-XM**)** and the University of Saskatchewan (Bio # 15-47). Dr. Dawnie W. Steadman, Director of the FAC, also approved a destructive analysis request for all individuals.

Forty-three bones were selected for SR micro-CT imaging from the fifty-five elements per skeleton sampled for DNA by Mundorff and Davoren (2014) (**Table 6.1**). Representatives from each skeletal element type were chosen and bones from the left side only were sampled for consistency. A total of 129 samples were prepared in the Molecular Anthropology laboratory at the University of Tennessee, Knoxville.

The analysis was limited by a small specimen size since the camera field of view cannot exceed 2 mm. Rectilinear bone blocks with dimensions of approximately 2 x 2 x 10 mm were

removed from each intact skeletal element directly adjacent to the DNA sampling site procured by Mundorff and Davoren (2014). This sampling location was selected in order to directly compare the osteocyte lacunar parameters with the DNA yield results from the same general location on each bone. Prior to sampling, the 2 x 2 x 10 mm area on each bone was measured with sliding calipers, marked in pencil (**Figure 6.1**), and photographed.

Each bone specimen was procured from the same region of each element for all three individuals to eliminate inter-individual variation in lacunar properties. Bones were secured in a gripping device for stability during sampling. All samples were removed using a Dremel 8200 drill at 15 RPM with a 7/8-inch diamond wheel attachment. The skeletal elements were photographed again following sampling (**Figure 6.2**). Specimens were further refined using an Isomet precision diamond-wafer saw to achieve dimensions of approximately 1.8 x 1.8 x 10 mm. All samples were fixed in a 70% ethanol solution and then dried. The author transported the prepared skeletal specimens to the CLS for SR micro-CT imaging.

The Canadian Light Source (CLS)

The CLS synchrotron facility is Canada's national centre for synchrotron research. One of only twenty-four synchrotron facilities globally, it is a cutting-edge research facility dedicated to advancing Canadian science, and enhancing the competitiveness of Canadian industry. Since 2005, the CLS has hosted approximately 2,500 researchers from academic institutions, government, and industry from 10 provinces and territories, and produced over 1,500 scientific publications (www.lightsource.ca). Organizations that contribute to CLS funded projects include the Canada Foundation for Innovation, the Natural Sciences and Engineering Research Council of Canada, the National Research Council of Canada, the Canadian Institutes of Health Research,

Table 6.1: Sample list of the forty-three skeletal elements and the specific sampling locations on the bone, apportioned by body region.

Body Region(s)	Skeletal Element	Sampling Location
Skull	Frontal	Posterior to DNA sampling site
	Parietal	Posterior to DNA sampling site
	Temporal	Superior to DNA sampling site
	Occipital	Posterior to DNA sampling site
	Maxilla	Antero-lateral of DNA sampling site
	Mandible	Inferior to DNA sampling site
Thorax and Abdomen	Cervical Vertebra	Posterolateral aspect of vertebral body; lateral to DNA sampling site
	Thoracic Vertebra	Posterolateral aspects of vertebral body; posterior to DNA sampling site
	Lumbar Vertebra	Posterolateral aspect of vertebral body; posterior to DNA sampling site
	First Rib	Medial surface; superior to DNA sampling site
	Middle Rib	Inferior surface; inferior to DNA sampling site
	Twelfth Rib	Medial surface; inferior aspect of DNA sampling site
	Scapula	Anterolateral aspect of scapula; ~1.5 cm from glenoid fossa
	Clavicle	Superior surface; lateral to DNA sampling site
	Ilium	Dorsal surface; directly inferior to iliac crest
	Ischium	Dorsal surface; 1.5 cm right of ischial tuberosity
	Pubis	Dorsal surface; ischiopubic ramus
	Sacrum	Ala; superior to DNA sampling site
Lower Limb	Femur	Anteromedial surface; inferior to DNA sampling site
	Tibia	Anteromedial surface; inferior to DNA sampling site
	Fibula	Medial surface; superior to DNA sampling site
	Patella	Medial facet on posterior surface; lateral to DNA sampling site
Foot	Metatarsal 1	Medial surface; proximal to DNA sampling site
	Metatarsal 2	Medial surface; distal to DNA sampling site
	Metatarsal 3	Lateral surface; distal to DNA sampling site
	Metatarsal 4	Medial surface; distal to DNA sampling site
	Cuneiform 1	Anteromedial surface
	Cuneiform 2	Medial surface
	Cuneiform 3	Lateral surface; ~0.2 cm from articular facet for metatarsal 2; lateral edge
	Navicular	Distal surface; articular facet for cuneiform 2; lateral edge
	Cuboid	Ventral surface; distal to sampling site
	Talus	Anterolateral and distal surface of talar dome
	Calcaneus	Superior surface; ~2 cm from posterior articular facet
	First Proximal Phalanx	Anterior surface; distal to DNA sampling site
	First Distal Phalanx	Anterior surface; distal to sampling site
Upper Limb	Humerus	Anterior mid-shaft; ~5 cm inferior from deltoid tuberosity; superior to DNA sampling site
	Ulna	Anteromedial surface; superior to DNA sampling site
	Radius	Superior aspect of DNA sampling site; distal third of diaphysis

Table 6.1: (cont).

Body Region(s)	Skeletal Element	Sampling Location
Hand	Capitate	Anterior surface; ~1 cm proximally from articular surface for metacarpal 3
	Metacarpal 2	Anterior surface; distal end; ~1 cm from head
	Metacarpal 3	Lateral surface; proximal to DNA sampling site
	Metacarpals 4	Anterior surface; distal end; ~1 cm from head
	First Proximal Hand Phalanx	Distal end; lateral surface; proximal to DNA sampling site
	First Distal Hand Phalanx	Anterior surface; distal to base, lateral to DNA sampling site

Figure 6.1: Left scapula from individual #3 displaying specimen site marked with pencil (black arrow), prior to removal.

Figure 6.2: Left scapula from individual #3 displaying specimen site (black arrow) following removal.

the Government of Saskatchewan, Western Economic Diversification Canada and the University of Saskatchewan.

Data collection for this study was performed at the BioMedical Imaging and Therapy (BMIT) beamlines at the CLS. The BMIT beamlines are designed for imaging biological tissues. Research time (beam time) for this research was awarded through a competitive peer-review process (Proposal #21-6666). The peer-review committee is composed of CLS scientists and external reviewers from synchrotron facilities worldwide. Beam time is allocated based on each proposal's ranking in scientific merit, in relation to all other proposals for a given beamline. The author received forty-six eight-hour research shifts during two cycles in 2015.

Justification for Use of SR micro-CT

As bone exists and remodels in three-dimensions, alternatives to high-resolution 3D imaging such as 2D histological methods will not achieve the resolution, efficiency, or precision required to address the proposed research question. Employing transmitted light to assess 2D cross-sections results in having to extrapolate histological feature counts, creating a potentially large margin of error.

Preliminary imaging of human femoral bone using the BMIT-ID beamline at the CLS previously revealed that high-resolution scans of approximately 0.9 μm can be achieved. The imaging protocol successfully demonstrated that osteocyte lacunae could be visualized and subsequently quantified. The Bruker (Kontich, Belgium) system at the CLS BMIT facility was specifically designed for imaging osteocyte lacunae.

The author collaborated with a local research group at the University of Saskatchewan lead by Dr. David Cooper. This group's success at BMIT is evidenced by multiple experimental projects and publications focused on 3D imaging of bone, resulting in peer-reviewed publications. Additionally, the availability of visualization and reconstruction software and sample preparation materials available at BMIT makes it an ideal facility for this type of imaging.

Employing SR micro-CT using the BMIT beamline at the CLS is a proven technique that yields high-resolution required to visualize the designated microscopic features. This set-up produced excellent results that allowed lacunar parameters such as density and volume to be analyzed. The resolution also allowed for visualization of other microstructural features including osteonal borders and remnants of soft tissue in the medullary cavity.

Imaging and Image Analysis Methodologies

Various specialized 3D imaging and image analysis techniques were used in order to increase the bone microstructural information gathered from all specimens. Skeletal elements were imaged using both clinical Computed Tomography (CT) and SR micro-CT to obtain data on the microstructural variables.

Imaging Methods

Clinical Computed Tomography

Clinical CT scans of the originally sampled bones were acquired to assess potential differences in cortical and cancellous bone volume contributing to the DNA results. For each sampling site, a 3/8" circular hole had been drilled to remove 0.2 grams of bone powder (Mundorff et al., 2012). CT scans were used to calculate the sample site's approximate volume in cortical and cancellous bone tissue.

CT images were acquired with assistance from Ms. Shelley Acuff and Dr. Yong Bradley at the University of Tennessee Medical Center. All CT scans were acquired using a Siemens Biograph mCT 64 slice scanner. Scans involved helical acquisition using a 0.6 mm slice thickness, 500 mAs, 120 kV, and bone window with kernel B70s. Data were stored on compact discs and transferred to workstations with image processing software (OsiriX 5.6, Geneva, Switzerland).

SR micro-CT

A custom built stage and Bruker (Kontich, Belgium) micro-CT set-up previously created by BMIT staff members was used for this study (**Figure 6.3**). Each fixed bone specimen was mounted on a brass pin holder on the stage (**Figure 6.4**). To ensure that the sample did not shift

during scan rotation, which would increase the possibility of motion artifacts, dental wax and an adhesive were applied to the brass pin. The adhesive was dissolved following scanning.

Images were obtained using monochromatic x-rays on the BMIT beamline. A Bruker (Kontich, Belgium) micro-CT system was used with a photon energy of 30 keV and an effective pixel size of 0.9 μm. An exposure time ranging from 360-1250 milliseconds and four-frame averaging was employed. As the storage ring current decreases from a peak of 250 mA over time following injection, the exposure time was tuned to maintain 20% saturation on the detector. A rotation step of 0.25 and 2x2 binning were used to obtain 720 projections spanning 180° of rotation. This protocol resulted in a scan time of approximately 75 minutes per sample. The projection images were reconstructed to create a 3D dataset of the 720 slices for each specimen.

The beam team assisting the author with 3D imaging included Isaac V. Pratt, Danielle Kabatoff, Kim Harrison, and Dr. David Cooper from the Anatomy and Cell Biology Department at the University of Saskatchewan.

Image Analysis

The following section describes the procedures used to visualize and quantify the data using commercial imaging packages.

Clinical CT Data

Clinical CT scans were evaluated using OsiriX 5.6. The DNA sampling site on each element was digitally measured using ImageJ (National Institutes of Health). A macro was created to detect and measure the areas of cortical and cancellous bone (mm) on each CT slice where the sampling site appeared. Measurements of cortical width and height (**Figure 6.5**) and cancellous width and height were taken separately for each cortical and cancellous bone region

for all bones. Average cortical and cancellous bone width and height measurements were then computed for each site.

SR micro-CT: 3D Quantitative Morphometry

The SR micro-CT projection images were reconstructed using NRecon (Bruker, Kontich, Belgium), a commercial GPU accelerated filtered back projection based reconstruction software package. Image stacks were cropped and analyzed using CT Analyser 1.15.4.0 (Bruker, Kontich, Belgium), following protocols described by Carter and colleagues (2013a). Cylindrical ROIs were identified within each bone sample with a diameter of 0.7 mm, a height of 0.7 mm, and a volume of 0.27 mm^3 for both cortical and cancellous bone regions. This produced matching ROI volumes of interest from which all measurements were acquired.

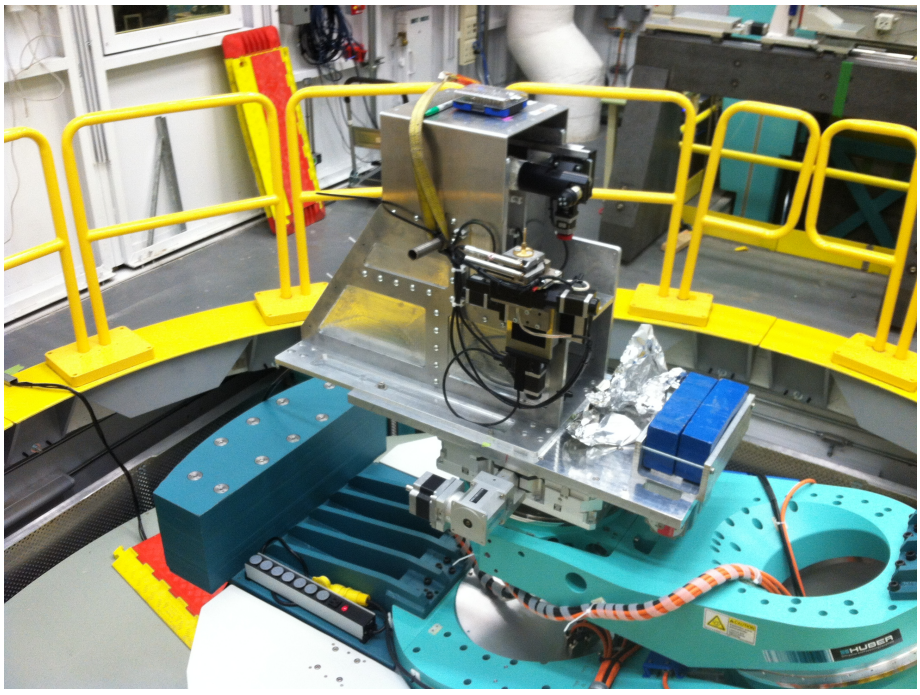

Figure 6.3: Custom built stage and Bruker (Kontich, Belgium) micro-CT set-up at BMIT.

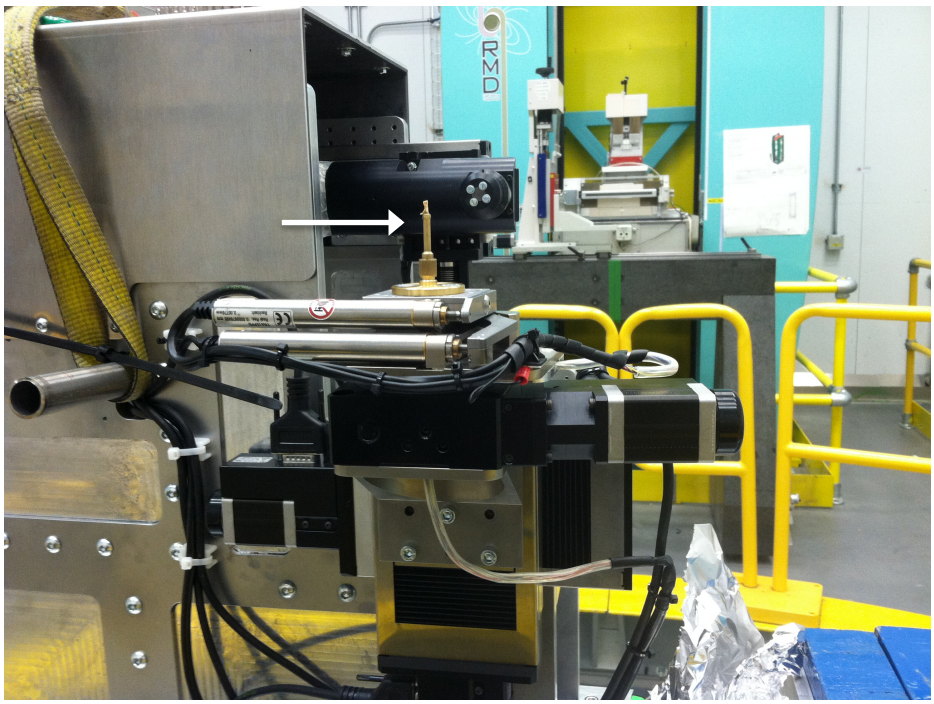

Figure 6.4: Fixed bone specimen mounted on brass pin holder (white arrow).

Visuals of single slices of cortical and cancellous bone ROIs are depicted in **Figures 6.6-6.7**, and 3D renders of the same bone specimens are presented below (**Figures 6.8-6.9**).

Osteocyte lacunae were separated from the high-density bone using global thresholding. Segmentation, a process of separating air-filled spaces, was applied to separate the lacunae from the surrounding higher-density bone. Despeckling (denoising) was conducted to remove noise (structures less than 10 μm^3). Elements above 2000 μm^3 were assumed to be canals and remaining structures were designated as lacunae. The above volume limits are based on previous confocal microscopy measurements, which determined human osteocyte volumes range from 28-1713 μm^3 (Carter et al., 2013a; McCreadie et al., 2004). Subsequently, 3D renders of bone microarchitecture were created using AMIRA (Visage Imaging, Berlin, Germany) imaging software.

Standard nomenclatures for canal and lacunar indices were applied for the analysis of three-dimensional lacunar parameters within the ROIs (Cooper et al., 2003; Schneider et al., 2007; Carter et al., 2013a). The variables measured included: (1) total ROI volume (TV); (2) total canal volume within ROI (Ca.V); (3) average canal diameter (Ca.Dm); (4) total number of lacunae (N.Lc); and (5) average lacunar volume (Lc.V). To determine lacunar density per mm^3 (N.Lc/BV), bone volume (BV) was calculated as total volume minus canal volume (TV-Ca.V). As cancellous bone lacks Haversian systems, and thus central vascular channels, BV for cancellous bone ROIs was calculated as total volume minus the volume of the marrow spaces.

To address the primary hypothesis, bones identified by Mundorff and Davoren (2014) to yield more DNA per mass of sample were directly correlated against the number of lacunae and osteocyte lacunar density data. The element types that produced higher quantities of DNA are hypothesized to have greater osteocyte lacunar densities.

Analytical Methods

This study aims to: (1) identify the approximate amount of cortical and cancellous bone tissue removed from the original nuclear DNA sampling sites; and (2) describe the relationship between osteocyte lacunar parameters and bone tissue type. Statistical analyses were accomplished using SPSS 23.0 statistical software (Chicago, IL, USA) with a significance of $\alpha \leq 0.05$.

It is important to note that the clinical CT and SR micro-CT data are cross-sectional and not longitudinal in nature, and thus can only infer cause and effect relationships between nuclear DNA yield and bone tissue type. The limitation of this approach is that it ignores variance in osteocyte lacunar parameters within and among individuals over time. As this study is focused on assessing histomorphometric variables from the Mundorff and Davoren (2014) study sample,

and not analyzing patterns in the parameters for each individual over time, the use of cross-sectional data is justified.

To assess within- and between-subject differences in bone tissue types for all clinical CT and SR micro-CT parameters, with the exception of the cortical canal measures, Repeated Measures Analysis of Variance (RM-ANOVA) statistical tests were selected. This approach considers dependency when two experimental units, parameters of cortical and cancellous bone tissue in this case, are being assessed within a single individual. The between-subjects effects also allows for the parameters to be evaluated among individuals. In addition to normality, RM-ANOVA has an assumption regarding the type of variance-covariance matrix. When the variances and covariances are equal, the matrix has compound symmetry and is sufficient for a repeated measures *F* test to be distributed as an *F* distribution (Rasmussen, 1987). If the assumption of variance-covariance homogeneity is violated, alternate approaches can be considered that include using: (1) a degrees of freedom adjustment, (2) only two repeated measures for the main analysis, and (3) a non-parametric bootstrapping procedure as an alternative to the RM-ANOVA.

The bootstrap uses a resampling approach to generate the sampling distribution of a statistic. Lunneborg and Tousignant (1985), who recommended the bootstrap approach as an alternative to the RM-ANOVA, cited two advantages of this method over parametric statistics: (1) the bootstrap is free from assumptions of normality and equality of variances, and (2) confidence intervals and significance levels are generated from the bootstrapped sampling distribution (Lunneborg & Tousignant, 1985). Calculation of confidence intervals using a non-parametric bootstrapping method provides more biologically meaningful information since it will determine which linear distances are statistically different between samples.

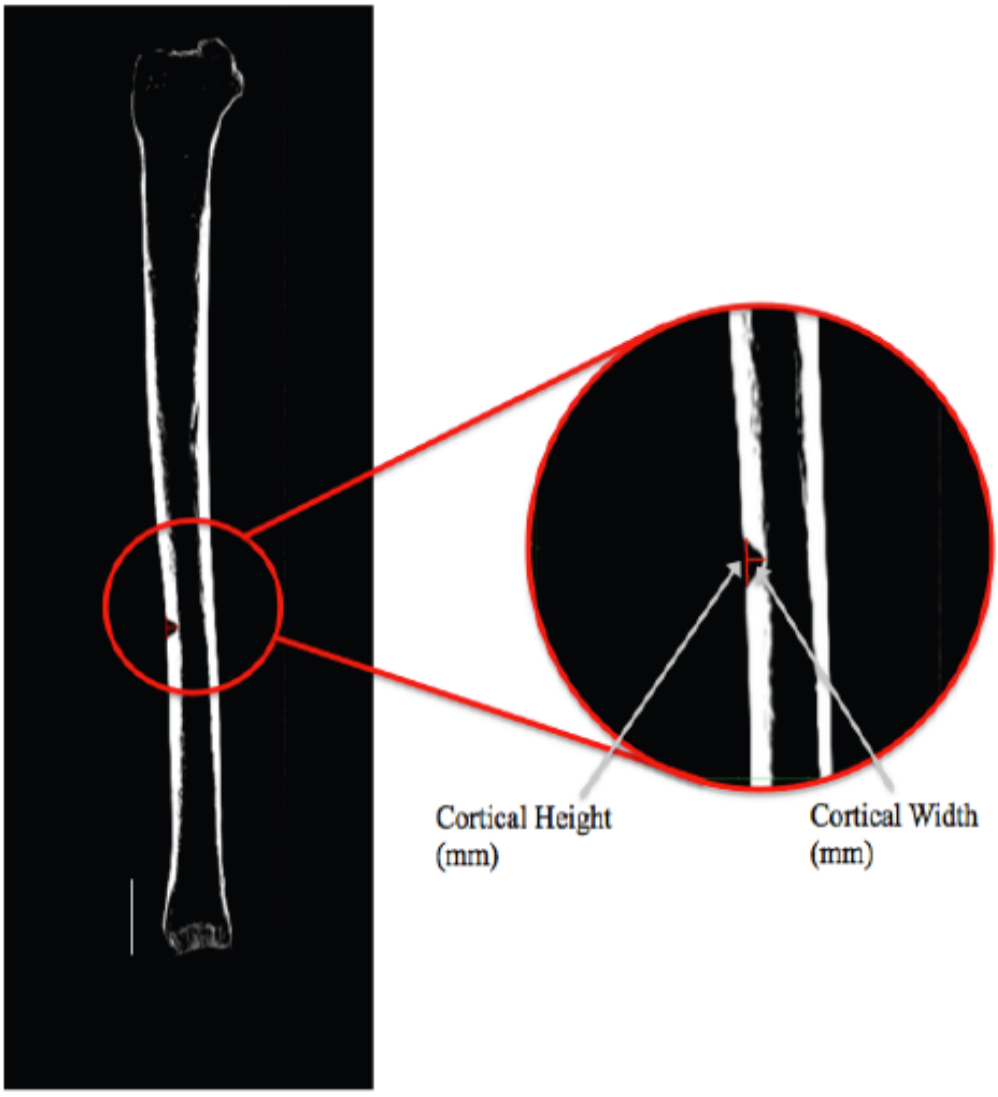

Figure 6.5: DICOM image from OsiriX software of a left tibia from a single CT projection. The circular window indicates the DNA sampling site. The superimposed enlargement displays the cortical height and width measurements (mm). Scale =400 mm. (Credit: JM. Andronowski).

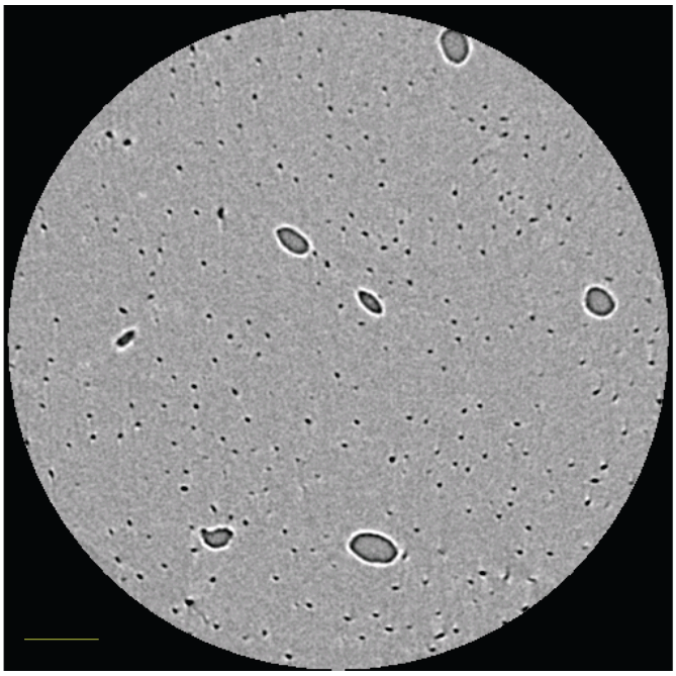

Figure 6.6: SR micro-CT single slice of a cortical bone circular ROI. (Credit: JM. Andronowski). Scale=100 μm.

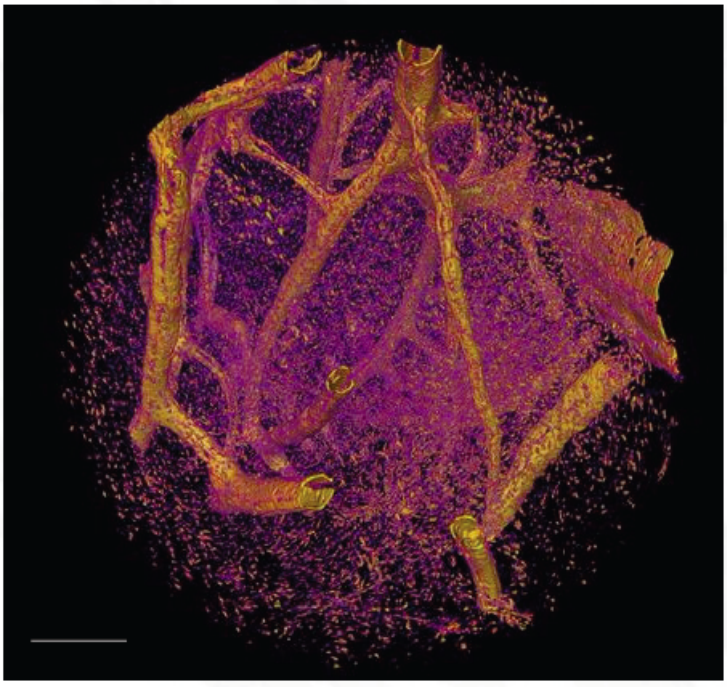

Figure 6.7: SR micro-CT 3D render of a cortical bone circular ROI. (Credit: JM. Andronowski). Scale=100 μm.

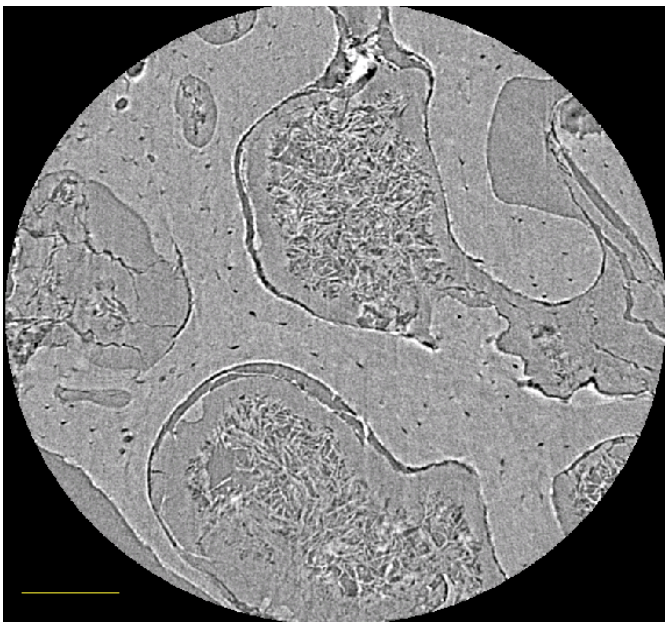

Figure 6.8: SR micro-CT single slice of a cancellous bone circular ROI. (Credit: JM. Andronowski). Scale=100 μm.

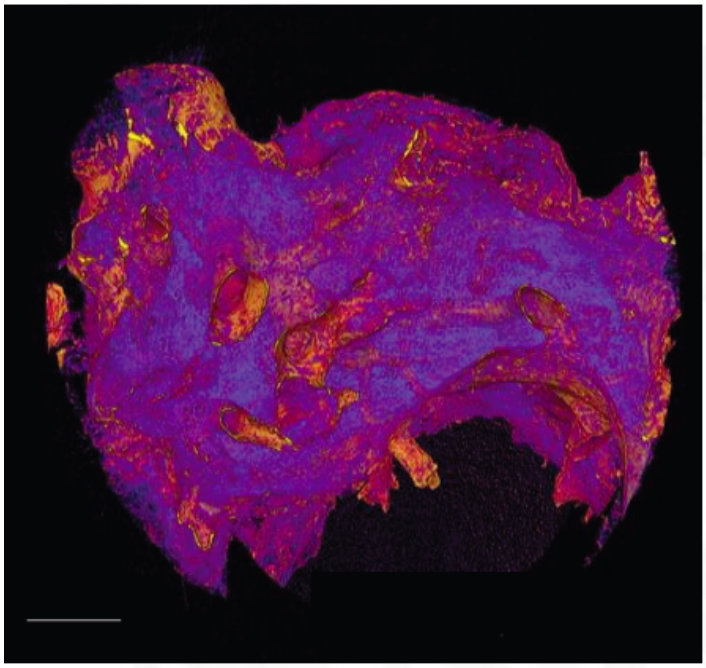

Figure 6.9: SR micro-CT 3D render of a cancellous bone circular ROI. (Credit: JM. Andronowski). Scale=100 μm.

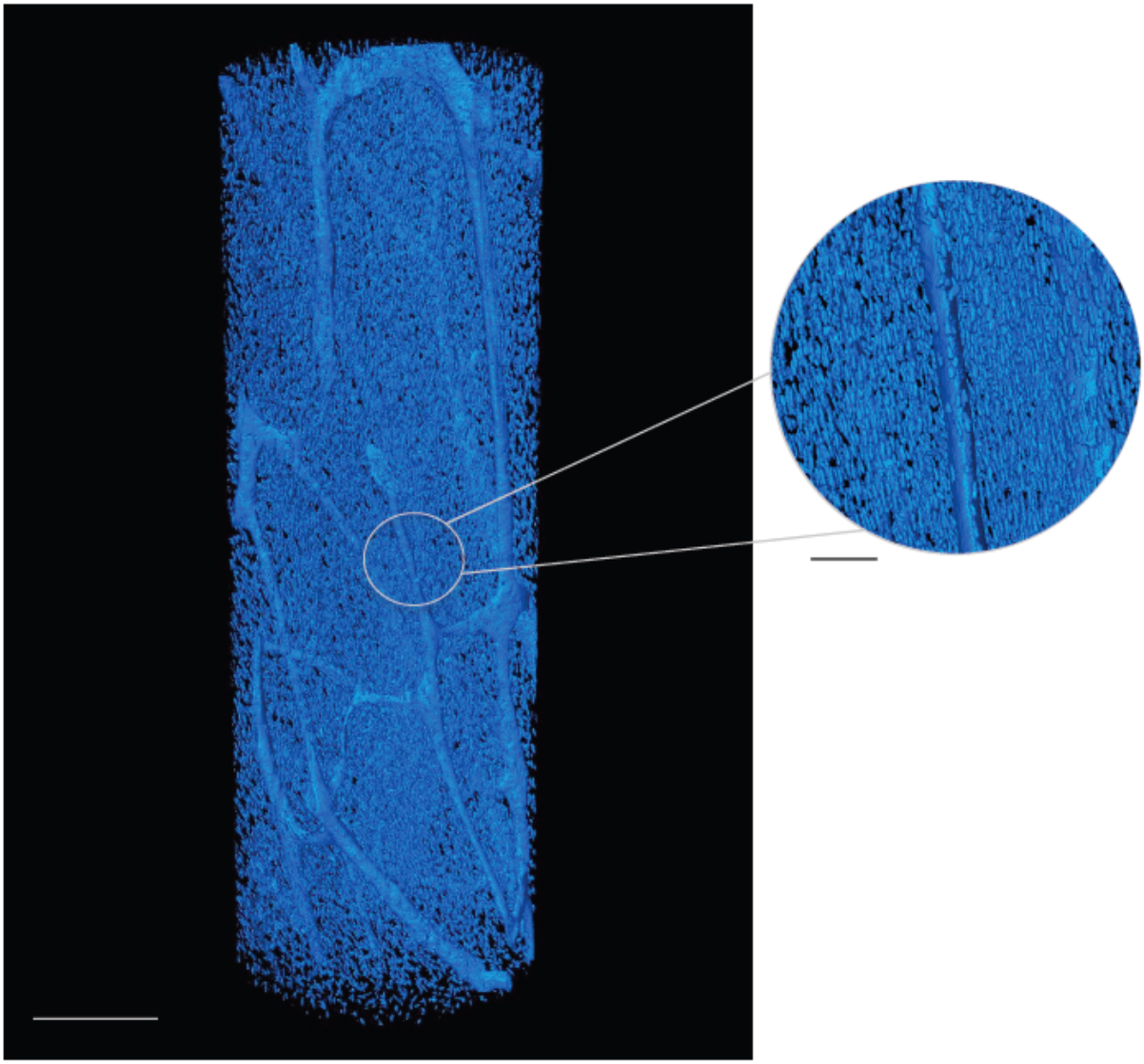

Figure 6.8: SR micro-CT 3D render of a 0.27 mm^3 cortical bone ROI from a mandible showing vascular porosity and osteocyte lacunae in blue (Credit: DML. Cooper; JM. Andronowski). Scale=300 μm. The superimposed enlargement displays the 3D microstructure in further detail. Scale=50 μm.

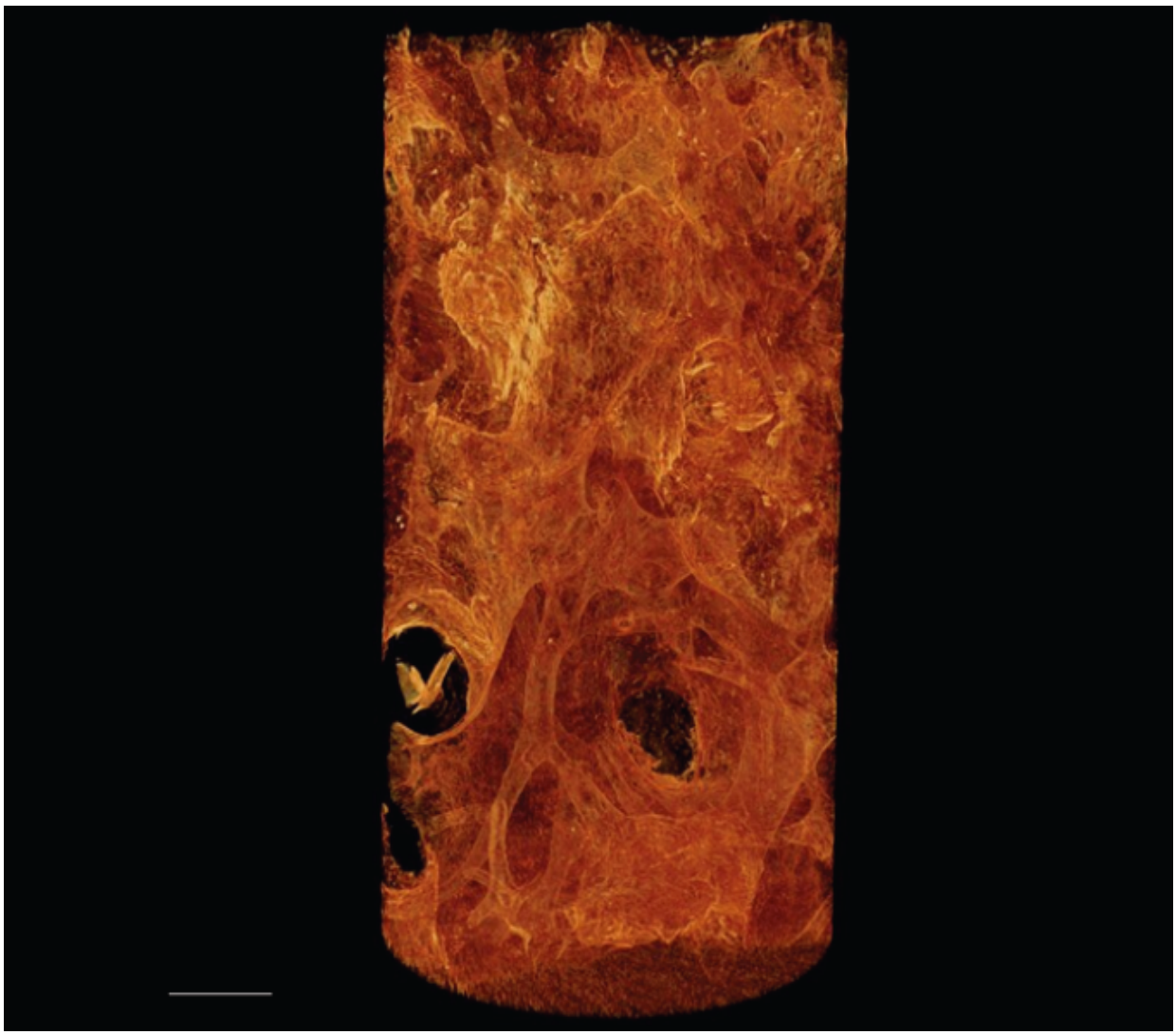

Figure 6.9: SR micro-CT 3D render of a 0.27 mm^3 cancellous bone ROI from a 2nd cuneiform showing cancellous bone microstructure (Credit: JM. Andronowski). Scale=300 μm.

Bootstrapping is a fairly robust way to address issues resulting from violations of statistical assumptions by resampling the data, thus allowing access to the true central tendency of the data. As such, it is considered a relatively powerful alternative to traditional non-parametric statistical approaches such as Kruskal Wallis, Mann-Whitney *U*, and rank transformations. However, statistical software packages such as SAS and SPSS limit bootstrap analysis to confidence intervals, and they do not contain bootstrapping implementations to directly apply to RM-ANOVA tests. Thus, this approach would require turning to a compatible statistical software package, such as R statistical programming language (R Development Core), to program the methodology. Alternatively, the analysis could be split into within- and between-subject effects, and separate analyses performed on the subsets.

To circumvent these measures due to time constraints, if a violation of the assumptions of normality or homogeneity of variances was revealed, RM-ANOVA tests were employed using rank transformed data. For future related work, however, a compatible statistical software package, such as R statistical programming language (R Development Core), will be considered and the bootstrapping approach applied.

For cortical canal measures (Ca.Dm and Ca.V), One-Way ANOVA tests were performed. This approach was appropriate as the aim was to compare single variables among experimental groups, or in this case, individuals. The mean for the variable is tested to determine if it is equal among all groups. Assumptions of the one-way ANOVA include: (1) normality of the data, and (2) homogeneity of variance. As a bootstrapped resampling function for the One-Way ANOVA is available in SPSS, it was applied to increase the number of samples, and thus, robustness. The number of data points was increased from 1,000 to 5,000 to increase robusticity. If either of the assumptions were violated, canal parameters were assessed using a non-parametric approach.

Kruskal-Wallis tests determined if differences in canal measures were present between individuals, and Mann-Whitney *U* tests were applied to assess where significant differences existed among individuals.

Spearman's Rank-Order Correlations were computed to examine the relationships between: (1) cortical and cancellous bone measurements from the clinical CT scans, and Mundorff and Davoren's (2014) nuclear DNA yield results per gram of sample (ng/g), and (2) lacunar abundance and density parameters and nuclear DNA yield results per gram of sample (ng/g). Spearman's Rank-Order Correlations were chosen over the parametric equivalent, Pearson Product-Moment Correlations, since the parameters of interest were ranked, and assumptions of normality were violated.

Further information regarding the analytical approaches applied to the clinical CT and lacunar parameters datasets are presented below.

Clinical CT Data

Percentiles were computed for the relative amounts of removed cortical and cancellous bone from the DNA sampling site for each element. Percentile data was averaged from each element type across the three individuals. RM-ANOVA tests were performed to compare the collected cortical and cancellous bone height and width measurements within and between individuals. If a value was found to be significant at $\alpha \leq 0.05$, the Bonferroni adjustment *post-hoc* test was used to identify factors contributing to significance. These computations were conducted on the entire sample rather than by skeletal element due to the limited sample size.

Spearman's Rank-Order Correlations were computed to examine the relationship between the amounts of cortical and cancellous bone tissue removed from the sampling sites and the nuclear DNA yield results per gram of sample (ng/g).

Lacunar Parameters

This statistical approach was modeled after Carter and colleagues (2013a). In accordance with their methodology, individual outliers were kept in the study since previous analyses have demonstrated that variation is normal and restricted to one or two variables (Carter et al., 2013a; 2014; 2014b). All statistical tests for the lacunar parameters were conducted on the entire sample rather than by skeletal element due to the limited sample size.

The total number of lacunae (N.Lc), lacunar density (N.Lc/BV), and lacunar volume (Lc.V) for cortical and cancellous bone ROIs were calculated using Individual Object Analysis. Individual Object Analysis **c**alculates the 3D parameters of each discreet object within the volume of interest after segmentation. In order to determine lacunae density per mm^3 (N.Lc/BV), bone volume (BV) was calculated as TV-Ca.V. RM-ANOVA tests were performed to compare the N.Lc, N.Lc/V, and Lc.V variables from cortical and cancellous bone ROIs within each individual and among individuals. If a value was found to be significant at $\alpha \leq 0.05$, a *post-hoc* Bonferroni adjustment was applied to identify factors contributing to significance.

Spearman's Rank-Order Correlations were computed to examine the relationship between N.Lc and N.Lc/BV values in cortical and cancellous bone ROIs and the nuclear DNA yield results per gram of sample (ng/g).

Canal Diameter and Volume

The microstructure of cancellous bone is similar to that of cortical bone, except that the former excludes Haversian systems (see **Figure 6.8** for a 3D render of isolated vascular canals from femoral cortical bone). As such, canal diameter (Ca.Dm) and canal volume (Ca.V) for only cortical bone ROIs were calculated using Individual Object Analysis. One-Way ANOVA tests

were employed using the original datasets for cortical bone ROIs. As the bootstrap option can be applied in SPSS, it was added to increase robusticity.

If assumptions of the One-Way ANOVA were violated, a rank transformation was employed and canal parameters were assessed using a non-parametric approach. Kruskal-Wallis tests will determine if differences in canal measures are present between individuals, and Mann-Whitney *U* tests will be applied to assess where significant differences exist among individuals.

Summary

Using the described imaging and analytical protocols, followed by graphical and statistical analyses of resulting data sets, it was possible for the evaluation of CT and osteocyte lacunar parameters in the study sample of cortical and cancellous bone tissue to determine their relationship to nuclear DNA yield.

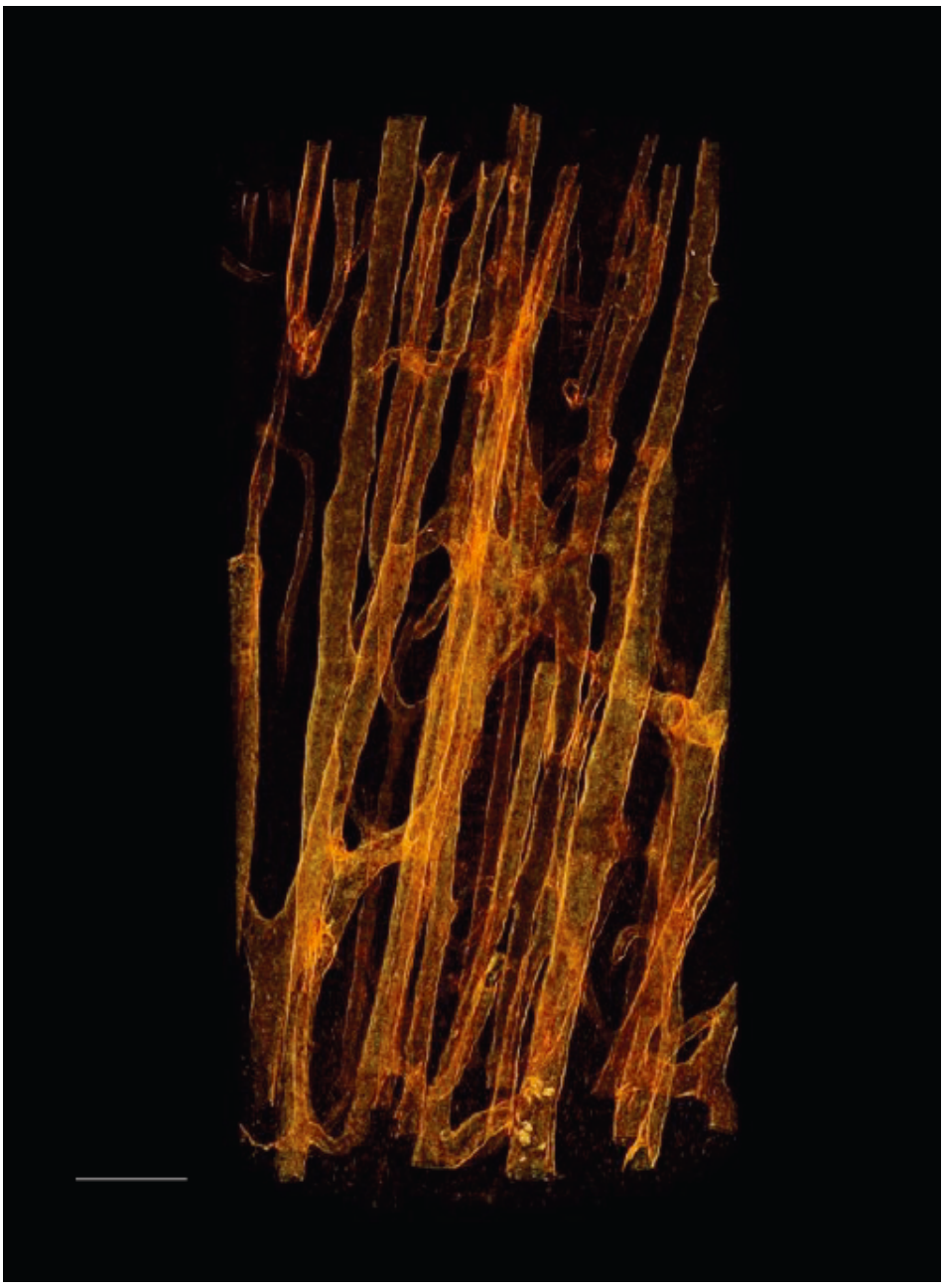

Figure 6.8: SR micro-CT 3D render of a 0.27 mm^3 cortical bone ROI from a left femur showing vascular canals (Credit: JM. Andronowski). Scale=300 μm.

CHAPTER SIX: RESULTS

The results chapter is divided into two main sections. Section I presents results from the statistical analyses of the measurement data from the clinical CT scans. Section II describes the results from all bone histomorphometric variables analyzed from the SR micro-CT scans.

Data were preliminarily inspected graphically using scatterplots and residual plots. Patterns of residuals were examined for unusual leverage, and the influence of observations was inspected using Cook's distance statistic. Descriptive statistics, including sample mean, range, standard error (SEM), and standard deviation were computed for all variables (**Appendix C**) for the clinical CT and SR micro-CT data sets. Normality of raw data was examined using Kolmogorov-Smirnov tests (**Appendix C**). Discussion of the results presented here is reserved for Chapter 8.

Section I: Clinical CT

Frequency Statistics: Examination of Percentile Values (%)

Due to issues with scan quality, ten of the original 129 samples were removed from the analysis. Percentiles of cortical and cancellous bone were computed from each DNA sampling site for all elements (**Table 7.1**). Percentile data were further averaged from each element type across all individuals. The majority of element types revealed consistent measurements between individuals, with standard deviations of 10% or less (**Table 7.2**). Three element types (temporal, occipital, cervical vertebra) exhibited high variability between the three individuals in the relative amount of cortical and cancellous bone removed from the sampling sites (**Figure 7.1).**

Mean percentiles of cortical bone composition at each sampling site were divided into seven categories by skeletal element: (1) 80-100%, (2) 70-79%, (3) 60-69%, (4) 50-59%, (5) 40-

49%, (6) 30-39%, and (7) 20-29%. The first category consists of bones whose sampling sites did not contain any cancellous bone, including the humerus, radius, ulna, femur, and tibia. The second, third, and fourth categories contained only three elements with sampling sites that were composed of over 50% cortical bone (**Table 7.3**).

Mean percentiles of cancellous bone composition at each sampling site were divided into nine categories by skeletal element: (1) 80-100%, (2) 70-79%, (3) 60-69%, (4) 50-59%, (5) 40-49%, (6) 30-39%, (7) 20-29%, (8) 10-19%, and (9) >10%. Though only the sacrum was represented in the first two categories, the majority of DNA sampling sites contained between 50-69% cancellous bone (**Table 7.4**).

Cortical and Cancellous Bone Height and Width Measurements

RM-ANOVA tests were performed to evaluate differences in average measurements of cortical and cancellous bone height and width from each DNA sampling site within- and between- individuals. The mean results and standard deviations for each parameter are summarized in **Appendix C**. Normality of raw data was examined using Kolmogorov-Smirnov tests. Mauchly's Tests of Sphericity, the RM-ANOVA equivalent of homogeneity of variances, were conducted to test for homogeneity of covariance matrices. Kolmogorov-Smirnov tests revealed that cancellous height and cortical width datasets were not normally distributed ($\alpha \leq 0.05$) (**Appendix C**). Results from Mauchly's Tests of Sphericity indicated that the assumption of homogeneity of variances was met for each parameter (p=1.00). Although analysis with non-parametric statistics is warranted due to the violation of normality, the Kolmogorov-Smirnov test statistics and associated normal Q-Q Plots revealed that these variables only slightly deviated from a normal distribution (**Figures 7.2-7.5**), despite one individual outlier in the cortical height dataset.

Table 7.1: Percentiles of Cortical and Cancellous Bone from each DNA Sampling Site Procured by Mundorff & Davoren (2014) by Skeletal Element.

Skeletal Element	Research #	Cortical Bone (%)	Cancellous Bone (%)
Pubis	#1	44	56
	#2	28	72
	#3	40	60
Ilium	#1	35	65
	#2	30	70
	#3	N/A	N/A
Ischium	#1	38	62
	#2	39	61
	#3	N/A	N/A
Sacrum	#1	34	66
	#2	25	75
	#3	N/A	N/A
Cuboid	#1	40	60
	#2	29	71
	#3	30	70
Calcaneus	#1	40	60
	#2	32	68
	#3	31	69
Talus	#1	40	60
	#2	29	71
	#3	30	70
1st Cuneiform	#1	36	64
	#2	31	69
	#3	36	64
2nd Cuneiform	#1	38	62
	#2	31	69
	#3	32	68
3rd Cuneiform	#1	35	65
	#2	34	66
	#3	37	63
Navicular	#1	36	64
	#2	33	67
	#3	37	63
Capitate	#1	39	61
	#2	28	72
	#3	39	61
Twelfth Rib	#1	N/A	N/A

Table 7.1: (cont).

Skeletal Element	Research #	Cortical Bone (%)	Cancellous Bone (%)
	#2	N/A	N/A
	#3	41	59
Fibula	#1	60	40
	#2	62	38
	#3	52	48
Femur	#1	100	0
	#2	100	0
	#3	100	0
Tibia	#1	100	0
	#2	100	0
	#3	100	0
Patella	#1	34	66
	#2	36	64
	#3	34	66
Humerus	#1	100	0
	#2	100	0
	#3	100	0
Ulna	#1	100	0
	#2	100	0
	#3	100	0
Radius	#1	100	0
	#2	100	0
	#3	100	0
Scapula	#1	N/A	N/A
	#2	51	49
	#3	48	52
Clavicle	#1	N/A	N/A
	#2	40	60
	#3	47	53
Cervical Vertebra	#1	37	63
	#2	30	40
	#3	45	55
Lumbar Vertebra	#1	33	67
	#2	29	71
	#3	34	66
Thoracic Vertebra	#1	34	66
	#2	39	61
	#3	36	64

Table 7.1: (cont).

Skeletal Element	Research #	Cortical Bone (%)	Cancellous Bone (%)
Frontal	#1	49	51
	#2	62	38
	#3	58	41
Parietal	#1	46	54
	#2	56	44
	#3	52	48
Temporal	#1	N/A	N/A
	#2	52	48
	#3	35	65
Maxilla	#1	42	58
	#2	39	61
	#3	N/A	N/A
Mandible	#1	45	55
	#2	46	54
	#3	51	49
Occipital	#1	53	47
	#2	64	36
	#3	100	0
First Rib	#1	47	53
	#2	48	52
	#3	51	49
Middle Rib	#1	40	60
	#2	42	58
	#3	47	53
Metatarsal 1	#1	39	61
	#2	44	56
	#3	41	59
Metatarsal 2	#1	44	56
	#2	48	52
	#3	32	68
Metatarsal 3	#1	45	55
	#2	45	55
	#3	48	52
Metatarsal 4	#1	38	62
	#2	45	55
	#3	36	64
First Proximal Hand Phalanx	#1	37	63
	#2	38	62

Table 7.1: (cont).

Skeletal Element	Research #	Cortical Bone (%)	Cancellous Bone (%)
	#3	37	63
First Distal Hand Phalanx	#1	47	54
	#2	37	63
	#3	N/A	N/A
First Distal Foot Phalanx	#1	45	55
	#2	40	60
	#3	32	68
Metacarpal 4	#1	34	66
	#2	42	58
	#3	39	61
Metacarpal 2	#1	36	64
	#2	42	58
	#3	39	61
Metacarpal 3	#1	42	58
	#2	33	67
	#3	40	60
First Proximal Foot Phalanx	#1	32	68
	#2	35	65
	#3	37	63

Table 7.2: Mean Percentiles and Standard Deviations for Cortical and Cancellous Bone Measurements by Bone Type from each DNA Sampling Site.

Bone Type	Mean Cortical (%)	St. Dev	Mean Cancellous (%)	St. Dev
First Distal Hand Phalanx	42	7	58	6
Cuneiform 2	34	4	66	4
Talus	33	6	67	6
Cuneiform 3	35	2	65	2
Cuboid	33	6	67	6
First Rib	49	2	51	2
Capitate	35	6	65	6
Navicular	35	2	65	3
Calcaneus	34	5	66	5
Metacarpal 4	38	4	62	4
Metatarsal 2	41	8	59	8
Cuneiform 1	34	3	66	3
Patella	35	1	65	1
Metacarpal 3	38	5	62	5
Metatarsal 4	40	5	60	5
Metatarsal 3	46	2	54	2
Maxilla	40	2	60	2
Pubis	37	8	63	8
Ilium	35	4	65	4
Thoracic Vertebra	36	3	54	3
Sacrum	29	6	71	10
Ischium	38	1	62	1
First Proximal Foot Phalanx	35	3	65	3
Metacarpal 2	39	3	61	3
Mandible	47	6	53	3
Humerus	100	0	0	0
Tibia	100	0	0	0
Twelfth Rib	41	0	59	0
First Proximal Hand Phalanx	37	1	63	1
Middle Rib	43	7	57	7
Cervical Vertebra	37	8	53	12
Frontal	57	7	43	7
Clavicle	43	5	57	5
Parietal	49	5	51	5
Lumbar Vertebra	32	3	68	3
Metatarsal 1	41	3	59	3

Table 7.2: (cont).

Bone Type	Mean Cortical (%)	St. Dev	Mean Cancellous (%)	St. Dev
First Distal Foot Phalanx	39	7	61	7
Femur	100	0	0	0
Fibula	58	5	42	5
Temporal	43	12	57	12
Scapula	50	2	50	2
Occipital	72	25	28	25
Radius	100	0	0	0
Ulna	100	0	0	0

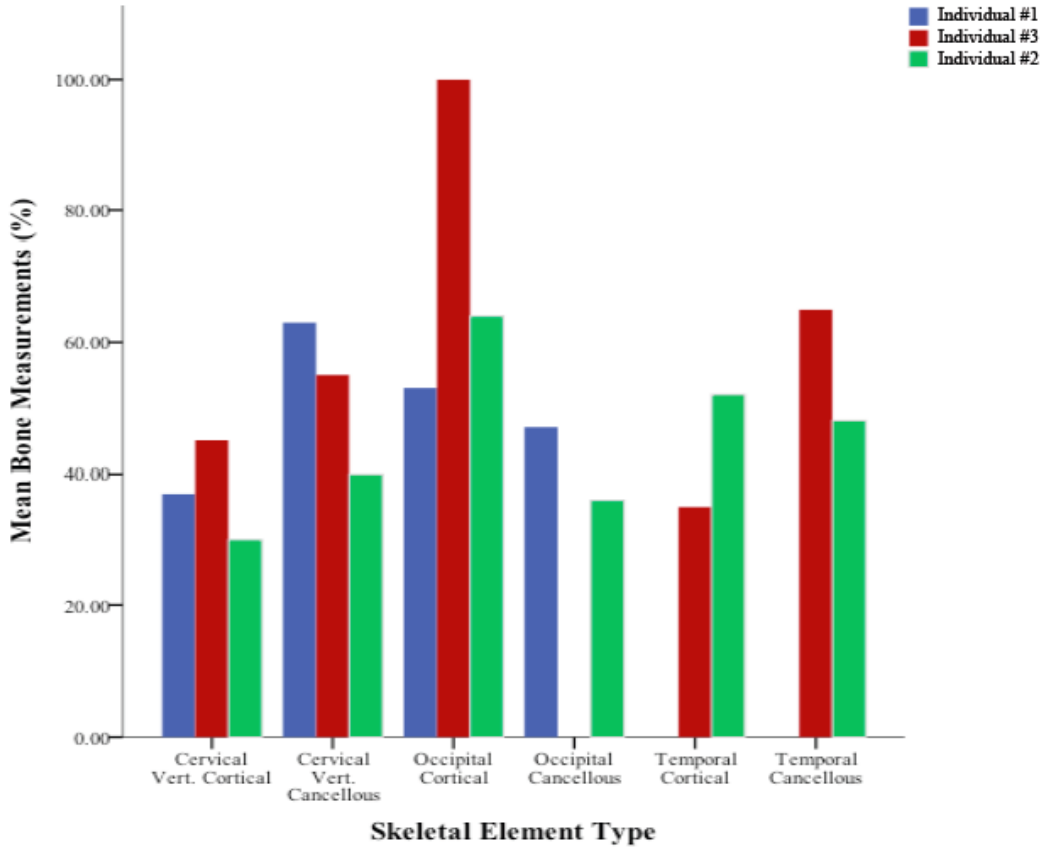

Figure 7.1: Skeletal Elements Exhibiting High Variability in Cortical and Cancellous Bone Measurements.

Table 7.3: Average Percentage of Cortical Bone Removed from the DNA Sampling Sites by Skeletal Element.

Average Amount of Cortical Bone (%)	Skeletal Element(s)
80-100	Humerus, Radius, Ulna, Femur, Tibia
70-79	Occipital
60-69	N/A
50-59	Scapula, Fibula
40-49	Maxilla, Mandible, Frontal, Parietal, Temporal, Clavicle, First Distal Hand Phalanx, First Rib, Middle Rib Twelfth Rib, Metatarsal 1, Metatarsal 2, Metatarsal 4, Metatarsal 3
30-39	Patella, Cuneiform 1, Cuneiform 2, Cuneiform 3, Talus, Cuboid, Capitate, Navicular, Calcaneus Metacarpal 2, Metacarpal 3, Metacarpal 4, Cervical Vertebra, Thoracic Vertebra, Lumbar Vertebra, Pubis, Ilium, Ischium
30-39	First Proximal Foot Phalanx, First Distal Foot Phalanx, First Proximal Hand Phalanx

Table 7.4: Average Percentage of Cancellous Bone Removed from the DNA Sampling Sites Procured by Mundorff & Davoren (2014) by Skeletal Element.

Average Amount of Cancellous Bone (%)	Skeletal Element(s)
80-100	N/A
70-79	Sacrum
60-69	Maxilla, Cuneiform 1, Cuneiform 2, Cuneiform 3 Talus, Cuboid, Navicular Calcaneus, Capitate, Metatarsal 4, Metacarpal 2, Metacarpal 3 Metacarpal 4, Lumbar Vertebra, Pubis, Ilium Ischium, Patella, First Proximal Foot Phalanx, First Distal Foot Phalanx, First Proximal Hand Phalanx

Table 7.4: (cont).

Average Amount of Cancellous Bone (%)	Skeletal Element(s)
50-59	Mandible, Parietal, Temporal Twelfth Rib, Middle Rib Clavicle, Scapula, First Rib Metatarsal 1, Metatarsal 2 Metatarsal 3, Cervical Vertebra, Thoracic Vertebra, First Distal Hand Phalanx
40-49	Frontal, Fibula
30-39	N/A
20-29	Occipital
10-19	N/A
>10	Humerus, Radius, Ulna, Femur, Tibia

Individual outliers were kept in the study since variation is normal and often restricted to one or two variables. RM-ANOVA tests were first employed using the original datasets for cortical and cancellous bone height and width variables from cortical and cancellous bone ROIs, and then a rank transformation was performed on each dataset. Additional RM-ANOVA tests were employed using the rank transformed data to determine if the results remained consistent. Since parametric statistical tests are more powerful, and more robust to deviations, including these additional results is warranted to provide a more complete picture of the relationships between variables. It should be noted, however, that future publications resulting from this work will report results from the non-parametric analyses.

RM-ANOVA Original Dataset: Cortical and Cancellous Bone Height and Width

Results of the test of within-subjects effects revealed no significant differences in the main effect for cortical and cancellous bone height measurements ($F_{(1,95)}$=0.118, p=0.732) (**Table 7.5**), indicating that height measurements do not significantly differ according to bone tissue

type. However, the interaction effect between cortical and cancellous bone height and individual is significant ($F_{(1,95)}$=5.293, p=0.007). Because of the significant interaction effect, the main effect will not be further considered. In this case, the significant interaction effect indicates that height measurements are dependent on the individual the measurements were retrieved from, but differences in measurements are not consistent among individuals. The interaction can be visualized in **Figure 7.6**, as the trends are not parallel among individuals. The sampling sites for individual #3 displayed low cortical and cancellous bone height measurements, and exhibited the lowest cancellous bone height measurements overall. Individual #2 displayed greater cancellous bone height measurements compared to the other individuals, but the lower cortical bone height measurements. Individual #1 possessed the greatest cortical height measurement values. The test of between-subjects effects (**Table 7.6)** demonstrated that there are no significant differences in cortical and cancellous bone height between individuals ($F_{(1,95)}$=1.013, p=0.367).

For cortical and cancellous bone width measurements, results of the test of within-subjects main effects (**Table 7.7**) revealed significant differences in cortical and cancellous bone width measurements overall ($F_{(1,95)}$=267.514, p=0.000). However, the interaction effect between cortical and cancellous bone width and individual was not significant ($F_{(1,95)}$=0.542, p=0.583). **Figure 7.7** displays the parallel trends, indicating that the interaction is not significant. The test of between-subjects effects (**Table 7.8)** demonstrated that cortical and cancellous width measurements were not significantly different among individuals ($F_{(1,95)}$=1.726, p=0.183).

RM-ANOVA Following Rank Transformation: Cortical and Cancellous Bone Height and Width

Results of the test of within-subjects effects revealed no significant differences in the main effect for cortical and cancellous bone height measurements ($F_{(1,95)}$=0.273, p=0.603) (**Table**

7.9). The interaction effect between cortical and cancellous bone height and individual is significant ($F_{(1,95)}$=7.166, p=0.001), indicating that height measurements are dependent upon the individual that the measurements were retrieved from. This interaction can be visualized in **Figure 7.8**. The sampling sites for individual #3 displayed lower cortical and cancellous bone height measurements overall, and exhibited the lowest cancellous bone height measurements. Individual #2 displayed greater cancellous bone height measurements compared to the other individuals, and individual #1 possessed the greatest cortical height measurement values. The test of between-subjects effects (**Table 7.10)** demonstrated that there are no significant differences in cortical and cancellous bone height between individuals ($F_{(1,95)}$=1.373, p=0.258).

For cortical and cancellous bone width measurements, results of the test of within-subjects effects (**Table 7.11**) revealed significant differences in cortical and cancellous bone width measurements overall ($F_{(1,95)}$=304.445, p=0.000). However, the interaction effect between cortical and cancellous bone width and individual was not significant ($F_{(1,95)}$=0.168, p=0.583). **Figure 7.9** demonstrates that the trends are parallel, indicating that the interaction is not significant. The test of between-subjects effects (**Table 7.12)** demonstrated that cortical and cancellous width measurements were not significantly different among individuals ($F_{(1,95)}$=2.324, p=0.103).

The results of the parametric and non-parametric approaches are comparable. As such, it was not warranted to either: (1) divide the dataset into within- and between- subjects groups and bootstrap the results to make determinations from the resulting confidence intervals, or (2) create a new implementation in the R statistical package. It is concluded that employing both statistical approaches confirms that the results are reliable.

Clinical CT Parameters and Nuclear DNA Yield

Of the 55 elements selected for nuclear DNA analysis by Mundorff and Davoren (2014), the sampling sites from the 34 top ranked bones had higher percentages of cancellous than cortical bone (**Table 7.13**). The sampling sites from the lowest ranking samples, the radius and ulna, were composed entirely of cortical bone. Other poorly ranked bones with strictly cortical samples included the humerus, tibia, and femur, which ranked 35th, 36th, and 49th, respectively.

Normality of raw data examined using Kolmogorov-Smirnov tests and associated normal Q-Q Plots, revealed that the nuclear DNA and average cancellous bone volume datasets were not normally distributed ($\alpha \leq 0.05$) (**Appendix C and Figures 7.10-7.11**). Thus, Spearman's Rank-Order Correlations were computed to further examine the relationship between the relative amounts of cortical and cancellous bone tissue removed from the sampling sites and the nuclear DNA yield results per gram of sample (ng/g). Correlation coefficients indicated which variables shared significant relationships at $\alpha \leq 0.05$ (**Table 7.14**). A significant negative correlation was observed between average cortical bone volume and nuclear DNA yield (r=-0.340), suggesting that sampling sites comprised of primarily cortical bone do not share a positive relationship with nuclear DNA yield (**Figure 7.12**).

A positive significant correlation is evident between average cancellous bone volume and nuclear DNA yield (r=0.409), indicating that sampling sites with greater cancellous bone quantities produced higher nuclear DNA yields per mass of sample (**Figure 7.13**).

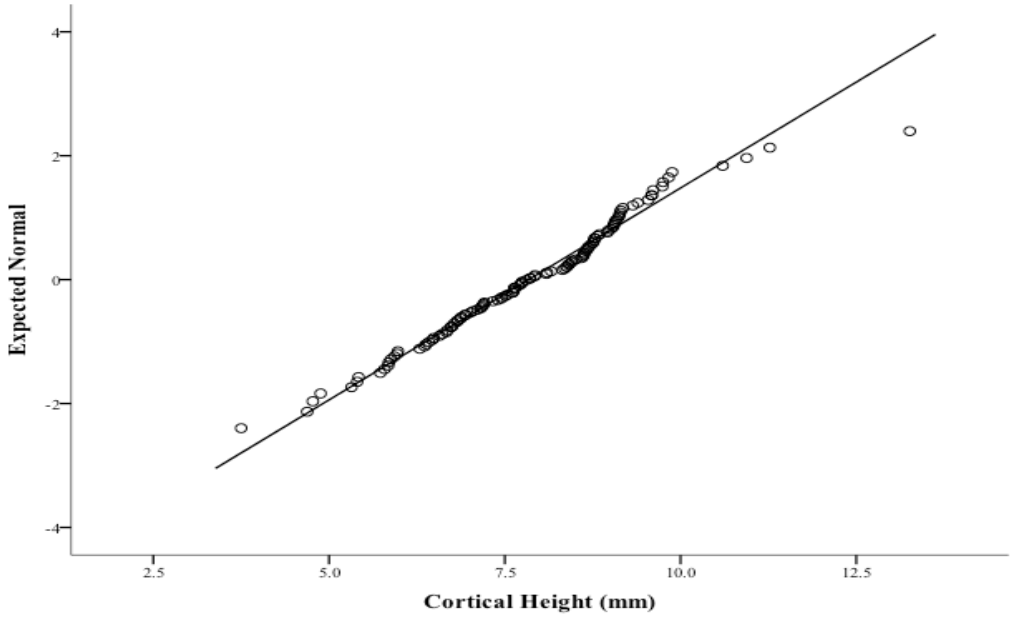

Figure 7.2: Normality Q-Q Plot for Cortical Height (mm).

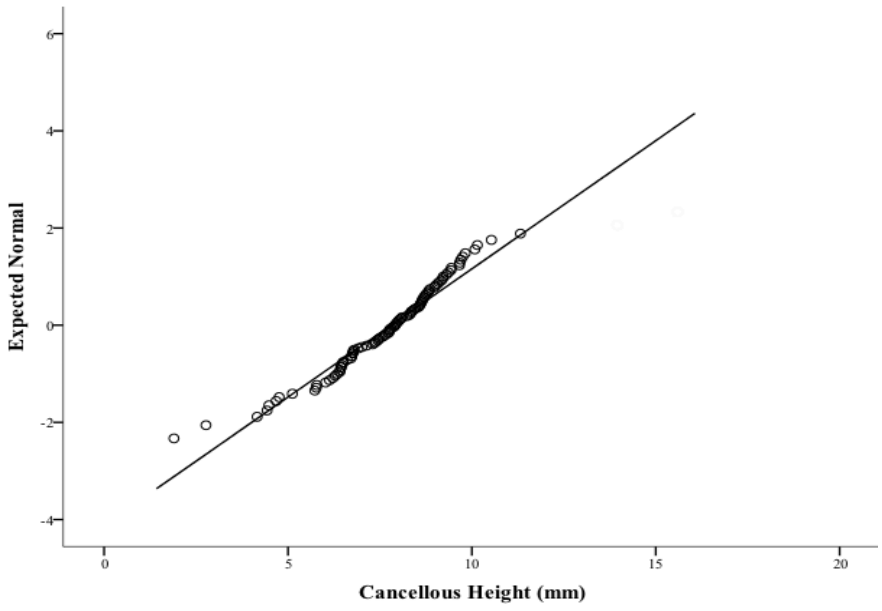

Figure 7.3: Normality Q-Q Plot for Cancellous Height (mm).

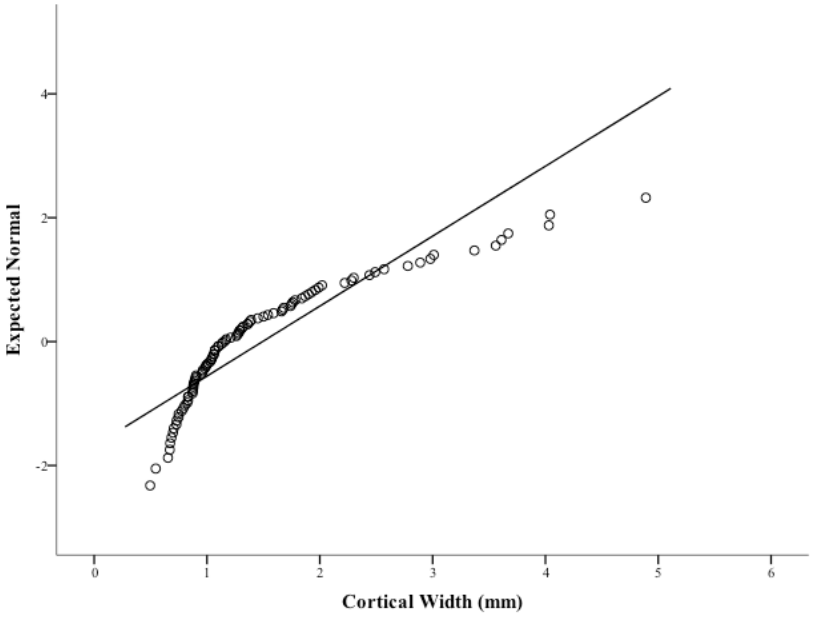

Figure 7.4: Normality Q-Q Plot for Cortical Height (mm).

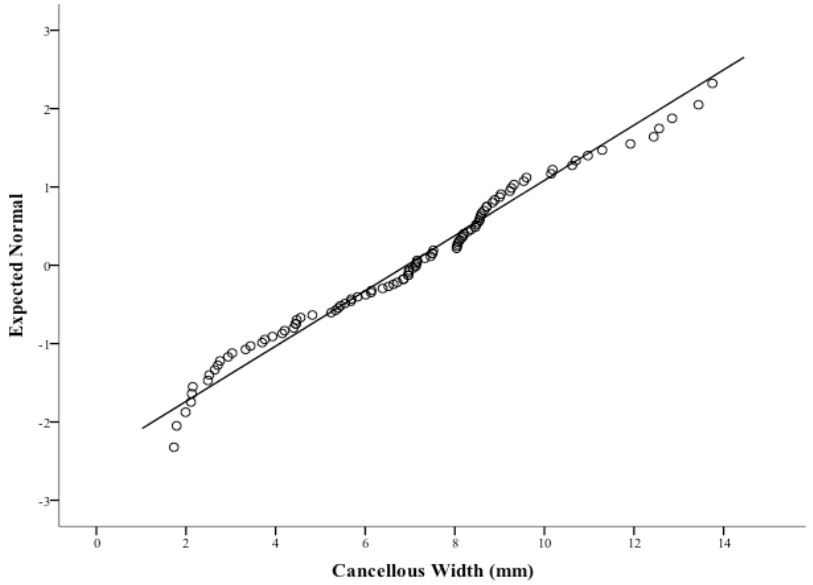

Figure 7.5: Normal Q-Q Plot for Cancellous Width (mm).

Table 7.5: RM-ANOVA Results from Cortical and Cancellous Height: Within-Subjects Effects.

Source	df	Mean Square	F	*p*-value
Cortical and Cancellous Height (mm)	1	0.111	0.118	0.732
Cortical and Cancellous Height (mm)*Individual	2	5.014	5.293	0.007*

**Significance at p=<0.05*

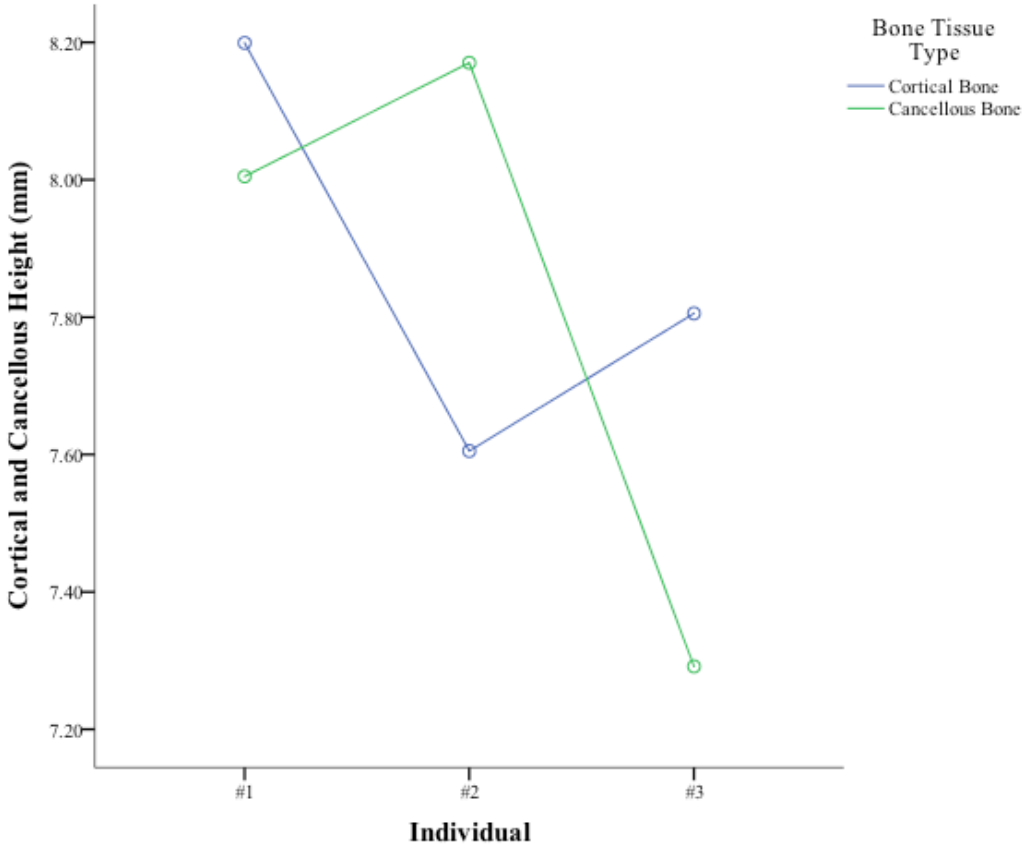

Figure 7.6: RM-ANOVA Within-Subjects Results Displaying Significant Interaction Effect for Cortical and Cancellous Bone Height (mm) and Individual.

Table 7.6: RM-ANOVA Results from Cortical and Cancellous Height: Between-Subjects Effects.

Source	df	Mean Square	F	*p*-value
Cortical and Cancellous Height (mm)/Individual	2	5.053	1.013	0.367

**Significance at =p <0.05*

Table 7.7: RM-ANOVA Results from Cortical and Cancellous Width: Within-Subjects Effects.

Source	df	Mean Square	F	*p*-value
Cortical and Cancellous Width (mm)	1	1448.862	267.514	0.000*
Cortical and Cancellous Width*Individual (mm)	2	2.938	0.542	0.583

**Significance at p=<0.05*

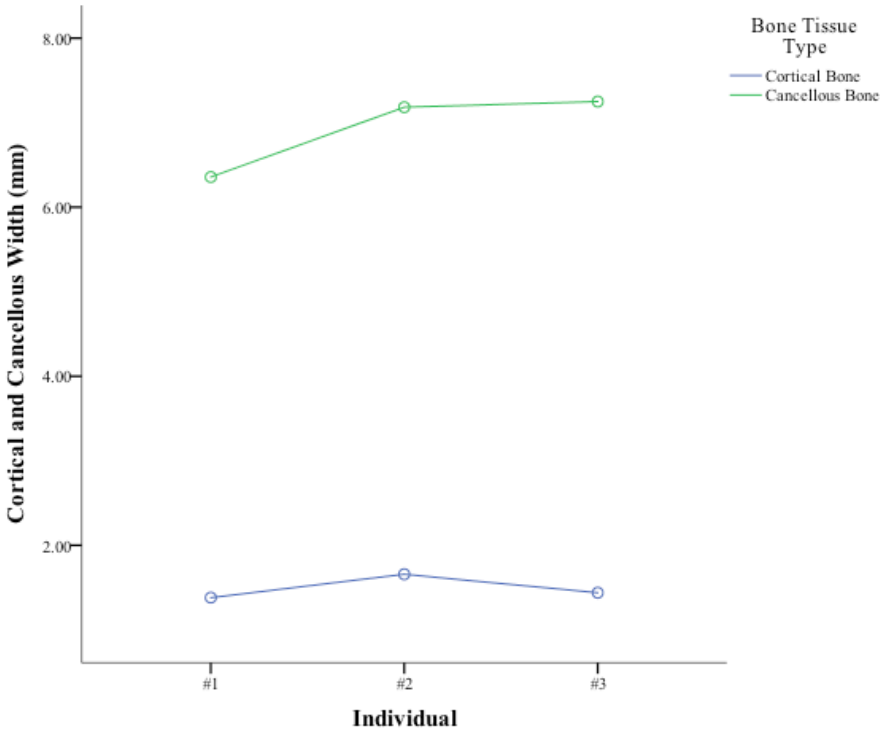

Figure 7.7: RM-ANOVA Within-Subjects Results Displaying No Interaction Effect for Cortical and Cancellous Bone Width (mm) and Individual.

Table 7.8: RM-ANOVA Results from Cortical and Cancellous Width: Between-Subjects Effects.

Source	df	Mean Square	F	*p*-value
Cortical and Cancellous Width (mm)/Individual	2	1767.66	1.726	0.183

**Significance at p=<0.05*

Table 7.9: RM-ANOVA Results from Rank Transformed Cortical and Cancellous Height: Within-Subjects Effects.

Source	df	Mean Square	F	*p*-value
Cortical and Cancellous Height (mm)	1	377.964	0.273	0.603
Cortical and Cancellous Height (mm)*Individual	2	9920.09	7.166	0.001*

**Significance at p=<0.05*

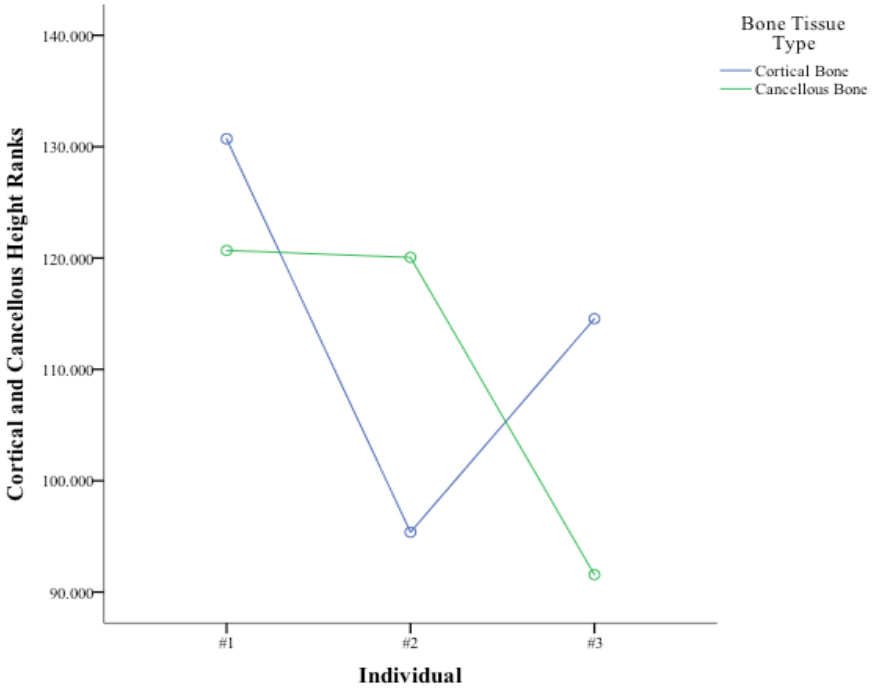

Figure 7.8: RM-ANOVA Results of Rank Transformed Data for Cortical and Cancellous Bone Height (mm): Within-Subjects Effects.

Table 7.10: RM-ANOVA Results from Rank Transformed Cortical and Cancellous Height: Between-Subjects Effects.

Source	df	Mean Square	F	*p*-value
Cortical and Cancellous Height (mm)/Individual	2	9350.09	1.373	0.258

**Significance at =p <0.05*

Table 7.11: RM-ANOVA Results from Rank Transformed Cortical and Cancellous Width: Within-Subjects Effects.

Source	df	Mean Square	F	*p*-value
Cortical and Cancellous Width (mm)	1	1448.862	304.445	0.000*
Cortical and Cancellous Width*Individual (mm)	2	2.938	0.168	0.845

**Significance at p=<0.05*

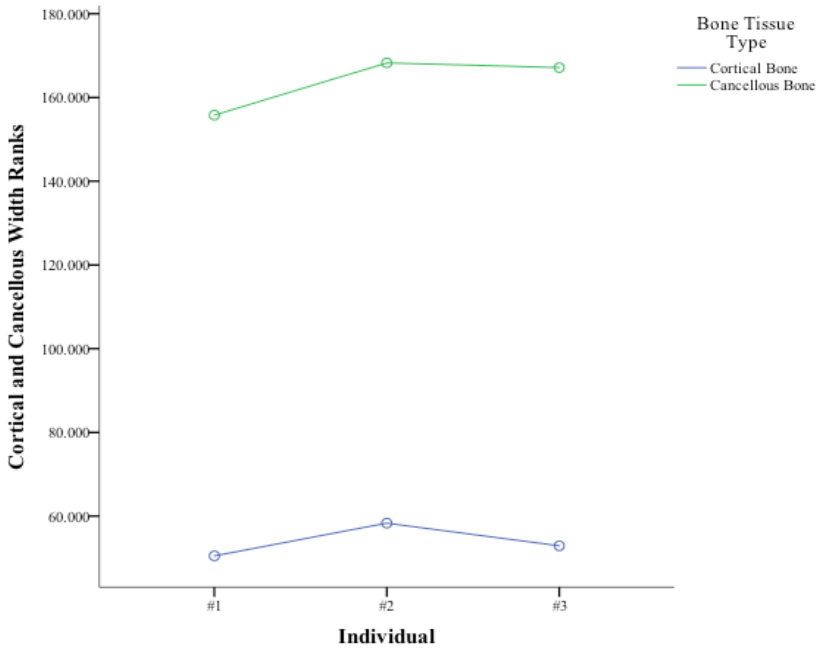

Figure 7.9: RM-ANOVA Results of Rank Transformed Data for Cortical and Cancellous Bone Width (mm): Within-Subjects Effects.

Table 7.12: RM-ANOVA Results from Rank Transformed Cortical and Cancellous Width: Between-Subjects Effects.

Source	df	Mean Square	F	*p*-value
Cortical and Cancellous Width (mm)/Individual	2	1767.66	2.324	0.103

**Significance at =p <0.05*

Section II: SR micro-CT

Lacunar Parameters

Due to the minute specimen size required for SR micro-CT imaging, certain bone blocks with dense cortical regions (femur, tibia, fibula, humerus, radius, ulna, temporal, mandible, occipital) did not contain sufficient cancellous bone for the evaluation of a separate ROI. For the noted skeletal elements, only cortical bone ROIs were quantitatively analyzed.

Results from the Individual Object Analysis for N.Lc, N.Lc/BV, and Lc.V are presented in **Appendix A**. The mean results and standard deviations for each parameter are summarized in **Appendix C**. Normality of raw data was examined using Kolmogorov-Smirnov tests. Mauchly's Tests of Sphericity were conducted to test for homogeneity of covariance matrices. Kolmogorov-Smirnov tests revealed that all datasets, with the exception of cortical bone N.Lc and N.Lc/BV, were not normally distributed ($\alpha \leq 0.05$) (**Appendix C**). Results from Mauchly's Tests of Sphericity indicated that the assumption of homogeneity of variances was met for all parameters (p=1.00), except for the Lc.V variables.

Though analysis with non-parametric statistics is warranted due to the violation of normality (**Appendix C**), the Kolmogorov-Smirnov tests revealed that certain variables only slightly deviated from a normal distribution, with the exception of the Lc.V parameters (**Figures 7.14-7.17**).

Table 7.13: Ranking of DNA Quantification Results by Average Yield per Mass of Sample and Average Percentages of Cortical and Cancellous Bone from each DNA Sampling Site.

Rank	Bone Type	Avg. Cortical (%)	Avg. Cancellous (%)
1	First Distal Hand Phalanx	42	58
2	Cuneiform 2	34	66
5	Talus	33	67
7	Cuneiform 3	35	65
8	Cuboid	33	67
9	First Rib	49	51
10	Capitate	35	65
12	Navicular	35	65
15	Calcaneus	34	66
16	Metacarpal 4	38	62
18	Metatarsal 2	41	59
20	Cuneiform 1	34	66
21	Patella	35	65
22	Metacarpal 3	38	62
23	Metatarsal 4	40	60
24	Metatarsal 3	46	54
25	Maxilla	40	60
26	Pubis	37	63
27	Ilium	35	65
28	Thoracic Vertebrae	36	54
29	Sacrum	29	71
30	Ischium	38	62
31	First Proximal Foot Phalanx	35	65
32	Metacarpal 2	39	61
34	Mandible	47	53
35	Humerus	100	0
36	Tibia	100	0
37	Twelfth Rib	41	59
38	First Proximal Hand Phalanx	37	63
39	Middle Rib	43	57
40	Cervical Vertebrae	37	53
41	Frontal	57	43
42	Clavicle	43	57
43	Parietal	49	51
45	Lumbar Vertebrae	32	68
46	Metatarsal 1	41	59
48	First Distal Foot Phalanx	39	61

Table 7.13: (cont).

Rank	Bone Type	Avg. Cortical (%)	Avg. Cancellous (%)
49	Femur	100	0
50	Fibula	58	42
51	Temporal	43	57
52	Scapula	50	50
53	Occipital	72	28
54	Radius	100	0
55	Ulna	100	0

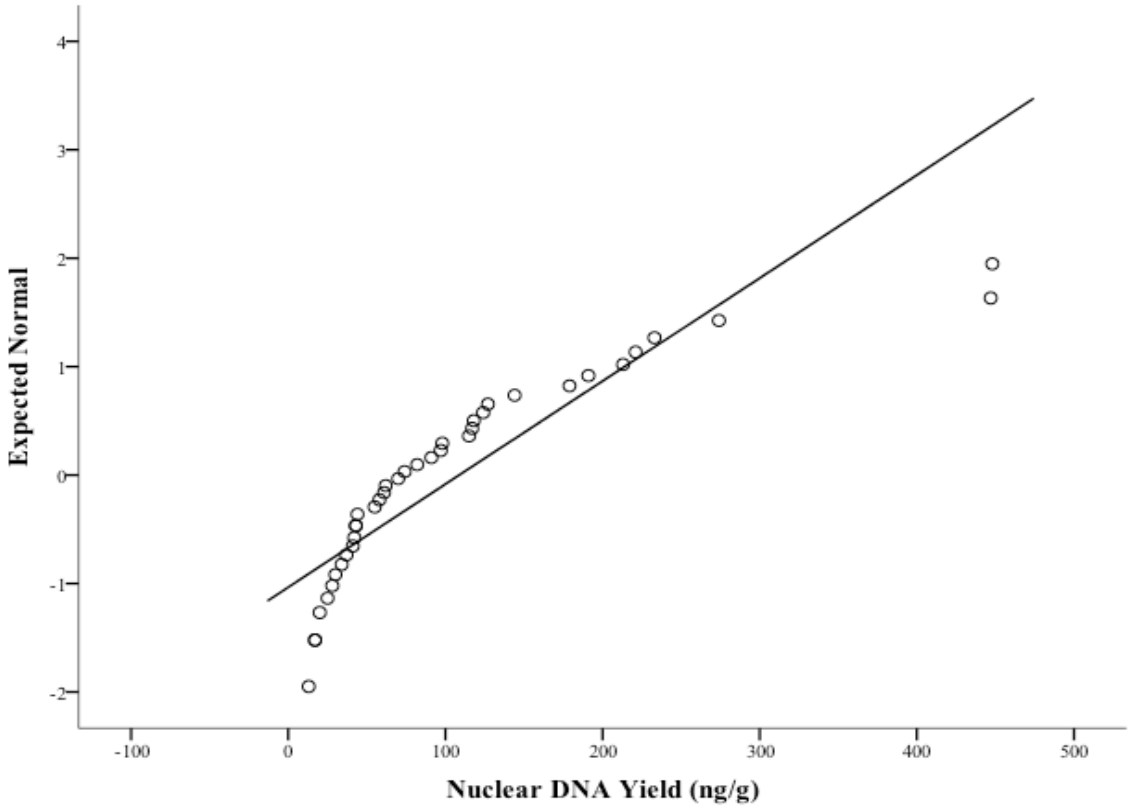

Figure 7.10: Normality Q-Q Plot for Nuclear DNA Yield (ng/g).

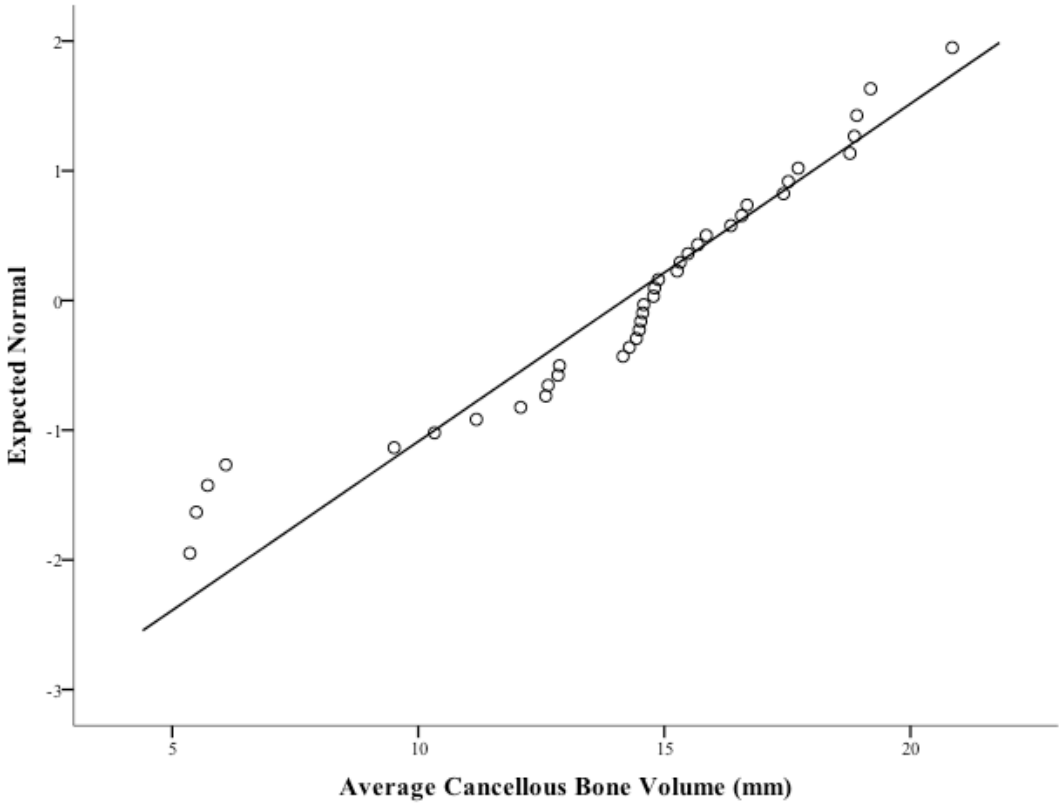

Figure 7.11: Normality Q-Q Plot for Average Cancellous Bone Volume.

Table 7.14: Spearman's Correlation Coefficients for Clinical CT Scan Parameters and Nuclear DNA Yield.

	Nuclear DNA Yield (ng/g)	**Avg. Cortical Bone (mm)**	**Avg. Cancellous Bone (mm)**
Nuclear DNA Yield (ng/g)	1.00	-0.340*	0.409*
Avg. Cortical Bone (mm)	-0.340*	1.00	-0.092
Avg. Cancellous Bone (mm)	0.409*	-0.092	1.00

**Significance at =p <0.05*

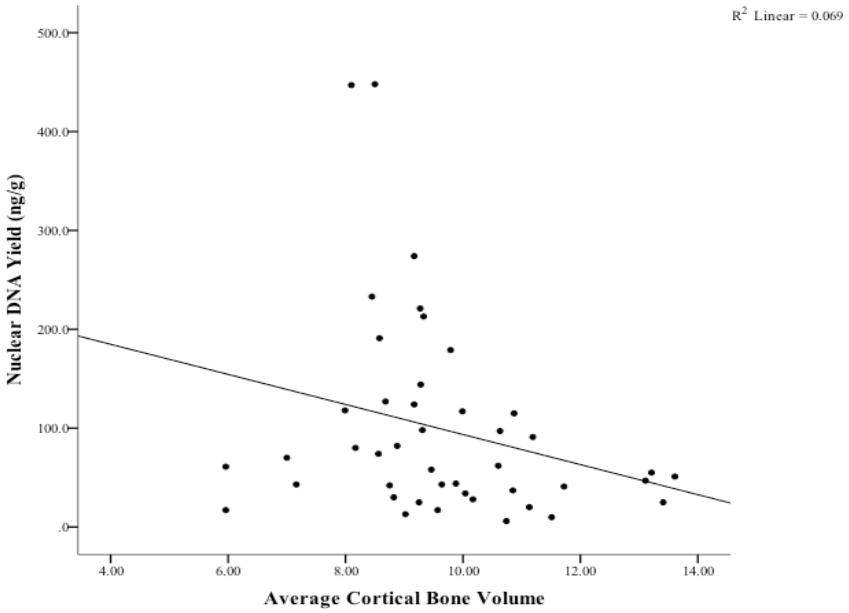

Figure 7.12: Scatterplot Depicting Average Cortical Bone Volume and Nuclear DNA Yield (ng/g).

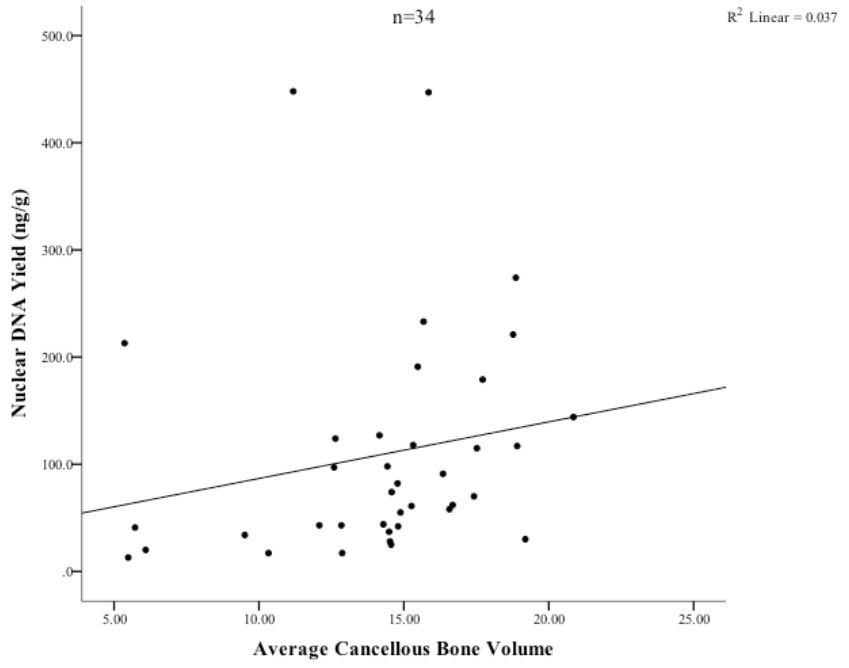

Figure 7.13: Scatterplot Depicting Average Cancellous Bone Volume and Nuclear DNA Yield (ng/g).

As such, RM-ANOVA tests were employed using the original datasets for N.Lc and N.Lc/BV variables from cortical and cancellous bone ROIs, and then a rank transformation was performed on each dataset. Additional RM-ANOVA tests were employed using the rank transformed data to determine if the results remained consistent. As parametric statistical tests are more powerful, including these results is warranted if results are comparable.

For the Lc.V parameters, only RM-ANOVA tests using the rank transformed data were performed since assumptions of normality and homogeneity of variances were violated (**Figures 7.18-7.19**).

RM-ANOVA Original Dataset: Number of Lacunae (N.Lc)

Results of the within-subjects test (**Table 7.15**) indicated that mean N.Lc in cortical and cancellous bone were significantly different overall ($F_{(1,99)=}171.928$, $p=0.000$). There was no significant interaction observed between overall N.Lc in cortical and cancellous bone and individual ($F_{(1,99)=}2.561$, $p=0.082$). The test of between-subjects effects demonstrated significant differences in N.Lc between cortical and cancellous bone among the three individuals ($F_{(1,99)=}47.969$, $p=0.000$) (**Table 7.16**). As such, lacunar counts in cortical and cancellous bone were significantly different between individuals. **Figure 7.20** provides a visual representation of the mean N.Lc in cortical and cancellous bone tissues for the three individuals. Lower N.Lc values are evident for individual #3 in both cortical and cancellous bone tissues. Alternatively, individual #2 exhibited higher lacunar counts than #3 and #1 in both cortical and cancellous bone tissues.

The Bonferroni *post-hoc* test revealed significant differences between individuals at $\alpha \leq 0.05$ (**Table 7.17**). Differences were noted in N.Lc between individual #3, #2 ($p=0.000$), and #1

(p=0.000). Significant differences were also noted between individual #2 and #3 (p=0.000), and individual #1 and #3 (p=0.000).

RM-ANOVA Following Rank Transformation: Number of Lacunae (N.Lc)

Results of the within-subjects test (**Table 7.18**) indicated that mean N.Lc in cortical and cancellous bone were significantly different overall ($F_{(1,99)}$=214.658, p=0.000). There was no significant interaction observed between overall N.Lc in cortical and cancellous bone and individual ($F_{(1,99)}$=1.189, p=0.309). The test of between-subjects effects demonstrated significant differences in N.Lc between cortical and cancellous bone among the three individuals ($F_{(1,99)}$=67.024, p=0.000) (**Table 7.19**).

Figure 7.21 provides a visual representation of the mean N.Lc in cortical and cancellous bone tissues for the three individuals. Lower N.Lc values are evident for individual #3 in both cortical and cancellous bone tissues. Alternatively, individual #2 exhibited higher lacunar counts than #3 and #1 in both cortical and cancellous bone tissues.

The Bonferroni *post-hoc* test revealed significant differences between individuals at $\alpha \leq 0.05$ (**Table 7.20**). Differences were noted in N.Lc between individual #3, individual #2 (p=0.000), and individual #1 (p=0.000). Significant differences were also noted between individual #2 and #3 (p=0.000), and individual #1 and #3 (p=0.000).

RM-ANOVA Original Dataset: Lacunar Density (N.Lc/BV)

Results of the within-subjects test (**Table 7.21**) indicated that mean N.Lc/BV in cortical and cancellous bone are significantly different overall ($F_{(1,99)}$=196.189, p=0.000). There is no significant interaction observed between overall N.Lc/BV in cortical and cancellous bone and individual ($F_{(1,99)}$=0.406, p=0.668). The test of between-subjects effects demonstrated significant

differences in N.Lc/BV between cortical and cancellous bone among the three individuals ($F_{(1,99)}$=14.205, p=0.000) (**Table 7.22**). N.Lc/BV in cortical and cancellous bone was significantly different between individuals, with lower lacunar density overall in cancellous bone tissue (**Figure 7.22**).

Figure 7.22 provides a visual representation of the mean N.Lc/BV in cortical and cancellous bone tissues for the three individuals. Lower N.Lc/BV values are evident for individual #3 in both cortical and cancellous bone tissues. Alternatively, higher lacunar counts are evident in both cortical and cancellous bone tissues for individual #2 compared to individuals #3 and #1. These differences are more substantial in cancellous bone than cortical bone.

The Bonferroni *post-hoc* test revealed significant differences between individuals at $\alpha \leq 0.05$ (**Table 7.23**). Differences were noted in N.Lc/BV between individual #3, individual #2 (p=0.000), and individual #1 (p=0.001). Significant differences were also noted between individual #2 and #3 (p=0.000), and individuals #1 and #3 (p=0.001).

RM-ANOVA Following Rank Transformation: Lacunar Density (N.Lc/BV)

Results of the within-subjects test (**Table 7.24**) indicated that mean N.Lc/BV in cortical and cancellous bone are significantly different overall ($F_{(1,99)}$=245.952, p=0.000). There is no significant interaction observed between overall N.Lc/BV in cortical and cancellous bone and individual ($F_{(1,99)}$=2.850, p=0.063). The test of between-subjects effects demonstrated significant differences in N.Lc/BV between cortical and cancellous bone among the three individuals ($F_{(1,99)}$=26.372, p=0.000) (**Table 7.25**). N.Lc/BV in cortical and cancellous bone remains significantly different between individuals using rank the transformed data, with lower lacunar density overall in cancellous bone tissue.

Figure 7.23 provides a visual representation of the mean N.Lc/BV in cortical and cancellous bone tissues for the three individuals. Lower N.Lc/BV values are evident for individual #3 in both cortical and cancellous bone tissues. Alternatively, higher lacunar counts are evident in both cortical and cancellous bone tissues for individual #2 compared to individuals #3 and #1. These differences are more substantial in cancellous bone than cortical bone.

The Bonferroni *post-hoc* test revealed significant differences between individuals at $\alpha \leq 0.05$ (**Table 7.26**). Differences were noted in N.Lc/BV between individual #3, individuals #2 (p=0.000), and #1 (p=0.000). Significant differences were also noted between individuals #2 and #3 (p=0.000), and individuals #1 and #3 (p=0.000).

RM-ANOVA Following Rank Transformation: Lacunar Volume (Lc.V)

Results of the within-subjects test (**Table 7.27**) indicated that mean Lc.V in cortical and cancellous bone are significantly different overall ($F_{(1,99)}$=839.825, p=0.000). There was no significant interaction effect observed between Lc.V and individual in cortical and cancellous bone ($F_{(1,99)}$=1.693, p=0.189).

The test of between-subjects effects demonstrated significant differences in Lc.V between cortical and cancellous bone among the three individuals ($F_{(1,99)}$=135.454, p=0.000) (**Table 7.28**). Lc.V in cortical and cancellous bone is significantly different between individuals, with lower Lc.V overall in cancellous bone tissue.

Figure 7.23 provides a visual representation of the mean Lc.V in cortical and cancellous bone tissues for the three individuals. Lower Lc.V values are evident for individual #3 in both cortical and cancellous bone tissues. For individual #2, higher Lc.V is visible in both cortical and cancellous bone tissues compared to individuals #3 and #1, though a higher Lc.V is seen in

cortical bone. The Bonferroni *post-hoc* test revealed significant differences in Lc.V between all individuals at $\alpha \leq 0.05$ (**Table 7.29**).

Summary

Results from the parametric RM-ANOVA tests and non-parametric approach using rank transformed data are comparable for N.Lc and N.Lc/BV. As such, dividing the datasets into within- and between- subjects groups and bootstrapping the results to make determinations from bootstrapped confidence intervals, or creating an implementation in the R statistical package, was not warranted. It is concluded that employing both statistical approaches on these parameters confirms that the results are reliable.

However, Lc.V variables violated both assumptions of the RM-ANOVA and analyses were solely run on rank transformed data. Following the rank transformation, a number of ties, represented by the same values of Lc.V for multiple observations, were noted in the resulting cortical bone ROI dataset. This observation may be contributing to the violation of assumptions revealed during review of the summary statistics. As such, further investigation into measures of lacunar volume parameters with a larger sample size is warranted.

Lacunar Parameters and Nuclear DNA Yield

Normality of raw data was examined using Kolmogorov-Smirnov tests, and revealed that the nuclear DNA dataset was not normally distributed ($\alpha \leq 0.05$) (**Appendix C and Figure 7.24**). Thus, Spearman's Rank-Order Correlations were used to examine the relationship between N.Lc and N.Lc/BV values in cortical and cancellous bone ROIs and the nuclear DNA yield results per gram of sample (ng/g).

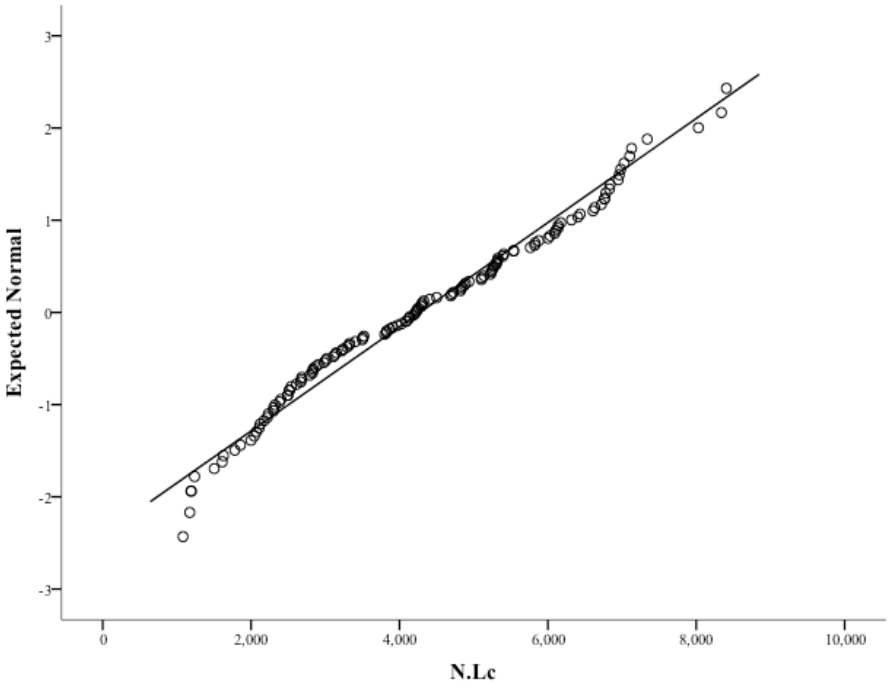

Figure 7.14: Normality Q-Q Plot for Cortical Bone N.Lc.

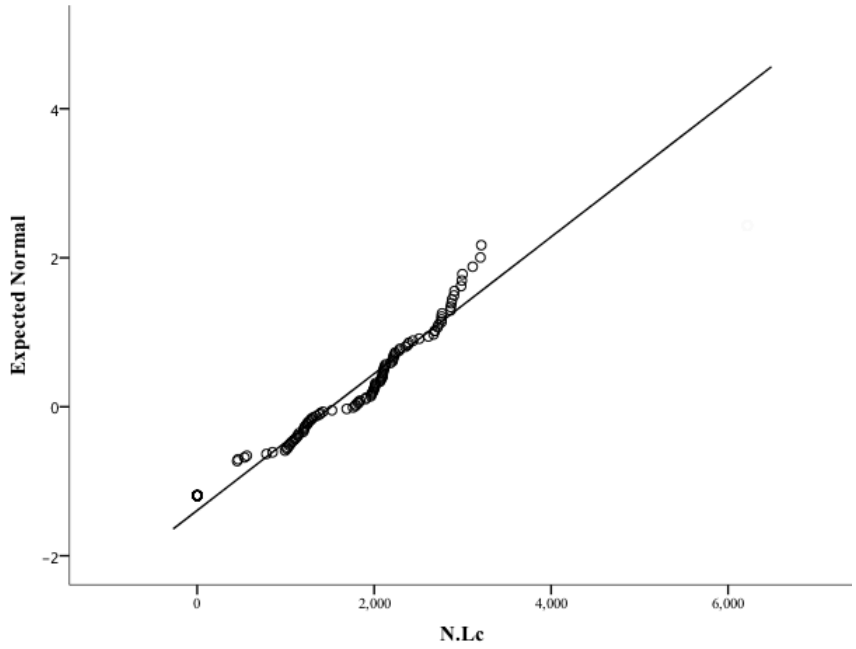

Figure 7.15: Normality Q-Q Plot for Cancellous Bone N.Lc.

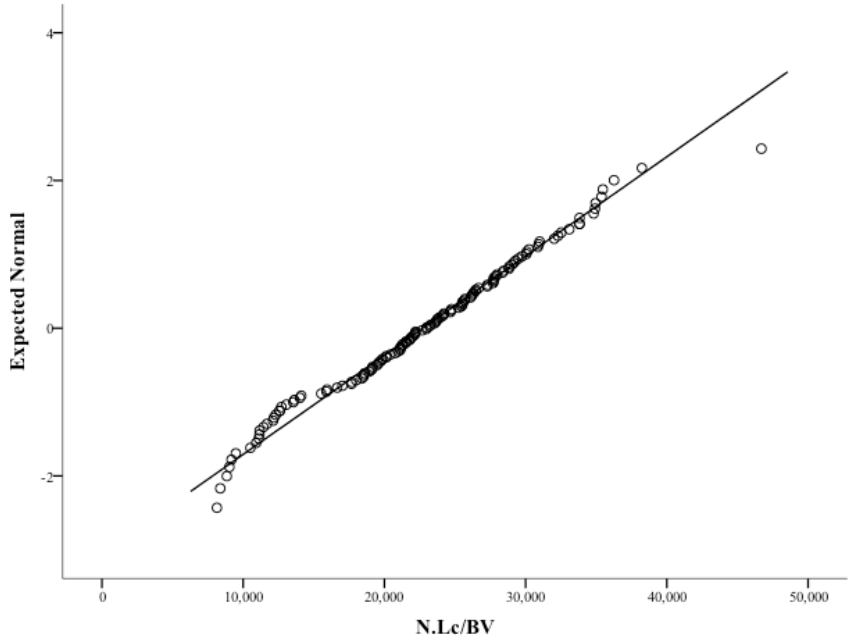

Figure 7.16: Normality Q-Q Plot for Cortical Bone N.Lc/BV (mm^3).

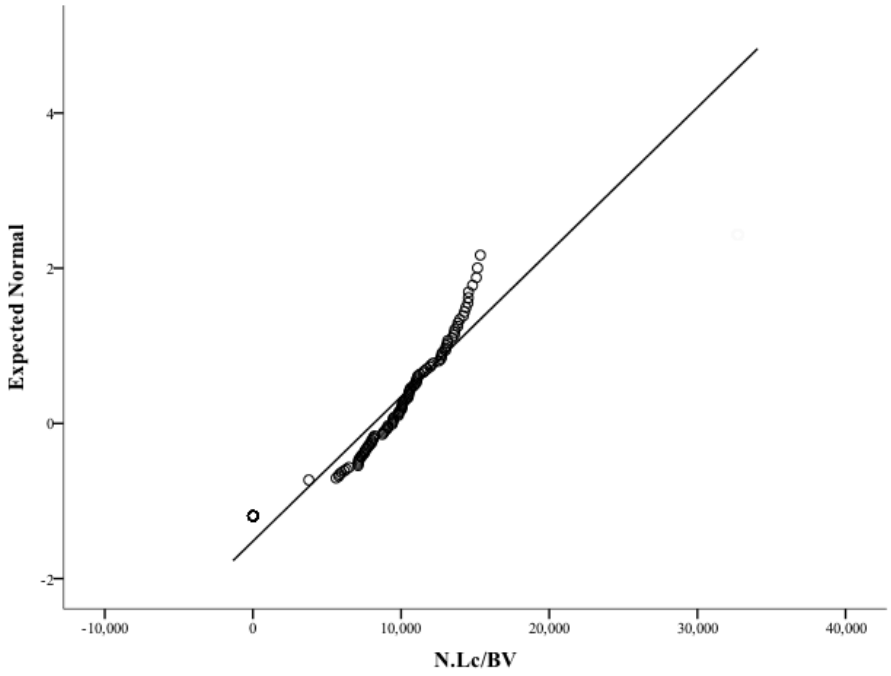

Figure 7.17: Normality Q-Q Plot for Cancellous Bone N.Lc/BV (mm^3).

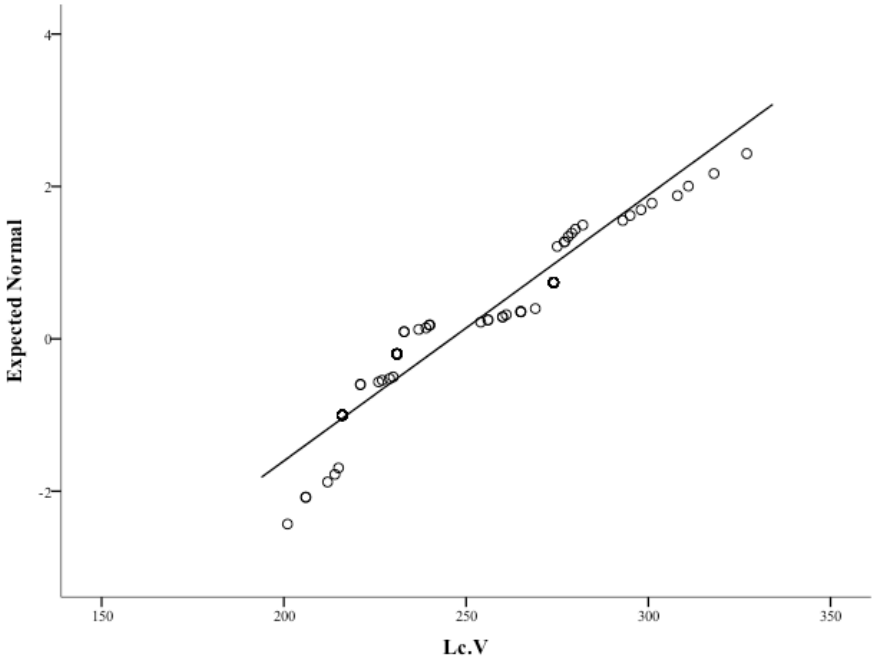

Figure 7.18: Normality Q-Q Plot for Cortical Bone Lc.V (μm).

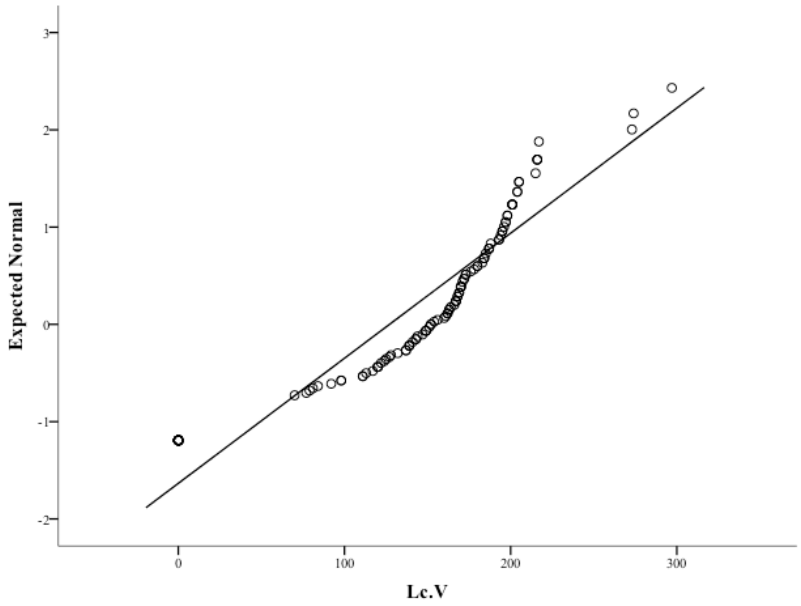

Figure 7.19: Normality Q-Q Plot for Cancellous Bone Lc.V (μm).

Table 7.15: RM-ANOVA Results for N.Lc in Cortical and Cancellous Bone: Within-Subjects Effects.

Source	df	Mean Square	F	*p*-value
N.Lc	1	233129658	171.928	0.000*
N.Lc*Individual	2	3473326.43	2.561	0.082

**Significance at =p <0.05*

Table 7.16: RM-ANOVA Results for N.Lc in Cortical and Cancellous Bone: Between-Subjects Effects.

Source	df	Mean Square	F	*p*-value
N.Lc/Individual	2	65004213.5	47.969	0.000*

**Significance at =p <0.05*

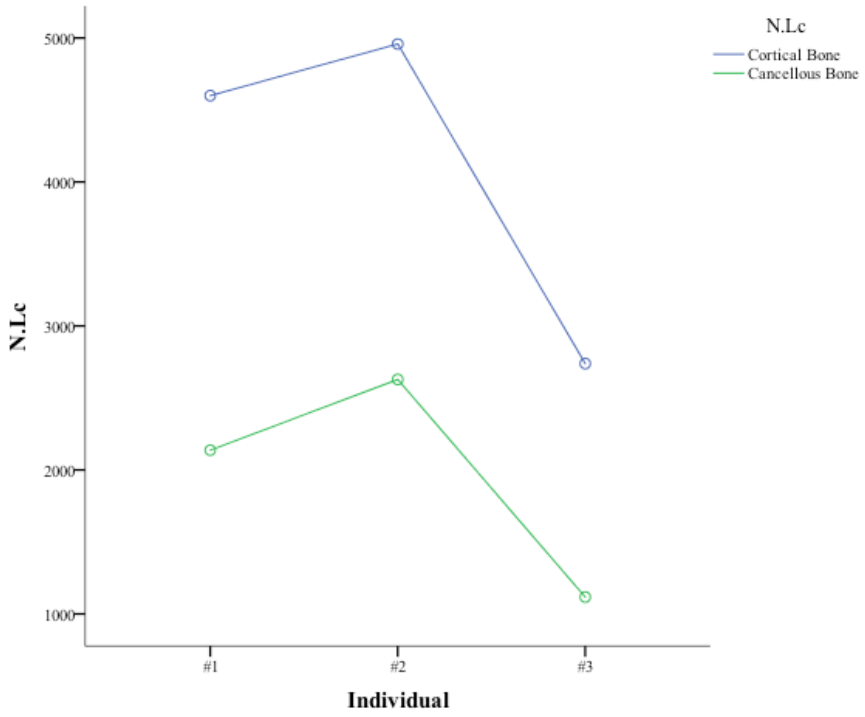

Figure 7.20: Estimated Marginal Means for Cortical and Cancellous Bone N.Lc by Individual from the RM-ANOVA.

Table 7.17: RM-ANOVA Bonferroni Adjustment *post-hoc* Results for N.Lc in Cortical and Cancellous Bone.

(I) Individual	(J) Individual	Mean Difference (I-J)	Std. Error	*p*-value	95% Confidence Interval	
					Lower Bound	Upper Bound
#1	#2	-425.044	199.6417	0.107	-911.239	61.151
	#3	1440.456	199.6417	0.000*	954.261	1926.651
#2	#1	425.044	199.6417	0.107	-61.151	911.239
	#3	1865.500	199.6417	0.000*	1379.305	2351.695
#3	#1	-1440.456	199.6417	0.000*	-1926.651	-954.261
	#2	-1865.500	199.6417	0.000*	-2351.695	-1379.305

**Significance at =p <0.05*

Table 7.18: RM-ANOVA Results for Rank Transformed N.Lc in Cortical and Cancellous Bone: Within-Subjects Effects.

Source	df	Mean Square	F	*p*-value
N.Lc	1	348812	214.658	0.000*
N.Lc*Individual	2	1931.68	1.189	0.309

**Significance at =p <0.05*

Table 7.19: RM-ANOVA Results for Rank Transformed N.Lc in Cortical and Cancellous Bone: Between-Subjects Effects.

Source	df	Mean Square	F	*p*-value
N.Lc/Individual	2	110633	67.024	0.000*

**Significance at =p <0.05*

Table 7.20: RM-ANOVA Bonferroni Adjustment *post-hoc* Results for Rank Transformed N.Lc in Cortical and Cancellous Bone.

(I) Individual	(J) Individual	Mean Difference (I-J)	Std. Error	*p*-value	95% Confidence Interval	
					Lower Bound	Upper Bound
#1	#2	-20.06	6.96768	0.013*	-36.638	-3.4794
	#3	57.640	6.96768	0.000*	41.0603	74.2191
#2	#1	20.059	6.96768	0.013*	3.47941	36.6382
	#3	77.699	6.96768	0.000*	61.1191	-41.060
#3	#1	-57.64	6.96768	0.000*	-74.219	-954.261
	#2	-77.70	6.96768	0.000*	-94.278	-61.119

**Significance at =p <0.05*

Table 7.21: RM-ANOVA Results for N.Lc/BV in Cortical and Cancellous Bone: Within-Subjects Effects.

Source	df	Mean Square	F	*p*-value
N.Lc/BV	1	6.484E+9	196.189	0.000*
N.Lc/BV*Individual	2	13413143.5	0.406	0.668

**Significance at p=<0.05*

Table 7.22: RM-ANOVA Results for N.Lc/BV in Cortical and Cancellous Bone: Between-Subjects Effects.

Source	df	Mean Square	F	*p*-value
N.Lc/BV/Individual	2	459448156	14.205	0.000*

**Significance at =p <0.05*

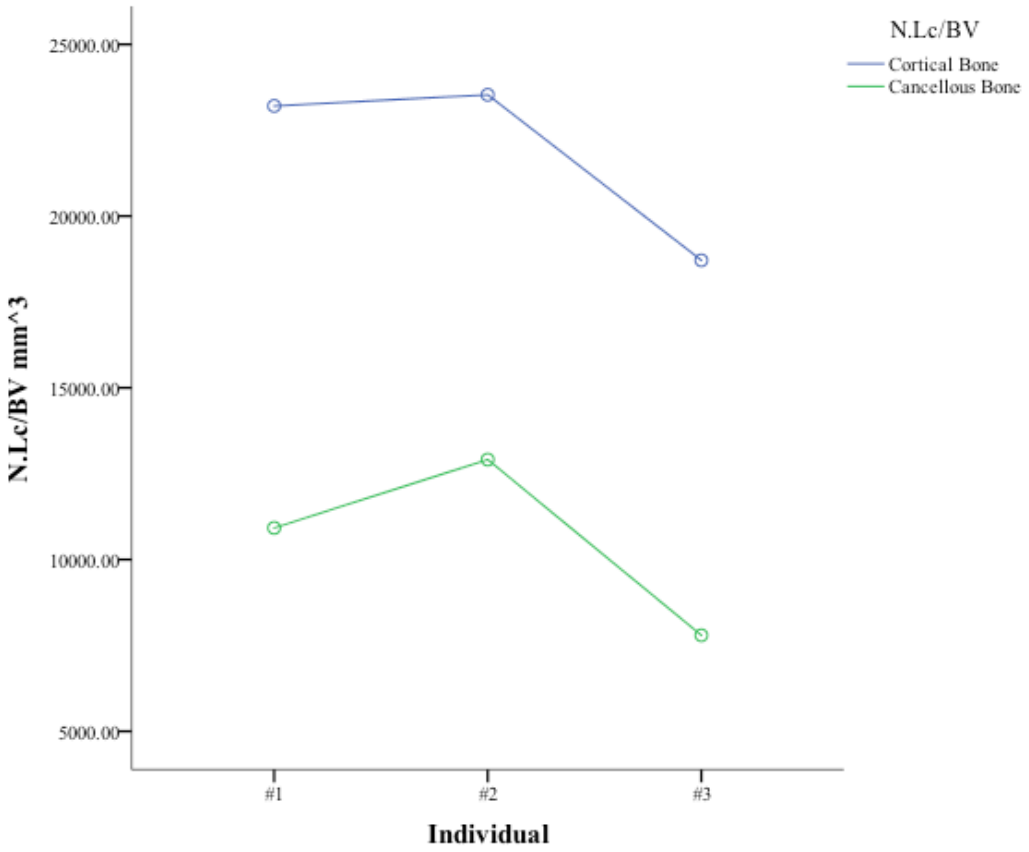

Figure 7.21: Estimated Marginal Means for Cortical and Cancellous Bone N.Lc/BV by Individual from the RM-ANOVA.

Table 7.23: RM-ANOVA Bonferroni Adjustment *post-hoc* Results for N.Lc/BV in Cortical and Cancellous Bone.

(I) Individual	(J) Individual	Mean Difference (I-J)	Std. Error	*p*-value	95% Confidence Interval	
					Lower Bound	Upper Bound
#1	#2	-1156.6779	975.333196	0.715	-3531.9452	1218.58937
	#3	3811.0054	975.333196	0.001*	1435.73814	1926.651
#2	#1	-1156.67789	975.333196	0.715	-1218.5894	3531.94515
	#3	4967.6833	975.333196	0.000*	2592.41603	7342.95055
#3	#1	-3811.005	975.333196	0.001*	-6186.2727	-1435.7381
	#2	-4967.683	975.333196	0.000*	-7342.9506	-2592.4160

**Significance at =p <0.05*

Table 7.24: RM-ANOVA Results for Rank Transformed N.Lc/BV in Cortical and Cancellous Bone: Within-Subjects Effects.

Source	df	Mean Square	F	*p*-value
N.Lc/BV	1	433045	245.952	0.000*
N.Lc/BV*Individual	2	5018.49	2.850	0.063

**Significance at p=<0.05*

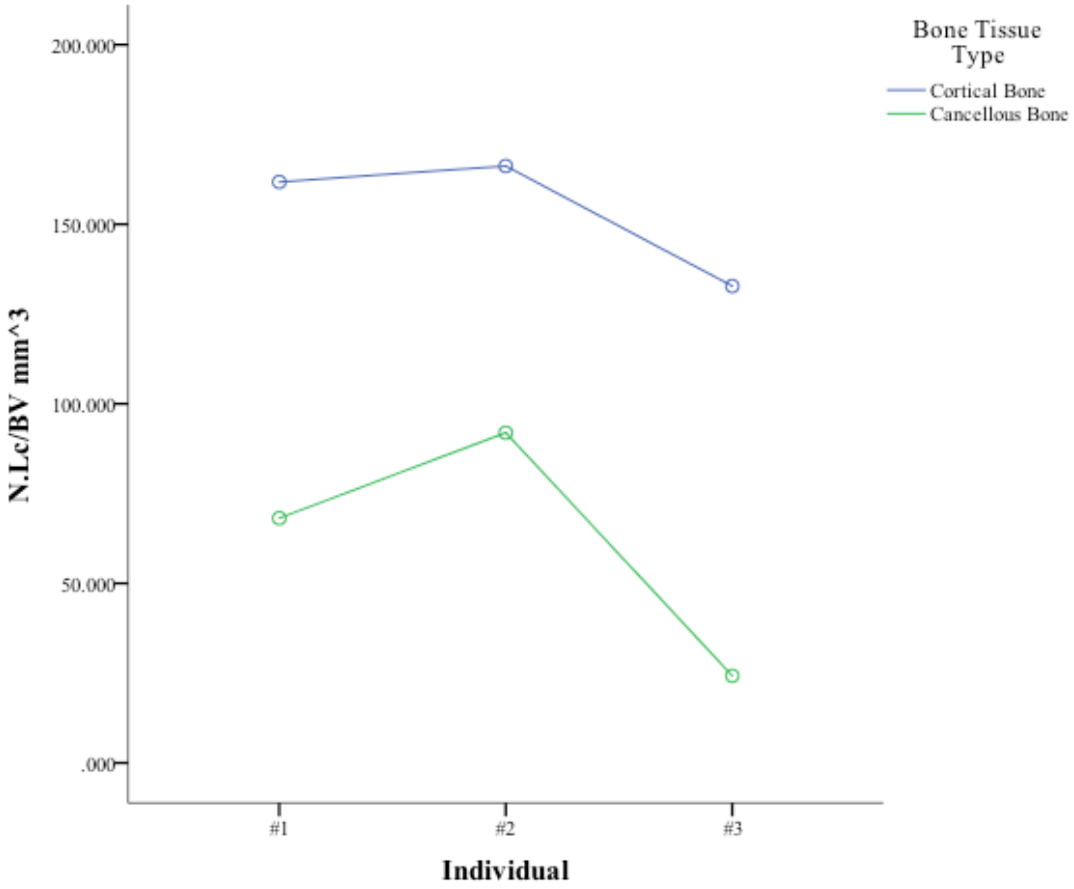

Figure 7.22: Estimated Marginal Means for Rank Transformed Cortical and Cancellous Bone N.Lc/BV by Individual from the RM-ANOVA.

Table 7.25: RM-ANOVA Results for Rank Transformed N.Lc/BV in Cortical and Cancellous Bone: Between-Subjects Effects.

Source	df	Mean Square	F	*p*-value
N.Lc/BV/Individual	2	46300.8	26.372	0.000*

**Significance at =p <0.05*

Table 7.26: RM-ANOVA Bonferroini Adjustment *post-hoc* Results for Rank Transformed N.Lc/BV in Cortical and Cancellous Bone.

(I) Individual	(J) Individual	Mean Difference (I-J)	Std. Error	*p*-value	95% Confidence Interval	
					Lower Bound	Upper Bound
#1	#2	-14.132	7.18590	0.126	-31.231	2.96631
	#3	36.441	7.18590	0.000*	19.3425	53.5398
#2	#1	14.1324	7.18590	0.126	-2.9663	31.2310
	#3	50.574	7.18590	0.000*	33.4749	67.6722
#3	#1	-36.44	7.18590	0.001*	-53.540	-19.343
	#2	-50.57	7.18590	0.000*	-67.672	-33.475

**Significance at =p <0.05*

Table 7.27: RM-ANOVA Results for Rank Transformed Lc.V in Cortical and Cancellous Bone: Within-Subjects Effects.

Source	df	Mean Square	F	*p*-value
Lc.V	1	619192	839.825	0.000*
Lc.V *Individual	2	1247.91	1.693	0.189

**Significance at p=<0.05*

Table 7.28: RM-ANOVA Results for Rank Transformed Lc.V in Cortical and Cancellous Bone: Between-Subjects Effects.

Source	df	Mean Square	F	*p*-value
Lc.V/Individual	2	93636.5	135.454	0.000*

**Significance at =p <0.05*

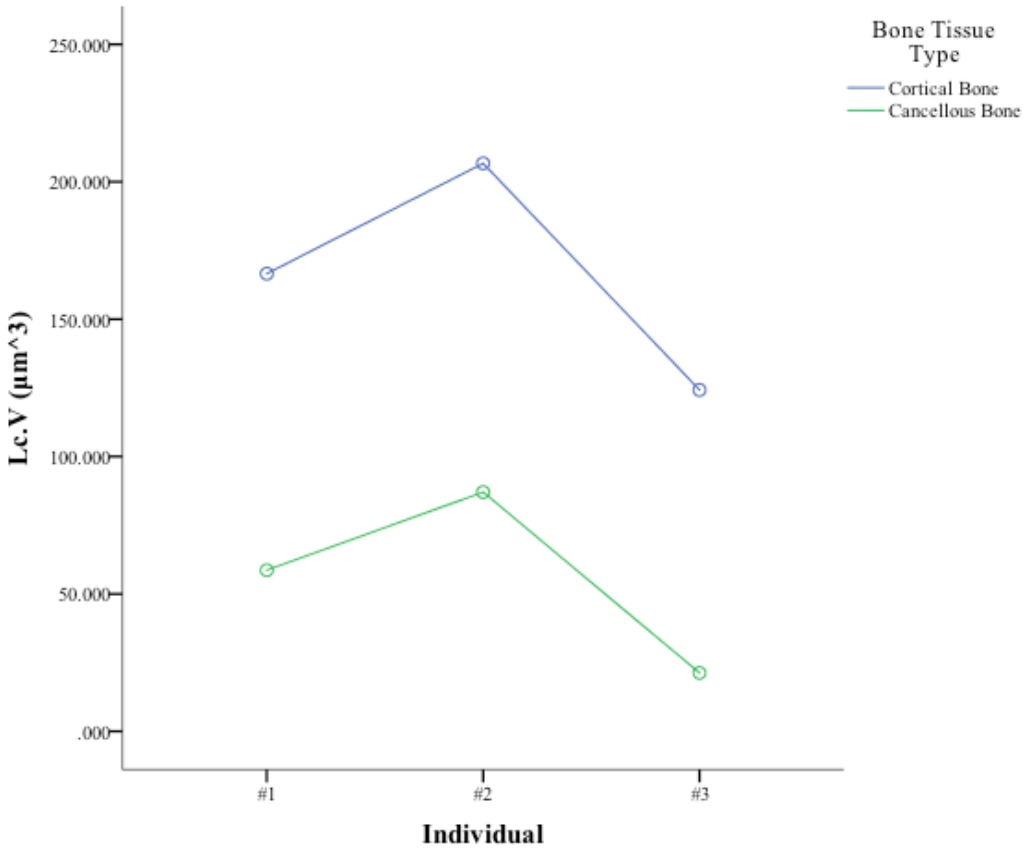

Figure 7.23: Estimated Marginal Means for Cortical and Cancellous Bone Lc.V by Individual from the RM-ANOVA.

Table 7.29: RM-ANOVA Bonferroni Adjustment *post-hoc* Results for Rank Transformed Lc.V in Cortical and Cancellous Bone.

(I) Individual	(J) Individual	Mean Difference (I-J)	Std. Error	*p*-value	95% Confidence Interval	
					Lower Bound	Upper Bound
#1	#2	-34.30	4.50907	0.000*	-45.031	-23.572
	#3	39.846	4.50907	0.000*	29.1164	50.5748
#2	#1	34.301	4.50907	0.000*	23.5722	45.0307
	#3	74.147	4.50907	0.000*	63.4178	84.8763
#3	#1	-39.85	4.50907	0.000*	-50.575	-29.116
	#2	-74.15	4.50907	0.000*	-84.876	-63.418

**Significance at =p <0.05*

Correlation coefficients indicated which variables shared significant relationships at $\alpha \leq 0.05$ (**Table 7.30**). Significant negative correlations are observed between cortical bone N.Lc and nuclear DNA yield ng/g (r=-0.410), and cortical bone N.Lc/BV and nuclear DNA yield ng/g (r=-0.408). These results suggest that although osteocyte lacunar counts are higher in cortical bone tissue, these specimens do not share a positive relationship with nuclear DNA yield per mass of sample, indicating an alternative factor at play. **Figures 7.25-7.26** display the negative associations between the cortical bone lacunar parameters and nuclear DNA yield. Positive correlations exist between cancellous bone N.Lc and nuclear DNA yield ng/g (0.150), and cancellous bone N.Lc/BV and nuclear DNA yield ng/g (r=0.107), though they are not statistically significant. Despite the low correlation, a slight positive trend was observed between cancellous bone N.Lc and nuclear DNA yield ng/g (0.150) (**Figure 7.27**), though a positive trend was not evident for cancellous bone N.Lc/BV and nuclear DNA yield ng/g (**Figure 7.28**).

Canal Diameter and Volume

Individual Object Analysis results for cortical bone canal diameter and volume are summarized in **Appendix A**. The mean results and standard deviations for each parameter are summarized in **Appendix C**. Kolmogorov-Smirnov tests revealed that the datasets were not normally distributed ($\alpha \leq 0.05$) (**Appendix C)**. Levene's tests of equality of variances revealed that the assumption of homogeneity of variances was met for both parameters (**Appendix C**). Though analysis with non-parametric statistics is warranted due to the violation of normality, parametric statistical tests are more powerful, and thus including these additional results is warranted to provide a more complete picture of the relationships between variables.

One-Way ANOVA tests were employed using the original datasets for cortical bone ROIs. A bootstrap for multiple comparisons was performed, followed by a rank transformation

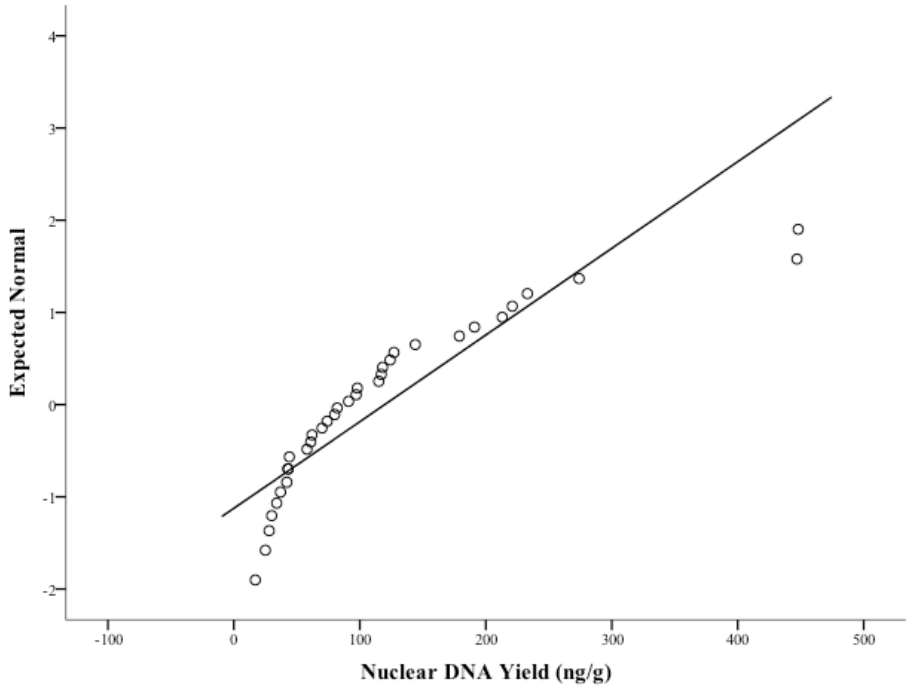

Figure 7.24: Normality Q-Q Plot for Nuclear DNA Yield (ng/g).

Table 7.30: Spearman's Correlation Coefficients for Osteocyte Lacunar Parameters and Nuclear DNA Yield.

	Nuclear DNA Yield (ng/g)	Cort. Bone N.Lc	Canc. Bone N.Lc	Cort. Bone N.Lc/BV (mm^3)	Canc. Bone N.Lc/BV (mm^3)
Nuclear DNA Yield (ng/g)	1.00	-0.410*	0.150	-0.408*	0.107
Cort.Bone N.Lc	-0.410*	1.00	0.073	0.939*	-0.018
Canc.Bone N.Lc	0.150	0.073	1.00	0.043	0.925*
Cort. Bone N.Lc/BV	-0.408*	0.939*	0.043	1.00	0.001
Canc. Bone N.Lc/BV	0.107	-0.018	0.925*	0.001	1.00

**Significance at p=<0.05*

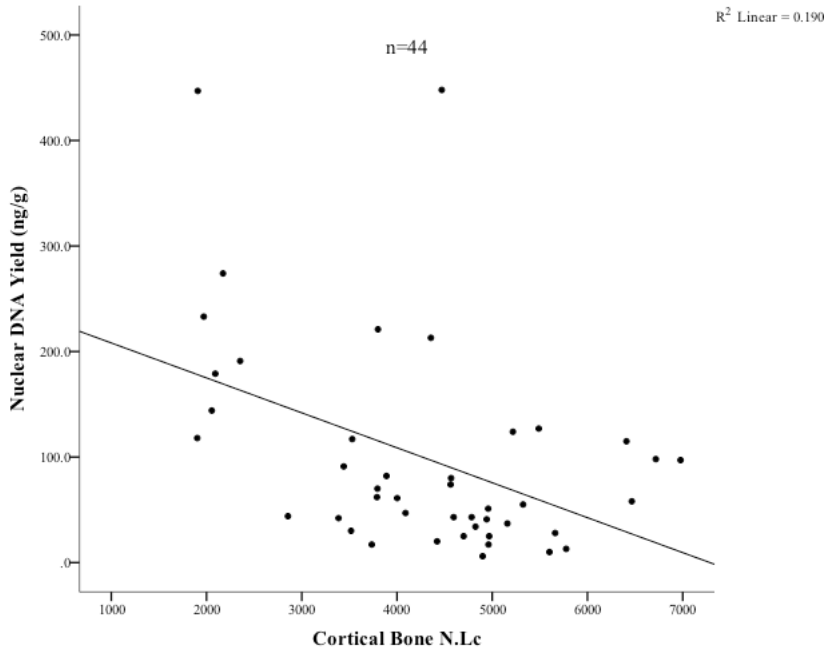

Figure 7.25: Scatterplot Depicting Average Cortical Bone N.Lc and Nuclear DNA Yield (ng/g).

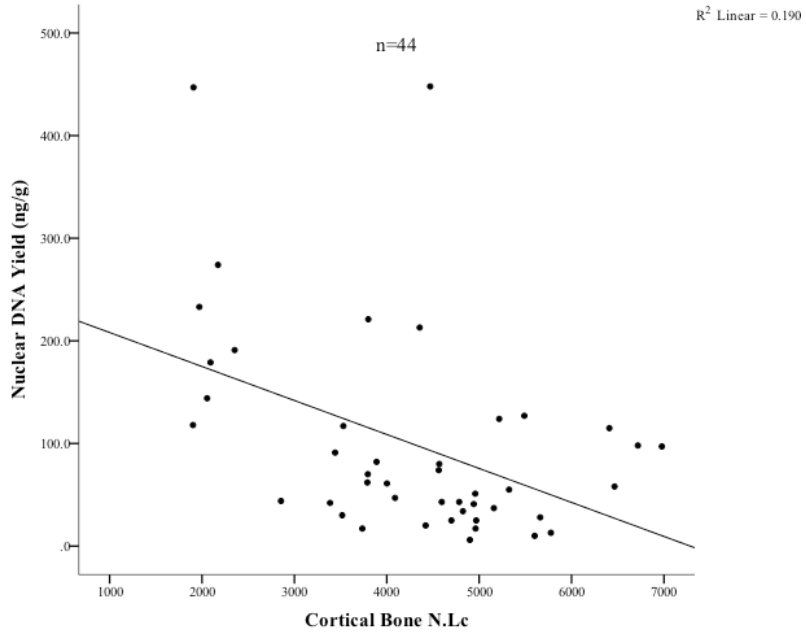

Figure 7.26: Scatterplot Depicting Average Cortical Bone N.Lc/BV and Nuclear DNA Yield (ng/g).

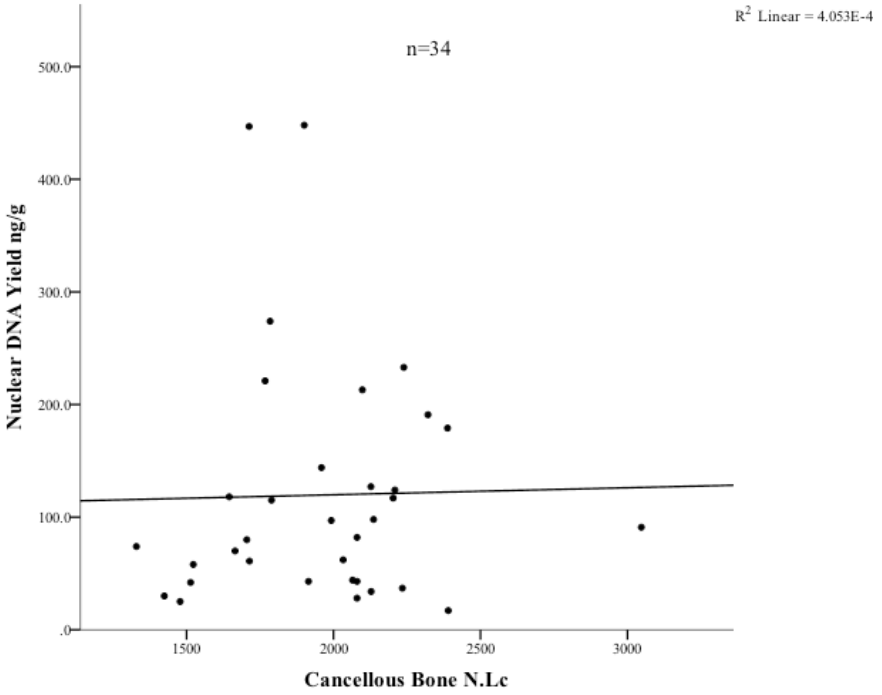

Figure 7.27: Scatterplot Depicting Average Cancellous Bone N.Lc and Nuclear DNA Yield (ng/g).

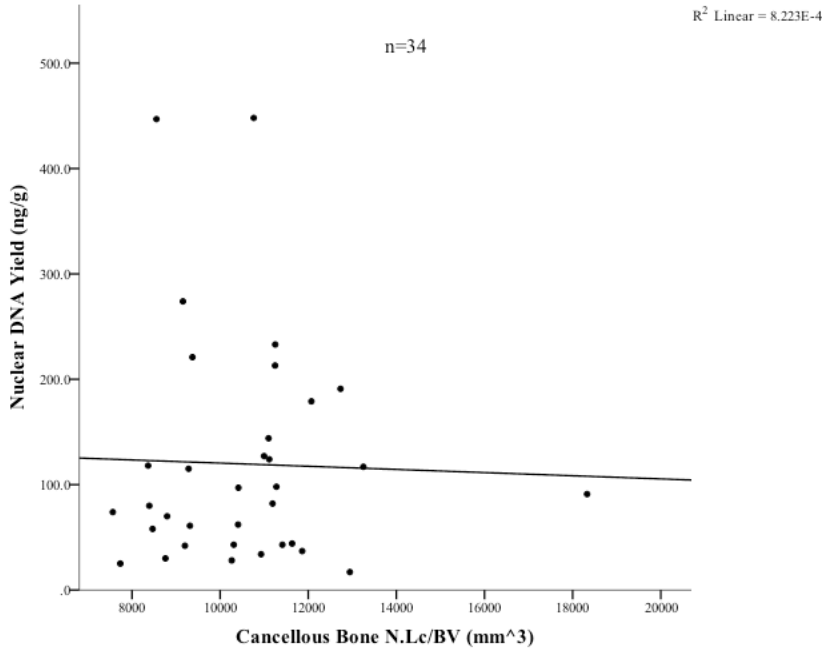

Figure 7.28: Scatterplot Depicting Average Cancellous Bone N.Lc/BV and Nuclear DNA Yield (ng/g).

on each dataset. Ranks of Ca.Dm and Ca.V parameters were further assessed using Kruskal-Wallis tests to evaluate if the results remained consistent. Mann-Whitney *U* tests were used to determine where significant differences existed among individuals.

One-Way ANOVA: Ca.Dm

Results of the One-Way ANOVA (**Table 7.31**) indicated that mean Ca.Dm in cortical bone is significantly different between the three individuals ($F_{(2,129)=}86.962$, p=0.000). The interaction effect between cortical bone Ca.Dm and individual is significant ($F_{(1,129)=}11399.8$, p=0.000), indicating that Ca.Dm measurements are dependent on the individual the measurements were retrieved from, but differences in measurements are not consistent among individuals. A Bonferroni adjustment *post-hoc* test revealed significant differences between all individuals at $\alpha \leq 0.05$ (**Table 7.32**).

The bootstrapping function revealed lower and upper confidence intervals around the means for each individual (**Table 7.33**): (1) #1, M=49.98, 95% CI(48.48, 51.66); (2) #2, M=46.11, 95% CI(44.84, 47.80); and (3) #3, M=61.39, 95% CI(59.15,63.35). As the SPSS software package does not save the 5,000 resampled bootstrapped values, an error bar chart was created from the lower confidence intervals, mean, and upper confidence intervals generated by the One-Way ANOVA (**Figure 7.29**). Significant overlap was not present between the lower and upper confidence interval ranges across individuals, indicating that Ca.Dm measures are significantly different between all three individuals. Thus, it can be concluded that the observations are independent of one another.

Kruskal-Wallis and Mann-Whitney U Tests: Ca.Dm

A Kruskal-Wallis test for Ca.Dm revealed a statistically significant difference among individuals, $x^2(2)=66.038$, $p=0.000$ (**Table 7.34)**, with a mean rank score of 58.58 for individual #1, 38.16 for individual #2, and 102.76 for individual #3. The highest rank overall is associated with individual #3 (**Table 7.35**), indicative of possessing the largest measures of canal diameter (**Figure 7.30**). Mann-Whitney *U* tests determined where significant differences existed among individuals. Ca.Dm of individual #1 was significantly higher than it was for individual #2 ($U_{0.05(2)}=563$, $p=0.001$) (**Table 7.36)**, and Ca.Dm of individual #3 was statistically significantly greater than it was for individuals #1 ($U_{0.05(2)}=214.500$, $p=0.000$) (**Table 7.37)**, and #2 ($U_{0.05(2)}=126$, $p=0.000$) (**Table 7.38)**.

Figure 7.31 provides a visual representation of the mean Ca.Dm in cortical bone tissue for the three individuals. Larger values for Ca.Dm were observed for individual #3. Alternatively, lower values for Ca.Dm are evident in cortical bone tissue for individual #2 compared to individuals #3 and #1.

One-Way ANOVA: Ca.V

Results of the One-Way ANOVA (**Table 7.39**) indicated that mean Ca.V in cortical bone is significantly different between the three individuals ($F_{(2,129)=}124.817$, $p=0.000$). The interaction effect between cortical bone Ca.V and individual is significant ($F_{(1,129)=}22419.73$, $p=0.000$). The significant interaction effect indicates that Ca.V measurements are dependent on the individual the measurements were retrieved from, but differences in measurements are not consistent among individuals. A Bonferroni adjustment *post-hoc* test revealed significant differences between individuals at $\alpha \leq 0.05$ (**Table 7.40**). Differences were noted in Ca.V

between individual #3, individuals #2 (p=0.000), and #1 (p=0.000). Significant differences were also noted between individual #2 and #3 (p=0.000), and individual #1 and #3 (p=0.000).

The bootstrapping function revealed lower and upper confidence intervals around the means for each individual (**Table 7.41**): (1) #1, M=0.072, 95% CI(0.068, 0.075); (2) #2, M=0.060, 95% CI(0.056, 0.064); and (3) #3, M=0.123, 95% CI(0.115,0.132). Since the SPSS software package does not save the 5,000 resampled bootstrapped values, an error bar chart was created from the lower confidence intervals, mean, and upper confidence intervals generated by the One-Way ANOVA (**Figure 7.32**). Significant overlap was not present between the lower and upper confidence interval ranges across individuals, indicating that Ca.V measures are significantly different between each of the three individuals. Thus, it can be concluded that the observations are independent of one another.

Kruskal-Wallis and Mann-Whitney U Tests: Ca.V

A Kruskal-Wallis test for Ca.V revealed a statistically significant difference among individuals, $x^2(2)=92.408$, p=0.000, with a mean rank score of 54.73 for individual #1, 34.89 for individual #2, and 109.89 for individual #3 (**Table 7.42**). Again, individual #3 revealed the highest rank overall (**Table 7.43**), indicative of possessing the largest canal volume. Mann-Whitney U tests determined where significant differences existed among individuals. Ca.V of individual #1 was significantly higher than it was for individual #2 ($U_{0.05(2)}$=542, p=0.000) (**Table 7.44)**. Ca.V of individual #3 was statistically significantly greater than it was for individuals #1 ($U_{0.05(2)}$=24, p=0.000) **(Table 7.45)**, and #2 ($U_{0.05(2)}$=3, p=0.000) **(Table 7.46)**.

A dramatically high Ca.V value is evident for individual #3 (**Figure 7.33**). Conversely, lower Ca.V were noted in cortical bone tissue for individual #2 compared to individuals #3 and #1.

Summary

Results from the parametric One-Way ANOVA tests and non-parametric Kruskal Wallis and Mann-Whitney *U* tests are comparable for Ca.Dm and Ca.V parameters. Applying the bootstrap resampling approach to the parametric tests confirmed that the lower and upper confidence intervals do not overlap, indicating the measures of Ca.Dm and Ca.V are significantly different between all three individuals. It is concluded that employing both statistical approaches on these parameters confirms that the results are reliable.

Table 7.31: One-Way ANOVA Results for Ca.Dm in Cortical Bone.

Source	df	Mean Square	F	*p*-value
Ca.Dm	2	2774.58	86.962	0.000*
Ca.Dm*Individual	1	363720	11399.8	0.000*

**Significance at =p <0.05*

Table 7.32: RM-ANOVA Bonferroni Adjustment *post-hoc* Results for Ca.Dm in Cortical Bone.

(I) Individual	(J) Individual	Mean Difference (I-J)	Std. Error	*p*-value	95% Confidence Interval	
					Lower Bound	Upper Bound
#1	#2	3.86	1.204	0.005*	-0.0027	-0.0197
	#3	-11.41	1.204	0.000*	-0.0638	-0.0412
#2	#1	-3.86	1.204	0.005*	-0.0197	0.0027
	#3	-15.27	1.204	0.000*	-0.0720	-0.0500
#3	#1	11.41	1.204	0.000*	-0.0412	0.0638
	#2	15.27	1.204	0.000*	0.0500	0.0720

**Significance at =p <0.05*

Table 7.33: One-Way ANOVA: Bootstrapped 95% Confidence Intervals for Ca.Dm.

Individual		Statistic	Bias	Std. Error	95% Confidence Interval	
					Lower Bound	Upper Bound
#1	Mean	49.98	0.02	0.85	48.48	51.66
	Std. Deviation	5.634	-0.145	0.908	3.901	6.979
	N	44	0	5	34	54
#2	Mean	46.11	0.01	0.64	44.84	47.40
	Std. Deviation	4.238	-0.059	0.432	3.507	4.926
	N	44	0	5	34	54
#3	Mean	61.39	0.01	1.01	59.15	63.35
	Std. Deviation	6.783	-0.197	1.194	4.342	8.506
	N	44	0	5	34	54

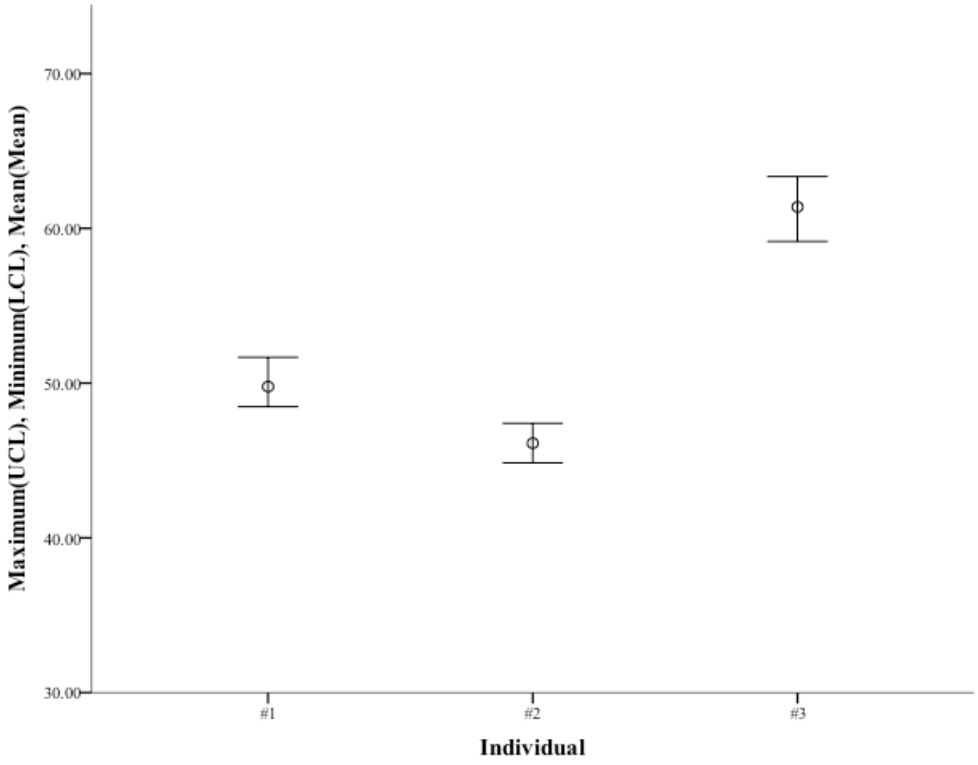

Figure 7.29: Error Bar Chart Displaying the Ca.Dm Bootstrapped 95% Upper and Lower Confidence Intervals and Mean.

Table 7.34: Kruskal-Wallis Test for Significance for Ca.Dm in Cortical Bone.

	C.Dm Cortical Bone
Chi-Square	66.038
df	2
Sig.	0.000

Table 7.35: Kruskal-Wallis Test Rank Results for Ca.Dm in Cortical Bone.

Source	**Individual**	**N**	**Mean Rank**
Ca.Dm Cortical Bone	#1	44	58.58
	#2	44	38.16
	#3	44	102.76

Table 7.36: Mann-Whitney *U* Test for Significance in Ca.Dm in Cortical Bone: Individuals #1 and #2.

	C.Dm Cortical Bone
Mann-Whitney *U*	563.000
Wilcoxin W	1553.00
Z	-3.413
Asymp, Sig. (2-tailed)	0.001

Table 7.37: Mann-Whitney *U* Test for Significant Differences in Ca.Dm in Cortical Bone: Individuals #1 and #3.

	C.Dm Cortical Bone
Mann-Whitney *U*	214.500
Wilcoxin W	1204.50
Z	-6.308
Asymp, Sig. (2-tailed)	0.000

Table 7.38: Mann-Whitney *U* Test for Significance in Ca.Dm in Cortical Bone: Individuals #2 and #3.

	C.Dm Cortical Bone
Mann-Whitney *U*	126.000
Wilcoxin W	1116.00
Z	-7.050
Asymp, Sig. (2-tailed)	0.000

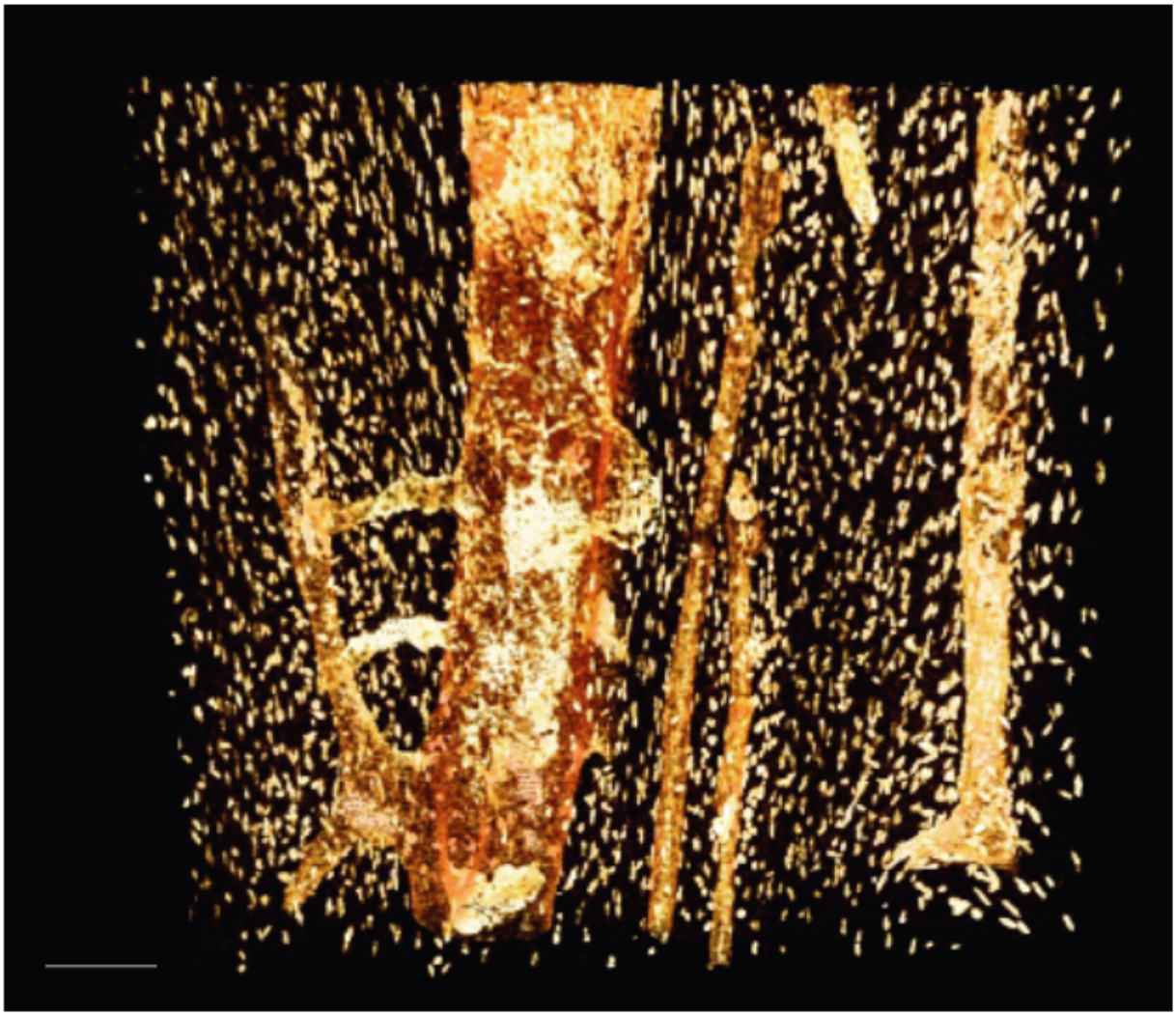

Figure 7.30: SR micro-CT 3D render of the cortical bone ROI from the left first rib of individual #3 displaying large canals. Scale bar=200 μm (Credit: JM. Andronowski).

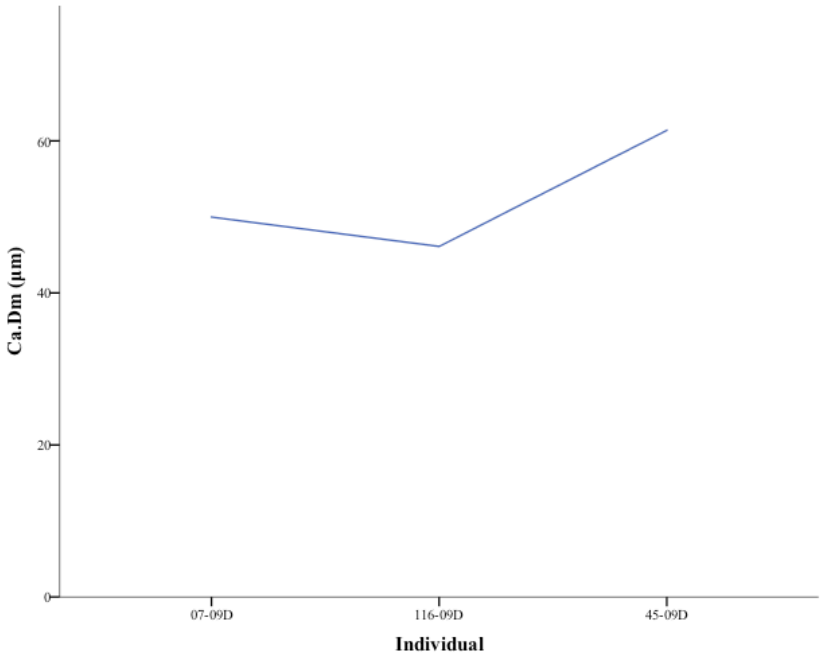

Figure 7.31: Mean Ca.Dm in Cortical Bone for All Individuals.

Table 7.39: One-Way ANOVA Results for Ca.V.

Source	df	Mean Square	F	*p*-value
Ca.V	2	0.049	124.817	0.000*
Ca.V*Individual	1	0.955	22419.73	0.000*

**Significance at =p <0.05*

Table 7.40: RM-ANOVA Bonferroni Adjustment *post-hoc* Results for Ca.V in Cortical Bone.

(I) Individual	(J) Individual	Mean Difference (I-J)	Std. Error	*p*-value	95% Confidence Interval	
					Lower Bound	Upper Bound
#1	#2	0.0111	0.00424	0.026	0.0011	0.0212
	#3	-0.0516	0.00424	0.000*	-0.0616	-0.0415
#2	#1	-0.0111	0.00424	0.026	-0.0212	-0.0011
	#3	-0.0627	0.00424	0.000*	-0.0728	-0.0527
#3	#1	-0.0516	0.00424	0.000*	0.0415	0.0616
	#2	0.0627	0.00424	0.000*	0.0527	0.0728

**Significance at =p <0.05*

Table 7.41: One-Way ANOVA: Bootstrapped 95% Confidence Intervals for Ca.V.

Individual		Statistic	Bias	Std. Error	95% Confidence Interval	
					Lower Bound	Upper Bound
#1	Mean	0.0716	0.0000	0.0017	0.0682	0.0750
	Std. Deviation	0.01140	-0.00018	0.00101	0.00949	0.01289
	N	44	0	5	35	53
#2	Mean	0.0605	0.0000	0.0020	0.0564	0.0643
	Std. Deviation	0.01363	-0.00019	0.00116	0.1156	0.01527
	N	44	0	5	35	54
#3	Mean	0.1232	0.0000	0.0044	0.1150	0.1319
	Std. Deviation	0.02947	-0.00048	0.00333	0.02327	0.03462
	N	44	0	5	35	54

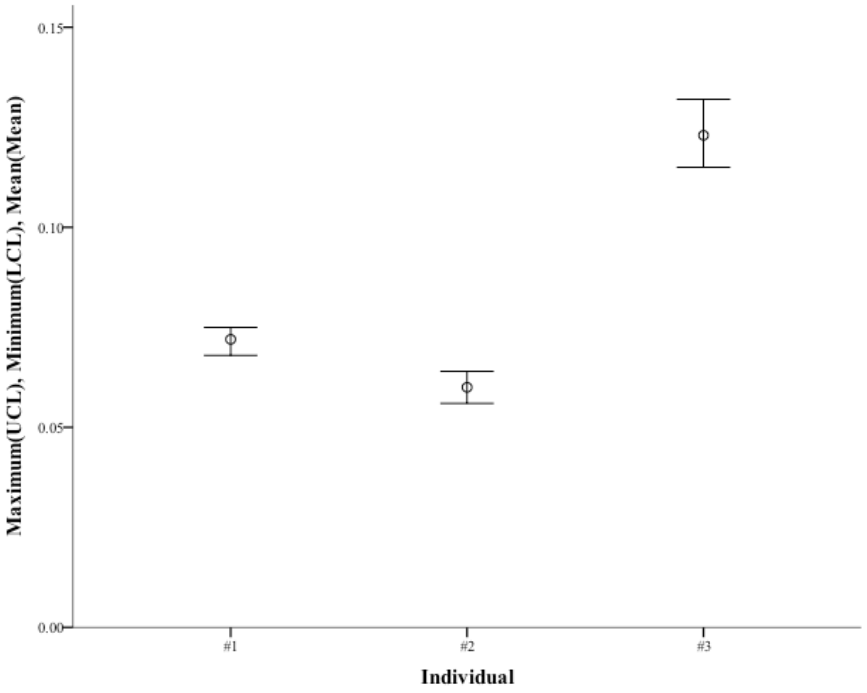

Figure 7.32: Error Bar Chart Displaying the Ca.V Bootstrapped 95% Upper and Lower Confidence Intervals and Mean.

Table 7.42: Kruskal-Wallis Test for Significance for Ca.V in Cortical Bone.

	C.V Cortical Bone
Chi-Square	92.408
df	2
Sig.	0.000

Table 7.43: Kruskal-Wallis Test Rank Results for Ca.V in Cortical Bone.

Source	Individual	N	Mean Rank
Ca.V Cortical Bone	#1	44	54.73
	#2	44	34.89
	#3	44	109.89

Table 7.44: Mann-Whitney *U* Test for Significant Differences in Ca.V in Cortical Bone: Individuals #1 and #3.

	C.Dm Cortical Bone
Mann-Whitney *U*	24.000
Wilcoxin W	1014.00
Z	-7.932
Asymp, Sig. (2-tailed)	0.000

Table 7.45: Mann-Whitney *U* Test for Significance in Ca.V in Cortical Bone: Individuals #1 and #2.

	C.Dm Cortical Bone
Mann-Whitney *U*	542.000
Wilcoxin W	1532.00
Z	-3.649
Asymp, Sig. (2-tailed)	0.000

Table 7.46: Mann-Whitney *U* Test for Significance in Ca.V in Cortical Bone: Individuals #2 and #3.

	C.Dm Cortical Bone
Mann-Whitney *U*	3.000
Wilcoxin W	993.00
Z	-8.094
Asymp, Sig. (2-tailed)	0.000

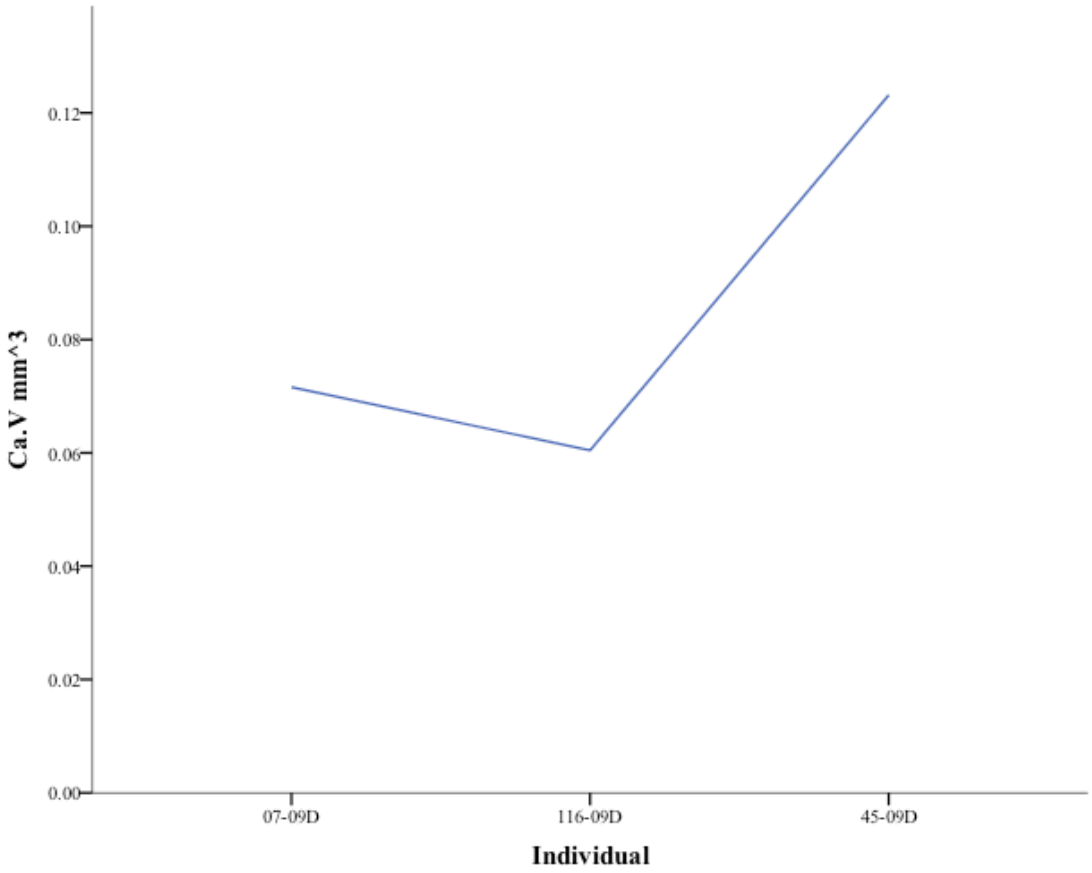

Figure 7.33: Mean Ca.V in Cortical Bone for All Individuals.

CHAPTER SEVEN: DISCUSSION

This study aimed to determine whether differences in bone microstructure can be used to explain differential nuclear DNA yield among bone tissue types. At the time of this writing, the current work represents the first examination of inter-element variation in osteocyte lacunar properties from cortical and cancellous bone tissues in various human skeletal elements. The use of SR micro-CT allowed for a scale of analysis that revealed a high range of variation in lacunar abundance in both tissue types. As this is the first study to use this approach, the results have implications that improve current understandings of the relationship between nuclear DNA yield and osteocyte lacunar abundance, and normal variation of osteocyte lacunar parameters in adult males. Results of this work also have broader applications as it offers promise for the development of a refined method for identifying the bone tissue type most likely to yield nuclear DNA.

This chapter synthesizes the main results from the statistical analyses presented in Chapter 6 and discusses their implications for the hypotheses presented in Chapter 1. Though these hypotheses were derived from three broader questions (see Chapter 1), the study focuses on one central inquiry: Why do different bone tissue types seem to yield DNA differently? A discussion of the supplemental research questions will further examine the relationship of bone tissue type and nuclear DNA yield. The four hypotheses proposed in the introduction generally expected there to be variation in osteocyte lacunar parameters between bone tissue types.

The current research methodology offered promise to refine understanding of DNA bone sample-selection protocols for human identification. The implications of the research findings for forensic identification within the fields of biological anthropology, and forensic anthropology will also be discussed below.

It is important to note the limitations of the study that could potentially be contributing to the observed differences in osteocyte lacunar density between bone tissue types. Overall, two of the greatest challenges encountered were restricted access to human skeletal specimens and synchrotron beam time. Related methodological considerations, limitations of this work, and possible confounding factors will be discussed in a later section of this chapter.

Summary of Principal Findings

Analyses reported in Chapter 6 examined the proposed hypotheses, and the general results are reported here prior to fully discussing their implications. From the exploration of the hypotheses, four main conclusions emerged:

1) The relative amounts of cortical and cancellous bone removed from the DNA sampling sites varied to achieve the desired weight of bone powder for DNA analysis.
2) Osteocyte lacunar abundance and density differs between cortical and cancellous bone tissue types.
3) The cortical bone ROIs contained higher lacunar abundance and density values than their cancellous bone counterparts.
4) Osteocyte lacunar density appears to be independent of nuclear DNA yield, suggesting there may be an alternative explanation regarding why yields were higher from bones with higher cancellous content.

The following sections will provide a synthesis of the results for each of the hypotheses along with explanations regarding how the results inform understanding of nuclear DNA yield and osteocyte lacunar parameters.

Addressing Research Hypotheses

Synthesis of Hypotheses One and Two Results

Hypotheses one and two focused on differences in osteocyte lacunar abundance and density in cortical and cancellous bone tissues. The first hypothesis offered the prediction that osteocyte lacunar density would vary between bone tissue types. The second hypothesis expanded on this notion by stating that osteocyte lacunar density is expected to be greater in skeletal elements with high cancellous bone content.

Hypothesis One

There will be differences in osteocyte lacunar density between cortical and cancellous bone.

This study made an initial investigation into variation in nuclear DNA yields from cortical and cancellous bone tissues, focusing on the examination of osteocyte lacunae. The first hypothesis argued that osteocyte lacunar density varies between bone tissue types. Results of the RM-ANOVAs for N.Lc and N.Lc/BV variables demonstrated that variation exists in osteocyte lacunar parameters between human bone tissue types, with a greater abundance and density of lacunae in cortical bone. As such, the first hypothesis was supported. The following section offers potential explanations for the observed differences in osteocyte lacunar density between bone tissue types.

Developmental Factors

As mentioned in Chapter 3, adult human bone tissue is a product of ongoing growth and development, involving ossification, growth, fusion, appositional growth and eventual bone loss. Developmental differences during bone formation among skeletal elements and tissue types may

play a role in explaining the varying osteocyte concentrations in cortical and cancellous bone tissues. This variability may be attributed to the mechanical environment during bone formation, such as during primary growth or secondary bone remodeling. Possible mechanisms for this variation in lacunar density could include differences in the bone formation rates across the diaphysis, differential remodeling of these areas, the presence of hematopoetic portions of cancellous bone regions, or differences in the local strain environment (Qiu et al., 2002; 2003; Vatsa et al., 2008; Carter et al., 2014b). Further, lacunar infilling, or micropetrosis (Frost, 1960), could be another possible source of density variation since the skeletal sample contained one elderly individual (individual #3) with marked differences in lacunar parameters. Thus, implications of age-related changes associated with individual #3 are described in the following section.

Age-Related Factors

Individual #3 possessed lower osteocyte N.Lc, N.Lc/BV, Lc.V and larger Ca.D and Ca.V compared to the other two individuals. Individual #3 was 69 years-old at the time of death, while individuals #2 and #1 were 47 and 50 years of age at death, respectively. Thus, it is suggested that the microstructural differences observed in individual #3 may be associated with advancing age.

Osteocytes die and disappear from the lacunae of adult humans. Osteocyte deaths are particularly prevalent in elderly individuals, as the bone cortex remodels more slowly (Power et al., 2001). Investigations into age-associated changes in osteocyte lacunar parameters have concentrated largely on lacunar density. Though it is proposed that lacunar density declines with age in males and females (Mori et al., 1997; Mullender et al., 1996; Qiu et al., 2002; Carter et al., 2014a; 2014b), the majority of work on sex differences in bone histological parameters has

focused on women. This interest in the aging female skeleton is due to the increased incidence of age-related bone diseases, such as osteoporosis. The timing of lacunar density decline in females, however, is debated and under further investigation. For example, Mori and colleagues (1997) examined osteocyte lacunar density in femoral head cancellous bone from females. The authors reported that osteocyte lacunar density did not decline until age 70, which was followed by a marked decrease in density thereafter. Further studies have reported this decline to be either linear (Mullender et al., 2005) or exponential (Qiu et al., 2002) in nature. Recent research by Carter and colleagues (2014a; 2014b) examined differences in osteocyte lacunar parameters in males and females across the lifespan. The authors revealed that younger males and females had similar osteocyte lacunar densities. Males demonstrated a significant decrease in lacunar density with advancing age, though females only revealed a downward trend in lacunar density with age. Lacunar volume was found to remain consistent in males, likening the values to those seen in older females (Carter et al., 2014b).

For the most part, lacunar abundance and density values for individual #3 are in agreement with the trends for adult males presented by Carter and colleagues (2014b). The authors reported that males demonstrated a significant decrease in lacunar density with advancing age, while canal diameter and volume increased with age. However, the same study noted that lacunar volume was found to remain consistent in males. In the current study, lacunar volume was lower in individual #3 in both cortical and cancellous bone tissues. Carter and colleagues (2014a) found a reduction in Lc.V in older females across the lifespan, with Lc.V in the over 50 age group reduced by approximately a third in comparison to the under 50 age category. As markedly low Lc.V measures were observed in only one individual in the current

study, further work using an expanded adult male sample is required to ascertain what biological process may be driving these results.

Carter and colleagues (2014b) were the first to identify sex-related differences in the osteocyte lacunar network over the lifespan, thus furthering understanding of the effects contributing to age-associated bone loss. However, one limitation of their female study sample was a lack of specimens representing the female middle-age group. Continuing the research of Carter and colleagues (2014a), expanding the middle-age category may allow for the possible identification of the timing associated with the reduction in lacunar volume. Future directions stemming from the above query and other observations will be described in a later section of this chapter.

Intra- and Inter-Element Variation

The differences in lacunar abundance and density between tissue types may also be attributed to intra- and inter-element variation. This is the first study to examine inter-element variation in osteocyte lacunar properties from cortical and cancellous bone, and only regions directly adjacent to DNA sampling sites were examined. However, certain studies have assessed intra-element analyses of human lacunar density, though these works have been limited and offer conflicting results (Carter et al., 2014b). For example, Power and colleagues (2001) examined osteocyte lacunar occupancy in the femoral neck and reported significant variation in lacunar densities within and between elderly females with hip fractures and those without. The authors identified more lacunae in the inferior region than the superior section (Power et al., 2001). Alternatively, Jordan and colleagues (2003) found no intra-element differences in femoral neck lacunar density in either men or women, with and without osteoporosis or osteoarthritis (Jordan et al., 2003).

Few studies have examined osteocyte parameters in cancellous bone, and all have employed a 2D approach. However, Qiu and colleagues (2002; 2003; 2006) have conducted comprehensive work on osteocyte lacunar density in cancellous bone using human iliac and rib specimens. The authors found significant differences between superficial cancellous (<25 μm from the surface) and deep cancellous bone (>45 μm) from the iliac crest, with superficial bone containing higher densities of osteocytes (Qiu et al., 2002).

Most recently, Carter and colleagues (2013a) examined regional lacunar variation within the femoral cortex of a young adult male using SR micro-CT. Results indicated that extensive regional variation (~30%) in osteocyte lacunar density exists, with the medial and lateral segments containing the most lacunae and the anterior and posterior displaying the least (Carter et al., 2013a). Though this study was limited to the evaluation of one femur within a single individual, it documented considerable variation in lacunar densities between regions. This site-specific variation warns against the extrapolation of lacunar values from single sections (Carter et al., 2013a), and thus further work is warranted.

The purpose of the current study was to compare lacunar parameters with nuclear DNA yield, thus all lacunar variables were only examined in a region of each bone directly adjacent to the DNA sampling sites. It would be valuable to examine multiple regions from each skeletal element to assess regional patterns of variation in lacunar parameters.

Inter-Element Variation and Bisphosphonates

Extensive preclinical research on the use of bisphosphonates (BPs), a class of drugs used to treat osteoporosis known to reduce remodeling and fracture risk, have revealed that their effects on bone turnover can be greatly site-specific (Allen & Burr, 2007; 2011). For example, Allen and colleagues (2010) treated canines (beagle dogs) with an oral BP at doses comparable

to those used to treat osteoporosis. The authors noted initiation of new bone remodeling sites of 15% in the mandible and 46% in the rib. However, no effects were noted in the tibial cortical bone tissue. These findings have implications for the examination of bone remodeling activity at certain skeletal sites, as evidence of bone turnover may be over- or under-estimated in individuals treated with BPs. Thus, differences in remodeling rates among varying skeletal elements may affect the accumulation of osteoblasts that become entombed in osteoid and undergo osteocytogenesis, potentially affecting osteocyte density.

Additionally, the mineralization profile of bone is altered by suppressing bone remodeling and reducing the formation of BMUs (Allen & Burr, 2007). The degree of mineralization is documented to increase in individuals taking BPs, though the mechanisms in which they alter the mineralization process are unclear (Allen & Burr, 2007). Future research should further address why these differences in mineralization exist and how they relate to osteocyte density.

Hypothesis Two

Cancellous bone will have greater osteocyte lacunar densities.

This second hypothesis argued that osteocyte lacunar density varies between bone tissue types, with higher osteocyte densities in cancellous bone. Results of the RM-ANOVAs for N.Lc and N.Lc/BV variables demonstrated that there is a greater abundance and density of lacunae in cortical bone, failing to support this hypothesis.

Bone Turnover Rates

As discussed in Chapter 3, cortical and cancellous bone tissues are continuously modified throughout life. It is often asserted that cancellous bone has higher turnover than cortical bone.

The following section will explore this claim and assess if differences in turnover rates between bone tissue types may be contributing to the variation in osteocyte lacunar densities.

Cortical bone tissue is altered in three ways through: (1) formative bone modeling, including periosteal or endosteal apposition, which adds primary lamellar bone to existing bone tissue; (2) resorptive bone modeling that removes bone tissue; and (3) bone remodeling, which replaces existing bone tissue with secondary lamellar bone (Martin et al., 2015). In healthy adults, cortical bone has a slow turnover rate and a high elasticity modulus (Young's modulus), making it resistant to bending and torsion loads, but weaker in tension (Currey, 2002). The rigidity of cortical bone provides a sturdy attachment for muscles and tendons, and protects vital areas of the body.

It is widely accepted that cancellous bone remodeling operates in accordance with the activation-resorption-formation (ARF) sequence. Cancellous bone tissue is formed through the partial resorption of endosteal cortical bone tissue, and endocortical bone formation (Parfitt, 1994). Similar to cortical bone remodeling, cancellous bone is remodeled throughout life by hemiosteonal remodeling. It is often asserted that cancellous bone has a higher turnover rate and low Young's modulus compared to cortical bone. Though the latter is true, comparisons between the turnover rates and level of metabolic activity of cortical and cancellous bone, and the claims derived from these comparisons, have been questioned (Parfitt, 2002). Allen and Burr (2011) state that cortical bone takes longer to experience remodeling suppression after BP treatment than cancellous bone, implying that remodeling rates are lower in the former. However, Parfitt (2002) argues that although the surface-to-volume ratio of cancellous bone is greater, turnover in cancellous bone will only be higher if it is assumed that the surface remodeling activity is comparable in both tissue types. Further, he suggests that remodeling activity will be greater in

the central skeleton since there is a close partnership between cancellous bone tissue, blood flow, and remodeling activity, as they relate to bone marrow composition (Parfitt, 2002). Additionally, osteoclast precursors migrate throughout the body via the circulatory system, and are shuttled to where they are needed (Parfitt, 1998; 2001). As such, turnover of cancellous bone will remain higher in the central skeleton due to its involvement in calcium homeostasis, and also possibly as support for hematopoiesis (Parfitt, 1993; 2002). According to Parfitt (2002), both cortical and cancellous bone tissues within the central skeleton will experience higher turnover than cortical and cancellous bone in the peripheral skeleton.

These differences in turnover between skeletal elements, and the intra-element variation within bones, suggests that there is not a simple relationship between bone tissue type and turnover rate. As such, generalizing that turnover rate is higher in cancellous bone should be done with caution, as this is only true in certain circumstances.

Osteocyte Lacunar Densities in Cortical and Cancellous Bone Tissues

Considering the current study's hypotheses and results, the following section will discuss the literature related to osteocyte lacunar densities in cortical and cancellous bone tissues.

The range in values for lacunar density in normal human bone is generally high, largely dependent on sampling location, tissue type, and the analytical technique employed (Carter et al., 2013a). Studies examining lacunar populations in human cortical bone are few, reveal high variation in density values, and often extrapolate 2D lacunar counts (mm^2) to 3D (mm^3), resulting in a potentially large margin of error. Recently, Bromage and colleagues (2016) used BSE-SEM to identify osteocyte lacunae in twelve mid-shaft human femora. The authors reported an average value of 100,000 osteocyte lacunae for whole adult femoral mid-shaft cross-sections. Further, Bromage and colleagues (2009) reported a lacunar density of 23,333 mm^3 from the

femur of an *Australopithecus afarensis* specimen (Lucy) by extrapolating from an original lacunar count of 63 (Bromage et al., 2009; Carter et al., 2013a). Sissons and O'Connor (1977) found cortical bone to have approximately 13,900 to 19,400 lacunae mm^3 depending on the sectioning technique applied.

The current study reported osteocyte densities in cortical bone ranging from ~8,000 to 47,000, exhibiting high variance compared to the findings of the above earlier studies. It also reveals a considerable range in density values not previously reported, possibly due to the array of skeletal elements examined. However, the upper values do agree well with those reported by Carter and colleagues (2013a), who devised the applied analytical and quantitative techniques used in this study. The current study found lacunar densities in femoral bone ranging from ~26,000 to 35,000 per mm^3, which are consistent with the densities of ~26,000 to 37,000 per mm^3 reported by Carter and colleagues (2013a). The high counts presented in the current work and those observed by Carter and colleagues (2013a) are likely related to the improved sampling of the 3D imaging modality used, which allowed for larger region of interests to be evaluated and much greater numbers of lacunae to be quantified.

Studies examining lacunar populations in cancellous bone are scarce, and have relied on animal models, and/or 2D traditional histological techniques. For example, Hobdell and Howe (1971) recorded lacunar densities of 13,000 mm^3 in mammalian and reptilian cancellous bone. As mentioned above, Qiu and colleagues have performed substantial 2D research examining osteocyte lacunar properties from human cancellous bone in iliac and rib biopsy specimens (Qiu et al., 2002; 2003a; 2003b; 2006). Differences were observed in lacunar densities between superficial cancellous and deep cancellous bone from the iliac crest, with superficial bone containing higher densities of osteocyte lacunae. The current study revealed a wide range in

osteocyte density in human cancellous bone, ~3,800 to 33,000, which is significantly different from the lacunar density values found in cortical bone tissue specimens. This variability may be attributed to differences in intra- and inter-element cancellous bone turnover rates. However, this study is limited by its focus on only three individuals. Despite this limitation, the current work adds to the growing body of literature addressing the possible variances in lacunae populations within human cortical (Carter et al., 2013a; 2013b; 2014a) and cancellous bone tissues (Qiu et al., 2002; 2003a; 2003b; 2006). The findings further demonstrate that existing pathological and functional interpretations of bone microstructure must be better situated within the broader context of normal variation, as such interpretations are often deduced from the high-resolution 3D imaging of osteocyte lacunae. Further research in this area is warranted to determine whether the observed pattern exists as a part of normal variation.

Synthesis of Hypotheses Three and Four Results

Hypotheses three and four centered on the relationship between the clinical CT and SR micro-CT histomorphometric variables and nuclear DNA yield. The third hypothesis offered the expectation that osteocyte lacunar density would correlate with DNA yield results obtained from the same general location on the bones. The fourth hypothesis examined whether relative measures of cortical and cancellous bone were consistent between sampling DNA sites to achieve the desired testing weight (0.2g bone powder) for nuclear DNA analysis.

Hypothesis Three

The osteocyte lacunar density in cortical and cancellous bone is correlated with differential DNA yield.

Significant differences in osteocyte lacunar abundance and density were found between cortical and cancellous bone tissues, with greater lacunar counts found in cortical bone. As such,

this hypothesis fails to be supported since cancellous bone had a significantly lower lacunar density overall. Results suggest that an alternative explanation exists to describe why Mundorff and Davoren (2014) found elements with higher cancellous content to yield greater quantities of nuclear DNA. A plausible explanation focuses on remnants of soft tissue between trabeculae observed using SR micro-CT. Though soft tissue was not present on the surface of the bones, 3D scans consistently revealed soft tissue within the medullary cavities of skeletal elements with high cancellous content (**Figure 8.1**). It is hypothesized that these residual soft tissues, which likely include periosteum and osteological lining cells, contributed to the higher DNA yields from cancellous bone.

Cancellous bone tissue has an open, porous structure characterized by interconnected trabecular struts. It is found in five primary locations: (1) at the metaphyses of long bones; (2) filling short bones; (3) between flat bones; (4) beneath bony protuberances where muscles attach and; (5) in the medullary cavities of certain long bones (Currey, 2002). In growing bone, spaces around and within cancellous tissue are sites for hematopoietic marrow. With age, the majority of hematopoietic marrow tissue is modified to yellow bone marrow and found within medullary cavities (Nanci, 2008; Carter & Beaupré, 2001). The internal surfaces of cancellous bone are also covered by endosteum. This soft tissue layer consists of connective tissue housing bone cells, and physically separates the bone surface from the marrow (Nanci, 2008). Due to this composition, the surface to volume ratio of cancellous bone and adhering soft tissues removed during DNA sampling is likely much higher compared to cortical bone samples.

As noted in Chapter 5, the three individuals selected for Mundorff and Davoren's (2014) original study were of modern origin and died in the same calendar year, 2009.

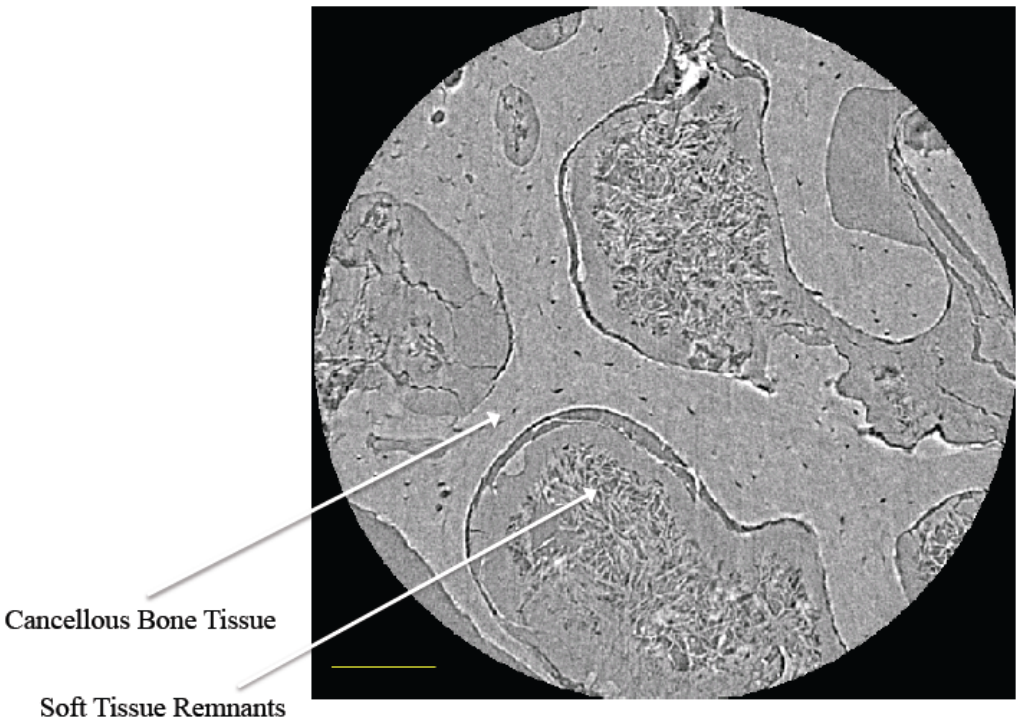

Figure 8.1: SR micro-CT cancellous bone ROI slice from a left 2nd cuneiform. Soft tissue remnants are evident between the trabecular struts. Scale bar=100 μm. (Credit: JM. Andronowski).

Following recovery, all skeletons were only washed with water prior to nuclear DNA sampling to limit possible effects of maceration techniques on DNA recovery (Frank et al., 2015). Bone washing protocols used to remove blood and bone marrow components from the medullary cavities are extensive and time consuming (Eagle et al., 2015), and such measures were not employed. During tissue procurement for SR micro-CT, bones were noted to be greasy but remnants of soft tissue were not evident on the surface of the bones.

Though the presence of soft tissue remnants in cancellous bones was consistent for all three individuals in this study, skeletal elements from individuals of increased postmortem intervals (PMI) were not assessed for the presence of similar amounts of soft tissue. In a follow-up study (Phase 2), Mundorff and Davoren (2014) examined a subset of skeletal elements

(*n*=120) from twelve additional skeletons of increasing PMIs. Phase 2 comprised the eight highest DNA yielding skeletal elements from the primary study plus the femur and tibia, which did not rank highly but are typically sampled for DNA by practitioners. Four predetermined postmortem intervals (0-3 years, 4-10 years, 11-20 years and <20 years) were identified and three skeletons were selected to represent each interval (*n*=12). Skeletons with similar demographics to those examined in the current study were selected. This second phase was designed to determine if the same rank order of skeletal elements by DNA yield would maintain over increased PMIs, and to give an indication of how nuclear DNA degradation occurs over time.

The nuclear DNA results revealed that as PMI increased, the skeletal elements generally maintained a comparable rank order as the first phase, though certain bones did not conform to this pattern. Consistent with phase one, the first distal hand phalanx maintained relatively high yields of DNA while the femur and tibia possessed the lowest (Mundorff & Davoren, 2014). The first distal hand phalanx had the highest yields of DNA from six individuals at three different PMI ranges. The fourth metacarpal was the highest yielding sample from three individuals, the talus was the highest yielding sample from two individuals, and the first cuneiform was the highest yielding sample for one individual (Mundorff et al., 2012). Overall, skeletal elements predominantly comprised of cortical bone were generally low yielding, with the femur possessing the lowest yields from three individuals at three varying PMI ranges, while the tibia had the lowest yields for four individuals at three different PMI ranges (Mundorff et al., 2012).

Skeletal elements that did not consistently conform to the original pattern include a talus and a first cuneiform. Counter-intuitively, a talus from 0-3 years PMI revealed ~50% more DNA than the first distal hand phalanges, which typically exhibited the highest yield rates overall.

Additionally, the first cuneiforms from the 0-3 years PMI range had the lowest average yield, although this was likely due to inhibition (Mundorff et al., 2012). All three first cuneiforms from this PMI interval, however, produced full sixteen-loci profiles. Interestingly, the 10-20 year PMI group had significantly higher DNA yields than the shorter PMI ranges for the majority of samples.

To further the argument that soft tissue between trabeculae of cancellous bone tissue is driving higher nuclear DNA yields, it is recommended that all skeletal elements from phase two be evaluated using 3D imaging modalities including clinical CT and SR micro-CT. If remaining soft tissue is revealed within medullary cavities of bone with differing PMIs, this could aid in explaining why the DNA yields observed by Mundorff and Davoren (2014) remained generally consistent over time, and strengthen the argument that soft tissue remnants may be driving this trend. Future directions stemming from this query will be described in a later section of this chapter.

The proposed "soft tissue hypothesis", as an alternative explanation, has forensic implications for bone sampling protocols in DVI. An alteration to DNA sampling guidelines is proposed that involves the procurement of small, primarily cancellous bones. Though this study did not discover a higher density of osteocyte lacunae in cancellous bone tissue as hypothesized, the residual soft tissue in the medullary cavities likely contributed to the higher DNA yields found by Mundorff and Davoren (2014). As such, removing small elements with high cancellous content, thus housing DNA rich soft tissues, offers promise for selecting elements that will yield higher quantities of nuclear DNA. These smaller bones are straightforward to remove since they can be easily sampled whole in a field or lab setting with the use of a disposable scalpel blade. In turn, this protocol would minimize contamination effects, safety hazards, and the time spent

recovering samples by forensic personnel (Mundorff et al., 2009).

As this sampling recommendation depends on the preservation of remaining soft tissues within the medullary cavities of bones, it is likely that this hypothesis will not hold true for archaeological samples, though further investigation is warranted for confirmation. Over time, diagenetic alterations such as microbial degradation and infiltration of soil into medullary cavities and cancellous bone tissues will cause deterioration of remaining soft tissues and eventually the bone histology. In severely degraded samples, there is often no clear demarcation between the cortical and cancellous bone tissues, and internal porosity increases (Turner-Walker & Mays, 2008). As this porosity increases, soil and associated bacteria begin infilling the open spaces. The concurrent breakdown of bone tissues and invasion of diagenetic agents will result in the decomposition of remaining soft tissue remnants. Eventually, distinguishing histological features such as osteonal boundaries and circumferential lamellae will be difficult to discern. This 'ghost histology' can inform understandings of diagenetic processes and their effects on bone microarchitecture, but do little to assist in the description of life history or health variables related to an individual.

Hypothesis Four

> *The relative volumes of cortical and cancellous bone procured by Mundorff and Davoren (2014) will vary between sampling sites to achieve the desired testing weight for nuclear DNA analysis.*

This hypothesis was upheld by quantifying the relative amounts of cortical and cancellous bone tissue comprising the 0.2g bone powder sample removed from each sampling site. The majority of DNA sampling sites contained between 50-69% cancellous bone, suggesting that unequal amounts of cortical and cancellous bone tissues were removed from each sampling site to achieve the desired testing weight. Mundorff and Davoren (2014) also noted,

"that in most cases, a single hole was sufficient to collect 0.2g of bone powder" (Mundorff & Davoren, 2014, p.56), suggesting that an additional sampling site was drilled for certain elements to achieve a consistent testing weight. However, the skeletal elements that were sampled more than once were not noted. It is plausible that these bones possessed a high cancellous content since cancellous bone is porous and lightweight compared to cortical bone (Martin et al., 2015). As such, bone- sampling protocol differences between skeletal elements, and the associated soft tissues, may be contributing to the high DNA yield from cancellous elements.

The sampling sites from the top-ranked 34 top skeletal elements (of the 55 tested) contained higher amounts of cancellous bone than cortical bone. The assumption that residual soft tissue was consistently present in bones with higher cancellous content may explain why the sampling sites from the top ranked bones were comprised primarily of cancellous bone. Additionally, sampling sites from low ranking skeletal elements, such as the femur, tibia, humerus, radius and ulna, were composed entirely of cortical bone. For these specimens, there was not ample cancellous bone present for a separate ROI to be assessed, further supporting the alternative hypothesis.

Results of the RM-ANOVAs indicated that cortical and cancellous bone height measurements were not significantly different within individuals, and the height and width measurements were not significantly different between individuals. This lack of significance may be attributable to small sample sizes among groups. Though due to the low degrees of freedom in these analyses, increasing the sample size may not have necessarily increased the ability to distinguish subtle differences observed in the results (J. Price, personal communication). However, the interaction effect for cortical and cancellous height and individual was significant. This result indicated that height measurements are dependent on the individual the measurements

were retrieved from, but the differences in measurements were not consistent among individuals. For example, the sampling sites for individual #3 displayed markedly low cancellous bone height measurements. As discussed earlier in this chapter, individual #3 was 69 years old at the time of death and age-associated changes were observed in lacunar abundance, density, and canal parameters. The decreased cancellous bone height measurements may be attributed to a loss of trabecular connectivity and increased porosity of cortical bone associated with age. Human bone undergoes a constant process of remodeling throughout life, in which older bone is resorbed and replaced with new bone. In younger individuals, these paired processes are balanced. With advancing age, however, there is an increase in bone resorption and an overall loss of bone's microarchitectural quality. The modification of cortical bone with age is referred to as trabecularization (Zebaze et al., 2009), and this conversion increases the endosteal area and displays a decreasing network of interconnecting trabecular struts.

Despite subtle differences in the cortical and cancellous height and width measures, future work is needed to further investigate the observed trends among DNA sampling sites using a dataset larger than three individuals. Replicating this study with additional subsets of bones (n=120) from the twelve skeletons of increasing PMIs will increase the sample size and allow for further 3D visualization and quantification of comparable DNA sampling sites.

Overall, the above synthesis of hypotheses three and four suggest broader implications of this work in a forensic context. General recommendations for the improvement of DNA sampling guidelines, and a refined DNA bone sampling guideline, are presented below which in turn may inform future forensic identification efforts.

General Recommendations for the Improvement of DNA Sampling Guidelines

Results demonstrated that primarily cancellous elements from the Mundorff and Davoren (2014) study housed soft tissue within the medullary cavities resulting in higher nuclear DNA yields than cortical bone tissues from the same individuals. These findings have significant implications in a forensic context since cancellous bone is typically dismissed as a potential DNA source in favor of cortical bone. The following section will use the observations made in this dissertation to offer several general DNA sampling guidelines and recommendations to guide those who plan and implement DVI projects.

In the last decade, there have been significant changes in MFI management fueled by large-scale disasters such as the World Trade Center terrorist attacks, hurricane Katrina (2005), and the 2004 Boxing Day tsunami. DVI is a critical part of a response to a mass disaster in order to recover, identify and, repatriate all decedents and their associated body parts (Sledzik & Rodriguez, 2002). It is a multidisciplinary approach, in which forensic anthropologists currently play a critical role (Mundorff et al., 2012).

In conjunction with changes to mass fatality response protocols, DNA extraction and amplification techniques have been improved, especially with regard to the analysis of small and degraded samples. Although DNA analysis has become a common tool used in human identification, current DVI DNA sampling choices are highly variable, and often customized for each unique disaster situation (Mundorff et al., 2009). As described in Chapter 2, there are few empirically based studies informing current guidelines that outline DNA sampling recommendations following mass fatality incidents. The available DVI manuals provide comprehensive information to create a mass disaster response plan, but only general DNA sampling guidelines. They do not consistently define, however, how their guidelines can be

modified for different disaster situations, and sometimes fail to differentiate between best practices and minimum standards. As such, this author aims to present a set of generic DNA sampling guidelines for DVI, provide explanations of how they can be modified based on various scenarios, discuss considerations for sufficient sample preservation, and suggest recommendations for best practices.

Due to challenging field conditions often encountered in a mass context, and the lack of universally applied DNA sampling guidelines, it is not rare to encounter forensic field teams working without previously determined tissue extraction protocols (Sledzik & Rodriquez, 2002; Milos et al., 2007). In response to this evidence, and the discrepancies evident in mass disaster management manuals and DNA sampling guidelines for DVI, a set of generic recommendations are presented below for those who intend to rely on DNA as the primary modality of identification.

1. Disaster response plans and DVI guides are typically comprehensive and dense, therefore it is essential that these manuals be clearly and intuitively organized. As is evident in the NIJ manual (2005), poor organization and disorganized appendices lead to a lot of back-and-forth browsing that is not intuitive. Difficulty in following this material can lead to further distress for forensic personnel in mass disaster situations.

2. Responses to mass disaster are multidisciplinary. The various forensic disciplines should be adequately represented (if possible) with individual roles and responsibilities defined. For example, anthropology and radiology are underrepresented in the NIJ and Interpol

manuals, although forensic anthropologists and archaeologists are crucial during victim recovery, initial triage, and identification.

3. DNA sampling guidelines should be adaptable to various DVI scenarios such as large- and small-scale disasters, open and closed populations, and intact or fragmentary remains.

Most Significant Recommendation for DNA Bone Sampling Guidelines

The most significant recommended alteration to current DNA sampling guidelines is the procurement of small, cancellous bones. As demonstrated by Mundorff and Davoren (2014) small bones such as hand phalanges, tarsals, and patellae were shown to yield sufficient DNA profiles. Though this study did not discover a higher density of osteocyte lacunae in cancellous bone tissue as hypothesized, an alternative explanation suggests that remnants of soft tissue found in between trabeculae likely contributed to the higher DNA yields found by Mundorff and Davoren (2014). As such, removing small elements with higher cancellous content would allow for straightforward sample removal since small bones can be easily sampled whole in a field or lab setting with the use of a disposable scalpel blade. In turn, this protocol would minimize contamination effects from sampling a wedge of cortical bone, safety hazards due to the use of an electric saw, and the time spent recovering samples by forensic personnel (Mundorff & Davoren, 2014).

Caveats and Methodological Limitations

Caveats

In the analyses summarized above, the research hypothesis proposing a link between high lacunar density in cancellous bone tissue and DNA yield was not supported. On the statistical argument, power analyses may reveal that the sample sizes were insufficient to reach statistical significance. Due to the low degrees of freedom in these analyses, increasing the sample size may not have necessarily increased the ability to distinguish many of the subtle differences observed in the results (J. Price, personal communication). Statistical power is also dependent on effect sizes. To reach relatively large effect sizes would require sample sizes much greater than the total sample available for this study and even then an increase in sample size is not a guarantee for increased effect sizes.

Methodological Limitations

One of the greatest challenges for the current work was the restricted access to human skeletal specimens and synchrotron beam time. In order to accurately illustrate the variation in lacunar density among bone tissue types, a dedicated project would be required with a larger number of human samples from additional individuals and sufficient beam time.

A major limitation of the employed SR micro-CT technique is the ratio of field of view to image resolution. In order to visualize a sufficient number of lacunae to be biologically and statistically relevant some resolution was sacrificed. While the majority of images were clear, others displayed artifacts and noise that limited the visibility of microstructural features. Though the protocol allowed for visualization of lacunae and other microstructural features, it only permitted intermittent quantification of shape parameters. As such, all shape data were removed

from the analysis. However, there are other synchrotron facilities that are capable of achieving suffice resolution for quantifying shape parameters. For example, imaging of osteocyte density and shape was conducted by Carter and colleagues (2013a; 2013b; 2014a) using an established protocol at the Advanced Photon Source (APS), Argonne National Laboratory, Il, USA. This protocol provided excellent quantitative information, and allowed for short scan times. Comparable scans per specimen were achieved in approximately twenty-two minutes (Carter et al., 2014b).

The current study was limited by its focus on three adult male individuals. Human tissue procurement for histological analysis is destructive and it is difficult to acquisition a large number of specimens for research purposes. However, as a proof of principle study, the results from this project justify destructive analysis of a larger dataset to further assess the relationship between nuclear DNA yield and bone tissue type.

Notably, the cortical and cancellous bone ROIs assessed herein only represent portions of the entire cross-section of these bone specimens. Despite this limitation, hundreds of thousands of lacunae were analyzed with consistent results. This work further highlighted the high variation in lacunar populations within human cortical and cancellous bone. Further exploration of the variation identified in lacunar abundance and density using a larger sample that is representative of the adult male life span will allow for a clearer understanding of lacunar populations.

Future work should focus on refining bone sampling, imaging, and image-processing protocols for cancellous bone for SR micro-CT. Due to the small width of the beam at the BMIT-ID line, the field of view is limited to 2 mm. As such, the cancellous bone of certain specimens did not fit into the field of view. Additional beam time would have permitted for multiple scans of a single specimen, allowing for each bone tissue type to be successfully imaged. Embedding

tissue specimens may also allow for greater cancellous bone volumes to be visualized. Due to the nature of hard-tissue procurement, some trabeculae were broken during sampling. Embedding bone blocks in an epoxy resin, however, would likely increase the presence of artifacts in the scans (D.M.L. Cooper, personal communication). Later imaging experiments on the BMIT-ID line utilized human femoral bone specimens embedded in methylmethacrylate (MMA). This technique has been widely used for undecalcified bone tissue for bone histomorphometry in both clinical and experimental contexts (Erben, 1997). MMA can also be fully removed from bone tissue sections, while epoxy resin cannot. As such, embedding bone in MMA will be considered for future research focused on the 3D imaging of cancellous bone. This study aimed to follow the methodology outlined by Carter and colleagues (2013a), along with time and budgetary constraints, thus embedding in MMA was not carried out.

Image processing of cancellous bone ROIs was laborious and time consuming. As discussed in Chapter 6, CT Analyser and ImageJ software programs were used to segment 3D image stacks and separate lacunar spaces from canals and cavity spaces. Issues were encountered during cancellous bone processing due to phase fringe (areas of high frequency), as these regions often did not contain adequate frequency information. Future work should consider using image-processing software such as AMIRA (Visage Imaging, Berlin, Germany), or Avizo (Visage Imaging, Berlin, Germany) as they may provide more powerful analysis tools than CT Analyser and ImageJ.

Even taking into account the methodological limitations of this study, the results do address interpretations of variation in osteocyte lacunar parameters in cortical and cancellous bone tissues, providing a basis for further assessment.

Future Directions

This dissertation demonstrated differences in lacunar density between human bone tissue types on a scale of two comparable ROIs per specimen. Attempts to measure osteocyte lacunar parameters beyond abundance, such as morphology and spatial distribution, could not be evaluated from the SR micro-CT scans due to resolution limitations at the BMIT-ID line. The majority of lacunae had a generally spherical appearance and accurate shape assessments could not be quantified from all scans. As such, it would be valuable to assess differences in osteocyte lacunar morphology in cortical and cancellous ROIs from individual specimens. Lacunar morphology has not been widely studied in either animal or human models. Work by van Hove and colleagues (2009) compared diseased human bone samples and found that osteopenic bone had relatively large and round lacunae, while lacunae in osteoarthritic bone were large and elongated. In an animal model, Vatsa and colleagues (2008) found osteocyte lacunae in the fibula, an element experiencing uni-directional loading, were elongated relative to those of the cranial vault, a region undergoing multi-directional loading. In each of these studies, the authors linked the results to adaptation of the bone matrix due to different external loading conditions. Recent work by Carter and colleagues (2013a) revealed differences in lacunar morphology between various regions within human femora. The authors revealed more elongated lacunae in anterior and posterior regions than in the other segments.

It would be beneficial to investigate lacunar abundance and density in relation to additional microstructural features such as vascular canals, lamellae, and BMUs. Since BMUs accomplish bone remodeling, and thus the mechanism for the removal and embedding of

osteocytes, description of lacunar parameters around BMUs, may illuminate the relationship between remodeling and the osteocyte mechanotransduction system.

Another topic necessitating further exploration is the reported differences in osteocyte lacunar parameters (density, volume, orientation, and morphology) with age between adult women and men (Carter et al., 2013b). The Carter and colleagues (2013b) study was limited by a lack of specimens representing the female middle-age group. Continuing Carter and colleagues' (2013b) work by expanding the middle-age category would possibly allow for the identification of the timing associated with the reduction of osteocyte lacunar volume. Due to the preferential bias of particular bone diseases in females, such as osteoporosis, further exploration of age-associated sex differences in lacunar parameters is warranted. Revealing a sudden decline in lacunar volume during middle age may suggest a potential link to menopause, which may have implications for selecting possible targets for intervention during menopause linked to the bone remodeling process.

For the results to be better understood and applicable to forensic identification, this study will be replicated using the additional subsets of bones (n=120) from the twelve skeletons of increasing PMIs selected by Mundorff and Davoren (2014). Findings from bones at increased PMIs may clarify the link between residual soft tissue between the trabeculae of cancellous bone and higher nuclear DNA yields. Recommendations further include evaluation of all skeletal elements from the Mundorff and Davoren (2014) phase two study using 3D imaging modalities including clinical CT and SR micro-CT. Revealing residual soft tissue within medullary cavities of bone with increased PMIs could aid in explaining why the DNA yield patterns observed by Mundorff and Davoren (2014) generally persisted over time.

CHAPTER EIGHT: CONCLUSION

The overarching goal of this dissertation was to determine whether differences in bone microstructure can be used to explain differential nuclear DNA yield among bone tissue types. Increased interest in bone cellular properties resulting from the availability of 3D imaging modalities, allows researchers to quantify osteocyte lacunar parameters. By employing SR micro-CT, this study has been able explore osteocyte lacunar density in representatives of each skeletal element type within a single individual and among multiple individuals for the first time. The current work raises more questions than it answered. However, the most important intellectual contributions of this dissertation are that it: (1) highlights the variance in osteocyte lacunar populations within human cortical and cancellous bone tissues, which is an area of growing interest due to emerging high-resolution imaging techniques, and (2) provides evidence for preferentially sampling bones with primarily cancellous content with associated soft tissue remnants in forensic contexts.

Although the 3D analysis of bone microstructure did not result in a concrete explanation for differential DNA yields among bone tissues types, the results encourage further exploration. Three research questions were posed in Chapter 1, and conclusions drawn from the current work will be briefly summarized in response to these questions.

How does osteocyte lacunar density and the amount of bone matrix surrounding osteocytes compare between cortical and cancellous bone tissue types?

SR micro-CT scans consistently revealed remnants of soft tissue within the medullary cavities of bones with high cancellous content, suggesting that the adherent soft tissues contributed to higher DNA yields from cancellous bone. A follow-up study using additional subsets of bones (n=120) from the twelve skeletons of increasing PMIs will replicate the

methodological approaches outlined here to potentially further the evidence supporting this hypothesis. Future results may have implications for DNA bone sampling protocols in a forensic context. If remaining soft tissue within cancellous bone is driving the high DNA yields, this suggests that these elements should be preferentially sampled in cases involving modern skeletal remains.

Can osteocyte lacunar density in cortical and cancellous bone be used to explain differential DNA yield?

Osteocyte lacunar density appears to be independent of nuclear DNA yield, as lacunar abundance and density was greater overall in cortical bone specimens. Results suggest that an alternative explanation exists that describes why Mundorff and Davoren (2014) found elements with higher cancellous content to yield greater quantities of nuclear DNA.

Do the relative volumes of cortical and cancellous bone, procured by Mundorff and Davoren (2014), vary between each sampling site procured to achieve the desired testing weight for nuclear DNA analysis?

Overall, the amount of cortical and cancellous bone tissues varied between the DNA sampling sites procured by Mundorff and Davoren (2014), with increased amounts of cancellous bone removed from higher-ranking skeletal elements. This suggests that the sampling protocol for cortical and cancellous bone may be contributing to the variation observed in DNA yield among skeletal element types.

Summary

Chapter one outlined the rationale for the study, research objectives, questions, and hypotheses. The second chapter examined broad issues associated with DNA bone sampling protocols in the forensic identification literature, and reviewed previous studies examining DNA

yield rate by skeletal element. Chapter three provided a comprehensive overview of basic bone biological principles including normal human bone gross composition, histomorphology and basic mechanisms of bone turnover. Chapter four introduced 3D imaging modalities as alternatives to traditional 2D methods, provided a brief history of the conception of 3D imaging techniques, and examined various imaging modalities used in both clinical and anthropological research. Chapter five provided details on the skeletal sample chosen for this study and the methods involved in preparing bone specimens suitable for the analyses needed to complete the project. An overview of the 3D imaging modalities used for data collection and the subsequent analyses were also discussed here. Chapter six presented the results. Chapter seven contained a discussion that provided perspectives gained from the study and the potential for future research as they relate to anthropology and bone biology. Chapter eight concludes the dissertation, providing an overview of the results and potential future research directions.

LIST OF REFERENCES

Adam JF, Nemoz C, Bravin A, Fiedler S, Bayat S, Monfraix S, Berruyer G, Charvet AM, Le Bas JF, Elleaume E, Estève F. 2005. High-resolution blood-brain barrier permeability and blood volume imaging using quantitative synchrotron radiation computed tomography: Study on an F98 rat brain glioma. J Cereb Blood Flow Metab(25):145-153.

Agarwal SC. 2008. Light and broken bones: Examining and interpreting bone loss and osteoporosis in past populations. In Katzenberg AK and Saunders S (Eds) Biological Anthropology of the human skeleton (2nd Ed). Wiley-Liss: NY.

Allen MR, Kubek DJ, Burr DB. 2010. Cancer treatment dosing regimens of zoledronic acid result in near-complete suppression of mandible intracortical bone remodeling in beagle dogs. J Bone Miner Res 25:98-105.

Allen MR, Burr DB. 2011. Bisphosphonate effects on bone turnover, microdamage, and mechanical properties: What we think we know what we know that we don't know. Bone 49:56-65.

Allen MR, Burr DB. 2007. Mineralization, microdamage, and matrix: How bisphosphonates influence material properties of bone. BoneKEy-Osteovision 4(2):49-60.

Allen-Hall A, McNevin D. 2012 Human tissue preservation for disaster victim identification (DVI) in tropical climates. Forensic Science International: Genetics 6(5):653-357.

Allouche M, Hamdoum M, Mangin P and Castella V. 2008. Genetic identification of decomposed cadavers using nails as DNA source. Forensic Science International: Genetics 3:46-49.

Alonso A, Anđelinović S, Martin P, Sutlovic D, Erceg I, Huffine E, de Simon LF, Albarran C, Definis-Gojanovic M, Fernandez-Rodriguez A, Garcia P, Drmic I, Rezic B, Kuret S, Sancho M, Primorac D. 2001. DNA Typing from Skeletal Remains: Evaluation of Multiplex and Megaplex STR Systems on DNA Isolated from Bone and Teeth Samples. Croatian Medical Journal 42(3):260-266.

Amory S, Huel R, Bilic A, Loreille O, Parsons T. 2012. Automatable Full Demineralization DNA extraction Procedure from Degraded Skeletal Remains. Forens Sci Internat: Genetics 6:398-406.

Amprino R. 1948. A Contribution to the Functional Meaning of the Substitution of Primary by Secondary Bone Tissue. Acta Anat 5:291-300.

Anđelinović S, Sutlović D, Ivkošić IE, Škaro V, Ivkošić A, Paić F, Režić B, Definis-Gojanović M, Primorac D. 2005. Twelve-year experience in identification of skeletal remains from mass graves. Croat Med J 46(4): 530-539.

Bar W, Kratzer A, Machler M, Schmid W. 1988. Postmortem stability of DNA. Forens Sci Internat 39(1): 59-70.

Barta JL, Monroe C, Crockford SJ, Kemp BM. 2014. Mitochondrial DNA preservation across 3000-year old northern fur seal ribs is not related to bone density: Implications for forensic investigations. Forensic Sci Internat 139:11-18.

Basillais A, Chappard C, Bensamoun S, Brunet-Imbault B, Ho Ba Tho M, Benhamou C. 2004. Three Dimensional Characterization of Cortical Bone Porosity on Microcomputed Tomography Images: A New Method of Evaluation. J Bone Miner Res 19:s112-113.

Bell LS. 1990. Palaeopathology and diagenesis: a SEM evaluation of structural changes using backscattered electron imaging. J Arch Sci 17: 85-102.

Bell LS. 1995. Post mortem microstructural change to the skeleton. Ph.D. thesis, University College London, Department of Anatomy and Developmental Biology.

Bell LS, Elkerton A. 2008. Unique marine taphonomy in human skeletal material recovered from the medieval warship Mary Rose. Int J Osteoarcheol 18: 523-535.

Biesecker LG, Bailey-Wilson JE, Ballantyne J, Baum H, Bieber FR, Brenner C, Biomech 29:161-9.

Boles T, Snow C, Stover E. 1995. Forensic DNA Testing of Skeletal Remains from Mass Graves: A Pilot Study in Guatemala. J Forensic Sci 40:349-355.

Borah B, Gross GJ, Dufresne TE, Smith TS, Cockman MD, Chmielewski PA, Lundy MW, Hartke JR, Sod EW. 2001. Three-dimensional microimaging (MRmicroI and microCT), finite element modeling, and rapid prototyping provide unique insights into bone architecture in osteoporosis. Anat Rec 265(2):101-110.

Boushey HA,Warnock DG. 1983. Osteoporosis: Part I: Advanced Radiologic Assessment Using Quantitative Computed Tomography. West J Med 139(1):75–84.

Boutroy S, Bouxsein ML, Munoz F, Delmas PD. 2005. In vivo assessment of trabecular bone microarchitecture by high-resolution peripheral quantitative computed tomography. Clin Endocrinol Metab 90(12):6508-15.

Bouvier M, Ubelaker DH. 1977. A comparison of two methods for the microscopic determination of age at death. Am J Phys Anthropol 46:391-394.

Bromage TG, Juwayeyi YM, Katris JA, Gomez S, Ovsiy O, Goldstein J, Janal MN, Schrenk F. 2016. The scaling of human osteocyte lacuna density with body size and metabolism. Human Palaeo and Prehist 15:33-40.

Bromage TG, Goldman HM, McFarlin SC, Perez Ochoa A, Boyde A. 2009. Confocal scanning optical microscopy of a 3-million-year-old Australopithecus afarensis femur. Scanning 31: 1-10.

Budowle B, Butler JM, Carmody G, Conneally PM, Duceman B, Eisenberg A, Burger J, Hummel S, Herrmann B, Henke W. 1999. DNA Preservation: A microsatellite-DNA study on ancient skeletal remains. Electrophoresis 20(8): 1722-1728.

Burghardt AJ, Buie HR, Laib A, Majumdar S, Boyd SK. 2010. Reproducibility of direct quantitative measures of cortical bone microarchitecture of the distal radius and tibia by HR-pQCT. Bone 47(3):519-28.

Burr DB. 2002. Targeted and nontargeted remodeling. Bone 30:2-4

Burr DB, Martin RB. 1993. Calculating the probability that microcracks initiate resorption spaces. J Biomech 26: 613-616.

Burr DB, Allen MR. 2013. Basic and applied bone biology. London, UK: Elsevier.

Brooks ST, Suchey JM. 1990. Skeletal age determination based on the os pubis: A comparison of the Ascadi-Nemeskeri and Suchey-Brooks methods. Hum Evol 5:227-238.

Canadian Light Source. 2016. About the Canadian Light Source. www.lightsource.ca accessed January 2016.

Campos PF, Craig OE, Turner-Walker G, Peacock E, Willerslev E, Gilbert MTP. 2012. DNA in ancient bone - Where is it located and how should we extract it? Annals of Anatomy - Anatomischer Anzeiger 194: 7-16.

Caputo M, Bosio LA, Corach D. 2011. Long-term room temperature preservation of corpse soft tissue: an approach for tissue sample storage. Investigative Genetics 2:17-22.

Carlson DS, Armelagos GJ, Van Gerven DP. 1976. Patterns of age-related cortical bone loss (osteoporosis) within the femoral diaphysis. Hum Biol, 48: 295-314.

Carter D, Beaupré G. 2001. Skeletal Function and Form: Mechanobiology of Skeletal Development, Aging, and Generation. Cambridge University Press: NY.

Carter Y, Thomas CDL, Clement JG, Peele AG, Hannah K, Cooper DML. 2013. Variation in osteocyte lacunar morphology and density in the human femur – a synchrotron radiation micro-CT study. Bone 52: 126-132.

Carter Y, Thomas CDL, Clement JG, Cooper DML. 2013. Femoral Osteocyte Lacunar Density, Volume and Morphology in Women Across the Lifespan. J Struct Biol183(3), 519-26.

Carter Y, Suchorab JL, Thomas CDL, Clement JG, Cooper DML. 2014a. Normal variation in cortical osteocyte lacunar parameters in health young males. J Anat 225:328-336.

Carter Y. 2014b. Quantitative imaging of sex and age differences in human cortical bone osteocyte lacunae. Ph.D. Dissertation, University of Saskatchewan, Department of Anatomy & Cell Biology.

Chapman D, Thomlinson W, Johnston RE, Washburn D, Pisano E, Gmur N, Zhong Z, Menk R, Arfelli F, Sayers D. 1997. Diffraction enhanced x-ray imaging. Phys Med Biol 42(11):2015-2025.

Chen T, Catcheside DEA, Stephenson A, Hefford C, Kirkbride KP, Burgoyne LA. 2012. A rapid wire-based sampling method for DNA profiling. Journal of Forensic Sciences 57(2):472-477.

Cho H, Stout SD, Madsen RW, Streeter MA. 2002. Population-specific histological age-estimating method: A model for known African-American and European-American skeletal remains. J Forensic Sci 47: 12-18.

Cobaugh KL, Schaeffer SM, DeBruyn JM. 2015. Functional and structural succession of soil microbial communities below decomposing human cadavers. PLoS ONE 10(6): e0130201.

Cockle D, Andrews D, Thompson D. 2005. Tsunami Thailand: Disaster Victim Identification. Identification Canada: The Art and Science of Forensic Identification 28(3):4-15.

Cohen J, Harris W. 1958. The three-dimensional anatomy of haversian systems. J Bone Joint Surg Am 40A:419-434.

Collins, MJ, Nielsen-Marsh CM, Hiller J, Smith CI, Roberts JP, Prigodich RV, Computer-assisted 3D reconstruction of serial sections of cortical bone to determine

Cooper DML, Thomas CD, Clement JG, Hallgrimsson B. 2006. Three-dimensional microcomputed tomography imaging of basic multicellular unit-related resorption spaces in human cortical bone. Anat RecA: 288(7):806-816.

Cooper DML, Turinsky AL, Sensen CW, Hallgrimsson B. 2003. Quantitative 3D analysis of the canal network in cortical bone by micro-computed tomography. Anat RecB: 274(1):169-179.

Cooper DML, Turinski A, Sensen C, Hallgrimsson B. 2007. Effect of voxel size on 3D micro-CT analysis of cortical bone porosity. Calcif Tiss Int 80(3):211-219.

Cooper DML, Erickson B, Peele A, Hannah K, Thomas CDL, Clement JG. 2011. Visualization of 3D Osteon Morphology by Synchrotron Radiation Micro-CT. J Anat 219(4):481-489.

Cooper DML, Thomas CDL, Clement JG. 2012a. Technological Developments in the Analysis of Cortical Bone Histology: The Third Dimension and its potential in Anthropology. In C. and SD. Stout (Eds) Bone Histology: An Anthropological Perspective. CRC Press Boca Ranton, FL.

Cooper DML, Chapman LD, Carter Y, Wu Y, Panahifar A, Britz HM, Bewer B, Zhouping W, Duke MJ, Doschak M. 2012b. Three dimensional mapping of strontium in bone by dual energy K-edge subtraction imaging. Phys Med Biol 57(18):5777-5786.

Cooper DML. 2005. 3D Micro-CT Imaging of Human Cortical Bone Porosity: A Novel Method for Estimating Age at Death. Ph.D. Dissertation, University of Calgary, Departments of Archaeology and Medical Science.

Crainic K, Paraire F, Leterreux M, Durigon M, de Mazencourt P. 2002. Skeletal remains presumed submerged in water for three years identified using PCR-STR analysis. J Forensic Sci 47(5): 1-3.

Crowder C, Heinrich J, Stout S. 2012. Rib Histomorphometry for Adult Age Estimation. In Bell, L. (Ed): Forensic Microscopy for Skeletal Tissue: Methods and Protocols. Springer.

Crowder C. 2005. Evaluating the use of quantitative bone histology to estimate adult age at death. Ph.D. Dissertation, University of Toronto, Department of Anthropology.

Currey JD. 2002. Bones: Structure and Mechanics. Chapter 1 The Structure of Bone Tissue pp. 3-25; Chapter 2 The Mechanical Properties of Materials pp. 27-51; Chapter 3 The Mechanical Properties of Bone pp. 54-122. Princeton University Press.

Damann FE. 2010. Human decomposition ecology at the University of Tennessee Anthropology Research Facility. Ph.D. dissertation, University of Tennessee, Knoxville, Department of Anthropology.

Damann FE, Tanittaisong A, Carter DO. 2012. Potential carcass enrichment of the University of Tennessee Anthropology Research Facility: A baseline survey of edaphic features. Forensic Sci Internat 222:4-10.

Davoren, J, Vanek D, Konjhodzic R, Crews J, Huffine E, Parsons T. 2007. Highly Effective DNA Extraction Method for Nuclear Short Tandem Repeat Testing of Skeletal Remains from Mass Graves. Croatian Medical Journal 48(4):478-485.

DeHoff RT. 1983. Quantitative Serial Sectioning analysis: preview. J Microsc 131:259-263.

Dibbets JMH. 1992. One century of Wolff's Law. In Carlson DS, and Goldstein SA (Eds) Bone biodynamics in Orthodontic and Orthopedic Treatment, Centre for Growth and Development, the University of Michigan, Ann Arbor;1-13.

Eagle MJ, Man J, Rooney P, Hogg P, Kearney JN. 2015. Assessment of an improved bone washing protocol for deceased donor human bone. Cell Tissue Bank 16:83-90.

Edson S, Ross J, Coble M, Parsons TJ, Barritt S. 2004. Naming the Dead: Confronting the Realities of Rapid Identification of Degraded Skeletal Remains. Forensic Science Review 16(1): 63-90.

Emmons AL. 2015. The preservation and persistence of human DNA in soil during cadaver decomposition. M.A. thesis, University of Tennessee, Knoxville, Department of Anthropology.

Evison MP, Smillie DM, Chamberlain AT. 1997. Extraction of Single-Copy Nuclear DNA from forensic specimens with a variety of postmortem histories. J Forensic Sci 42(6): 1032-1038.

Feldkamp LA, Goldstein SA, Parfitt AM, Jesion G, and Kleerekoper M. 1989. The direct examination of three-dimensional bone architecture in vitro by computed tomography. J Bone Miner Res 4:3-11.

Ferreira STG, Kuser HH, Garrido RG, Trindade-Filho A, Paula KA, Galvão MF, Moraes AV. 2011. Floods and mudslides in the State of Rio de Janeiro and a plane crash in the Brazilian Amazon rainforest: A study of two different experiences in disaster victim identification (DVI). Forensic Sci. Internat: Gene. Suppl: 3:e516-e517.

Ferreira STG, Garrido RG, Paula KA, Nogueira RC, Oliveira ES, Moraes AV. 2013. Cartilage and phalanges from hallux: Alternative sources of samples for DNA typing in disaster victim identification (DVI). A comparative study. Forensic Sci. Internat: Gene. Suppl: 4:e366-e367.

Forman L, Kidd KK, Leclair B, Niezgoda S, Parsons TJ, Pugh E, Shaler R, Fredericks J, Brown K, Williams A, Bennett P. 2013. DNA analysis of skeletal tissue recovered from the English Channel. J Forensic Sci and Legal Medicine 20(6):757-759.

Frank F, Mundorff AZ, Davoren J. 2015. The effect of common imaging and hot water maceration on DNA recovery from skeletal remains. Forensic Sci Internat 257:189-195.

Frost HM. 1960. Micropetrosis. J Bone Joint Surg Am 42-A:144-150.

Frost HM. 1969. Tetracycline-based histological analysis of bone remodeling. Calcif
Golubic S, Radtke G, Le Campion-Alsumund T. 2005. Endolithic fungi in marine ecosystems. Trends Microbiol, 13(5): 229-235.

Frost HM. 1983. The skeletal intermediary organization. 1: Metab Bone Dis Relat Res. 4(5):281-90.

Frost HM. 1987. Secondary osteon populations: An algorithm for determining mean bone tissue age. Yearbk Phys Anthropol 30: 221-238.

Frost HM. 1997. Why do marathon runners have less bone than weight lifters? A vital biomechanical view and explanation. Bone 20(3): 183-189.

Frost HM. 1998. Changing concepts in skeletal physiology: Wolff's Law, the Mechanostat, and the "Utah Paradigm". Am J Hum Biol, 10: 599-605.

Frost HM. 2000a. Does bone design intend to minimize fatigue failures? A case for the affirmative. J Bone Miner Metab 18:278-282.

Frost HM. 2000b. The Utah paradigm of skeletal physiology: An overview of its insights for bone, cartilage and collagenous tissue organs. J Bone Miner Metab 18:305-316.

Frost HM. 2004. A 2003 update for bone physiology and Wolff's Law for clinicians. Angle Orthod, 74(1): 3-15.

Georgia R, Albu I, Sicoe M, and Georoceanu M. 1982. Comparative aspects of the density and diameter of Haversian canals in the diaphyseal compact bone of man and dog. Morphol Embryol (Bucur) 28:11-4.

Goldman HM. 2001. Histocomposition and geometry at the human mid-shaft femur. Ph.D. Dissertation, The City University of New York.

Gotherstrom A, Collins MJ, Angerbjorn A, Liden K. 2002. Bone Preservation and DNA Amplification. Archaeometry 44:395-404.

Goulet GC, Cooper DM, Coombe D, Zernicke RF. 2008. Influence of cortical canal architecture on lacunocanalicular pore pressure and fluid flow. Comput Methods Biomech and Biomed Engin 11:379-387.

Graham EAM, Turk EE, Rutty GN. 2008. Room temperature DNA preservation of soft tissue for rapid DNA extraction: An addition to the disaster victim identification investigators toolkit? Forensic Science International: Genetics 2:29-34.

Graw M, Weisser HJ, Lutz S. 2000. DNA Typing of Human Remains Found in Damp Environments. Forensic Science International 113(1-3):91-95.

Gunderson HJG. 1986. Steriology of arbitrary particles. J Microsc 143:3-45.

Hackett CJ. 1981. Microscopical focal destruction (tunnels) in excavated human bones. Med Sci Law 21: 243-265.

Havers C repr.1977, c1691. Osteologia nova, or, Some new observations of the bones: and the parts belonging to them, with the manner of their accretion, and nutrition,
Hedges REM. 2002. Bone diagenesis: An overview of Processes. Archaeometry 44(3):319-328.

Hedges REM, Millard AR, Pike AWG. 1995. Measurements and Relationships of Diagenetic Alteration of Bone from Three Archaeological Sites. Journal of Archaeological Science 22:201-209.

Hedges REM, Millard AR. 1995. Bones and ground water: towards the modelling of diagenetic processes, Journal of Archaeological Science 22:155–164.

Hert J, Fiala P, Petrtyl M. 1994. Osteon orientation of the diaphysis of the long bones Hildebrand T, Ruegsegger P. 1997a. A new method for the model-independent assessment of thickness in three-dimensional images. J Microsc-Oxford 185:67-75.

Hesse B, Langer M, Varga P, Pacureanu A, Dong P, Schrof S, Männicke N, Suhonen H, Olivier C, Maurer P, Kazakia GJ, Raum K, Peyrin F. 2014. Alterations of mass density and 3D osteocyte lacunar properties in biophosphate-related osteonecrotic human jaw bone, a synchrotron μCT study. PLoS One 9(2):e88481.

Higgins D, Rohriach AB, Kaldonis J, Townsend G, Austin JJ. 2015. Differential nuclear and mitochondrial DNA preservation in post-mortem teeth with implications for forensic and ancient DNA studies. PLoS One 10(5): e0126935.

Hildebrand T, Rüegsegger P. 1997b. Quantification of Bone Microarchitecture with the Structure Model Index. Computer methods in biomechanics and biomedical engineering 1(1):15-23.

Hines D, Vennemeyer M, Amory S, Huel R, Hanson I, Katzmarzyk C, Parsons T. 2014. Prioritizing Sampling of Bone and Teeth for DNA Analysis in Commingled Cases. In Adams BJ, Byrd JE (editors), Commingled Human Remains: Methods in Recovery, Analysis, and Identification. Elsevier Science, Oxford; pp. 275-305.

Hobdell MH, Howe CE. 1971. Variation in bone matrix volume associated with osteocyte lucunae in mammalian and reptilian bone. Isr J Med Sci 7(3):492-493.

Hochmeister MN, Budowle B, Borer UV, Eggmann U, Comey CT, Dirnhofer R. 1991. Typing of Deoxyribonucleic-Acid (DNA) Extracted from Compact-Bone from Human Remains. J Forensic Sci 36(6):1649-1661.

Holland MM, Cave CA, Holland CA, Bille TW. 2003. Development of a Quality, High Throughput DNA Analysis Procedure for Skeletal Samples to Assist with the Identification of Victims from the World Trade Center Attacks. Croatian Medical Journal 44(3):264-72.

Imaizumi K, Miyasaka S, and Yoshino M. 2004. Quantitative Analysis of Amplifiable DNA in Tissue Exposed to Various Environments Using Competitive PCR Assays. Science and Justice 44(4):199-208.

International Commission on Missing Persons. 2015. Standard Operating Procedure for Sampling Bone and Tooth Specimens from Human Remains for DNA Testing at the ICMP. http://www.icmp.int/wp-content/uploads/2015/04/icmp-sop-aa-136-2-doc.pdf accessed January 2016.

Interpol. 2009. Disaster Victim Identification Guide. International Criminal Police Organization. Available online at http://www.interpol.int/INTERPOLexpertise/Forensics/DVI-Pages/DVI-guide accessed November 2013.

Interpol. 2014. Disaster Victim Identification Guide. International Criminal Police Organization. Available online at http://www.interpol.int/INTERPOLexpertise/Forensics/DVI-Pages/DVI-guide accessed January 2016.

Iwamura ESM, Regina C, Oliveira C, Soares-Vieira JA, Nascimento SAB, Munoz DR. 2005. A Qualitative Study of Compact Bone Microstructure and Nuclear Short Tandem Repeat Obtained from Femur of Human Remains Found on the Ground and Exhumed 3 Years after Death. American Journal of Forensic Medicine and Pathology 26(1):33-44.

Jackes M, Sherburne R, Lubell D, Barker C, Wayman M. 2001. Destruction of Microstructure in Archaeological Bone: A Case Study from Portugal. Int J Osteoarchaeol 11:415-432.

Jans MME. 2008. Microbial bioerosion of bone: A review. Current developments in Bioerosion. Erlangan Earth Conference Series.

Jans MME, Neilson-Marsh CM, Smith CI, Collins MJ, Kars H. 2004. Characterisation of microbial attack on archeological bone. J Archaeol Sci, 31: 87-95.

Jordan GR, Loveridge N, Power J, Clarke MT, Parker M, Reeve J. 2003. The ratio of osteocytic incorporation to bone matrix formation in femoral neck cancellous bone: An enhanced osteoblast work rate in the vicinity of hip osteoarthritis. Calcif Tissue Internat 73:190-196.

Just RS, Leney MD, Barritt SM, Los CW, Smith BC, Hollard TD, Parsons CJ. 2009. The use of mitochondrial DNA single nucleotide polymorphisms to assist in the resolution of three challenging forensic cases. J Forensic Sci 54(4): 887-891.

Kabel J, Odgaard A, van Rietbergen B, Huiskes R. 1999. Connectivity and the elastic properties of cancellous bone. Bone 24(2):115-120.

Kaneko Y, Ohira H, Tsuda Y, Yamada Y. 2015. Comparison of hard tissues that are useful for DNA analysis in forensic autopsy. Legal Medicine 17:547-552.

Kelly ME, Schultke E, Fielder S, Nemoz C, Guzman R, Corde S, Esteve F, Leduc G, Juurlink BHJ, Meguro K. 2007. Synchrotron-based intravenous cerebral angiography in a small animal model. Phys Med Biol(52):1001-1112.

Kerley ER. 1965. The microscopic determination of age in human bone. Am J Phys Anthropol 23:149-164.

Kleerekoper M, Villaneuva AR, Stanciu J, Rao DS, Parfitt AM. 1985. The role of three-dimensional trabecular microstructure in the pathogenesis of vertebral compression fractures. Calcif Tissue Int 37:594-597.

Klinck RJ, Campbell GM, Boyd SK. 2008. Radiation effects on bone architecture in mice and rats resulting from in vivo micro-computed tomography scanning. Med Eng Phys 30(7):888-95.

Kline MC, Duewer DL, Redman JW, Butler JM. 2005. Results from the NIST 2004 DNA quantitation study, J. Forensic Sci. 50 (3): 570–578.

Kolta S, Fechtenbaum J, Roux C. 2010. Bone macroarchitecture by 3D imaging and osteoporosis. In EH. Duke and SR. Aguirre (Eds) 3D Imaging: Theory, Technology and Applications. Nova Science Publishers, NY, pp 175-88.

Kvaal SI. 2006. Collection of Post Mortem Data: DVI Protocols and Quality Assurance. Forensic Sci Internat 159(1):S12-14.

Lauber CL, Metcalf JL, Keepers K, Ackermann G, Carter DO, Knight R. (2014). Vertebrate decomposition is accelerated by soil microbes. Appl Environ Microbiol 80(16):4920-4929.

Lee HY, Park MJ, Kim NY, Sim JE, Yang WI, Shin KJ. 2010. Simple and highly effective DNA extraction methods from old skeletal remains using silica columns, Forensic Sci Int Genet 4:275-280.

Leeuwenhoeck A. 1677-78. Microscopical Observations of the Structure of Teeth and other Bones: Made and Communicated, in a Letter by Mr. Anthony Leeuwenhoeck. Philos. Trans. R. Soc. Lond., B, Biol. Sci 12:1002-1003.

Leney MD. 2006. Sampling Skeletal Remains for Ancient DNA (aDNA): A Measure of
Li RC, Application of Proteinases for DNA Isolation of Bone Specimens, NIJ Award 2006-DN-BX-K010.

Li RC. 2006. Application of Proteinases for DNA Isolation of Bone Specimens, NIJ Award 2006-DN-BX-K010.

Lunneborg CE, Tousignant. 1985. Efron's bootstrap with application the repeated measures design. Multivariate Behavioural Research 20:161-178.

MacDonald, HM, Cooper DML, McKay HA. 2008. A school-based physical activity intervention positively affects change in Imax in pre- and early pubertal boys. Osteoporosis International Jan 20(1):61-70.

Maggiano IS, Maggiano CM, Clement JG, Thomas CDL, Carter Y, Cooper DML. 2016. Three-dimensional reconstruction of Haversian systems in human cortical bone using synchrotron radiation-based micro-CT: Morphology and quantification of branching and transverse connections across age. J Anat doi:10.111/joa.12430.

Marjanović D, Durmić-Pasić A, Bakal N, Haverić S, Kalamujić B, Kovacević L, Ramić J, Pojskić N, Skaro V, Projić P. 2007. DNA Identification of Skeletal Remains from World War II Mass Graves Uncovered in Slovenia, Croat. Med. J. 48: 513-519.

Marks SC, Odgren PR. 2002. Structure and development of the skeleton. In: Bilezikian JP, Raisz LG, Rodan GA, editors. Principles of bone biology, Second edition. California: Academic Press. p 3-17.

Mameli A, Piras G, Delogu G. 2014. The successful recovery of low copy number and degraded DNA from bones exposed to seawater suitable for generating a DNA STR profile. J Forensic Sci 49(2): 470-473.

Martin RB, Burr DB, Sharkey NA. 2015. Skeletal Tissue Mechanics (2nd Ed). Springer Press, NY.

Martin RB. 2000. Toward a unifying theory of bone remodeling. Bone, 26:1-6.

Martin RB. 2003a. Functional adaptation and fragility of the skeleton. In Agarwal SC and Stout SD. (Eds): Bone loss and osteoporosis: An anthropological perspective. Kluwer Academic/Plenum Publishers:NY; 121-136.

Martin RB. 2003b. Fatigue damage, remodeling, and the minimization of skeletal weight. J Theor Biol 220:271-276.

Martin RB. 2007. Targeted bone remodeling involves BMU steering as well as activation. Bone, 40: 1574-1580.

McCreadie BR, Hollister SJ, Schaffler MB, Goldstein SA. 2004. Osteocyte lacuna size and shape in women with and without osteoporotic fracture. J Biomech 37: 563-572.

Michaud CL, Foran DR. 2011. Simplified field preservation of tissues for subsequent DNA analyses. Journal of Forensic Sciences 56(4):846-852.

Milos A, Selmanovic A, Smajlovic L, Huel R, Katzmarzyk C, Rizvic A, Parsons T. 2007. Success Rates of Nuclear Short Tandem Repeat Typing from Different Skeletal Elements. Croatian Medical Journal 48:486-493.

Misner L, Halvorson A, Dreier J, Ubelaker D, Foran D. 2009. The Correlation Between Skeletal Weathering and DNA quantity and Quality. J Foren Sci 54(4): 822-828.
Mol Cell Evol Biol 282:157-62.

Mori S, Harruff R, Ambrosius W, Burr DB. 1997. Trabecular bone volume and microdamage accumulation in femoral heads of women with and without femoral neck fractures. Bone 21:521-526.

Mullender MG, van der Meer DD, Huiskes R, Lips P. 1996. Osteocyte density changes in aging and osteoporosis. Bone 18(2):109-113.

Muller R, Ruegsegger P. 1995. Three-dimensional finite element modelling of noninvasively assessed trabecular bone structures. Med Eng Phys 17(2):126-133.

Mundorff AZ, Davoren JM. 2014. Examination of DNA yield rates for different skeletal elements at increasing post mortem intervals. Forensic Science International: Genetics (8): 55-63.

Mundorff AZ, Davoren J, Huffine E, Frank E, Bettinger S, Weitz S, Jeanguenat A. 2012. Developing an empirically based ranking order for bone sampling: Examining differential yield rates between human skeletal elements – *Final Results*. U.S. Department of Justice, OJP, NIJ. The NIJ Conference June 2012, Arlington, Virginia.

Mundorff AZ, Bartelink E, Mar-Cash E. 2009. DNA preservation in skeletal elements from the World Trade Center disaster: Recommendations for mass fatality management. J Forensic Sci 54(3): 739-745.

Nanci A. 2008. Ten Cate's oral histology: Development, structure and function (7th ed). California: Elsevier.

National Association of Medical Examiners. 2010. Standard Operating Procedures for Mass Fatality Management. Available online at: http://thename.org/index.php?option=com_docman&task=cat_view&gid=38&Item

National Institute of Justice. 2005. Mass Fatality Incidents: A Guide for Human Forensic Identification. U.S. Department of Justice, Washington.

Narasaki S. 1990. Estimation of age at death by femoral osteon remodeling: Application of Thompson's core technique to modern Japanese. J Anthrop Soc Nippon 98(1):29-38.

Neilson-Marsh CM, Hedges REM. 1999. Bone Porosity and the use of Mercury Intrusion Porosimetry in Bone Diagenesis studies. Archaeometry 43(1):165-174.

Neilson-Marsh CM, Hedges REM. 2000. Patterns of Diagenesis in Bone I: The Effects of Site Environments. J Archaeol Sci 27(12):1139-1150.

Neilson-Marsh CM, Hedges REM. 2000. Patterns of Diagenesis in Bone II: Effects of acetic acid treatment and the removal of diagenetic CO32. J Archaeol Sci 27(12):1151-1159.

Odgaard A. 1997. Three-dimensional methods for quantification of cancellous bone architecture. Bone 20(4):315-328.

Odgaard A, Gundersen HJ. 1993. Quantification of connectivity in cancellous bone, with special emphasis on 3-D reconstructions. Bone 14(2):173-182.

Odgaard A, Andersen K, Melsen F, Gundersen HJG. 1990. A direct method for fast three-dimensional serial reconstruction. J Microsc 159:335-342.

Ortner DJ, Turner-Walker G. 2003. The biology of skeletal tissues. In Ortner DJ (Ed), Identification of pathological conditions in human skeletal remains (2nd ed). Academic Press: Amsterdam.

Ott SM. 2002. Histomorphometric Analysis of Bone Remodeling. In Bilezikian JP, Raisz LG, Rodan GA, editors. Principles of bone biology, Second edition. California: Academic Press. p 303-320.

Parfitt AM. 1983a. Calcium homeostasis. In Mundy GR & Martin TJ (editors), Handbook of Experimental Pharmacology. Vol. 107. Physiology and Pharmacology of Bone. Heidelberg: Springer, 1-65.

Parfitt AM, Matthews CHE, Villaneuva AR, Kleerekoper M, Frame B, Rao DS. 1983b. Relationships between surface, volume, and thickness of iliac trabecular bone in aging and osteoporosis. J Clin Invest 72:1396-1409.

Parfitt AM, Drezner MK, Glorieux FH, Kanis JA, Malluche H, Meunier PJ, Ott SM, Recker RR. 1987. Bone histomorphometry: Standardization of nomenclature, symbols, and units. J Bone Miner Res 6(2): 595-610.

Parfitt AM. 1998. Mini review – Osteoclast precursors as leukocytes: Importance of the area code. Bone 23:291-494.

Parfitt AM. 2001. The bone remodeling compartment: A circulatory function for bone lining cells. J Bone Miner Res 16:1583-1585.

Parfitt AM. 2002. Misconceptions (2): Turnover is always higher in cancellous than in cortical bone. Bone 30(6):807-809.

Parfitt AM. 2003. New concepts of bone remodeling: A unified spatial and temporal model with physiological and pathophysiologic implications. In Agarwal SC, Stout SD (Eds), Bone loss and osteoporosis: An anthropological perspective. Kluwer Academic/Plenum Publishers: NY; 3-15.

Parsons TJ, Huel J, Davoren J, Katzmarzyk C, Milos A, Selmanovic A, Smajlovic L, Coble MD, Rizvic A. 2007. Application of novel "Mini-Amplicon" STR Multiplexes to high volume casework on degraded skeletal remains. Forensic Sci Int: Genetics, 1(2): 175-179.

Parsons TJ, Weedn WN. 1997. Preservation and Recovery of DNA in Postmortem Specimens and Trace Samples. In Haglund W and Sorg M (Eds) Forensic Taphonomy: The Postmortem Fate of Human Remains, pp. 109-138. CRC Press, Boca Raton.

Pearson OM, Liberman DE. 2004. The aging of Wolff's "law": Ontogeny and responses to mechanical loading in cortical bone. Yearbk Phys Anthropol, 47: 63-99.

Pesquier B, Taille A, Garcin G, Frackowiak S and Coiffait P.E. 2006. Automation of postmortem or nonstandard reference samples genotyping using FTA®. International Congress Series 1288:728-730.

Petrtyl M, Hert J, Fiala P. 1996. Spatial organization of the haversian bone in man. J Biomech 29:161-9.

Power J, Noble BS, Loveridge N, Bell KL, Rushton N, Reeve J. 2001. Osteocyte lacunar occupancy in the femoral neck cortex: An association with cortical remodeling in hip fracture cases and controls. Calcif Tissue Internat 69:13-19.

Prinz M, Carracedo A, Mayr WR, Morling N, Parsons TJ, Sajantila A, Scheithauer R, Schmitter H, Schneider PM. 2007. DNA Commission of the International Society for Forensic Genetics (ISFG): Recommendations Regarding the Role of Forensic Genetics for Disaster Victim Identification (DVI). Forens Sci International: Genetics 1(1):3-12.

Putkonen MT, Palo JU, Cano JM, Hedman M, Sajantial A. 2010. Factors affecting the STR amplification success in poorly preserved bone samples, Investigative Generics: 1-9.

Qiu S, Rao DS, Palnitkar S, Parfitt AM. 2006. Differences in osteocyte and lacunar density between Black and White American women. Bone 38:130-5.

Qiu S, Rao DS, Palnitkar S, Parfitt AM. 2003. Reduced iliac cancellous osteocyte density in patients with osteoporotic vertebral fracture. J Bone Miner Res 18:1657-63.

Qiu S, Rao DS, Palnitkar S, Parfitt AM. 2002. Age and distance from the surface but not menopause reduce osteocyte density in human cancellous bone. Bone 31:
313-8.

Qiu S, Fyhrie DP, Palnitkar S, Rao DS. 2003. Histomorphometric assessment of Haversian canal and osteocyte lacunae in different-sized osteons in human rib. Anat Rec A Discov Mol Cell Evol Biol 272:520-5.

Rasmussen JL. 1987. Parametric and bootstrap approaches to repeated measures design. Behav Res Methods 19(4):357-360.

Robling AG, Castillo AB, Turner CH. 2006. Biomechanical and Molecular Regulation of Bone Remodeling. Annual Review of Biomedical Engineering 8:455-498.

Robling AG, Turner CH. 2009. Mechanical signaling for bone modeling and remodeling. Crit Rev Eukaryot Gene Expr 19(4):319-338.

Robling AG, Stout SD. 2008. Histomorphometry of human cortical bone: Applications to age estimation. In Katzenberg MA , Saunders SR, editors. Biological anthropology of the human skeleton (2nd edition). New York: Wiley-Liss. p 149-171.

Robling AG. 1998. Histomorphometric assessment of mechanical loading history from human skeletal remains: The relation between micromorphology and macromorphology at the femoral midshaft. Ph.D. Dissertation, University of Missouri at Columbia.

Roeder A, Elsmore P, Greenhaulgh M. 2009. Maximizing DNA profiling success
Ruth EB.1947. Gross Demonstration of the Vascular Channels. Anat Rec 98:59-66.

Ruff CB, Hayes WC. 1983a. Cross-sectional geometry of Pecos Pueblo femora and tibiae—a biomechanical investigation: I. Method and general patterns of variation. Am J Phys Anthropol 60: 359-381.

Ruff CB, Hayes WC. 1983b. Cross-sectional geometry of Pecos Pueblo femora and tibiae—a biomechanical investigation: II. Sex, age, and side differences. Am J Phys Anthropol 60: 383-400.

Ruff CB. 2008. Biomechanical analyses of archaeological human skeletons. In: Katzenberg MA, Saunders SR, editors. Biological anthropology of the human skeleton (2nd edition). New York: Wiley-Liss. p 71-102.

Ruff CB, Holt B, Trinkhaus E. 2006. Who's afraid of the big bad Wolff? "Wolff's law" and bone functional adaptation. Am J Phys Anthropol, 129: 484-498.

Salmon P, Sasov A. 2004. New Nano-CT Technology Allows Ultrastructural Study of Bone Quality Including Microcracks and Osteocyte Lacunae. J Bone Miner Res

Scheithauer R, Schmitter H, Schneider PM. 2007. DNA Commission of the International Society for Forensic Genetics (ISFG): Recommendations Regarding the Role of Forensic Genetics for Disaster Victim Identification (DVI). Forens Sci International: Genetics 1(1):3-12.

Scheuer L, Black SM. 2000. Developmental juvenile osteology. Academic Press.

Schnapper A, Reumann K, Meyer W. 2002. The architecture of growing compact bone
Schneider P, Stauber M, Voide R, Stampanoni M, Donahue LR, Muller R. 2007.

Schneider P, Stauber M, Voide R, Stampanoni M, Donahue LR, Muller R. 2007. Ultrastructural properties in cortical bone vary greatly in two inbred strains of mice as assessed by synchrotron light based micro- and nano-CT. 1: J Bone Miner Res 22(10):1557-70.

Schultz M. 2001. Palaeohistopathology of bone: A new approach to the study of ancient diseases. Yearbk Phys Anthropol, 44: 106-147.

Schwark T, Heinrich A, von Wurmb-Schwark N. 2011. Genetic identification of highly putrefied bodies using DNA from soft tissues. International Journal of Legal Medicine 125:891-894.

Sherry ST, Sozer A,Walsh A. 2005. Epidemiology - DNA Identifications After the 9/11 World Trade Center Attack. Science 310(5751):1122-1123.

Shirley NR, Wilson, RJ, Jantz LM. 2011. Cadaver use at the University of Tennessee's Anthropological Research Facility. Clinical Anatomy 24:372-380.

Shook BAS, Smith DG. 2008. Using ancient mtDNA to reconstruct the population history of Northeastern North America. Am J Phys Anthropol 137:14-29.

Singh IJ, Gunberg DL. 1970. Estimation of age at death in human males from quantitative histology of bone fragments. Am J Phys Anthropol 33:373-382.

Sissons HA, O'Connor P. 1977. Quantitative histology of osteocyte lacunae in normal human cortical bone. Calcif Tissue Res 22:530-533.

Skedros JG, Hunt KJ, Hughes PE, Winet H. 2003. Ontogenic and regional morphologic variations in the turkey ulna diaphysis: Implications for functional adaptation of cortical bone. Anat Rec 273:609-629.

Skedros JG, Dayton MR, Sybrowsky CL, Bloebaum RD, Bachus KN. 2006. The influence of collagen fiber orientation and other histocompositional characteristics on the mechanical properties of equine cortical bone. J Exp Biol 209: 3025-3042.

Sledzik PS, Rodriguez WC. 2002. Damnum fatale: the taphonomic fate of human remains in mass disasters, in: W.D. Hagulund, M.H. Sorg (Eds.), Advances in forensic taphonomy: method, theory, and archaeological perspectives, CRC Press, Boca Raton: 321-330.

Soler MP, Alves MTS, Silva MS, Guimarães MA, Sousa, MLAPO., Almeida JS, Iwamura ESM, 2011. Morphological and DNA analysis in human skeletal remains exposed to environmental conditions in Brazil. Forensic Sci Internat: Gene. Suppl: 3: e339-e340.

Sosa C, Vispe E, Nunez C, Baeta M, Casalod Y, Bolea M, Hedges REM, Martinez-Jarreta B. 2013. Association between ancient bone preservation and DNA yield: A multidisciplinary approach. Am J Phys Anthropol 151(1):102-109.

Sozer A, Baird M, Beckwith M, Harmon B, Lee D, Riley G, Schmitt S. 2010. Guidelines for Mass Fatality DNA Identification Operations. American Association of Blood Banks. Bethesda, Maryland.

Sterio DC. 1984. The unbiased estimator of number and sizes of arbitrary particles using the dissector. J Microsc 134:127-136.

Stout SD, Crowder CM. 2012. Bone remodeling, histomorphology, and histomorphometry. In Stout SD, Crowder CM (Eds), Bone histology: An anthropological perspective. CRC Press: FL;1-21.

Suhonen H, Porra L, Bayat S, Sovijärvi ARA, Suortti P. 2008. Simultaneous *in vivo* synchrotron radiation computed tomography of regional ventilation and blood volume in rabbit lung using combined *K*-edge and temporal subtraction. Phys Med Biol(53):775-791.

Tappen NC. 1977. Three-dimensional studies of resorption spaces and developing osteons. Am J Anat 149:301-332.

Teitelbaum SL. 2000. Bone resorption by osteoclasts. Science. 289(5484):1504-1508.

Thompson AC, Llacer J, Finman LC, Hughes EB, Otis JN, Wilson S, Zeman HD. 1984. Computed tomography using synchrotron radiation. Nucl Instrum Methods Phys Res. A(222): 319-323.

Tibbett M, Carter DO. 2008. Soil analysis in forensic taphonomy: chemical and biological effects of buried human remains, CRC Press, Boca Raton.
Tissue Res 3:211-37.

Todd RB, Bowmann W. 1845. The Physiological Anatomy and Physiology of Man.

Turner-Walker G. 2008. The chemical and microbial degradation of bones and teeth. In Pinhasi R, Mays S (Eds), Advances in Human Palaeopathology. John Wiley & Sons, Ltd, p 3-30.

Turner-Walker G, Jans, MME. 2008. Reconstructing taphonomic histories using histological analysis. Palaeogeogr Palaeocl 266: 227-235.

Turner CH, Forwood MR. 1995. What role does the osteocyte network play in bone adaptation? Bone 16(3):283-285.

Turner CH. 1999. Toward a mathematical description of bone biology: The principle of cellular accommodation. Calcif Tissue Int 65:466-481.

Turner CH. 2000. Letter to the Editor Reply. Toward a mathematical description of bone biology: The principle of cellular accommodation. Calcif Tissue Int 67:184-187.

Vanek D, Saskova L, Votrubova J, Emmerova B. 2015 (in press). Factors influencing the reliability of DNA typing results for bone samples. Forensic Sci. Internat.: Gene. Suppl.

Vasciaveo F, Bartoli E. 1961. Vascular Channels and Resorption Cavities in the Long Bone Cortex the Bovine Bone. Acta Anat 47:1-33.

Vashishth D, Gibson GJ, Fyhrie DP. 2005. Sexual dimorphism and age dependence of osteocyte lacunar density for human vertebral cancellous bone. Anat Rec A Discov Mol Cell Evol Biol 282:157-62.

Vashishth D, Gibson G, Kimura J, Schaffler MB, Fyhrie DP. 2002. Determination of bone volume by osteocyte population. Anat Rec 267:292-5.

van Hove RP, Nolte PA, Vatsa A, Semeins CM, Salmon PL, Smit TH, Klein-Nuland J. 2009. Osteocyte morphology in human tibiae of different bone pathologies with different bone mineral density – is there a role for mechanosensing? Bone 45: 321-329.

Vatsa A, Breuls RG, Semeins CM, Salmon PL, Smit TH, Klein-Nulend J. 2008. Osteocyte morphology in fibula and calvaria – is there a role for mechanosensing? Bone 43:252-258.

Vidoli GM. 2015. Introduction to Human Identification and the Forensic Anthropology Center. Presentation for Human Identification Course, University of Tennessee, Knoxville.

Waarsing JH, Day JS, van der Linden JC, Ederveen AG, Spanjers C, De Clerck N, Sasov A, Verhaar JA, Weinans H. 2004. Detecting and tracking local changes in the tibiae of individual rats: a novel method to analyse longitudinal in vivo micro-CT data. Bone 34(1):163-9.

Wachter NJ, Augat P, Krischak GD, Mentzel M, Kinzl L, Claes L 2001. Prediction of cortical bone porosity in vitro by microcomputed tomography. Clinical Biomech 16:221-256.

Weedn VW, Baum HJ. 2011. DNA identification in mass fatality incidents. American Journal of Forensic Medicine and Pathology 32(4):393-397.

Weiss TJ, Csapo J, Millard AR, Turner-Walker G. 2002. The Survival of Organic Matter in Bone: A Review. Archaeometry 44:383-394.

Wurtz W. 2014. CLS Summer School Lecture: Synchrotron 101. Canadian Light Source, Saskatoon, Saskatchewan, Canada.

Yazedjian L, Kesetovic R. 2008. The Application of Traditional Anthropological Methods in a DNA-Led Identification Project. In Recovery, Analysis, and Identification of Commingled Human Remains, B Adams and J Byrd (Eds), pp. 271-284. Humana Press.

Ye J, Ji AQ, Parra EJ, Zheng XF, Jiang CT, Zhao XC, Hu L, Tu Z. 2004. A simple and efficient method for extracting DNA from old and burned bone. J Forensic Sci, 49(4): 754-759.

Zaidi M. 2007. Skeletal remodeling in health and disease. Nat Med 13:791-801.

Zebaze R, Ghasem-Zadeh A, Bohte A, Iuliano-Burns S, Mackie E, Seeman E. 2009. Age-related bone loss: The effect of neglecting intracortical porosity. Bone, 44: S117-S118.

Zhou SA, Brahme A. 2008. Development of phase-contrast X-ray imaging techniques and potential medical applications. Phys Med 24(3):129-148.

Zhu Y, Samadi N, Martinson M, Bassey B, Wei Z, Belev G, Chapman D. 2014. Spectral *K*-edge subtraction imaging. Phys Med Biol 59:2485-2503.

APPENDICES

APPENDIX A: Raw Data from Clinical CT Scans for Cortical and Cancellous Bone Height and Width Measurements.

Table A.1: Individual #1 Average Cortical and Cancellous Measurement Raw Data (mm).

Skeletal Element	Cortical Height (mm)	Cortical Width (mm)	Cancellous Height (mm)	Cancellous Width (mm)
Pubis	7.61	1.68	7.57	6.14
Ilium	7.46	0.7041	N/A	N/A
Ischium	N/A	N/A	N/A	N/A
Sacrum	N/A	N/A	N/A	N/A
Cuboid	8.45	1.17	8.36	13.75
Calcaneus	9.12	0.7053	8.98	12.44
Talus	8.68	0.6539	8.3	13.44
1st Cuneiform	6.78	0.7753	6.73	6.72
2nd Cuneiform	7.01	0.7305	7.14	9.26
3rd Cuneiform	8.38	0.8025	8.77	7.16
Navicular	9.04	0.8753	6.77	10.18
Capitate	8.78	0.9638	8.46	6.98
12th Rib	8.75	1.13	8.74	5.55
Fibula	8.38	2.3	6.8	3.03
Femur	8.35	6.03	N/A	N/A
Tibia	7.4	5.71	N/A	N/A
Patella	8.75	0.995	8.63	10.15
Humerus	9.61	4.97	N/A	N/A
Ulna	6.38	3.99	N/A	N/A
Radius	6.94	3.86	N/A	N/A
Scapula	7.05	1.35	N/A	N/A
Clavicle	6.47	3.37	4.43	6.85
Cervical Vertebra	9.14	1.29	8.08	4.47
Lumbar Vertebra	7.21	1.1	7.46	8.71
Thoracic Vertebra	5.42	0.7476	4.76	6.01
Frontal	8.16	2.89	5.73	2.15
Parietal	7.64	1.93	6.22	2.64
Temporal	9.07	1.06	9.75	8.89
Maxilla	N/A	N/A	N/A	N/A
Mandible	7.93	2.98	6.76	3.7
Occipital	7.64	4	N/A	N/A
1st Rib	3.75	1.03	1.9	2.76
Middle Rib	7.75	0.8787	6.13	3.44

Table A.1: (cont).

Skeletal Element	Cortical Height (mm)	Cortical Width (mm)	Cancellous Height (mm)	Cancellous Width (mm)
1st Metatarsal	8.42	2.49	8.1	7.5
2nd Metatarsal	4.88	1.21	7.66	5.24
3rd Metatarsal	9.13	2.44	7.92	4.82
4th Metatarsal	8.69	0.8894	8.57	8.19
1st Proximal Hand Phalanx	6.94	1.29	6.5	7.46
1st Distal Foot Phalanx	6.36	1.05	6.41	9.54
4th Metacarpal	8.41	1.67	7.8	8.05
2nd Metacarpal	8.51	1.28	7.87	10.97
3rd Metacarpal	8.63	1.99	8.59	7.52
1st Proximal Foot Phalanx	7.54	1.66	7.44	8.29

Table A.2: Individual #2 Average Cortical and Cancellous Measurement Raw Data (mm).

Skeletal Element	Cortical Height (mm)	Cortical Width (mm)	Cancellous Height (mm)	Cancellous Width (mm)
Pubis	0.8794	5.97	8.87	8.56
Ilium	6.29	1.88	N/A	N/A
Ischium	4.04	7.2	9.21	8.2
Sacrum	5.88	0.791	11.32	9
Cuboid	5.85	0.9611	8.42	8.55
Calcaneus	6.87	1.1	7.01	12.85
Talus	6.74	1.07	9.66	9.32
1st Cuneiform	7.11	1.26	9.82	8.47
2nd Cuneiform	5.93	0.5454	6.02	8.46
3rd Cuneiform	5.84	0.7286	4.48	8.37
Navicular	7.7	1.27	9.11	8.84
Capitate	5.4	0.7485	7.76	8.08
12th Rib	N/A	N/A	N/A	N/A
Fibula	7.73	2.23	N/A	N/A
Femur	7.16	6.21	N/A	N/A
Tibia	6.74	5.11	N/A	N/A
Patella	8.67	0.981	9.01	8.04
Humerus	6.42	6.61	N/A	N/A
Ulna	8.62	2.6	N/A	N/A
Radius	8.32	3.27	N/A	N/A
Scapula	8.77	1.96	7.62	2.71

Table A.2: (cont).

Skeletal Element	Cortical Height (mm)	Cortical Width (mm)	Cancellous Height (mm)	Cancellous Width (mm)
Clavicle	7.45	0.904	7.75	11.29
Cervical Vertebra	10.94	0.8712	10.08	8.11
Lumbar Vertebra	9.88	0.8314	15.59	10.7
Thoracic Vertebra	8.82	6.36	N/A	N/A
Frontal	8.85	3.01	9.17	8.52
Parietal	7.33	3.67	6.44	2.13
Temporal	5.73	2.02	4.16	2.94
Maxilla	10.6	0.6847	10.53	6.97
Mandible	13.26	4.89	13.95	7.13
Occipital	5.32	2.78	2.77	1.79
1st Rib	9.83	3.16	N/A	N/A
Middle Rib	7.8	1.9	7.9	5.45
1st Metatarsal	6.61	2.22	5.78	5.34
2nd Metatarsal	7.92	3.56	6.42	5.83
3rd Metatarsal	7.63	1.78	7.38	4.2
4th Metatarsal	7.61	1.84	7.97	3.76
1st Proximal Hand Phalanx	4.69	1.74	5.12	5.4
1st Distal Foot Phalanx	N/A	N/A	6.61	5.96
4th Metacarpal	9.39	1.14	8.82	6.96
2nd Metacarpal	7.17	1.01	6.91	4.56
3rd Metacarpal	8.59	1.07	8.61	10.62
1st Proximal Foot Phalanx	8.63	1.38	8.23	7.33
Pubis	7.64	1.04	7.73	8.58
Ilium	6.34	5.82	3.97	
Ischium	7.26	7.32	N/A	N/A

Table A.3: Individual #3 Average Cortical and Cancellous Measurement Raw Data (mm).

Skeletal Element	Cortical Height (mm)	Cortical Width (mm)	Cancellous Height (mm)	Cancellous Width (mm)
Pubis	6.88	3.61	7.5	5.69
Ilium	N/A	N/A	N/A	N/A
Ischium	8.65	1.31	9.43	6.52
Sacrum	4.77	2.57	8.83	5.68
Cuboid	9.09	2.28	8.01	9.23
Calcaneus	9.54	0.4956	9.36	11.92

Table A.3: (cont).

Skeletal Element	Cortical Height (mm)	Cortical Width (mm)	Cancellous Height (mm)	Cancellous Width (mm)
Talus	8.97	1.39	8.7	7.15
1st Cuneiform	6.67	1.36	6.73	7.5
2nd Cuneiform	9.32	0.6981	9.7	6.96
3rd Cuneiform	8.78	0.8327	8.65	9.6
Navicular	9.59	0.8997	9.67	8.6
Capitate	8.96	0.8764	8.54	6.63
12th Rib	N/A	N/A	N/A	N/A
Fibula	8.72	4.03	6.34	2.11
Femur	6.68	5.8	N/A	N/A
Tibia	9.01	5.36	N/A	N/A
Patella	9.75	0.8244	8.35	12.56
Humerus	8.09	5.14	N/A	N/A
Ulna	7.19	3.43	N/A	N/A
Radius	7.51	4.63	N/A	N/A
Scapula	6.57	0.8943	5.77	7.14
Clavicle	6.49	0.9546	6.47	8.65
Cervical Vertebra	6.83	0.883	6.71	8.06
Lumbar Vertebra	7.86	1.07	6.76	2.52
Thoracic Vertebra	8.1	1.45	7.76	3.33
Frontal	N/A	N/A	N/A	N/A
Parietal	9.74	1.36	9.06	6.13
Temporal	9.06	1.5	8.66	4.45
Maxilla	5.79	1.54	4.68	1.73
Mandible	8.46	1.76	9.44	1.99
Occipital	9.59	0.9892	9.22	6.39
1st Rib	9.18	1.59	8.7	8.15
Middle Rib	8.61	1.32	8.32	4.45
1st Metatarsal	9.05	1.87	9.31	4.15
2nd Metatarsal	7.74	1.16	7.95	6.85
3rd Metatarsal	5.98	0.8327	7.35	4.4
4th Metatarsal	7.86	0.6728	7.3	2.49
1st Proximal Hand Phalanx	9.15	0.6705	8.03	3.93
1st Distal Foot Phalanx	6.74	1.04	6.44	8.71
4th Metacarpal	6.82	1.75	6.28	9.03
2nd Metacarpal	11.27	1.06	10.15	7.07
3rd Metacarpal	N/A	N/A	6.5	7.25

APPENDIX B: Quantitative Results of the Individual Object Analysis for Cortical and Cancellous Bone ROIs.

Table B.1: Quantitative Results for the Morphological Parameters of Osteocyte Lacunae from Cortical Bone ROIs.

Element Type	Research #	Bone Volume (TV-Ca.V)	Canal Diameter µm	Canal Volume mm^3	# of Lacunae (N.Lc)	Lacunar Volume $µm^3$	Lacunar Density (N.Lc/BV) mm^3
Pubis	#1	0.19	52	0.08	4138	231	21778.94737
	#3	0.17	62	0.1	3128	216	18400
	#2	0.2	48	0.07	4405	274	22025
Ilium	#1	0.21	42	0.06	4872	295	23200
	#3	0.18	58	0.09	3505	206	19472.22222
	#2	0.22	51	0.05	5328	318	24218.18182
Ischium	#1	0.19	47	0.08	4308	265	22673.68421
	#3	0.17	59	0.1	3149	240	18523.52941
	#2	0.2	53	0.07	3910	275	19550
Sacrum	#1	0.21	50	0.06	4128	269	19657.14286
	#3	0.17	62	0.1	3004	240	17670.58824
	#2	0.2	48	0.07	4254	308	21270
Cuboid	#1	0.2	56	0.07	4228	279	21140
	#3	0.14	61	0.13	2671	214	19078.57143
	#2	0.19	47	0.08	4501	230	23689.47368
Calcaneus	#1	0.19	51	0.08	2682	277	14115.78947
	#3	0.17	60	0.1	1856	256	10917.64706
	#2	0.2	47	0.07	1628	293	8140
Talus	#1	0.21	52	0.06	2401	260	11433.33333
	#3	0.17	63	0.1	1503	256	8841.176471
	#2	0.2	48	0.07	2612	277	13060

Table B.1: (cont).

Element Type	Research #	Bone Volume (TV-Ca.V)	Canal Diameter µm	Canal Volume mm^3	# of Lacunae (N.Lc)	Lacunar Volume μm^3	Lacunar Density (N.Lc/BV) mm^3
1st Cuneiform	#1	0.19	47	0.08	2109	233	11100
	#3	0.12	63	0.15	1083	201	9025
	#2	0.2	50	0.07	2517	301	12585
2nd Cuneiform	#1	0.2	48	0.07	2231	215	11155
	#3	0.13	63	0.14	1192	212	9169.230769
	#2	0.19	52	0.08	2302	239	12115.78947
3rd Cuneiform	#1	0.19	50	0.08	2221	265	11689.47368
	#3	0.14	60	0.13	1173	221	8378.571429
	#2	0.2	47	0.07	2517	298	12585
Navicular	#1	0.19	52	0.08	2121	233	11163.15789
	#3	0.17	63	0.1	1611	206	9476.470588
	#2	0.2	48	0.07	2541	280	12705
Capitate	#1	0.19	47	0.08	1998	265	10515.78947
	#3	0.17	64	0.1	2383	221	14017.64706
	#2	0.22	42	0.05	2679	327	12177.27273
Twelfth Rib	#1	0.19	48	0.08	3021	278	15900
	#3	0.15	55	0.12	2043	261	13620
	#2	0.21	47	0.06	3498	274	16657.14286
Fibula	#1	0.2	43	0.07	5249	282	26245
	#3	0.11	57	0.16	2908	254	26436.36364
	#2	0.2	40	0.07	5103	311	25515
Femur	#1	0.18	47	0.09	5308	237	29488.88889
	#3	0.11	66	0.16	2871	229	26100
	#2	0.19	41	0.08	6721	227	35373.68421

Table B.1: (cont).

Element Type	Research #	Bone Volume (TV-Ca.V)	Canal Diameter µm	Canal Volume mm^3	# of Lacunae (N.Lc)	Lacunar Volume $µm^3$	Lacunar Density (N.Lc/BV) mm^3
Tibia	#1	0.18	47	0.09	4237	260	23538.88889
	#3	0.13	66	0.14	2492	240	19169.23077
	#2	0.19	41	0.08	5539	226	29152.63158
Patella	#1	0.18	50	0.09	3872	231	21511.11111
	#3	0.09	67	0.18	1781	216	19788.88889
	#2	0.2	42	0.07	4937	274	24685
Humerus	#1	0.2	41	0.07	5262	231	26310
	#3	0.15	61	0.12	3290	216	21933.33333
	#2	0.21	39	0.06	6318	274	30085.71429
Ulna	#1	0.2	66	0.07	5237	231	26185
	#3	0.15	41	0.12	3322	216	22146.66667
	#2	0.22	47	0.05	6139	274	27904.54545
Radius	#1	0.19	66	0.08	5877	231	30931.57895
	#3	0.14	41	0.13	3823	216	27307.14286
	#2	0.21	47	0.06	7102	274	33819.04762
Scapula	#1	0.18	53	0.09	5105	231	28361.11111
	#3	0.11	67	0.16	2828	216	25709.09091
	#2	0.21	49	0.06	6948	274	33085.71429
Clavicle	#1	0.22	66	0.05	5229	231	23768.18182

Table B.1: (cont).

Element Type	Research #	Bone Volume (TV-Ca.V)	Canal Diameter µm	Canal Volume mm^3	# of Lacunae (N.Lc)	Lacunar Volume $µm^3$	Lacunar Density (N.Lc/BV) mm^3
	#2	0.16	41	0.11	3221	216	20131.25
	#3	0.24	47	0.03	7028	274	29283.33333
Cervical Vertebra	#1	0.2	50	0.07	4028	231	20140
	#3	0.07	67	0.2	1238	216	17685.71429
	#2	0.21	42	0.06	4891	274	23290.47619
Lumbar Vertebra	#1	0.2	50	0.07	3971	231	19855
	#3	0.07	67	0.2	1192	216	17028.57143
	#2	0.21	42	0.06	5392	274	25676.19048
Thoracic Vertebra	#1	0.19	50	0.08	5271	231	27742.10526
	#3	0.11	67	0.16	2323	216	21118.18182
	#2	0.21	42	0.06	6091	274	29004.7619
Frontal	#1	0.21	50	0.06	4291	231	20433.33333
	#3	0.18	67	0.09	3405	216	18916.66667
	#2	0.23	45	0.04	7128	274	30991.30435
Parietal	#1	0.21	40	0.06	4827	231	22985.71429
	#3	0.18	62	0.09	3241	216	18005.55556
	#2	0.2	52	0.07	6405	274	32025
Temporal	#1	0.22	51	0.05	4210	231	19136.36364
	#3	0.17	57	0.1	2303	216	13547.05882
	#2	0.19	58	0.08	4691	274	24689.47368

Table B.1: (cont).

Element Type	Research #	Bone Volume (TV-Ca.V)	Canal Diameter µm	Canal Volume mm^3	# of Lacunae (N.Lc)	Lacunar Volume $µm^3$	Lacunar Density (N.Lc/BV) mm^3
Maxilla	#1	0.19	46	0.08	3520	231	18526.31579
	#3	0.13	61	0.14	2072	216	15938.46154
	#2	0.2	42	0.07	4728	274	23640
Mandible	#1	0.2	42	0.07	5539	231	27695
	#3	0.18	58	0.09	4298	216	23877.77778
	#2	0.23	39	0.04	6135	274	26673.91304
Occipital	#1	0.22	50	0.05	6608	231	30036.36364
	#3	0.19	67	0.08	4092	216	21536.84211
	#2	0.23	42	0.04	6632	274	28834.78261
First Rib	#1	0.19	48	0.08	5405	231	28447.36842
	#3	0.13	55	0.14	2837	216	21823.07692
	#2	0.21	47	0.06	4824	274	22971.42857
Middle Rib	#1	0.2	48	0.07	6174	231	30870
	#3	0.15	55	0.12	3328	216	22186.66667
	#2	0.19	47	0.08	4848	274	25515.78947
Metatarsal 1	#1	0.21	47	0.06	5823	231	27728.57143
	#3	0.17	63	0.1	4327	216	25452.94118
	#2	0.21	50	0.06	6830	274	32523.80952

Table B.1: (cont).

Element Type	Research #	Bone Volume (TV-Ca.V)	Canal Diameter µm	Canal Volume mm^3	# of Lacunae (N.Lc)	Lacunar Volume $µm^3$	Lacunar Density (N.Lc/BV) mm^3
Metatarsal 2	#1	0.2	47	0.07	5763	231	28815
	#3	0.14	63	0.13	3109	216	22207.14286
	#2	0.21	50	0.06	6780	274	32285.71429
Metatarsal 3	#1	0.2	47	0.07	6763	231	33815
	#3	0.15	63	0.12	3829	216	25526.66667
	#2	0.21	50	0.06	7339	274	34947.61905
Metatarsal 4	#1	0.21	47	0.06	8028	231	38228.57143
	#3	0.17	63	0.1	5139	216	30229.41176
	#2	0.2	50	0.07	6983	274	34915
First Proximal Hand Phalanx	#1	0.19	54	0.08	4702	231	24747.36842
	#3	0.14	68	0.13	2980	216	21285.71429
	#2	0.22	48	0.05	6102	274	27736.36364
First Distal Hand Phalanx	#1	0.18	55	0.09	8405	231	46694.44444
	#3	0.14	67	0.13	2174	216	15528.57143
	#2	0.23	46	0.04	2830	274	12304.34783
First Distal Foot Phalanx	#1	0.21	50	0.06	5305	231	25261.90476
	#3	0.15	67	0.12	2790	216	18600
	#2	0.22	42	0.05	6002	274	27281.81818
Metacarpal 4	#1	0.22	51	0.05	5827	231	26486.36364
	#3	0.18	60	0.09	3801	216	21116.66667
	#2	0.23	42	0.04	6839	274	29734.78261

Table B.1: (cont).

Element Type	Research #	Bone Volume (TV-Ca.V)	Canal Diameter µm	Canal Volume mm^3	# of Lacunae (N.Lc)	Lacunar Volume $µm^3$	Lacunar Density (N.Lc/BV) mm^3
Metacarpal 2	#1	0.2	50	0.07	6963	231	34815
	#3	0.17	67	0.1	4092	216	24070.58824
	#2	0.23	42	0.04	8339	274	36256.52174
Metacarpal 3	#1	0.2	50	0.07	6763	231	33815
	#3	0.17	67	0.1	6029	216	35464.70588
	#2	0.23	42	0.04	6436	274	27982.6087
First Proximal Foot Phalanx	#1	0.2	55	0.07	4192	231	20960
	#3	0.12	70	0.15	2492	216	20766.66667
	#2	0.22	48	0.05	5322	274	24190.90909

Table B.2: Quantitative Results for the Morphological Parameters of Osteocyte Lacunae from Cancellous Bone ROIs.

Element Type	Research #	Bone Volume (TV-Ca.V)	# of Lacunae (N.Lc)	Lacunar Volume $µm^3$	Lacunar Density (N.Lc/BV) mm^3
Pubis	#1	0.18	2282	163	12677.77778
	#3	0.17	1242	139	7305.882353
	#2	0.2	2717	201	13585
Ilium	#1	0.21	2082	163	9914.285714
	#3	0.18	1042	139	5788.888889
	#2	0.21	1991	201	9480.952381
Ischium	#1	0.2	1912	152	9560
	#3	0.18	1313	120	7294.444444
	#2	0.2	2874	198	14370

Table B.2: (cont).

Element Type	Research #	Bone Volume (TV-Ca.V)	# of Lacunae (N.Lc)	Lacunar Volume μm^3	Lacunar Density (N.Lc/BV) mm^3
Sacrum	#1	0.2	1967	149	9835
	#3	0.17	1013	98	5958.823529
	#2	0.19	2014	167	10600
Cuboid	#1	0.2	2015	168	10075
	#3	0.17	1213	117	7135.294118
	#2	0.19	2072	156	10905.26316
Calcaneus	#1	0.19	1998	152	10515.78947
	#3	0.15	1116	120	7440
	#2	0.18	2762	198	15344.44444
Talus	#1	0.2	1962	187	9810
	#3	0.18	1290	111	7166.666667
	#2	0.2	2099	166	10495
1st Cuneiform	#1	0.2	1761	132	8805
	#3	0.17	1047	143	6158.823529
	#2	0.21	2128	170	10133.33333
2nd Cuneiform	#1	0.2	1821	162	9105
	#3	0.17	1102	113	6482.352941
	#2	0.22	2218	184	10081.81818
3rd Cuneiform	#1	0.2	2727	195	13635
	#3	0.17	993	98	5841.176471
	#2	0.21	2998	204	14276.19048
Navicular	#1	0.2	2768	197	13840
	#3	0.17	1283	128	7547.058824
	#2	0.21	3113	297	14823.80952
Capitate	#1	0.18	2292	180	12733.33333
	#3	0.15	1690	147	11266.66667
	#2	0.21	2982	201	14200
Twelfth Rib	#1	0.19	2093	164	11015.78947
	#3	0.14	1222	111	8728.571429
	#2	0.19	2880	201	15157.89474
Fibula	#1	0.2	N/A	N/A	N/A
	#3	0.17	N/A	N/A	N/A
	#2	0.19	N/A	N/A	N/A

Table B.2: (cont).

Element Type	Research #	Bone Volume (TV-Ca.V)	# of Lacunae (N.Lc)	Lacunar Volume μm^3	Lacunar Density (N.Lc/BV) mm^3
Femur	#1	0.21	N/A	N/A	N/A
	#3	0.18	N/A	N/A	N/A
	#2	0.21	N/A	N/A	N/A
Tibia	#1	0.21	N/A	N/A	N/A
	#3	0.15	N/A	N/A	N/A
	#2	0.22	N/A	N/A	N/A
Patella	#1	0.18	2352	184	13066.66667
	#3	0.12	1392	137	11600
	#2	0.19	2865	196	15078.94737
Humerus	#1	0.21	N/A	N/A	N/A
	#3	0.18	N/A	N/A	N/A
	#2	0.22	N/A	N/A	N/A
Ulna	#1	0.21	N/A	N/A	N/A
	#3	0.18	N/A	N/A	N/A
	#2	0.23	N/A	N/A	N/A
Radius	#1	0.19	N/A	N/A	N/A
	#3	0.17	N/A	N/A	N/A
	#2	0.21	N/A	N/A	N/A
Scapula	#1	0.18	2612	204	14511.11111
	#3	0.13	1347	139	10361.53846
	#2	0.23	3210	274	13956.52174
Clavicle	#1	0.2	2437	193	12185
	#3	0.12	1063	120	8858.333333
	#2	0.22	3201	273	14550
Cervical Vertebra	#1	0.19	1788	167	9410.526316
	#3	0.07	534	92	7628.571429
	#2	0.21	2219	187	10566.66667
Lumbar Vertebra	#1	0.2	1823	173	9115
	#3	0.06	462	84	7700
	#2	0.21	1987	149	9461.904762
Thoracic Vertebra	#1	0.19	1523	160	8015.789474
	#3	0.1	561	81	5610
	#2	0.21	1903	168	9061.904762

Table B.2: (cont).

Element Type	Research #	Bone Volume (TV-Ca.V)	# of Lacunae (N.Lc)	Lacunar Volume μm^3	Lacunar Density (N.Lc/BV) mm^3
Frontal	#1	0.2	N/A	N/A	N/A
	#3	0.21	N/A	N/A	N/A
	#2	0.18	N/A	N/A	N/A
Parietal	#1	0.22	2381	187	10822.72727
	#3	0.2	1792	171	8960
	#2	0.17	2210	183	13000
Temporal	#1	0.22	N/A	N/A	N/A
	#3	0.19	N/A	N/A	N/A
	#2	0.17	N/A	N/A	N/A
Maxilla	#1	0.18	1842	184	10233.33333
	#3	0.09	1082	122	12022.22222
	#2	0.19	3217	216	16931.57895
Mandible	#1	0.2	N/A	N/A	N/A
	#3	0.17	N/A	N/A	N/A
	#2	0.21	N/A	N/A	N/A
Occipital	#1	0.21	N/A	N/A	N/A
	#3	0.18	N/A	N/A	N/A
	#2	0.22	N/A	N/A	N/A
First Rib	#1	0.19	2113	170	11121.05263
	#2	0.15	1421	154	9473.333333
	#3	0.21	2760	205	13142.85714
Middle Rib	#1	0.19	2183	178	11489.47368
	#3	0.14	1149	216	8207.142857
	#2	0.2	2908	216	14540
Metatarsal 1	#1	0.21	2238	180	10657.14286
	#3	0.16	1139	125	7118.75
	#2	0.22	2863	176	13013.63636
Metatarsal 2	#1	0.2	2390	188	11950
	#3	0.16	1247	149	7793.75
	#2	0.22	2991	217	13595.45455

Table B.2: (cont).

Element Type	Research #	Bone Volume (TV-Ca.V)	# of Lacunae (N.Lc)	Lacunar Volume μm^3	Lacunar Density (N.Lc/BV) mm^3
Metatarsal 3	#1	0.2	2103	169	10515
	#3	0.15	1201	127	8006.666667
	#2	0.21	2672	195	12723.80952
Metatarsal 4	#1	0.2	2509	193	12545
	#3	0.14	1139	137	8135.714286
	#2	0.21	2761	205	13147.61905
First Proximal Hand Phalanx	#1	0.2	2209	173	11045
	#3	0.12	851	77	7091.666667
	#2	0.21	2686	194	12790.47619
First Distal Hand Phalanx	#1	0.19	2233	172	11752.63158
	#3	0.11	782	79	7109.090909
	#2	0.2	2686	197	13430
First Distal Foot Phalanx	#1	0.21	1973	185	9395.238095
	#3	0.12	452	70	3766.666667
	#2	0.2	2008	162	10040
Metacarpal 4	#1	0.19	2098	169	11042.10526
	#3	0.17	1382	144	8129.411765
	#2	0.21	2902	215	13819.04762
Metacarpal 2	#1	0.19	2109	170	11100
	#3	0.15	1198	141	7986.666667
	#2	0.2	1262	151	6310
Metacarpal 3	#1	0.21	2065	170	9833.333333
	#2	0.16	1207	143	7543.75
	#3	0.2	2096	167	10480

Table B.2: (cont).

Element Type	Research #	Bone Volume (TV-Ca.V)	# of Lacunae (N.Lc)	Lacunar Volume μm^3	Lacunar Density (N.Lc/BV) mm^3
First Proximal Foot Phalanx	#1	0.2	2004	161	10020
	#3	0.13	1017	124	7823.076923
	#2	0.21	2121	172	10100

APPENDIX C: Descriptive Statistics and Normality Tests for Clinical CT and SR micro-CT datasets.

Table C.1: Means and Standard Deviations for Cortical and Cancellous Bone Height Measurements Calculated from the Clinical CT Scans.

Variable	Individual	*n*	Mean	St.Dev
Average Cortical Bone Height (mm)	#1	33	8.1993	1.453593
	#2	33	7.6052	1.82317
	#3	32	7.8055	1.31113
Average Cancellous Bone Height (mm)	#1	33	8.0050	1.32470
	#2	33	8.1703	2.53998
	#3	32	7.2916	1.56041

Table C.2: Means and Standard Deviations for Cortical and Cancellous Bone Width Measurements Calculated from the Clinical CT Scans.

Variable	Individual	*n*	Mean	St.Dev
Average Cortical Bone Width (mm)	#1	33	1.3801	0.78390
	#2	33	1.6568	1.09018
	#3	32	1.4383	0.73980
Average Cancellous Bone Width (mm)	#1	33	6.3566	2.74554
	#2	33	7.1835	2.66714
	#3	32	6.9266	2.83561

Table C.3: Descriptive Statistics for Lacunar Parameters.

	n	Minimum	Maximum	Mean		St. Dev
	Statistic	Statistic	Statistic	Statistic	Std. Error	Statistic
N.Lc Cortical Bone	132	1083	8405	4274.50	154.088	1770.34
N.Lc Cancellous Bone	102	452	6217	1961.03	80.3374	811.37
N.Lc/BV Cortical Bone	132	8140	46694.44	22723.32	647.73	7441.88

Table C.3: (cont).

	n	Minimum	Maximum	Mean		St. Dev
	Statistic	Statistic	Statistic	Statistic	Std. Error	Statistic
N.Lc/BV Cancellous Bone	102	3766.67	32721.05	10542.87	340.62	3440.09
Lc.V Cortical Bone	132	201	327	245.93	2.495	28.66
Lc.V Cancellous Bone	102	70	297	164.431	4	40.45
Ca.Dm Cortical Bone	132	39	70	52.49	0.748	8.589
Ca.V Cortical Bone	132	0.03	0.20	0.0851	0.00294	0.03378

Tests of Normality

Table C.4: Kolmogorov-Smirnov Test for Normality for Cortical and Cancellous Bone Height and Width Measurements.

	Kolmogorov-Smirnov		
	Statistic	*df*	Sig.
Cortical Bone Height (mm)	0.099	98	0.020
Cancellous Bone Height (mm)	0.087	98	0.067
Cortical Bone Width (mm)	0.189	98	0.000
Cancellous Bone Width (mm)	0.071	98	0.200

Table C.5: Kolmogorov-Smirnov Test for Normality for Average Cortical and Cancellous Measurements (mm) and Nuclear DNA Data (ng/g).

	Kolmogorov-Smirnov		
	Statistic	*df*	Sig.
Average Cortical Bone Volume (mm)	0.118	38	0.200
Average Cancellous Bone Volume (mm)	0.183	38	0.003
Nuclear DNA Data (ng/g)	0.194	38	0.001

Table C.6: Kolmogorov-Smirnov Test for Normality for N.Lc.

	Kolmogorov-Smirnov		
	Statistic	***df***	**Sig.**
N.Lc Cortical Bone	0.075	132	0.068
N.Lc Cancellous Bone	0.145	132	0.000

Table C.7: Kolmogorov-Smirnov Test for Normality for N.Lc/BV.

	Kolmogorov-Smirnov		
	Statistic	***df***	**Sig.**
N.Lc/BV Cortical Bone	0.058	132	0.200
N.Lc/BV Cancellous Bone	0.163	132	0.000

Table C.8: Kolmogorov-Smirnov Test for Normality for Lc.V.

	Kolmogorov-Smirnov		
	Statistic	***df***	**Sig.**
Lc.V Cortical Bone	0.229	132	0.000
Lc.V Cancellous Bone	0.176	132	0.000

Table C.9: Kolmogorov-Smirnov Test for Normality for Average Cortical and Cancellous Measurements (mm) and Nuclear DNA Data (ng/g).

	Kolmogorov-Smirnov		
	Statistic	***df***	**Sig.**
Average Cortical Bone N.Lc	0.097	34	0.200
Average Cancellous Bone N.Lc	0.092	34	0.200
Average Cortical Bone N.Lc/BV (mm^3)	0.125	34	0.195
Average Cancellous Bone N.Lc/BV (mm^3)	0.129	34	0.167
Nuclear DNA Data (ng/g)	0.208	34	0.001

Table C.10: Kolmogorov-Smirnov Test for Normality for Ca.Dm and Ca.V.

	Kolmogorov-Smirnov		
	Statistic	***df***	**Sig.**
Ca.Dm Cortical Bone	0.160	132	0.000
Ca.V Cortical Bone	0.196	132	0.000

Table C.11: Levene's Tests of Equality of Variances for Ca.Dm and Ca.V.

Variable	F	df1	df2	Sig.
Ca.Dm Cortical Bone	1.210	2	129	0.302
Ca.V Cortical Bone	3.193	2	129	0.283

VITA

Janna M. Andronowski was born in Guelph, Ontario, Canada to parents Max and Karen Andronowski. She graduated from Centennial Collegiate Vocational Institute. Janna attended Simon Fraser University in Burnaby, British Columbia, Canada where she studied Criminology and Biological Sciences. During her undergraduate work she was a teaching assistant in the School of Criminology and research assistant at Simon Fraser University's Centre for Forensic Research, and the Mary Rose Trust in Portsmouth, UK. In 2010, Janna began a Master's program at the University of Toronto in anthropology with a specialization in biological anthropology. She graduated in 2012 with a Master's of Science and matriculated to the University of Tennessee, Knoxville to begin her doctorate degree that fall. Janna advanced to candidacy in November 2014 and received her Doctorate of Philosophy in May 2016. During her tenure in graduate school, Janna was a research intern with the Forensic Anthropology Unit at the Office of Chief Medical Examiner in New York City (NYC-OCME). She was also a graduate teaching associate for Human Origins and Principles of Biological Anthropology in the Department of Anthropology at the University of Tennessee, Knoxville, and a laboratory instructor for Human Anatomy in the Ecology and Evolutionary Biology department. Janna will be expanding her research program during a postdoctoral research fellowship in the Anatomy and Cell Biology department at the University of Saskatchewan beginning in June 2016 where she will be a Canadian Institutes of Health Research (CIHR) fellow in Health Research Using Synchrotron Techniques (THRUST).